UiT The Arctic University of Norway

Department of Geosciences

The rock slope failures at Låvan and Dusnjarga, Northern Norway

A comprehensive Quaternary, morphological and structural analysis

Frederic Blau

Master's thesis in Geology (GEO-3900), May 2020

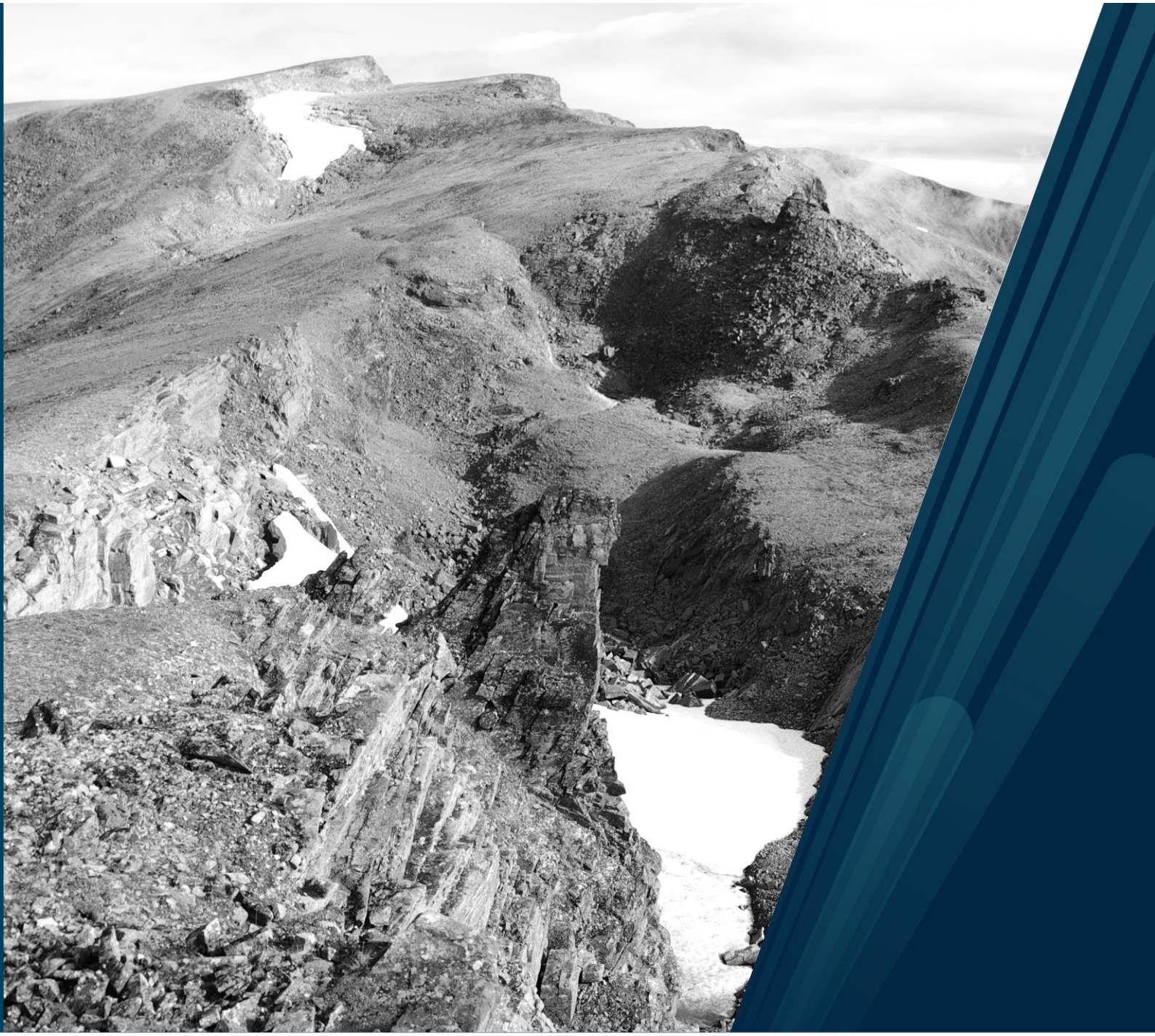

Declaration of Authorship

I hereby certify that this thesis is my own unaided work, unless stated otherwise. All directly or indirectly used sources are acknowledged as references.

This paper has neither been previously presented to another board of examiners, nor has been published.

Tromsø, May 14th 2020

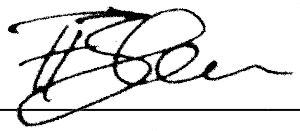

Frederic Blau (author)

UiT

NORGES
ARKTISKE
UNIVERSITET

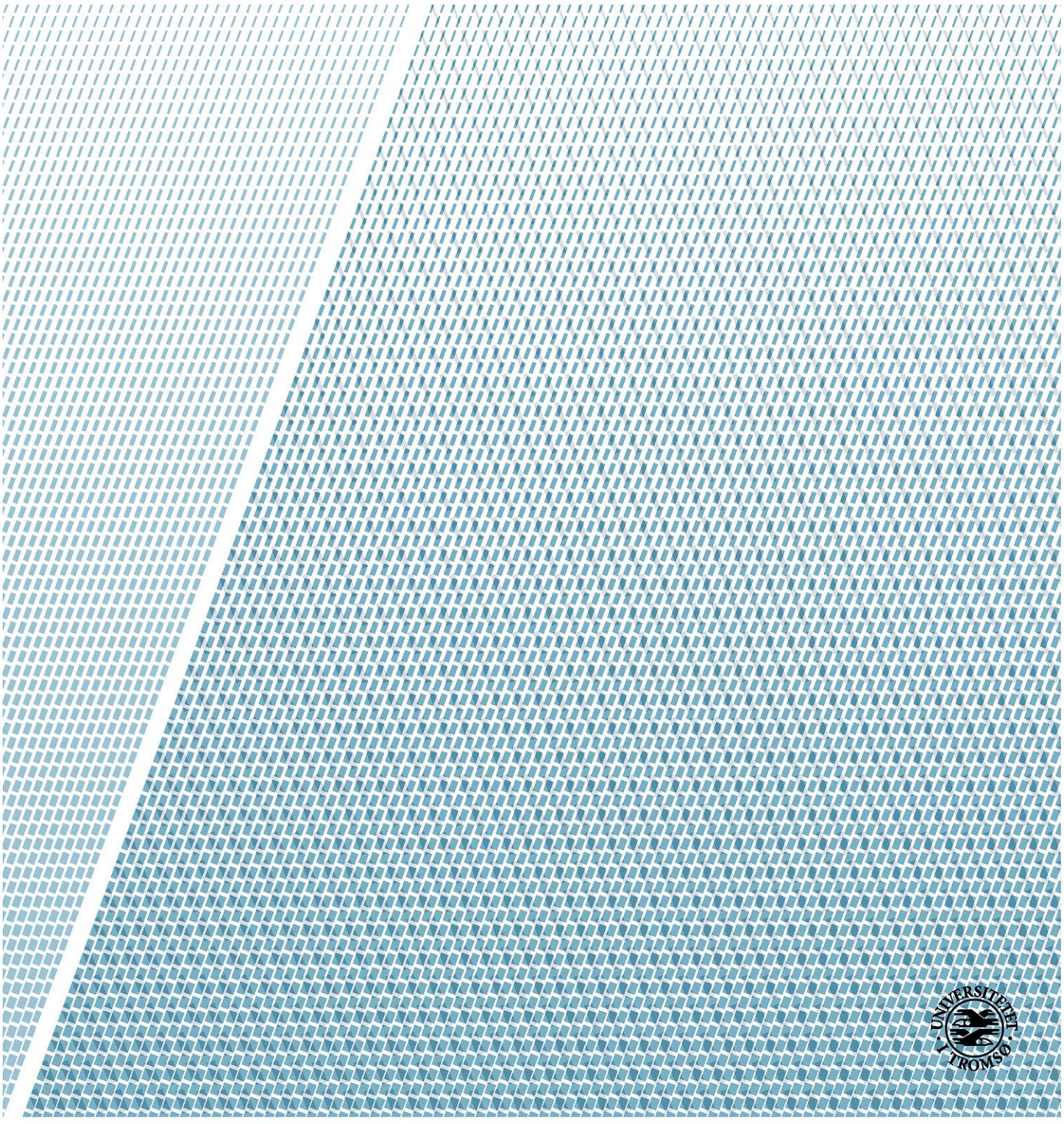

Abstract

Rock avalanches and subsequent displacement waves represented the deadliest natural disaster in Norway in the past century. The two deep-seated and unstable slopes Dusnjarga and Låvan in Troms county (Norway) are clearly defined by morphological deformation features. Due to the steep fjord setting, a potential catastrophic rock avalanche could pose a severe threat to people and infrastructure along the fjord and in particular for the settlement below Låvan.

Firstly, an analysis of Quaternary deposits and landforms in the study area was performed which involved e.g. the creation of a detailed Quaternary geological map, the sedimentary logs and particle size analyzes. The former glaciation and deglaciation were expressed by thin till layers, glaciomarine and redeposited glaciofluvial deposits as well as paleo-shorelines. Their analysis and interaction with the rock slope deformation allowed for several interpretations on the temporal behavior of the instabilities. For instance, for Dusnjarga's central and eastern parts, strong deformation is suggested for the approximate period of the Tapes transgression. Due to the general scarcity of Quaternary deposits in the study area further reaching chronological interpretations would however require the use of absolute dating methods.

Secondly, the rock slope deformation Låvan was investigated in detail using digital resources as well as data from the field which comprised structural measurements, scanline data and observations on the morphology and rock mass. Four discontinuity sets were clearly expressed in both the structural data and the morpho-structures: the foliation (SC) and the joint sets JN1, JN2 and JN3. Kinematically, planar failure on SC and wedge failure on JN1 and SC stood out as the most likely failure mechanisms. Bilinear compound sliding on multiple sliding surfaces was suggested as the controlling style of deformation. Sliding occurs as suggested principally on SC with the steeply dipping JN2 forming the linkage between low-persistent fractures. A change of the orientation of SC complicates the sliding movement in the lower slope and leads to compact blocks being pushed out frontally. This might pose a hazard for the settlement situated right below. However, the final hazard analysis resulted in a classification of Låvan as a low-hazard object which classification is largely based on the absence of significant displacement. In the future, some of the high uncertainties could be reduced by investigating longer time series and establishing further monitoring points.

Acknowledgements

First of all, I would like to thank both my supervisors Anne Hormes and Martina Böhme who were always present to give me helpful advice and to discuss my work; also thank you Anne for the good climbing days and belaying.

Further, I would like to thank Ellen Tyldum Skogen for the good time we had together in the field and especially for her warm down jacket during those snowy September days.

Thank you to all my Tromsø friends without who my Master studies in the north would not have been nearly as good as they were.

Since this is the moment to look back on my whole time as a student, I would also like to thank my best friends in Tübingen who made me who I am now.

I owe my parents more than just a thank you. Joachim and Gisela, throughout all my studies you have never lost confidence in me or stopped supporting me. Thanks a lot.

Finally, special thanks go to Charlotte Haugk who was always there to support me: as field assistant, writing and motivation coach, or just as the best girlfriend ever.

TABLE OF CONTENT

LIST OF FIGURES

LIST OF ABBREVIATIONS

a BP	= years before present
cal a BP	= calibrated radiocarbon years before present
DEM	= digital elevation model
dGNSS	= differential Global Navigation Satellite System
DSGSD	= deep-seated gravitational slope deformation
GIS	= geographical information system
InSAR	= Interferometric Synthetic Aperture Radar
IVF (value)	= intensity-value-frequency (value)
JN	= joint
ka	= 1,000 years
LGM	= last glacial maximum
LiDAR	= light detection and ranging (3D laser scanning)
NGU	= Geological Survey of Norway
NVE	= Norwegian Water Resources and Energy Directorate
RCP	= representative concentration pathway
SC	= schistosity/foliation
SIP	= Seiland Igneous Province
TCN (dating)	= terrestrial cosmogenic nuclide (dating)
UAV	= unmanned airborne vehicle

1 Introduction

Landslides and rock slope failures can be found almost everywhere around the globe in various settings on land and under water (Highland and Bobrowsky 2008). Over time these phenomena have caused large economic loss and numerous casualties. During this century, their impact is expected to rise even more. Causes can be the increase of settlements close to unstable areas, the decrease of slope stability due to deforestation and human construction as well as the consequences of climate change (Turner and Schuster 1996).

Norway's special topography is characterized in many parts by deep fjords and steep mountainous terrain that was subjected to several glacial cycles. Largely due to this particular situation, Norway is especially prone to rock avalanches and on average 2 - 6 major events have occurred along the Norwegian coast per century (Hermanns et al. 2014). Apart from the destructive impact itself, the major threat to the people and their settlements often arises from the rock avalanche's impact into water thereby triggering devastating displacement waves. In Norway, rock avalanches causing displacement waves represented the most disastrous natural disaster in the 20th century with a death toll of more than 175 (Hermanns and Longva 2012). In addition, many Norwegian settlements are presently located in fjord settings in hazardous proximity to the shore.

The present danger emanating from active unstable rock slopes has led to an extensive campaign by the Geological Survey of Norway (NGU) with the aim of systematically mapping and characterizing the unstable slopes in Norway (Hermanns et al. 2013; Oppikofer et al. 2015). In the course of this campaign more than 300 unstable slopes were mapped all over Norway and more are pending to be identified (Hermanns et al. 2013; NGU 2020a). Troms county in northern Norway stands out as the region with the most registered unstable rock slopes, so far counting 138 objects (NGU 2020a; Oppikofer et al. 2015). However, campaigns and detailed research efforts have focused predominantly on central Troms (particularly to the west of Lyngen), whereas the county's northernmost part has received comparably little attention (e.g. Bunkholt et al. 2012; NGU 2020a).

Dusnjarga and Låvan are two adjacent rock slopes in northernmost Troms that were registered as unstable in the context of NGU's mapping campaign (Bunkholt et al. 2013). On aerial imagery for instance, the local slope deformations are clearly identifiable by their morphology including characteristic elements such as sharp back scarps, minor scarps, and locally disaggregated rock mass. Both sites, Dusnjarga and Låvan, were described in several earlier reports by the NGU, e.g. Bunkholt et al. (2011, 2013), but only basic field work was carried out in 2007 and 2010 and detailed mapping of the deformed areas had not been performed before. NGU installed monitoring points during their field campaigns at Dusnjarga (3 points in 2007)

and Låvan (4 points in 2010). The data obtained from these dGNSS (differential Global Navigation Satellite System) measurements as well as from InSAR (interferometric synthetic aperture radar) clearly revealed active horizontal displacement for parts of Dusnjarga but not for Låvan.

Both slopes, Dusnjarga and Låvan, have a morphologically active appearance and a large sudden failure event at one of the rock slopes could have dramatic consequences for people and infrastructure in the adjacent fjords, particularly for the settlement directly below Låvan. In consequence to this and to so far inconclusive former research, it appears necessary to conduct a detailed and field-based study for Dusnjarga and Låvan.

2 Objectives of the study

The principal goal of this Master thesis is to perfom a detailed investigation of the unstable rock slopes of Dusnjarga and Låvan situated in the Kvænangen municipality (Troms). This thesis is related to a second Master thesis (Tyldum Skogen in prep.) conducted in the same study area. This is why this thesis focusses on two main aspects:

i. A detailed analysis of the Quaternary geology in the larger study area comprising Låvan and Dusnjarga. This includes the creation of a detailed Quaternary geological map for the study area and the analysis of relevant Quaternary deposits and sequences. The study of Quaternary deposits and particularly their interaction with the products of slope deformation allow final conclusions to be made on the temporal behavior of the slope deformations since the last glaciation.
ii. A detailed investigation and hazard analysis of the unstable rock slope Låvan. This is achieved through the analysis of a variety of field and digital data which includes analyzes of rock mass observations, scanline data, latest displacement data and structural data where the latter allows the modelling of different kinematic failure scenarios. These analyses allow for final conclusions to be made on the active deformation mechanisms and on the slope stability of Låvan which is also expressed in a concluding hazard assessment based on the system in Hermanns et al. (2012a; 2013a).

The Master thesis is part of the systematic mapping of unstable rock slopes in Norway and is a contribution to the national unstable rock slope database developed and maintained by the NGU (Oppikofer et al. 2015). This thesis will be an important resource for future decision making and planning related to Dusnjarga and Låvan. This concerns for instance future monitoring measures, safety precautions or follow-up studies. Furthermore, the presented

results and interpretations will contribute to a deeper understanding of past behaviour of unstable rock slopes in Norway and in formerly glaciated areas in general.

3 Available data

The presented and discussed results in this study are largely based on data that was collected by the author and Ellen Tyldum Skogen during a field campaign in August and September 2019 (in total 2.5 weeks), but data contributed from external sources was also essential. Table 1 gives an overview of the main external data resources as well as the origin and the quality of the data.

Table 1: Overview of the main data resources that were provided by external sources.

DATA	***SOURCE***	***RESOLUTION***
Digital elevation model	*Kartverket*	1 m
Orthophoto imagery	*Kartverket*	0.25 m, 0.5 m
Geological map	*NGU (Roberts 1974)* *Roberts and Elvevold (2018)*	1:250,000 1:50,000
Quaternary Map	*NGU (Riiber 2000)*	1:250,000
InSAR displacement data	*NGU (https://insar.ngu.no/)*	
dGNSS displacement data	*NGU*	

4 Study area

Dusnjarga (about 70.02°N, 21.95°E) was identified as the principal unstable rock slope in the study area, situated in Kvænangen community, Troms county, northern Norway. Låvan is a smaller unstable rock slope and is located directly to the east of Dusnjarga (Figure 1). Both sites are situated on the southern side of the Dusnjarga peninsula which is bounded by Jøkelfjorden to the north and Lille Altafjorden to the south. These two fjords extend in western direction into the larger Kvænangen fjord. The peninsula is very mountainous. Its highest elevation, Koppartind (923 m a.s.l.), forms the northern top of the Dusnjarga deformation area stretching on a length of about 2.5 km towards the fjord resulting in an approximate mean slope gradient of 37 %. The deformed area at Låvan is steeper (about 53 %) but less wide with a length of 850 m at an elevation difference of 453 m. The whole surrounding is sparsely populated with about 100 people living at Alteidet at the end of Lille Altafjorden and 400 people

living in Burfjorden 10 km to the south. However, a small settlement of 18 houses is directly situated at the foot of Låvan (Figure 1).

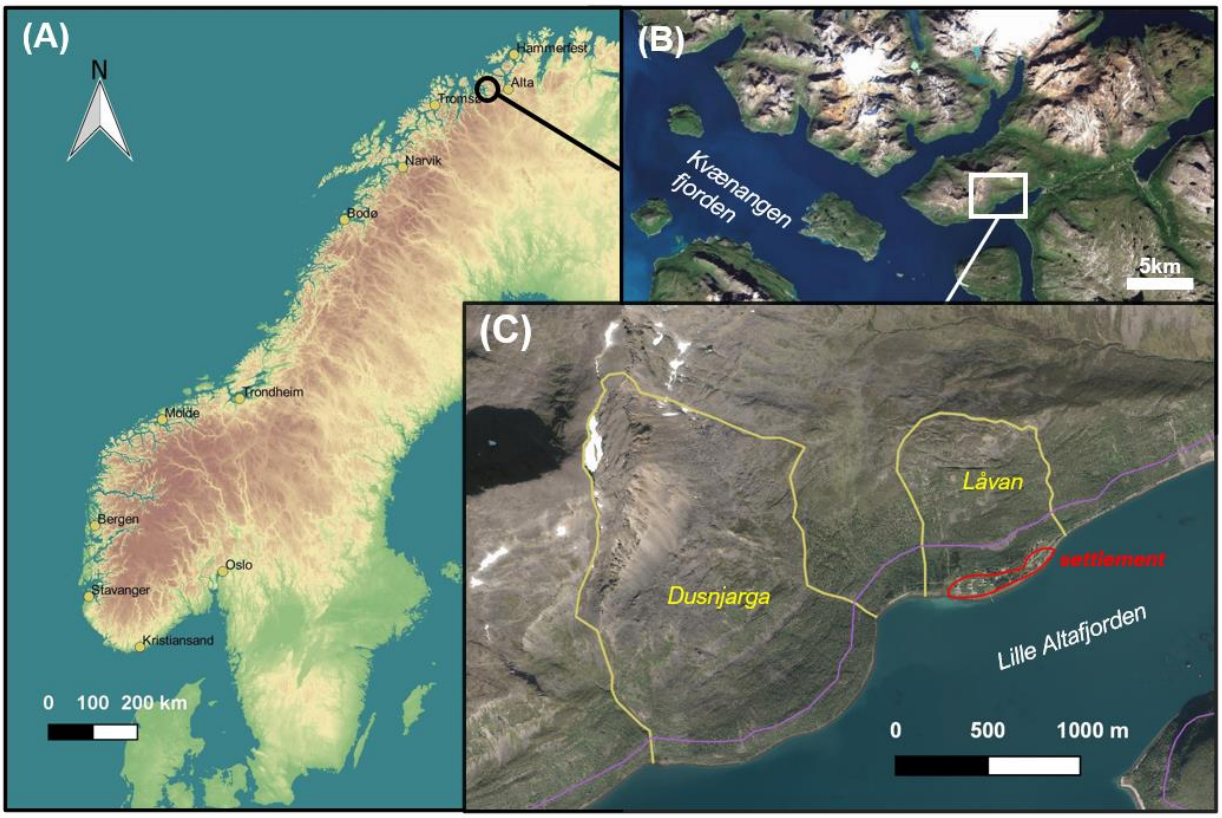

Figure 1: Overview and detailed maps of the study area located in the Troms county, Norway. (A) Small-scale map of Scandinavia: relief map including major cities (yellow points) and the location of Dusnjarga (red point). (B) Medium-scale map: aerial photo of the wider surrounding of the studied sites (red box) located on the Dusnjarga peninsula which is delimited by the large Kvænangen fjord to the west and the lateral branches of Jøkelfjorden and Lille Altafjorden to the north and south. *Adapted from: www.norgeibilder.no.* (C) Large-scale map: detailed aerial photo of the unstable rock slopes at Dusnjarga and at Låvan including the postglacial marine limit (purple line) as interpolated by NGU.

4.1 Climate and permafrost

- *Present-day climate*

Situated in northern Norway at a latitude of 70°, Dusnjarga has short cool summers (average July 12.1 °C) and long winters with at least seven months of snow cover (Meteorologisk Institutt et al. 2020). The immediate vicinity at the fjord and the short distance (about 40 km) to the open sea lead to a humid climate and relatively mild winter temperatures for the high latitude (average January -4.6 °C) (Meteorologisk Institutt et al. 2020). However, the coastal regions of Troms and Finnmark are generally less humid compared to the coasts of southern Norway. The closest weather station about 15 km east of Dusnjarga (Sopnesbukt) records a yearly precipitation of 728 mm for the time period 1998-2019 and an average temperature of 2.6 °C for the time period of 2009 - 2019 (Meteorologisk Institutt et al. 2020). Thus, the great

differences in elevation in the study area (up to 900 m a.s.l.) effect strongly the local climate, e.g. the tree line is at about 300 m a.s.l. and the vegetation line at about 500 m a.s.l.

- *Future climate*

An important factor for this study is the development of the regional precipitations because of its impact on the slope stability (section 5.4). Figure 2 displays the expected increase in precipitation according to climate projections from the Norwegian Climate Service Center (Meteorologisk Institutt et al. 2020). These projections are based on assumptions about emission scenarios concerning greenhouse gasses with global and regional climate models. Figure refers to scenario RCP8.5 (= Representative Concentration Pathways) which assumes an ongoing increase in greenhouse gas emissions following the development of the past ten years and probably leading to a global temperature increase of around 4°C until 2100 (compared to 1850-1900). Even in the past century precipitations in the Troms region rose considerably and according to this scenario they are expected to increase by 10 to 25 % this century (Figure 2).

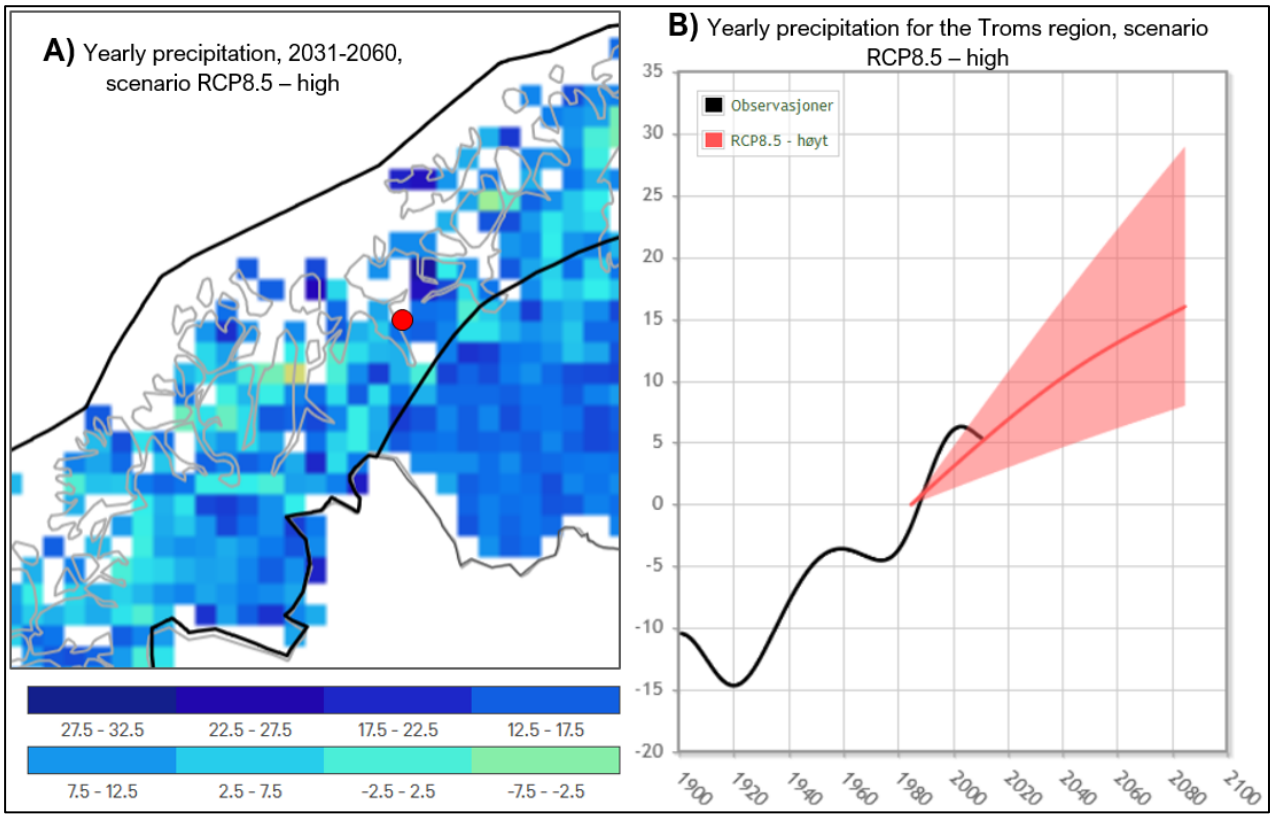

Figure 2: (A) Predicted change in total precipitation (%) from the period 1971-2000 to 2031-2060 for Eastern Troms considering a high emission scenario (RCP8.5). At the location of Dusnjarga (red point), the expected increase amounts more than 12.5%. (B) Development of the total precipitation in Troms, expressed as percentual deviation from the average of the time period of 1971 - 2000: the black curve shows the measured variations whereas the colored curve shows the trend of median values from several regional climate model simulations. The shaded area shows the spread between a high and low climate impact (10 and 90 percentiles). *Adapted from: Meteorologisk Institutt et al. (2020).*

However, with respect to rock slope failures, events of maximum precipitation play a more important role than the average precipitation (section 5.4). In 2100, rainfall-generated floods are expected to more frequently while fewer snow-melt generated floods will occur (Hanssen-Bauer et al. 2009).

In Figure 3 estimated IVF values (intensity-duration-frequency value) are plotted for the study area as presented by the Norwegian Climate Service Center (Meteorologisk Institutt et al. 2020). Thus, these IVF values represent estimations of the maximum precipitations in one to 24 hours that are likely to occur in a certain interval of years (2 to 200 years). The local IVF values are calculated using Bayesian hierarchical modelling based on a network of measuring stations all over Norway (Dyrrdal et al. 2015). The uncertainties increase for larger time intervals and for areas with few measuring stations like northern Norway. Nonetheless, it is necessary to think in longer terms regarding rock slope failures and in a century time scale, it is visible that maximum precipitation events with more than 60 mm in 24 hours would be possible at Dusnjarga (Figure 3).

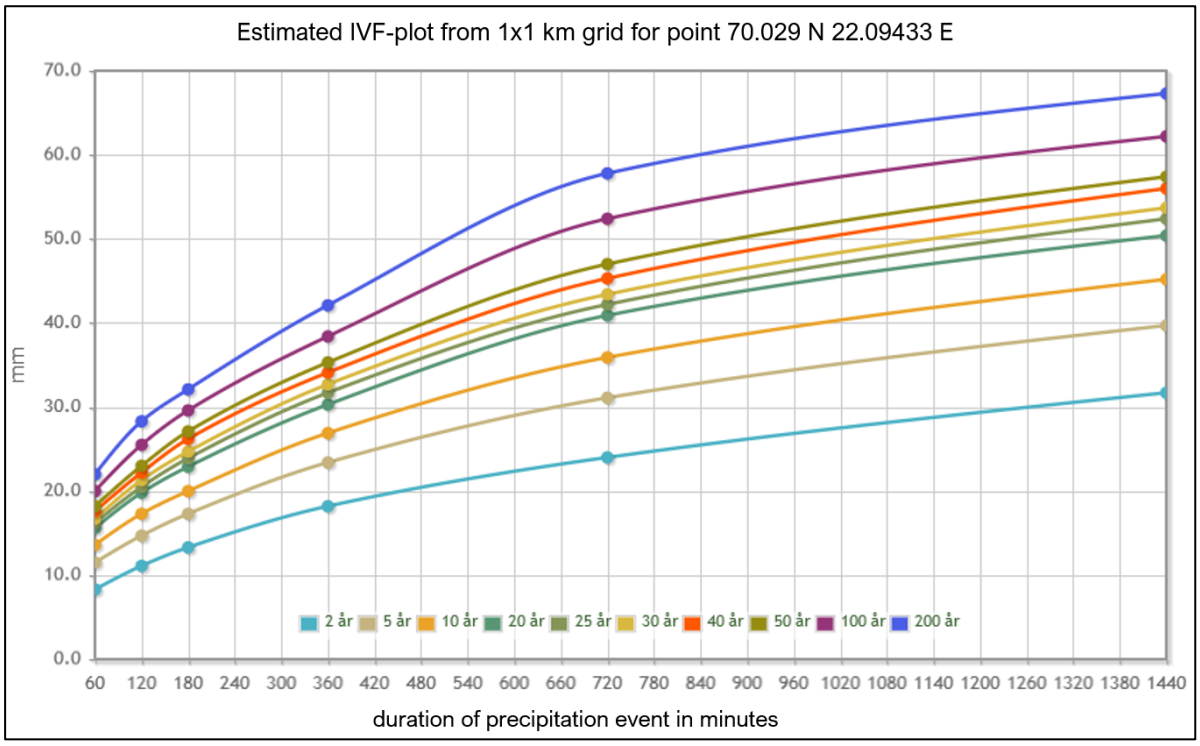

Figure 3: Plot of maximum expected precipitations in the study area presented as IVF values: the different curves represent the different time intervals of recurrence. The intensity (mm of precipitation) is plotted for durations of one to 24 hours (1440 minutes). IVF values were calculated using a GUMBEL-distribution (GEV-type 1) and Bayesian hierarchical modelling to extrapolate for a 1x1 km grid for whole Norway. *Adapted from: Meteorologisk Institutt et al. (2020).*

- *Permafrost conditions*

The existence of permafrost and its possible degradation as a result of future climatic changes can play an important role in terms of rock slope stability (chapter …).

Gisnås et al. (2017) created a baseline permafrost map for Scandinavia using the CryoGRID1 model with a resolution of 1 km² and Lilleøren et al. (2012) modelled the development as well as the distribution of permafrost in Norway reaching from 10 ka ago until today. Both models agree that the permafrost zone starts in NE-Troms further inland than e.g. for central Troms, and that discontinuous permafrost is probably not expectable on the Dusnjarga peninsula (Figure 4).

According to Lilleøren et al. (2012), the mid-Holocene thermal maximum (Figure 16B) was characterized by a vast permafrost degradation whereas during the 'Little Ice Age' permafrost had the biggest extent in the Holocene, but even during this time no discontinuous permafrost is indicated for Dusnjarga (the validating borehole data was however from central Troms).

However, it has to be taken into account that steep rock slopes and rock walls often show a significantly different behavior than other terrains which is why it is important to consider the nationwide permafrost probability map for steep slopes of Norway (*CryoWall map*) by Magnin et al. (2019). In this study, a permafrost probability (Figure 4B) was calculated for all the critical slopes in the NGU database (Oppikofer et al. 2015) which classified Dusnjarga as a permafrost slope (probability of permafrost > 0.5). Permafrost is possible at much lower elevations in steep rock slopes especially at north faces compared to other terrains (Magnin et al. 2019). The rock slopes of Dusnjarga and Låvan are S to SE facing and are at a maximum elevation of around 800 m a.s.l.. For these expositions discontinuous permafrost starts at above 1050 m a.s.l. in northern Norway (~70° N) indicating no discontinuous permafrost in the rock slopes of this study, whereas sporadic permafrost can even extend down to sea level (Magnin et al. 2019). For instance, sporadic permafrost extending into open fractures and sliding planes was identified as a likely controlling factor for the Nordnes rock slide in Troms (Blikra and Christiansen 2013).

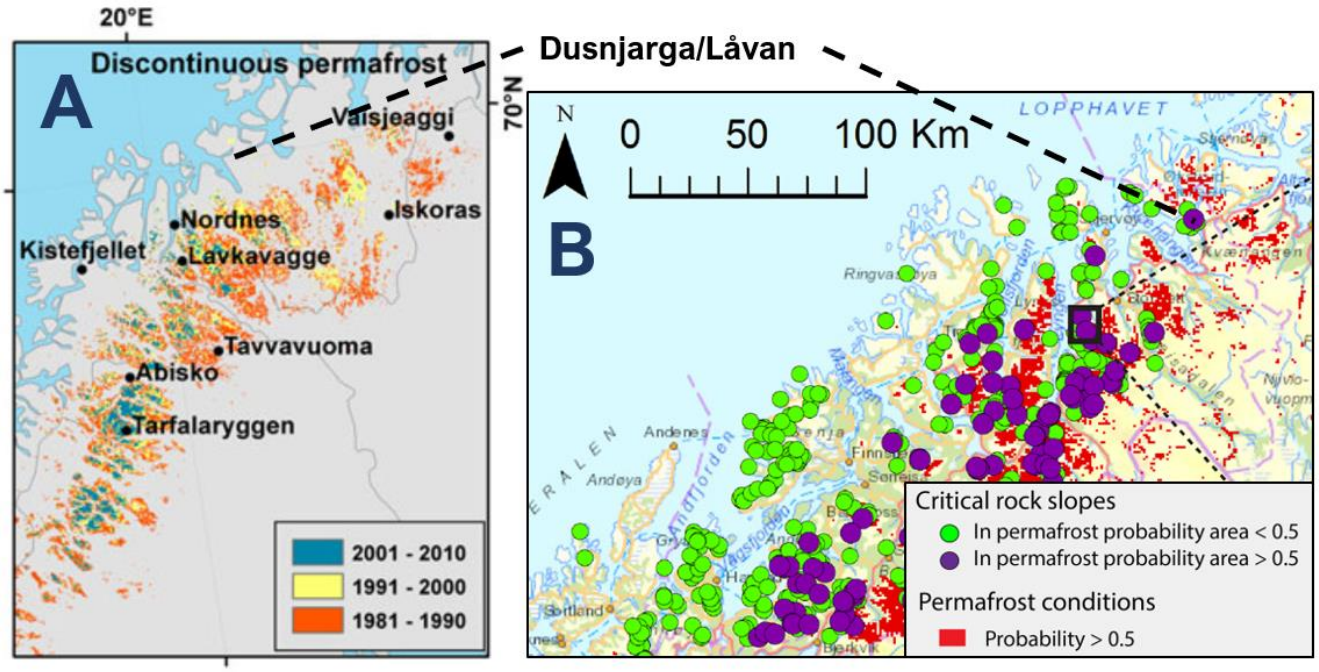

Figure 4: A) Modelled distribution of discontinuous permafrost in Northern Norway displaying a comparison for three decades in the period 1981- 2010. *Adapted from: Gisnås et al. (2017).* B) Distribution of critical slopes from the unstable rock slope compared CryoWall map and the Nordic permafrost map by Gisnås et al. (2017). This comparison led to the depicted division into permafrost (probability >0.5) and non-permafrost slopes. The highlighted rectangle is not of relevance for this adapted figure. *Adapted from: Magnin et al. (2019).*

4.2 Bedrock geology

The bedrock geology is highly relevant for the assessment of slope stability since rock mass behavior is controlled by rock mechanical properties as well as the structural features (folds, faults, discontinuities) depending on their orientations and on the intensity of the tectonic regime (Stead and Wolter 2015).

Roberts (1974) presented a 1:250,000-geological map which is currently the highest available map resolution for the study area (Figure 5). According to this map, the whole Dusnjarga peninsula is covered by one bedrock unit comprising layered clinopyroxene-gabbro, gabbro gneiss and pyroxene-granulite (purple color). However, for the area to the E of Dusnjarga a higher detailed geological map (1:50,000) by Roberts and Elvevold (2018) exists which displays a much higher lithologic diversity for the rocks in this unit. In this map the most dominant lithologies bordering our study area are different varieties of layered gabbros (e.g. Figure 6B).

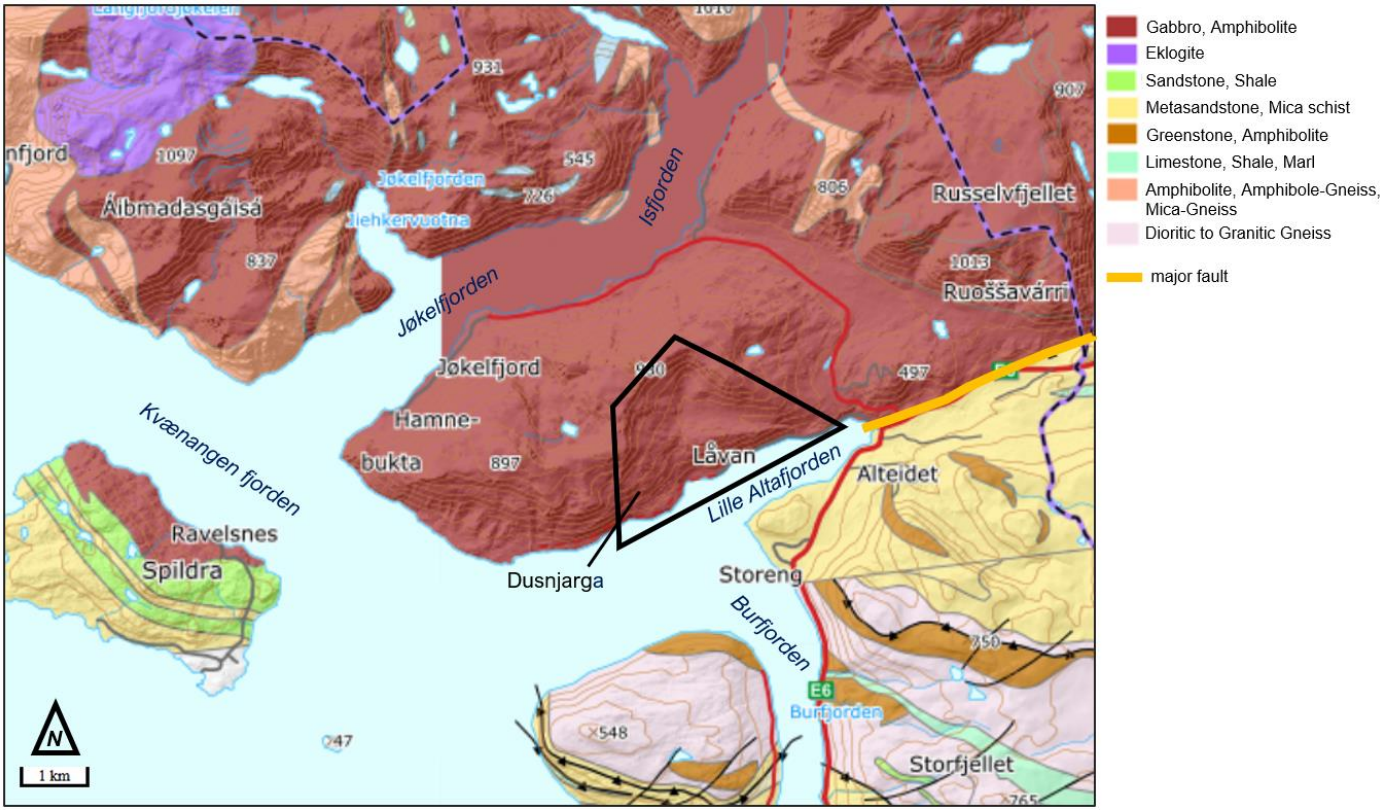

Figure 5: Map of bedrock geology (1:250,000): The Dusnjarga peninsula with the study area (black polygon) is depicted in the center: According to the map, the study area's bedrock shows little variation and is characterized as foliated Gabbro and Amphibolite. The major geologic fault is marked E of the study area: it separates intrusive rocks (purple) in the N from metasediments in the S. *Adapted from: NGU (2015).*

The bedrock on the peninsula is part of the so-called Seiland Igneous Province (SIP), a plutonic suite consisting mainly of gabbroic lithologies but also partly of ultramafic, felsic and syenitic intrusions (Stephens et al. 1985). The SIP stretches across the whole Øksfjord peninsula and the islands of Sørøy, Stjernøy, Seiland and Kvaløy (Figure 6A). Several studies (e.g. Krogh and Elvevold 1990) suggested long-lasting magmatic activity starting around 830 Ma ago forming the SIP. However, Roberts et al. (2006) attained Proterozoic ages from 570 to 560 Ma indicating a single tectonic event, probably an intracontinental rift setting, during which the rocks of the SIP were emplaced into the uppermost part of the Kalak Nappe Complex. The Kalak Nappe Complex (Figure 6A) consists of older Proterozoic basement and metasedimentary successions interpreted as an exotic mobile terrane belt that was amalgamated to the Baltic Shield during the Scandian phase of the Caledonian orogeny around 420 Ma (Kirkland et al. 2007). Probably by this event, the rocks of the SIP were deformed and metamorphosed to at least amphibolite facies (Roberts et al. 2006). The Caledonian deformation is probably responsible for the foliation observable at most of the rocks of the SIP which typically is formed by elongated pyroxene crystals (Krauskopf 1954). The foliated rocks show usually also layering (mostly 5 – 50 cm thick) caused by differences in

lithology and/or grain size (Krauskopf 1954). In the aftermath of the Caledonian deformation, the upper part of the intrusion body was eroded which means the still preserved rocks represent the root of the plutonic body (Roberts et al. 2006).

Directly south of Dusnjarga runs the so-called Langfjorden fault, a major geologic fault forming the border between the intrusive rocks of the SIP to the N and the Precambrian rocks of the upper Kalak Nappe Complex to the S. The WSW-ENE-striking fault follows the bottom of Lille Altafjorden directly in front of Dusnjarga and continues through Langfjorden to the E (Figure 6A). As depicted in the geologic transect across Langfjorden by Roberts and Elvevold (2018), the fault is interpreted as steeply dipping (roughly to N) with the plutonic rocks of the SIP in its hangingwall. The Langfjorden fault is part of the composite Vargsund-Langfjorden fault. This composite fault was most likely created during Devono-Carboniferous or Permo-Carboniferous rifting and was reactivated by dextral strike-slip or oblique-slip during the Mesozoic, thus post-Caledonian (Roberts and Lippard 2005).

The lithologies present S of the Langfjorden fault are of relevance with respect to the Quaternary transformation of the study area. These metasediments and Precambrian basement rocks in the area of Lille Altafjorden and neighbouring Burfjorden are dominated by dioritic to granitic gneisses, metasandstones, mica shists and greenstones (e.g. Figure 6B).

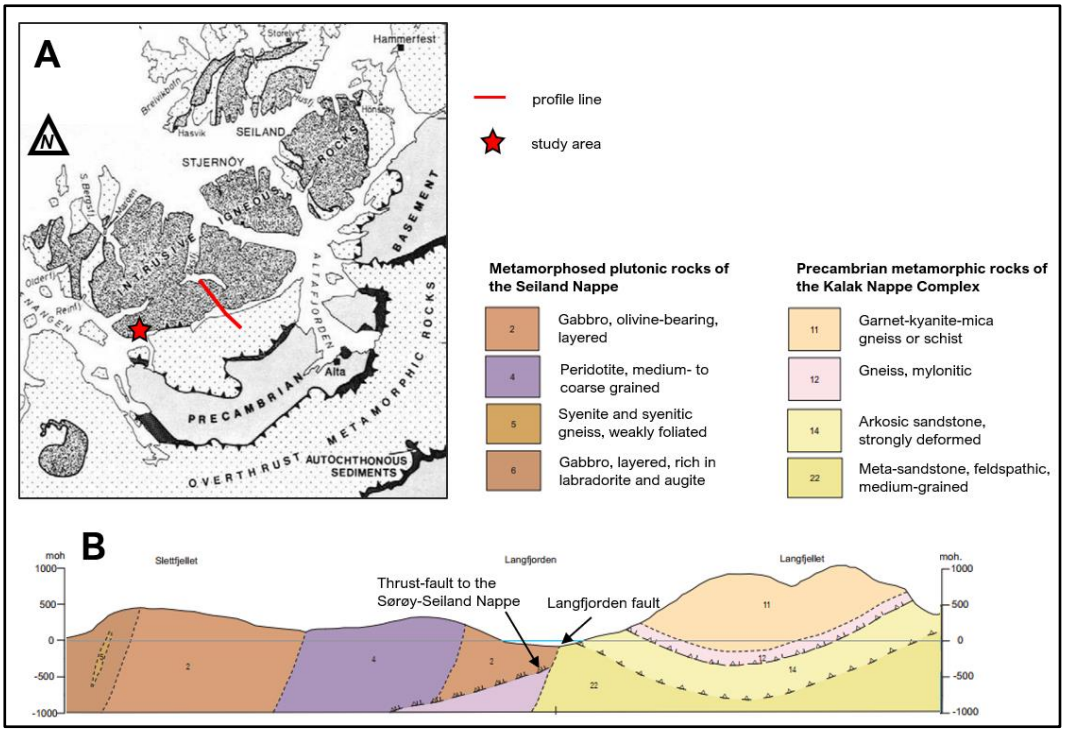

Figure 6: A) Overview map of the Seiland Igneous Province and its surrounding including central geological features. *Adapted from: Robins and Gardner (1975).* B) Geologic transect crossing Langfjorden in a NW-SE direction. The transect includes rocks from the SIP in the N and Precambrian metamorphic rocks in the S that are separated from each other by the Langfjorden fault. Adapted from: *Roberts and Elvevold (2018).*

4.3 Quaternary geology

Knowledge about Quaternary deposits and landforms is important for interpretations about the landscape evolution in the study area, especially regarding the temporal evolution of the large rock slope deformations. Quaternary maps and former studies about the local Quaternary geology are particularly valuable resources in this regard.

A 1:250,000 Quaternary geological map from NGU (Riiber 2000) exists and is presented in Figure 7. This map is based on roadside observations and aerial imagery and was not created based on extensive and detailed field work. It represents thus a resource of helpful information but for a rough orientation. As an example, the limits of the unstable areas Dusnjarga and Låvan are not given in this map.

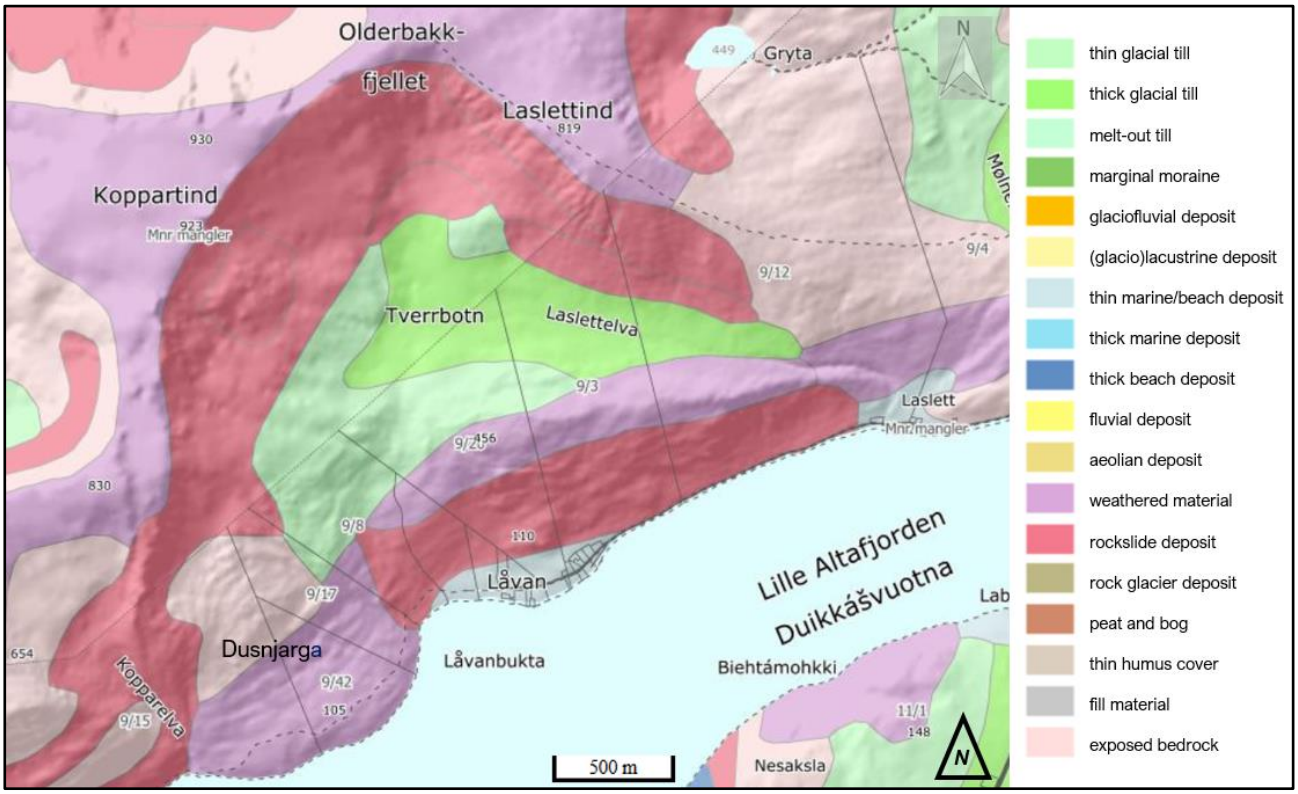

Figure 7: The official Quaternary map of the study area created and published by the Geological Survey of Norway (NGU). The Quaternary geology is expressed as semi-transparent polygons overlying a digital elevation model. *Adapted from: Riiber (2000).*

4.3.1 Glaciation and deglaciation of northern Norway

The cyclic changes between intense cold phases, the glacials, and the warmer interglacials characterize the Quaternary period. In the course of this time period, whole Scandinavia was repeatedly covered by ice sheets which shaped the local landscapes (e.g. U-shaped valleys, fjords, cirques). Especially, the Weichselian glacial cycle is responsible for the features and depositional landforms that can still be found locally (Fredin et al. 2013).

The maximum extent for the Eurasian ice sheet during the past 40 ka was not reached simultaneously for all areas but occurred between 29 and 21 ka (Böse et al. 2012; Hughes et al. 2016; Patton et al. 2017). The term last glacial maximum (LGM) refers to the last peak in global ice volume between 23 and 21 ka, and during which period the Fennoscandian ice sheet coalesced with the Barents Sea ice sheet until Svalbard and across the whole continental shelf (Clark et al. 2009; Hughes et al. 2016; Patton et al. 2017; 2016). During the LGM, the inland of Troms was entirely covered by the ice sheet but ice-free mountain peaks, so-called nunataks, are likely to have existed at alpine-relief mountains above 1000 m a.s.l. (Sveian 2004; 2005). The preservation of block fields and alpine pinnacle topography indicates that basically no glacially driven erosion took place in certain areas and at certain elevations. But the possible widespread prevalence of less erosive cold-based ice is another possibility that might be also relevant for Dusnjarga (e.g. Linge et al. 2006; 2007). In general, the thickness and surface geometry of the former ice sheet is more controversial than the discussion about its extent (Mangerud 2004).

After the LGM the ice sheet's margin retreated and reached the coast of northern Troms around 17 ka (Hughes et al. 2015; Patton et al. 2017). The Lateglacial interstadial, a phase again subdivided into Bølling interstadial (15.3 – 14.1 ka), Older Dryas stadial (14.1 – 13.8 ka) and Allerød interstadial (13.8 – 12.9 ka), was characterized by ice streams filling the fjords at the Scandinavian ice sheet's the western margin (Hughes et al. 2016; Olsen et al. 2013; Patton et al. 2017). Overall this period was accompanied by a strong retreat of the ice margin even though the Older Dryas brought an interim glacial readvance of a few kilometers (Olsen et al. 2013). The extent of the strong retreat in this lateglacial period is clearly shown in Figure 8 which presents the likely retreat scenario for the study area between 15 and 13 ka based on the DATED-1 time slice reconstruction by Hughes et al. (2015). According to the most likely scenario, the fjord section at Dusnjarga (Lille Altafjorden) was deglaciated shortly before 14 ka and certainly considerably before 13 ka (Figure 8B/C). This would mean a local deglaciation either during the later Bølling or early Allerød interstadial. Furthermore, Stokes et al. (2014) compiled an ice margin chronology for large fjord systems in northern Norway (Figure 8D). This reconstruction does not include the local fjord system (Kvænangen) but the two neighboring systems, Lyngen and Altafjorden, which can be taken as a reference for the deglaciation at Kvænangen fjorden. At both neighboring fjord systems, the reconstructed deglaciation was very rapid between 15 and 14 ka, as well as between 14 and 13 ka, and a connection line between the glacial extents at 14.2 ka matches the location of Dusnjarga (Figure 8D).

The last phase of strong climatic cooling, the Younger Dryas (12.9 - 11.7 ka), brought a general readvancement of at least 10 km for Norwegian glacier systems (Hughes et al. 2016; Patton

et al. 2017). Nonetheless, few exceptions for insignificant ice growth are known (Olsen et al. 2013). The Younger Dryas or so-called Tromsø-Lyngen moraines are often most prominent moraines and are traceable all along the Norwegian coast as visible in Figure 9 (Andersen 1980, 1995). At the end of the Younger Dryas period around 11.7 ka, the glaciers retreated rapidly from the Tromsø-Lyngen moraines (Patton et al. 2017).

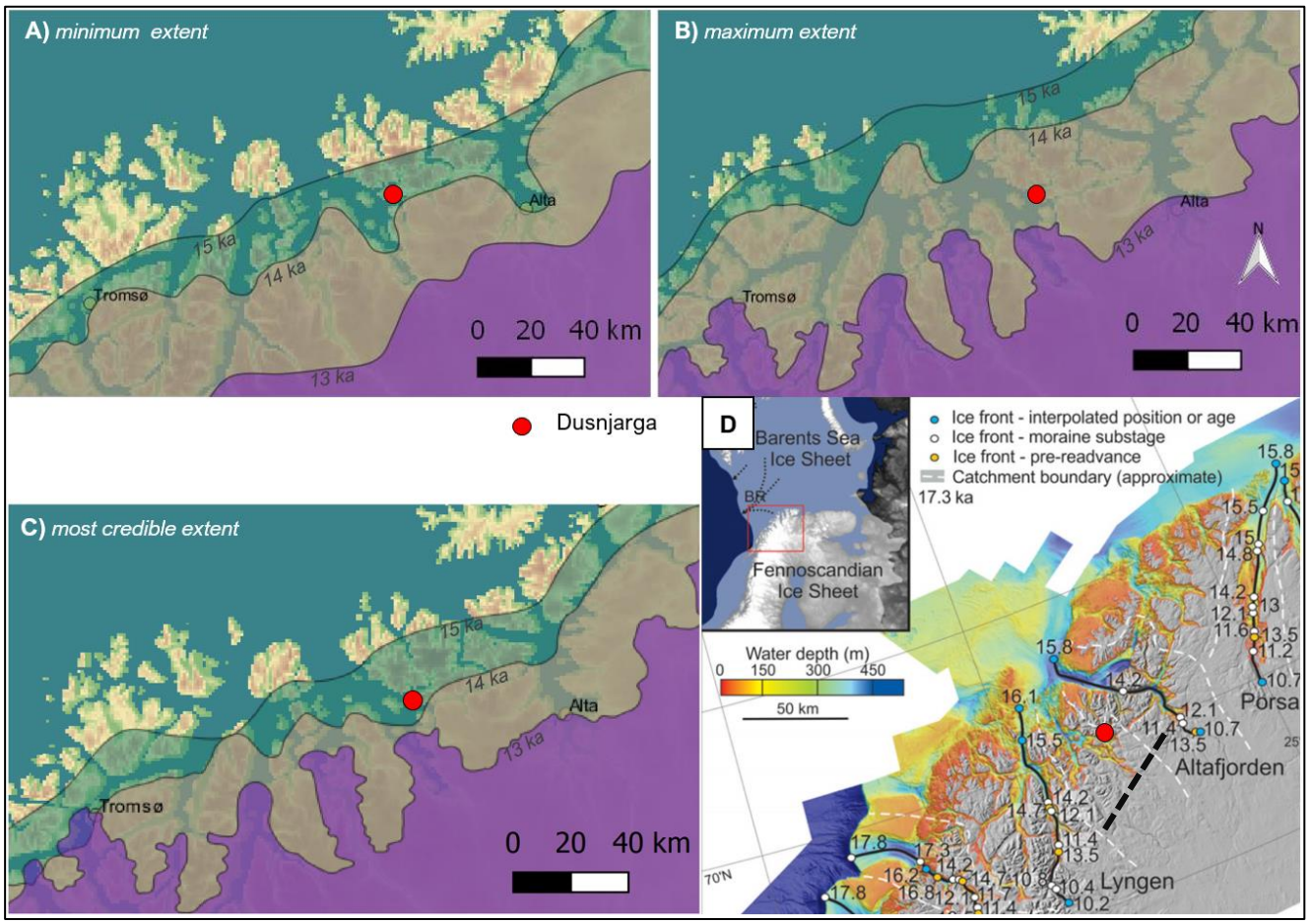

Figure 8: A) – C) Time slice reconstructions of the Scandinavian ice sheet's extent for 15, 14 and 13 ka according to the DATED-1 compilation by Hughes et al. (2015). This reconstruction is based on a compilation of published geological and chronologic data. A) and B) represent the extent's uncertainty bounds (minimum and maximum). C) depicts the most credible scenario according to which Dusnjarga was deglaciated around 14 ka. D) Ice margin chronology for major fjord systems of northern Norway including Lyngen- and Altafjorden which are the neighboring fjord systems to Kvænangenfjorden where Dusnjarga is located. The black dashed line connects the ice sheet's 14.2 ka extents of Lyngen and Altafjorden. *Adapted from: Stokes et al. (2014).*

4.3.2 Regional deglaciation sub-stages

The tracking of moraine ridges and paleo-shorelines plays a key role for the knowledge about the local and regional deglaciation in northern Norway. After having retreated onshore, the ice sheet had several still-stands and readvancements which are expressed in the moraine ridges and paleo-shorelines (Romundset et al. 2017). Partly, the moraine ridges and related ice-marginal deposits could be mapped across large areas. This made it possible to classify eight

to nine regional sub-stages of deglaciation for northern Norway (Sollid et al. 1973). A map depicting the location of the ice-marginal deposits defining these sub-stages is presented in Figure 9A.

The identification of past shorelines is equally important for the reconstruction of these sub-stages. These raised shorelines are common at the Norwegian coast and are usually products of prolonged erosion formed by wave action. They comprise beach ridges, terraces in sedimentary deposits, abrasion rock terraces, and deltaic surfaces, but boulder trains pushed up by the sea ice can also be found (Fredin et al. 2013; Sollid et al. 1973). The deglaciation resulted in a global sea level rise while at the same time the retreat of the Fennoscandian ice sheet caused an isostatic uplift of Norway's landscape (Vorren et al. 2008). The isostatic uplift decreases from inland towards the coast and it (mostly) outpaced the sea level rise. Both together, the deglaciation and the isostatic uplift, resulted in younger shorelines being lower than older ones and in shorelines sinking towards the coast (Vorren et al. 2008). As depicted in Figure 9B, paleo-shorelines are generally reconstructed using shoreline (and isobase) diagrams. Such diagrams are created by connecting identified shoreline markers through lines, thereby relying on the principles of isostatic uplift and on the fact that shorelines can only be formed after an area has been deglaciated (Vorren et al. 2008).

The highest post-glacial recorded sea level is known as the marine limit. In most locations, it is represented by the so-called 'main shoreline' created during the Younger Dryas and corresponding to the so-called 'Main sub-stage' (Vorren et al. 2008). The main shoreline can only be found beyond the Younger Dryas (or Tromsø-Lyngen) moraines and is therefore relevant for our study area as visible in Figure 9A (Andersen 1968; Mangerud 2004; Sollid et al. 1973).

Often, the younger 'Tapes shoreline' can also be found which sometimes intersects the main shoreline and was created through a transgression between 9,500 and 6,300 BP (Andersen 1968; Romundset et al. 2011; Vorren et al. 2008). Bondevik et al. (2019) dated the Tapes transgression maximum between 7600 and 5600 cal a BP.

Apart from that, only two older sub-stages are continuously represented in northern Norway, the Porsanger sub-stage (probably Older Dryas age) and the Repparfjord sub-stage (Romundset et al. 2017). These sub-stages can be relevant for the deposits and shorelines in our study area since it was presumably deglaciated before the Younger Dryas and most likely during the Allerød interstadial (compare to Figure 9A).

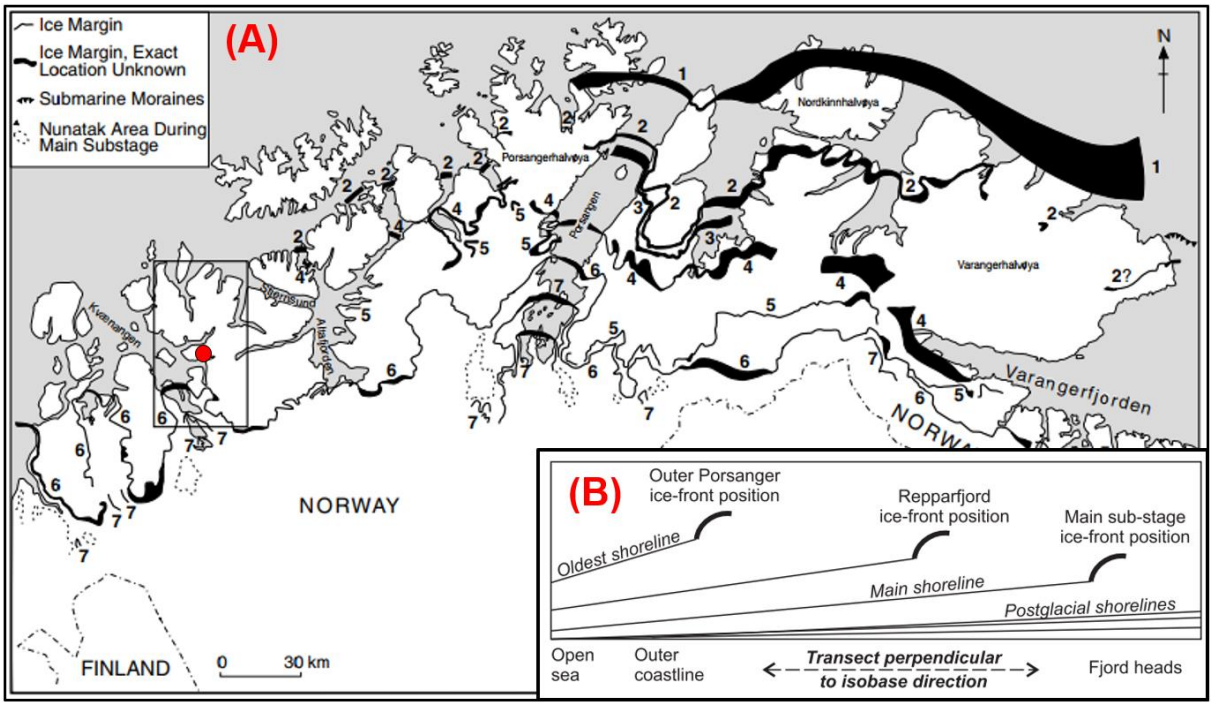

Figure 9: (A) Map of eastern Troms and Finnmark showing major regional ice marginal moraine systems after Sollid et al. (1973): The red point marks the location of Dusnjarga and the box the larger surrounding investigated by Evans et al. (2002). Moraine systems: 1 – Risvik sub-stage, 2 – Outer Porsanger sub-stage, 3 – Korsnes sub-stage, 4 – Repparfjord sub-stage, 5 – Gaissa sub-stage, 6 – Main (Tromsø-Lyngen) sub-stage, 7 – Post-Main (Stordal) sub-stages. (B) Simplified shoreline diagram depicting the three central sub-stages of regional deglaciation: in practice such diagrams are produced by connecting shoreline markers of the same age resulting in a modelled shoreline. *Adapted from: (A) Evans et al. (2002); (B) Romundset et al. (2017)*

It is important to notice that the absolute dates for the glacial and deglacial events are often accompanied by considerable uncertainties. Most of the available dates were retrieved by radiocarbon dating which dates can involve considerable uncertainties, especially in older studies e.g. because of inexact calibration to calendar years or variations in the marine reservoir age (Mangerud 2004). In the last years, progress has been made through enhanced calibration and new dating methods, for example surface exposure dating using ^{10}Be or ^{36}Cl which however still bears considerable uncertainties (e.g. Romundset et al. 2017).

4.3.3 Moraines and paleo-shorelines around Dusnjarga

Only very few local studies exist concerning the Quaternary geology and deglaciation in the Kvænangen area and even less for the Dusnjarga peninsula. The most important basic study on the regional Quaternary geology was done by Sollid et al. (1973) which presents the correlations and relative dating of shorelines and moraines in Finnmark, but also in the areas of Kvænangen and the Bergsfjord peninsula, thus in the proximity of Dusnjarga. The local

Quaternary study which is most relevant for this work, and the only one including the Dusnjarga peninsula, is the study by Evans et al. (2002).

Figure 10 displays the raised paleo-shorelines which were identified by Evans et al. (2002) in the neighboring fjords of the study area. These findings are very relevant for the interpretations of the Quaternary geology at Dusnjarga. Two sets of shoreline elevations seem to dominate regarding the Dusnjarga peninsula and Burfjorden: low marine limits were for example identified at deltas of Alteidet (47 m a.s.l.) and of Jøkelfjordeidet (34 m a.s.l.). These shorelines contrast high marine levels e.g. at the outer part of Jøkelfjorden (66m a.s.l.) and at the end of Burfjorden (67m a.s.l.). The latter shorelines match the marine limits found farther south at the head of Kvænangen (71 m a.s.l.) and at Badderen (72 m a.s.l.). These locations coincide with the 70m-isobase for the Main shoreline, and according to Evans et al. (2002) this indicates a nearby termination of the Tromsø-Lyngen moraines (Younger Dryas). Sollid et al. (1973) however attributed this ice margin to the postglacial Stordal substage and set the limit for the Tromsø-Lyngen moraines a bit farther north on the Skorpa island's south shore. Evans et al. (2002) classified the mentioned low shorelines (e.g. at Alteidet and Jøkelfjordeidet) not as 'true' marine limits but attributed them to the propagation of distal sediments as glaciers were receding stronger in the surrounding highlands. In wide fjords close and similar to the Kvænangen fjord, basal over-deepening was observed to induce rapid retreat rates reaching up to more than 100 m per year (Stokes et al. 2014). Following these interpretations, it seems clear that the fjord at the south side of the Dusnjarga peninsula called Lille Altafjorden was quite rapidly deglaciated in a warm phase preceding the Younger Dryas (either during the Allerød or the Bølling interstadial), similar to Jøkelfjorden in the north (Evans et al. 2002).

As a helpful tool the Geological Survey of Norway provides map information on the estimated location of the marine limit which is displayed in the map in Figure 19. This marine limit was interpolated based on the digital elevation model (DEM) and marker points registered in the national Quaternary database of the NGU (Høgaas et al. 2012). The marker points which are relevant for the interpolations of the marine limit in the study area are indicated on the map in Figure 10. In the study area, the interpolated marine limit is situated at an elevation between 65 m (E) and 66 m a.s.l. (W). It is shown in Figure 10 that the closest marker points are not close to the study area (about 10 km coastal distance) which raises the shoreline's uncertainty at Dusnjarga.

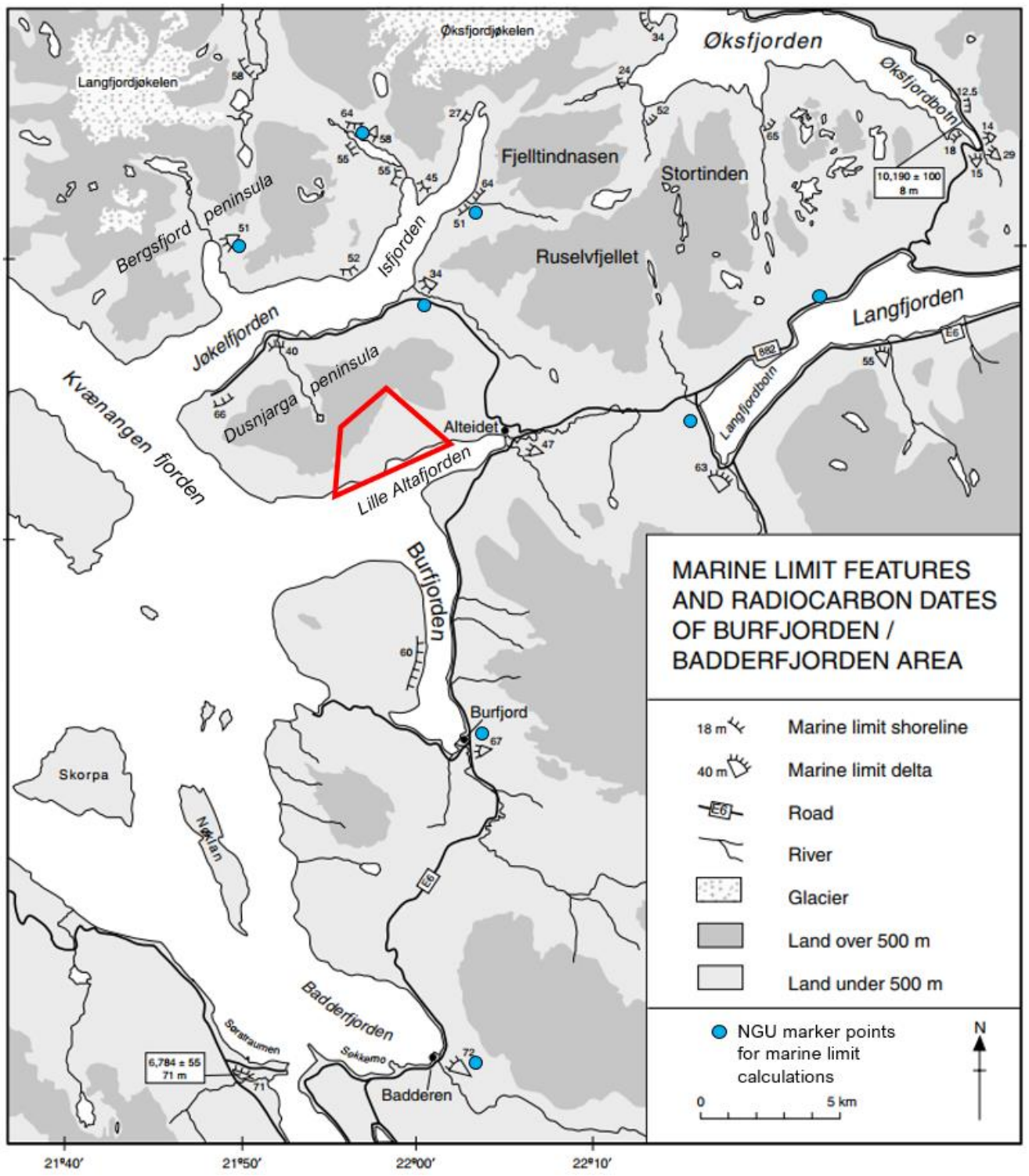

Figure 10: Topographic map of the larger surrounding of the study area depicting the marine limits identified by Evans et al. (2002). The location of the study area (red polygon) is marked on the Dusnjarga peninsula. One radiocarbon age was determined for organic material found in sediments at Sørstraumen which gives a minimum age of ca. 6,700 years for the deglaciation at the head of Kvænangen. *Adapted from: Evans et al. (2002).*

5 Rock slope failures – Theoretical background

The investigation of two large unstable rock slopes in Norway (Dusnjarga and Låvan) is the central topic of this thesis. Therefore, it is necessary to summarize the theoretical background regarding this topic.

5.1 Classification of landslides and rock slope failures

According to Böhme (2014), rock slope instabilities represent slopes that display signs of postglacial gravitational deformation. Such instabilities may develop rock slope failures, a failure of rock mass that results in a gravitational mass movement down a slope (Martina Böhme 2014). Rock slope failure means in this context the slope's most significant episode of movement during which episode the failure plane develops (Hungr et al. 2014; Leroueil et al. 1996). A "catastrophic rock slope failure" corresponds mostly to a rapid rock avalanche, showing substantial rock mass fragmentation and a run-out area larger than for a rockfall (Hermanns and Longva 2012). Generally, a (gravitational) mass movement is seen synonymous to a landslide, a mass of soil, rock or debris moving down a slope (Cruden 1991).

In this study, we classify mass movements or landslides according to the widely used classification system by Varnes (1978) and Cruden and Varnes (1996), and updated by Hungr (2014). In this system (Table 2), mass movements are classified according to the type of slope movement and the involved material (rock, ice, soil). The type of movement includes the five kinematic basic movement types: fall, topple, slide, spread, flow. The class slope deformation does not exactly refer to a basic kinematic mechanism, but it refers to large-scale deformations which cover whole rock or mountain slopes.

Table 2: Summary of the landslide classification system established by Varnes (1978) and updated by Hungr et al. (2014). This summary focusses on the material rock whereas the original classification also includes ice and soil.

Type of movement	*Landslide types (for rock)*
Fall	Rock fall
Topple	Rock block topple
	Rock flexural topple
Slide	Rock rotational slide
	Rock planar slide
	Rock wedge slide
	Rock compound slide

	Rock irregular slide
Spread	Rock slope spread
Flow	Rock avalanche
Slope deformation	Mountain slope deformation
	Rock slope deformation

5.2 Deep-seated gravitational slope deformations and their characteristics

Large-scale or mountain slope deformations (Table 2) typically involve multiple failure mechanisms and are kinematically complex objects which commonly are also defined by the term DSGSD (deep-seated gravitational slope deformation). DSGSDs are typical for high relief mountain slopes, stretch usually over the total length of the slope, show a considerable thickness and often not clearly defined boundaries (Agliardi et al. 2001; 2012; Crosta et al. 2013).

Furthermore, certain morphological surface features (Figure 11) are characteristic for DSGSDs and are often confined by its limits (Agliardi et al. 2001). The upper slope shows an extensional or mixed deformation regime which involves the formation of features like double-ridges, depressions, trenches, graben-structures, scarps, and counterscarps; whereas the frontal slope is rather marked by compression leading to toe bulging and buckling, as well as local secondary failures (Agliardi et al. 2001; Crosta et al. 2013). These characteristic features have the potential of controlling the slope deformation by the dissection of rock mass, change in water circulation or the alteration of rock mechanical properties (Crosta et al. 2013). They are often roughly linear but might also be concealed due to erosion or weathering (Crosta et al. 2013).

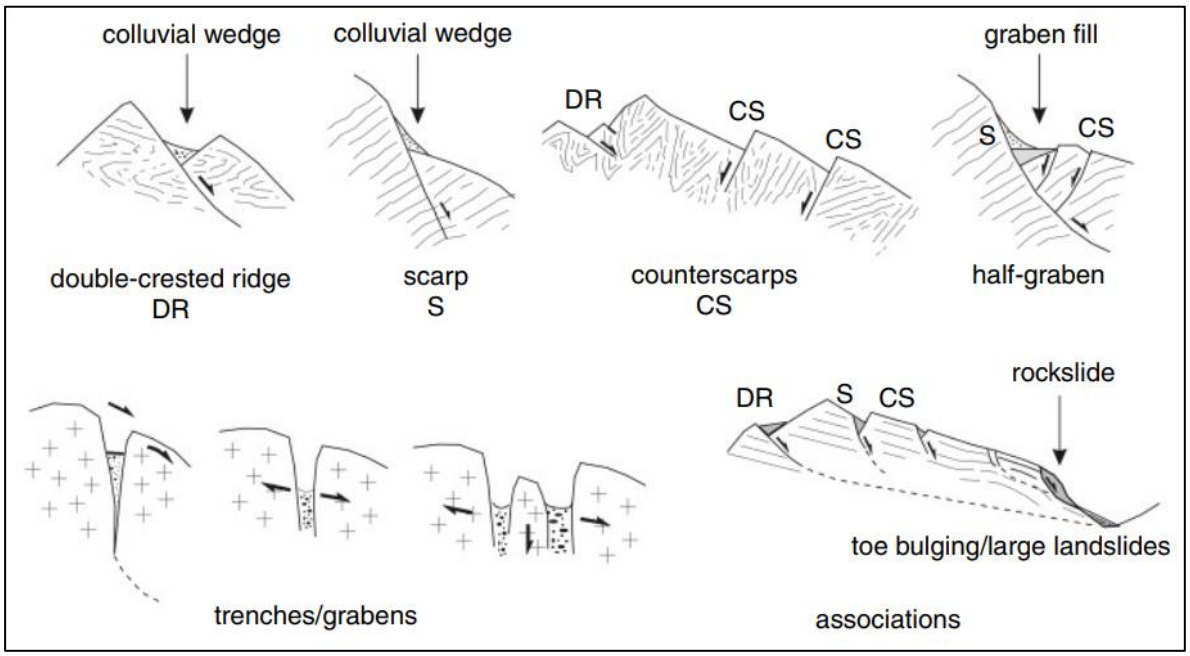

Figure 11: Schematized morpho-structural features that are diagnostic for DSGSD. *Source: Agliardi et al. (2012).*

DSGSDs are phenomena which usually evolve over very long times (often over more than 10,000 years) and whose deformation is mainly characterized by slow continuous creep movement (mm yr^{-1}) (McCalpin and Irvine 1995; Pánek and Klimeš 2016). The slow creep deformation modifies the slope topography and alters the mechanical rock properties, and thereby prepares conditions prone to catastrophic rock slope failures (Crosta et al. 2014; Pánek et al. 2009; Pánek and Klimeš 2016). Sudden failure in a single, massive catastrophic event is generally considered to be not very likely for DSGSDs, whereas the development of rather localized landslides is more typical (Agliardi et al. 2001; Oppikofer et al. 2017).

DSGSDs occur in multiple rock types but are especially common in post-glacial metamorphic mountain terrains, thus in highly anisotropic rocks (Stead and Wolter 2015). This indicates that DSGSDs are mainly controlled by rock structures. Many DSGSDs show a variety of deformation styles with complex deformation patterns which is commonly summarized under the term ‘sackung’ (Zischinsky 1969) or ‘sagging slope’ (Hutchinson 1988). Sagging slopes show typically significant displacements and deformation in the upper part usually involving multiple fractured sliding blocks and complex surface morphologies (especially counterscarps) whereas the lower slope shows considerably less deformation (Bunkholt et al. 2012; Zischinsky 1969). But a DSGSD may be also classified according to the dominant kinematic failure mechanism or as a particular subtype of sackung according to Hutchinson (1988). Sliding of the rock body on one or multiple basal sliding planes seems generally to be the central kinematic mechanism controlling large-scale rock slope failure as DSGSDs (Agliardi et

al. 2001; Hermanns and Longva 2012). These basal planes have been identified as shear zones of up to 10 m thickness marked by cataclastic breccias with a fine matrix (Crosta et al. 2013). Their low shear strength and permeability is supposed to largely control the present-day activity of DSGSDs (Crosta and Zanchi 2000; Crosta et al. 2013).

5.3 Sliding of large rock slopes

It was illustrated that large slope deformations as DSGSDs are usually controlled by a combination of several kinematic processes that form again own landslide classes in the classification by Hungr et al. (2014) (Table 2). Generally, the orientations and dimensions of structures determine the failure type of the instability (Stead and Wolter 2015).

Slides (or sliding) are defined as the movement of a rock mass on a rupture surface, whereby local failures enlarge gradually along zones of weakness to a rupture surface (Highland and Bobrowsky 2008). As was outlined in the previous chapter, sliding represents usually the essential kinematic mechanism controlling the large-scale deformation of phenomena such as a DSGSD. The sliding deformation inside a DSGSD is always accompanied by some grade of internal deformation progressing with the displacement resulting in different sliding blocks, as well as compressional and extensional features (Zangerl et al. 2008).

Slides can be separated into two endmember processes: rotational and translational slides whose clear separation is often difficult in practice (Zangerl et al. 2008).

Rotational slides (Figure 12) occur preferably in isotropic or homogeneous material and develop an upward curved, concave rupture surface (Highland and Bobrowsky 2008). The movement of rock mass is rather rotational accompanied by little internal deformation (Zangerl et al. 2008). At the head, displacement is almost vertical causing often the upper surface to tilt backwards toward the scarp forming depressions or trenches, whereas at the foot, uplift is possible (Highland and Bobrowsky 2008; Zangerl et al. 2008). They can only occur in weak rock masses, but often with a hard cap rock and tend to move at low or moderate velocities which is caused by a self-stabilizing effect (Hungr et al. 2014). But sometimes rapid rock avalanches have been induced through rotational slides (e.g. D'Alessandro et al. 2002; Hutchinson et al. 1980).

Translational slides (Figure 12) are mass movements along a planar surface which involves little rotation (Highland and Bobrowsky 2008). In contrast to rotational slides, that tend to restore the slide equilibrium, translational slides are shallower and can progress uninhibited over high distances if the rupture surface is steep enough (Highland and Bobrowsky 2008). They can be extremely rapid and move typically along geologic discontinuities in metamorphic

or sedimentary rocks (Hungr et al. 2014; Stead and Wolter 2015). Moreover, they occur often repetitively in areas where they have occurred before (Highland and Bobrowsky 2008).

Wedge slides (Figure 12) are a special type of translational slide and are thus similar in their kinematics but show higher stabilizing forces. The rupture surface originates from two downslope facing and intersecting sliding or discontinuity planes (Hungr et al. 2014; Zangerl et al. 2008).

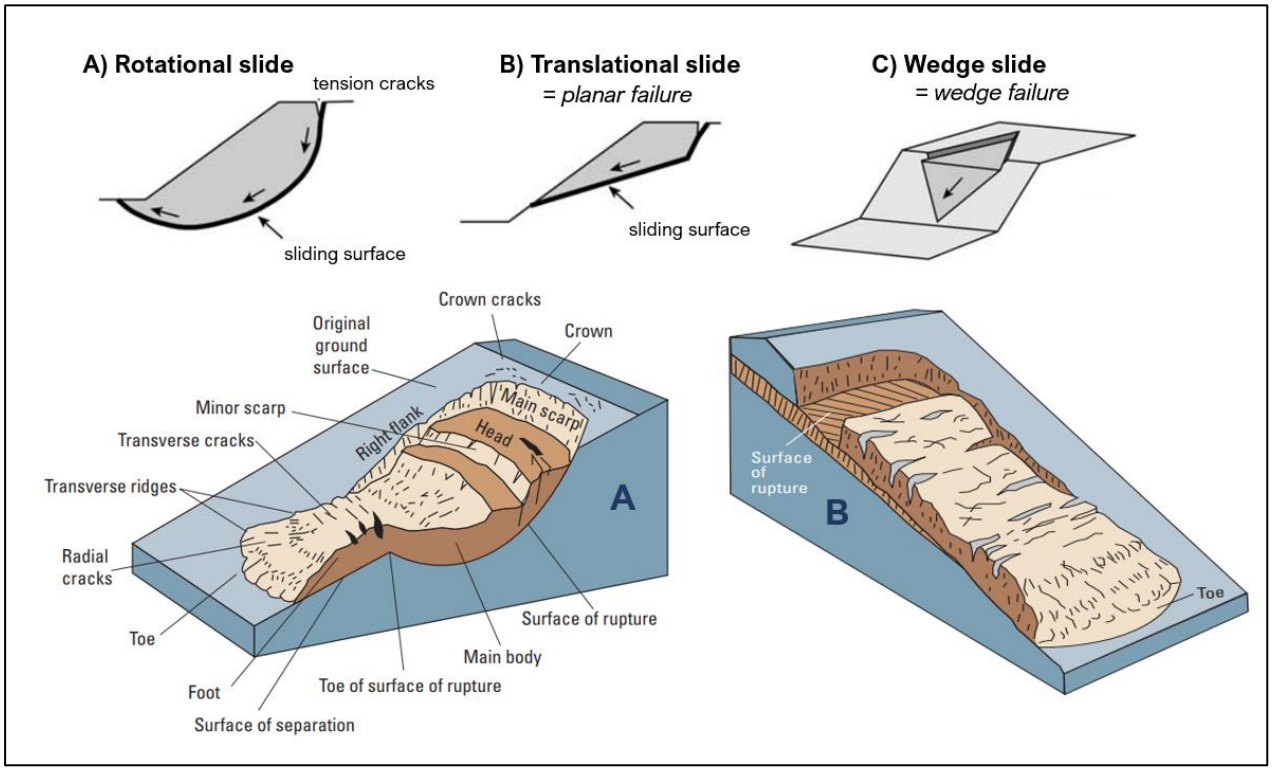

Figure 12: Schematics of central types of slides. Up (2D-schematics): Rotational slide (A) and translational slide (B) work as end members of further transitioning modes. Wedge failure/slide (C) constitutes a sub-type of the translational slide. Down: The colored schematics of a rotational (A) and translational (B) slide illustrate also the common parts or morpho-gravitational features of a landslide. *Adapted from: Highland and Bobrowsky (2008); Varnes (1978); Zangerl et al. (2008)*

Two special and more complex types of slides are compound and irregular slides. Compared to translational slides, compound slides have a more complex rupture surface consisting of several planes or showing an uneven curvature (Hungr et al. 2014). Much internal distortion is kinematically necessary, and features as horst and graben structures at the head are typical (Hungr et al. 2014).

Irregular slides form an irregular rupture surface that depends on randomly oriented joints separated by intact rock bridges (Hungr et al. 2014). These complex types of slides form usually in strong rock on steep slopes and happen often very sudden and extremely rapid, e.g. as in Willenberg et al. (2008) (Hungr et al. 2014).

5.4 Factors causing large rock slope failures

Rock slope failures are created through an interacting chain of events that alter the state of the slope and bring it to a state of critical stability (Eberhardt et al. 2001). Regarding these often complex interactions and great differences between rock slope settings, the quantification of the specific relevance of responsible parameters is difficult and remains an important research question (e.g. Crosta et al. 2013). Of great importance in this context are studies that examine the statistical relationships of these factors with the occurrence of slope instabilities based on sufficiently large inventories. Such studies exist for certain areas in the European Alps, e.g. Agliardi et al. (2013), Crosta et al. (2013), Fischer et al. (2012) or Pedrazzini (2012), but for Norway so far, only local studies exist investigating the influence of controlling factors, e.g. Blikra et al. (2015) or Böhme et al. (2013; 2011).

The controlling factors can be divided into three types according to Glade and Crozier (2005) and McColl (2012): (i) preconditioning factors which are static and inherent, (ii) preparatory factors which are dynamic and progressively reduce the slope stability, and (iii) triggering factors which eventually initiate the active movement (Table 3).

Table 3: Factors involved in the formation of (paraglacial) rock slope instabilities. They are divided into preconditioning and preparatory factors and triggers under which categories is given a qualitative and literature-based judgement of the factor's relevance. Glaciation and deglaciation are fully or partially responsible for the listed preparatory and triggering factors. Here, "debuttressing" refers to the removal of support through deglaciation whereas "sheet jointing" is an effect of the related stress release. *Source: McColl (2012).*

Factors	Preconditioning	Preparatory	Trigger
Lithology	Always		
Intact rock strength	Always		
Rock mass quality	Always		
Joint characteristics	Often		
Structure (e.g. bedding)	Often		
Pre-glacial erosion	Often		
Pre-existing stresses	Often		
Debuttressing		Sometimes	Sometimes?
Glacial erosion		Often	Unknown
Sheet jointing		Often	Often
Static fatigue		Always	Unknown
Seismicity		Unknown	Often
Climatic changes:			

Water	Unknown	Often
Permafrost	Sometimes	Often
Weathering	Always?	unknown

- *Preconditioning through geology and topography*

It is obvious that the fundamental conditions for a movement of rock mass is a potent combination of slope topography (inducing internal stresses and gravitational forces) and the local geology (involving rock strength and discontinuities).

There is overall agreement that the lithology and structural disposition are central preconditioning factors for DSGSDs that have often ultimate control over the occurrence of failure (e.g. Agliardi et al. 2001; Crosta et al. 2013; Pedrazzini 2012; Stead and Wolter 2015; Zischinsky 1966). In igneous and metamorphic rocks, the typical rock types in Norway, the rock strength is usually high. Therefore, the structures (e.g. joints, faults or foliation) control invariably the slope stability and often form the weak link. This relation is supported by many studies on slopes in Norway, e.g. Böhme et al. (2013; 2012; 2011) and Bunkholt et al. (2012). In this context, the most important discontinuity characteristics are persistence, orientation and frequency (Stead and Wolter 2015).

Clearly the size, steepness and shape of a slope are fundamental conditions determining the internal stress distribution which is relevant for the onset and geometry of a DSGSD (Ambrosi and Crosta 2011). The topographic stress can interact with the in-situ stress which is often inherited from past tectonic processes and is a further relevant preconditioning factor (Ambrosi and Crosta 2011; Kinakin and Stead 2005; Miller and Dunne 1996).

- *Preparatory and triggering factors following deglaciation*

The majority of DSGSDs in former studies was located in formerly glaciated areas with a high-alpine relief (Agliardi et al. 2001; Ambrosi and Crosta 2006). This correlation applies to all DSGSDs in Norway and is not a coincidence but is due to the strong imprint of glaciation and deglaciation. Basically, all the preparatory and triggering factors listed in Table 3 can fully or partially be caused through (de)glaciation.

The non-glacial shaping of the topography can also create steep slopes prone to failure, but studies, as Agliardi et al. (2013), have shown that areas with a glacial overprint have a higher density of DSGSDs than areas strongly intersected and shaped by hydrological processes. Preferential slope destabilization in deglaciated areas is mainly attributed to three factors: glacial erosion, debuttressing and isostatic uplift (Ballantyne 2002b; Böhme 2014).

Glacial erosion usually leads to a considerable steepening of slopes and deepens the valleys (MacGregor et al. 2000). Originally V-shaped valleys are transformed into steep-walled U-shaped valleys (Figure 13A), e.g. the Norwegian fjords (Harbor et al. 1988). The resulting higher and steeper rock faces cause increased self-weight shear stresses leading to failure if the rock mass strength is exceeded (e.g. Caine 1982). Ambrosi and Crosta (2011) applied numerical modelling that repeated glacial erosion through successive glaciations even enhances the failure susceptibility by creating broken slope profiles.

Deglaciation leads also to debuttressing, the process of removing the support and pressure of the glacier ice which is accompanied by the release of internal stress (Ballantyne 2002). In many studies, debuttressing was confirmed as one of the main parameters for the preparation and triggering of failure, for instance by several studies in the Alps (Agliardi et al. 2001; Ambrosi and Crosta 2006; Cossart et al. 2008) or by studies using numerical modelling (e.g. Agliardi et al. 2001; 2009a). Usually, debuttressing is associated with the formation of vertical, slope-parallel joints which according to Wyrwoll (1977) or Crosta et al. (2013) are the result of tensile stresses developed through elastic deformation from the former load of the glacier. McColl and Davies (2013) however doubt the long-term storage of elastic strain, and Hencher et al. (2011) and McColl (2012) attribute these so-called sheeting or exfoliation joints however to high slope-parallel stresses leading to uniaxial compression in the rock wall (Figure 13B).

The isostatic uplift in Norway is a consequence of the down-melting of the Scandinavian ice-sheet and leads to high uplift rates which currently amount around 1-3 mm per year in Norway's coastal areas as depicted in Figure 13C (Fjeldskaar et al. 2000). Glacial cycles and isostatic uplift are most likely associated with an increase in seismic activity (e.g. Hippolyte et al. 2006; Hormes et al. 2008; Sanchez et al. 2010). Many catastrophic rock-slope failures could be linked to seismicity as an important trigger, (e.g. Agliardi et al. 2009; Penna et al. 2011), but the cumulative effect of seismicity can also act preparatory by damaging and weakening slopes (e.g. Brain et al. 2014; Moore et al. 2011). For example, Henderson and Saintot (2011) were able to show for western Norway that historical slope failures and present instabilities cluster at an area with high uplift gradients. According to Keefer (1984), a minimum magnitude of M6 is needed to trigger spontaneous rockslides, and in Norway, the recurrence rate of a magnitude M5 earthquake is typically around 10 years whereas magnitude M7 earthquakes occur only every 1100 years (Hermanns et al. 2012a).

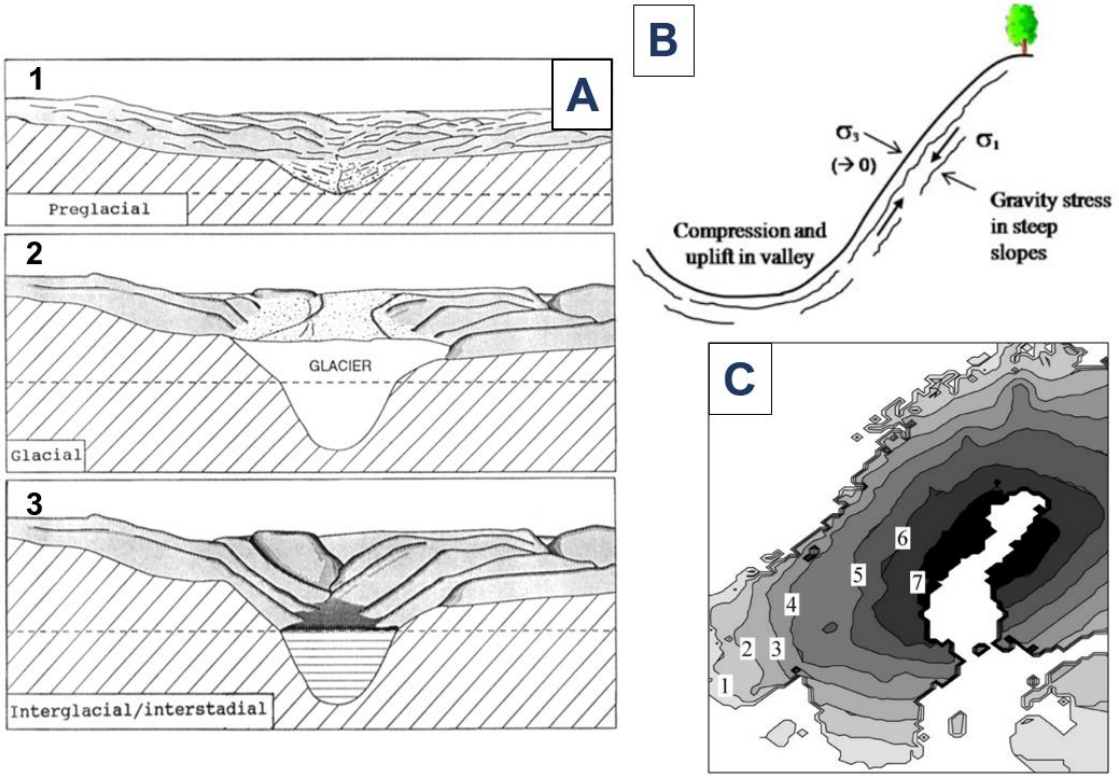

Figure 13: A) Schematized formation of the Norwegian fjords during the Quaternary glaciations: the dashed line shows the sea level during each stage. 1: Initial formation of fluvial valleys during uplift in the Tertiary. 2: Formation of a U-shaped fjord valley during the Quaternary glaciations. 3: The current interglacial situation with fjord walls that have been overprinted by erosion and gravitational movements. *Adapted from: Nesje and Whillans (1994).* B) Sheet jointing as an effect of debuttressing: surface parallel joints form on steep slopes where high gravity stresses act parallel to the slope surface; σ1/ σ3 = major/minor principal stress. *Source: Hencher et al. (2011).* C) The observed present-day rates of isostatic uplift in Scandinavia: The numbers and contour intervals indicate the rates in mm per year. *Source: Fjeldskaar et al. (2000).*

- *Climatic changes preparing or triggering landslides*

Climate and its changes are responsible for glacial cycles and can also directly prepare or trigger slope failure, especially by affecting the groundwater regime through high precipitation or snow melt events (e.g. Brückl and Parotidis 2005; Evans and Clague 1994; Trauth et al. 2000). An increase of ground water activity increases the pore pressure and reduces internal friction as well as the normal stress on sliding planes (Wyllie and Mah 2004). Landslide activity was linked to prolonged wet periods for instance in the Italian Alps (Porter and Orombelli 1981) or the Himalaya (Dortch et al. 2009), whereby deeper-seated landslides need prolonged periods of rainfall to be triggered (van Asch et al. 2009). Melting of snow and ice accompanies also deglaciation and is thought to have a similar effect as rainfall, potentially triggering or preparing landslides (McColl 2012). For instance, the seasonal snow melt in the Alps was shown to drive slope deformation (Le Roux et al. 2009). Additionally, the amount of surface

water has a strong control on chemical weathering which is known to reduce rock mass strength and can contribute to large rock slope failures as shown by Chemenda et al. (2009).

Climatic changes can also change permafrost conditions which have been suggested as an important preparatory and triggering factor for many large rock slope failures (e.g. Blikra et al. 2015; Fischer et al. 2012; Hormes et al. 2008). When permafrost levels rise, as during deglaciation, the bonding effect of the ice in pores and fractures disappears which reduces rock mass strength and joint friction as shown through mechanical models by Krautblatter et al. (2013) and Krautblatter and Leith (2015). Repeated freezing and thawing of interstitial water can follow the degradation of permafrost degradation. Experiments by Jia et al. (2015) showed that it promotes rock fatigue and decreases rock mass strength and thus may prepare or trigger large rock slope failures as also suggested by Davies et al. (2001).

5.5 Rock slope failures in Norway and Troms

In Norway, catastrophic rock slope failures have occurred repeatedly in historic times causing considerable damage and 175 fatalities during the past century (Blikra et al. 2006). In average 2 to 6 large catastrophic rock slope failure events occur in Norway per century (Blikra et al. 2006; Hermanns et al. 2013). The country's susceptibility to rock slope failures is largely due to its morphology characterized in many parts by a high-alpine relief deeply penetrated by fjord systems and over-steepened glacial valleys. Particularly important is the combination of this morphology with other factors, as the rock structures, heavy seasonal precipitation, the seasonal snow melting and the general cycles of freezing and thawing. For the population, that preferentially settles at the water front, the biggest danger emanates from displacement waves caused by the impact of rock avalanches into a fjord or lake (Harbitz et al. 1993). One dramatic example is the historic disaster at Tafjord where a displacement wave of more than 60 m height destroyed several villages in 1934 (Figure 14).

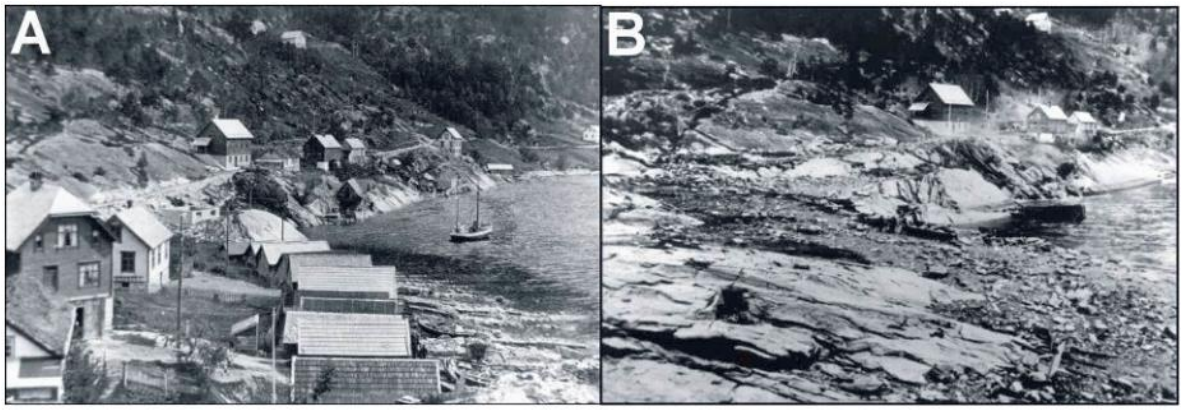

Figure 14: The pictures show the devastation caused in the village Fjøra by the tsunami at Tafjord in 1934. (A) before and (B) afte the event. *Source: Blikra et al. (2006); Furseth (1985)*

Due to Norway's critical natural predisposition, NGU carries out systematic mapping of unstable rock slopes in the whole country and has developed an unstable rock slope database (Oppikofer et al. 2015). So far, this effort has resulted in more than 300 recorded unstable rock slopes showing significant post-glacial deformation (Hermanns et al. 2013; NGU 2020a). Troms is one of the three key provinces of this mapping campaign and it is the one with the most recorded (138) unstable rock slopes (Figure 15B) and counts more than 150 mapped rock avalanches (Hermanns et al. 2013; NGU 2020a). The distribution of unstable rock slopes and landslides in Troms (Figure 15A,B) demonstrates a strong regional clustering with the strongest concentration of landslides to the East of Lyngen and Storfjorden (Bunkholt et al. 2012). The region's landslides occur in different rock types, but dominantly in mica schists and show a large variety of deformation styles comprising large sagging slopes, toppling failures, compound slides, stepped translational slides and one rotational landslide (Blikra et al. 2006; Bunkholt et al. 2012). In Troms, only one historic large rock avalanche event is known which happened in Lyngen killing 14 people in 1819 (Blikra et al. 2006). The rock avalanche deposits dated in Troms resulted in ages indicating a regionally high post-glacial activity but further information about temporal behavior is given in the following section (Blikra et al. 2006; Fenton et al. 2011).

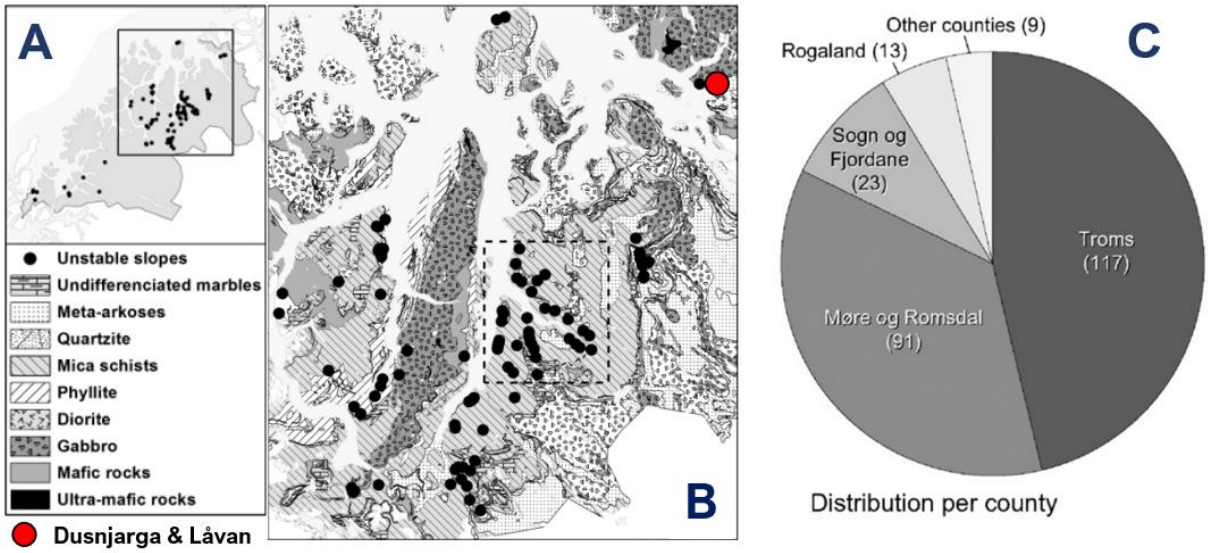

Figure 15: A) Overview map of the Troms county. B) Bedrock map of NE-Troms where most of the recorded unstable rock slopes are located. The area around Storfjorden and Kåfjorden (dashed rectangle) shows the highest concentration of instabilities. *Source: Bunkholt et al. (2012).* B) Pie chart displaying the county-wise distribution of registered unstable rock slopes with systematic mapping being performed in the counties Troms, Møre og Romsdal, Sogn og Fjordane and Rogaland since 2015. *Source: Oppikofer et al. (2015).*

5.6 Temporal behavior and dating of rock slope failures

The long-term temporal behavior of DSGSDs is especially relevant in order to assess the influence of past events on their activity, e.g. regarding the deglaciation, but it is also one of the least understood aspects (Pánek and Klimeš 2016). However during the past 20 years, many new insights have been made possible due to the improvement in absolute dating methods, in particular due to terrestrial cosmogenic nuclide (TCN) dating which allowed to date the rock surfaces of deformation features and landslide debris (e.g. Böhme et al. 2019; Hippolyte et al. 2006; 2012; Hormes et al. 2008). But also the advance in other dating techniques contributed to new insights, such as optically-stimulated luminescence and radiocarbon dating which often use the sediment filling of linear DSGSD features (like tension cracks or counterscarps) to obtain dateable material (e.g. Agliardi et al. 2009; McCalpin and Irvine 1995). Even without absolute dating it is still possible to establish relative chronologies by detailed investigations of deformation features and their relationship with younger sediment infill (e.g. Agliardi et al. 2009).

DSGSDs are long-lived phenomena that can show several reactivations spanning over time ranges of more than a glacial cycle (Crosta et al. 2013). Most likely, this long-term evolution is due to a progressive failure mechanism with failure surfaces typically starting to develop at one point, preferentially at the toe or as tension cracks on the head, from where failure

progressively propagates up- or downwards following the rhythm of influencing processes such as the deglaciation (Agliardi et al. 2012; Ambrosi and Crosta 2006).

Probability distributions of published DSGSD and deep-seated landslide ages from glaciated and non-glaciated areas are displayed in Figure 16A. A large proportion of slope deformations in glaciated areas showed an activation of deformation a few thousand years after the deglaciation (e.g. Augustinus 1995; Hippolyte et al. 2012; Moro et al. 2007) which time lag is attributed to the slope's gradual adjustment to debuttressing and stress release (McColl 2012). However, many DSGSDs and landslides seem to have been activated even later, clustering in the Mid-Holocene which is shown by a variety of studies from different regions such as the Pyrenees (Díez et al. 1996; Gutiérrez-Santolalla et al. 2005) or the Alps (e.g. Bigot-Cormier et al. 2005; Hormes et al. 2008; Ivy-Ochs et al. 2009). For the Alps, studies as Le Roux et al. (2009) or Ivy-Ochs et al. (2009) indicate an increased DSGSD activation coinciding with the end of the Holocene Climate optimum that lasted from around 9 to 5 ka. This suggests a potential linkage to climatic effects since these time-lags seem too long to be an answer to debuttressing even though this is still debated (Ballantyne et al. 1998; McColl 2012).

With respect to Norway, the rock avalanche inventory for S- and W-Norway analyzed by Hermanns et al. (2017) revealed that almost half of the 22 analyzed rock avalanches occurred less than 1000 a after the ice retreat. Rock slope failure activity clustering in the Mid-Holocene was also identified in the inventory by Hermanns et al. (2017) which showed that 6 of 22 rock avalanches occurred close to the Holocene thermal optimum around 8.5 ka. Further studies in W-Norway as Longva et al. (2009) and Böhme et al. (2015) identified a cluster of rock slope failures between 8 and 5 ka. In Hilger et al. (2018), catastrophic rock slope failures in W-Norway clustered a bit after this phase, between 5.5 and 4.5 ka. For northern Norway, TCN dates from the Gamanjunni rockslide by Böhme et al. (2019) support these findings where a slide initiation with high displacement rates was indicated between 6.6 and 4.3 ka. As presented in Figure 16B, the Holocene Climate optimum lasted in Norway from about 8 to 5 ka. The mentioned studies imply increased rock slope deformation for the maximum and especially for the end of this phase which most likely was characterized by a change to stronger seasonality with colder winter and increasing precipitation (Lilleøren et al. 2012). Therefore, even though an effect of seismicity cannot be ruled out, a link to climatic changes is suggested which could have affected slope stability through stronger freeze-thaw cycles, permafrost degradation or groundwater effects caused by increased rainfall or melt water (Böhme et al. 2019; Hilger et al. 2018).

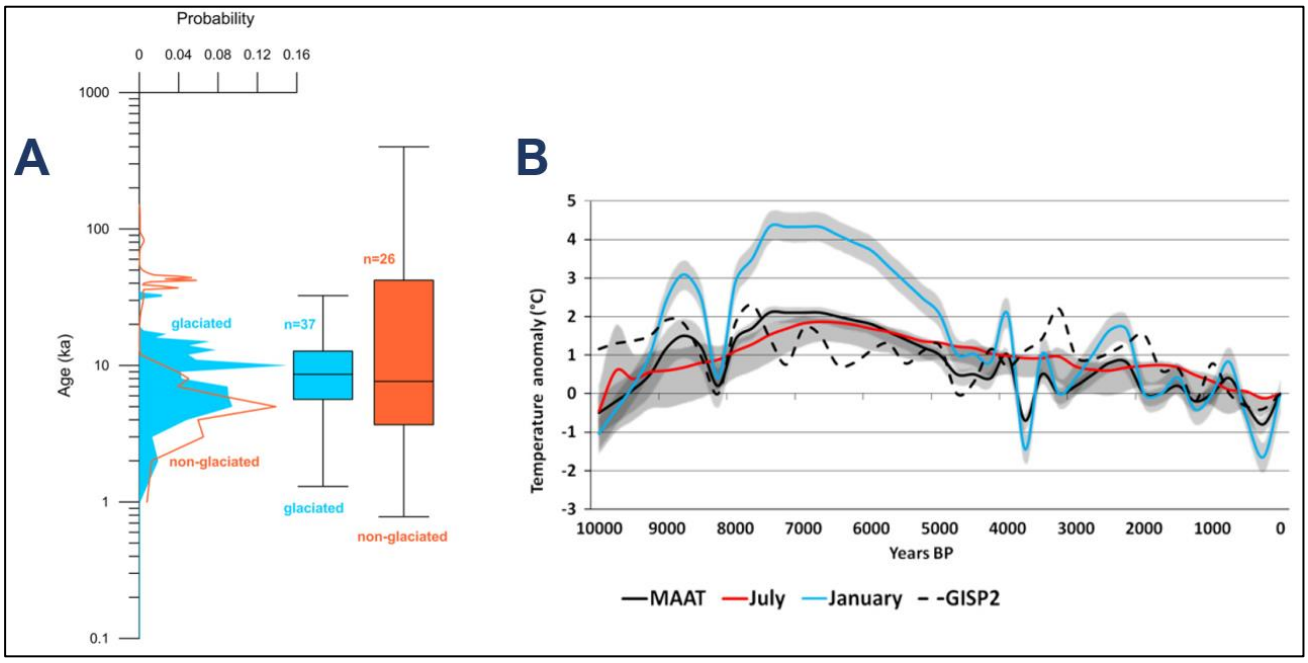

Figure 16: A) Published ages of DSGSDs and deep-seated landslides (until 2016): probability distributions (left) and whisker plots displaying the variability of ages (right), separated between formerly glaciated and non-glaciated terrains. *Source: Pánek and Klimeš (2016).* B) Temperature anomalies in Northern Norway over the Holocene in relation to present temperatures: displayed are the mean annual air temperature (MAAT) as well as the July and January temperature. The insecurities for each curve are indicated by the shades. Temperatures from the GISP2 Greenland ice core are displayed for comparison. *Source: Lilleøren et al. (2012).*

5.7 Susceptibility and hazard assessment of unstable rock slopes

The Norwegian hazard and risk classification system, described in detail in Hermanns et al. (2012a; 2013a) and implemented in this study, was developed by NGU, NVE (Norwegian Water Resources and Energy Directorate) and international experts. It uses a combination of a qualitative hazard analysis and a quantitative consequence analysis and serves to objectively rank the unstable areas in Norway and to prioritize the possible follow-up activities. The likelihood of a rock slope failure is one of the most difficult aspects to assess since there exists only very limited only very limited instrumental data on catastrophic rock slope failures. Therefore, a heuristic approach was chosen for the qualitative hazard analysis (Figure 17) thereby focusing on the evaluation of nine criteria which describe the present state of the slope and which are easy to determine using field-geological observations. One category of criteria refers to the structural development of the slope and a second refers to displacement rates and signs of activity since (aseismic) unstable rock slopes show deformation preceding their failure (Hermanns et al. 2012a; Hermanns and Longva 2012). As depicted in Figure 17A, one of several conditions with an assigned score is chosen for each criterion and a hazard score is calculated from the sum of these scores. The final hazard score ranging from 0 to 12 is divided again into five hazard classes of equal intervals which should give an indication for the

likelihood of failure. This hazard analysis allows additionally the inclusion of uncertainties for each criterion by choosing probability factors that are multiplied with the respective scores.

It is important to note that preliminary to the hazard analysis, different rock slope failure scenarios are defined for the unstable area since the failure of different subareas can lead to variations in critical volumes and run-out distances (Hermanns and Longva 2012). For each scenario a simple run-out assessment based on the approach by Scheidegger (1973) is done. If the assessment determines that buildings or a water body may be hit, the performance of a hazard analysis is required.

Subsequent to the hazard analysis, a risk estimation can be performed by using a risk matrix (Figure 17B) and combining the results from the hazard analysis (the event's likelihood) with the results of a consequence analysis (the suspectable loss of life).

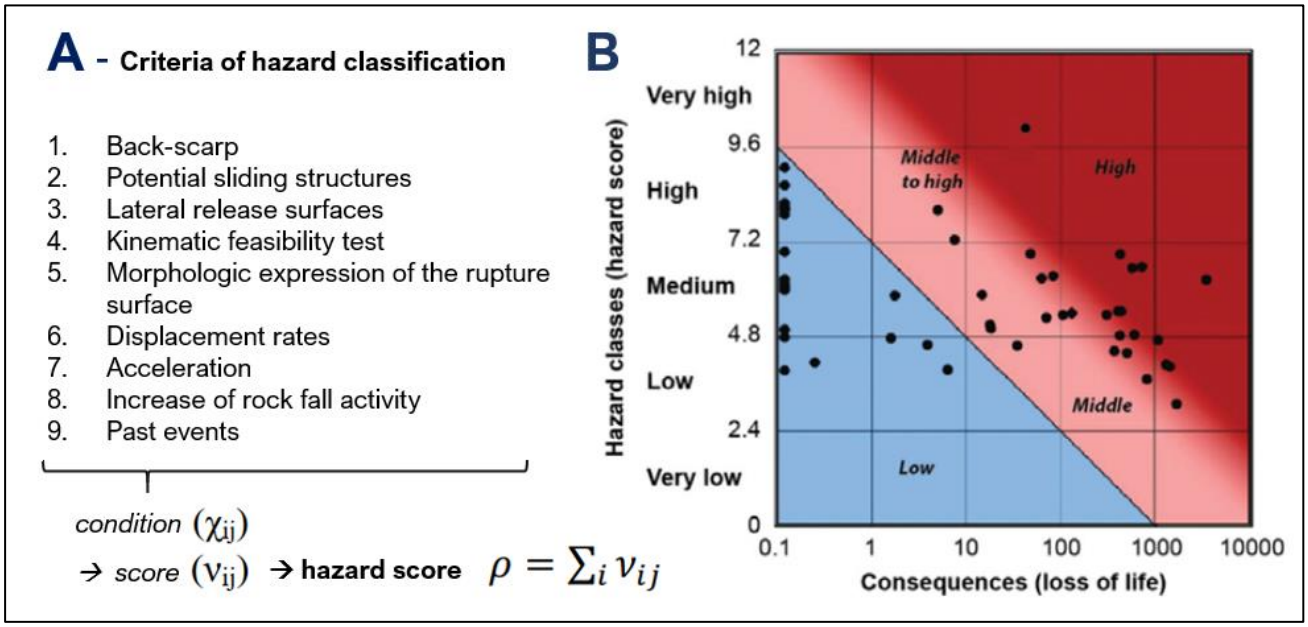

Figure 17: A) The nine criteria of the hazard classification that describe the present state of the slope. One of several possible conditions with an assigned score is chosen for each criterion. The final hazard score results from the sum of these nine scores. B) Hazard and risk matrix: The resulting hazard class/score can be used in combination with the results from a consequence analysis (loss of life) in order to perform a risk analysis. The result can plot in one of three risk classes: low, medium or high risk. This plot shows the 48 scenarios that were established for 22 unstable slopes classified in Norway until 2016. *Adapted from: Hermanns et al. (2013a); Hermanns et al. (2016).*

6 Data and methods

The results and interpretations presented in this thesis were achieved using a combination of methods based on different data sources: information provided by former studies (e.g. concerning the local glaciation or similar studies in Norway), digital map data as well as own field data.

The digital map data comprised orthophotos from 2015 and 2018 (resolution of 0.25 m and 0.5 m), a LiDAR-derived DEM of 1m-resolution, InSAR-data on ground motion, as well as the bedrock and Quaternary geologic maps, both in 1:250,000 (compare Table 1). This digital data was provided by the *Norwegian Mapping Authority* (*Kartverket*) and *NGU*. It was implemented in a geographical information system (GIS) using the applications *ArcGIS (ESRI)* and *QGIS*.

- *Field work*

Field data was collected in a field campaign in 2019. The campaign comprised 17 field days, three days in August and 14 in September. The collection of structural data was one of the main tasks in the field (e.g. Figure 18A). More than 1400 orientation measurements of joints and foliation were recorded at 29 outcrop localities (Figure 19) using both a geologic compass as well as the smartphone application *Fieldmove Clino (Midland Valley Ltd)*. Additionally, characteristics for each discontinuity set were recorded in detail for 20 outcrop localities (Figure 19) using a geotechnical scanline mapping sheet. We further observed and recorded the lithological characteristics and the morphological features especially elements with a gravitational origin.

A special focus was set on the observation of Quaternary deposits and features. We also excavated more than 20 sedimentological profiles (e.g. Figure 18B). From these profiles, we took a variety of sediment samples focusing on the most relevant Quaternary sediment types.

As a valuable supplement, additional aerial imagery was taken of the unstable rock slopes during the field campaign using an UAV platform (unmanned airborne vehicle).

Figure 18: Exemplary pictures of the field work at Dusnjarga in August-September 2019. (A) Acquisition of structural data, here: discontinuity plane measurements at Dusnjarga's head scarp. (B) Mapping of Quaternary geology, here: the recording of a sediment profile on a riverbank in the central high valley.

- *Quaternary map and analysis of Quaternary deposits*

We produced a high-detail Quaternary geological map of the study area using *ArcGIS* and *QGIS*. Mapping was carried out at a resolution of 1:5000 and covers an area of 10.4 km² including Dusnjarga, Låvan and the directly surrounding areas. For the mapping, the main sources of information were field observations, photos and sedimentological profiles, supplemented by the information through orthophotos and DEM, especially for areas which could not be covered by foot during field work.

Quaternary deposits were investigated and documented using standard sedimentological procedures, such as logging of profiles, measurements of clast characteristics and documentation. For selected profiles, sedimentological data charts were produced by using the vector graphics software *Inkscape 0.92* and based on the template by Krüger and Kjær (1999).

Particle size distributions of a selection of six sediment samples were obtained using manual wet sieving in a soil laboratory at the *University of Innsbruck*. We used a sieve column with five different mesh sizes: 6.3 mm, 2 mm, 0.63 mm, 0.2 mm, and 0.063 mm.

- *Morpho-gravitational map and analysis of slope morphology*

A map of morphological and gravitational features was created using *ArcGIS* for the central study area based on the information provided through field observations, field pictures, UAV imagery, orthophotos, the DEM and the DEM-based 3D-model. The role of the latter two resources was relatively larger than their role for the creation of the Quaternary map.

- *Structural, scanline and kinematic failure analysis*

The structural and kinematic failure analysis were performed using the stereographic projection software *Dips (Rocscience Inc.).* The discontinuity sets were calculated as mean values (and 1σ variabilities) of visibly distinguishable discontinuity clusters using *Dips*.

The scanline mapping comprised the following categories of discontinuity characteristics (joints and foliation): discontinuity type, orientation, spacing, length, type of termination, roughness, width, water condition, lithology, and strength. This data was analyzed statistically using *Excel (Microsoft Office 2016)*.

An interpreted geological cross section across Låvan (Figure 19) was created in *Inkscape 0.92* and was based on the analyses of structural data, digital map data and imagery, in particular with the help of an *ArcGIS pro (ESRI)* 3D-model.

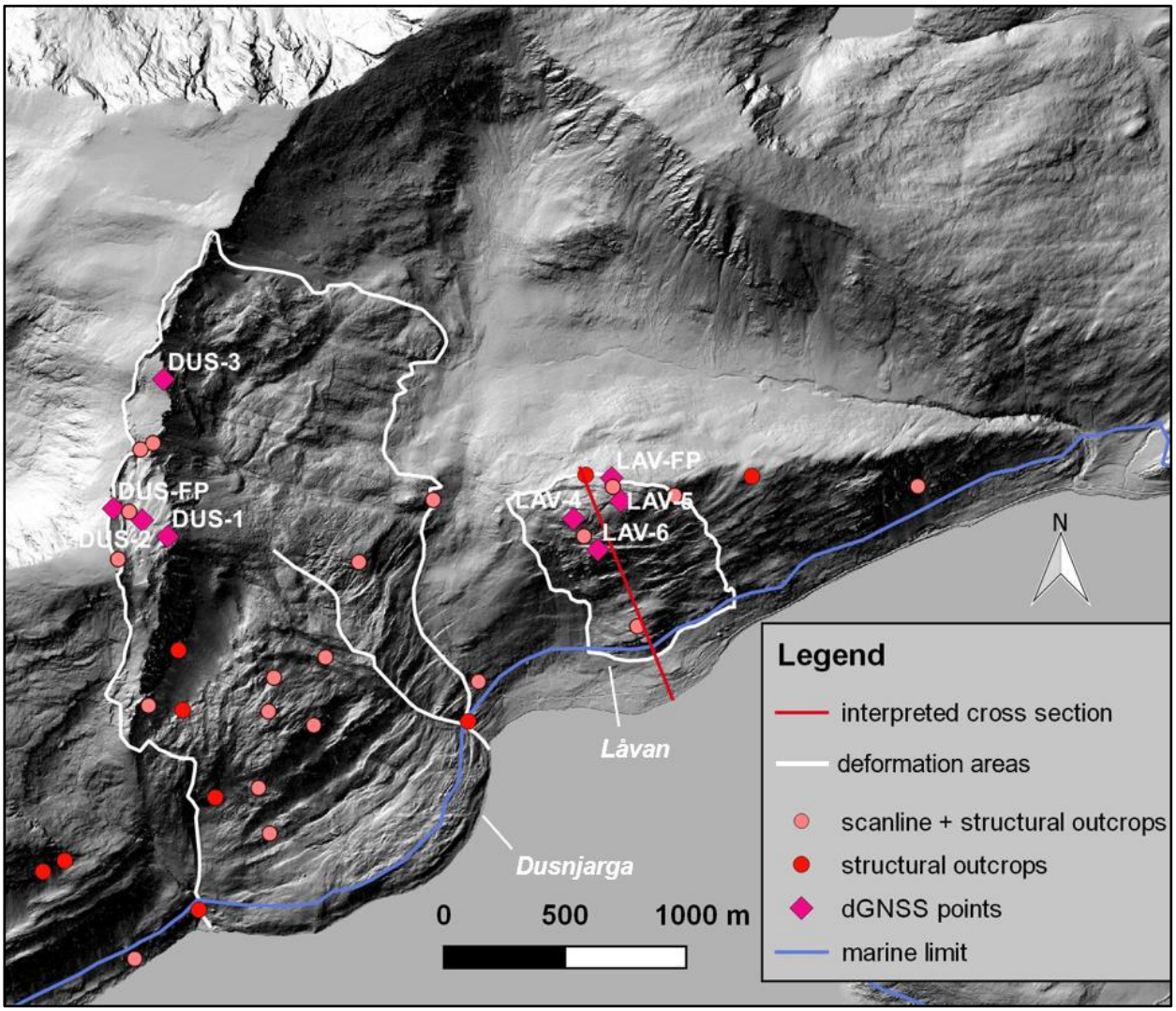

Figure 19: Hillshade map of the study area generated from the high-resolution DEM: The map includes the locations of the outcrops where structural and scanline data (pink/red points) was collected as well as the locations of the dGNSS-monitoring points (pink diamonds) installed by NGU. Furthermore, the marine (blue line) as interpolated by NGU and the boundaries of the deformation areas (white lines) are indicated.

- *Displacement measurements: InSAR and dGNSS*

For the analysis of current displacements, we used InSAR (Interferometric Synthetic Aperture Radar) and dGNSS (differential Global Navigation Satellite System) data from local monitoring points.

We had access to InSAR data from *InSAR Norway (https://insar.ngu.no/)* that was collected by Sentinel-1A/-1B from the EU Copernicus program between 2014 and 2019. The Sentinel-1 satellites move in polar orbits, either from N to S or from S to N, termed as descending or ascending pathway (Figure 20). The satellite's radar is oriented to its right and scans a swath of 250 km width and it is to note that the azimuth angle varies for both pathways (NGU 2020b). The displacement is measured relative to the moving satellite which implies that the

displacement vector's N- and S-components are missing. Furthermore, InSAR has incapacities with collecting data for very steep terrain (e.g. cliffs) as for vegetation- and snow-covered areas.

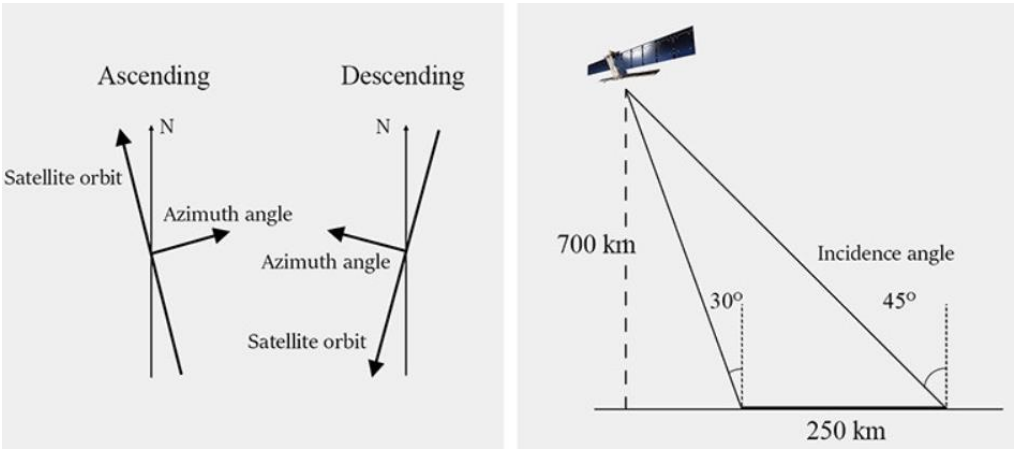

Figure 20: Satellite geometry for the collection fo InSAR data: data is collected for an ascending and descending satellite pathway whereby the line of sight is always orthogonal to the right of the satellite. The incidence angle is the angle between vertical and the line of sight and varies from 30 to 45°. *Source: NGU (2020)*

Since 2010, measurements using Differential Global Navigation Satellite System (dGNSS) have been carried out by NGU in a two-year cycle at Låvan. We had access to the dGNSS data of the period 2010 to 2014 from three monitoring points inside the deformation area (Figure 59). Every two years, the coordinates of these points were measured and compared to a fixed point installed in a stable position just above the main scarp. Measurements are declared as significant if the displacement between two measurements is higher than the uncertainty (3σ variability) of the method (Bunkholt et al. 2011). Followingly, displacement results can be declared either as certain gravitational movement or uncertain gravitational movement. It must be also considered that the vertical displacement has a larger uncertainty caused by atmospheric variations which is important to consider for the level of significance (Bunkholt et al. 2011). For certain gravitational movements, the average velocity can be calculated using regression models (e.g. least squares regression).

7 Results

An analysis of Quaternary deposits in the study area (7.2) and an analysis of rock mass and failure kinematics at Låvan (7.3 – 7.5) form the central parts of the study's results. An analysis of the slope morphology (7.1) and an analysis of current displacement data (7.6, 7.7) serve additionally to reach valid interpretations of the current deformation in the study area and particularly at Låvan.

Regarding the structures and failure mechanisms for Dusnjarga and the total study area, more detailed analyses are presented in a parallel Master thesis (Tyldum Skogen in prep.).

7.1 Morphology of the deformed rock slopes

This chapter presents firstly the created maps of slope inclination (7.1.1) and morpho-gravitational features (7.1.2) which is followed by detailed morphological descriptions of the deformed slopes Dusnjarga (7.1.3) and Låvan (7.1.4).

7.1.1 Slope inclination map

The slope inclination map for the study area was created based on the digital elevation data and is presented in Figure 21. A slope inclination map is an important tool in order to draw certain interpretations about the morphology and deformation.

It is clearly visible that Låvan's slope is steep (even >50°) in many smaller parts. This stands in contrast to the flat high plain at its top and the coastal flat at its foot.

The large cliff of Dusnjarga's lower head scarp stands out by its high slope gradients whereas the whole main part and frontal lobe of Dusnjarga has comparably low slope angles (usually 30° or less). Merely two transverse-running sections are obviously steeper in this central part.

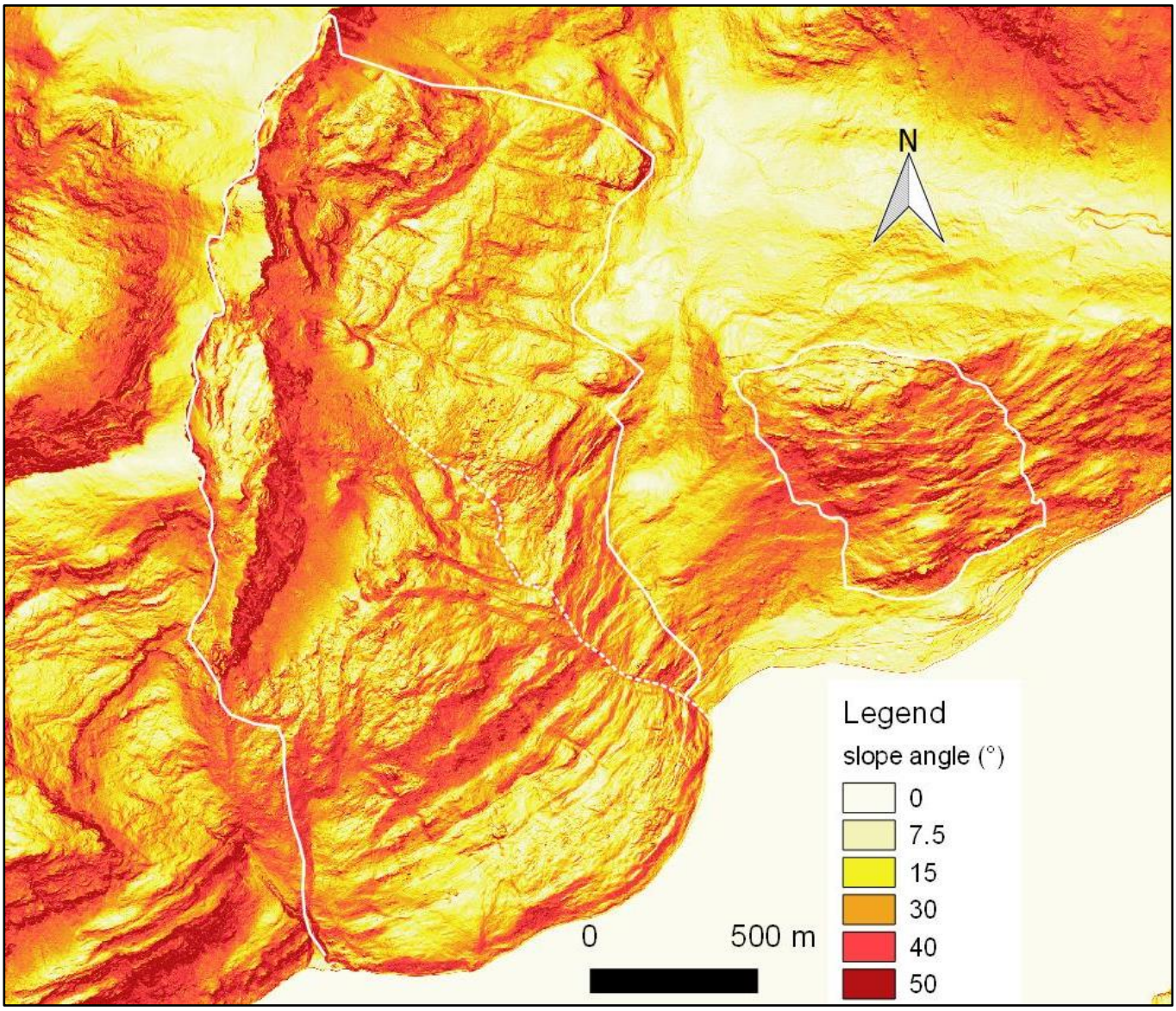

Figure 21: Slope angle map of the central study area: the map is based on the high-detail DEM. The contours delimit the deformation areas as morphologically indicated: Dusnjarga to the left (the dashed line delimits the actively deforming area) and Låvan to the right. Very steep slopes (red colors) are found e.g. at large sections of Låvan or at the lower head scarp of Dusnjarga. Low slope gradients (light and yellowish colors) stand out for instance at Dusnjarga's frontal part or at coastal section in front of Låvan.

7.1.2 Morpho-gravitational map

A morphological map that includes indicative features for the gravitational deformation (morpho-gravitational map) was composed for the central study area comprising the deformation areas Låvan and Dusnjarga. It is presented in Figure 22. The following sections refer in more detail to the morpho-gravitational features indicated on this map.

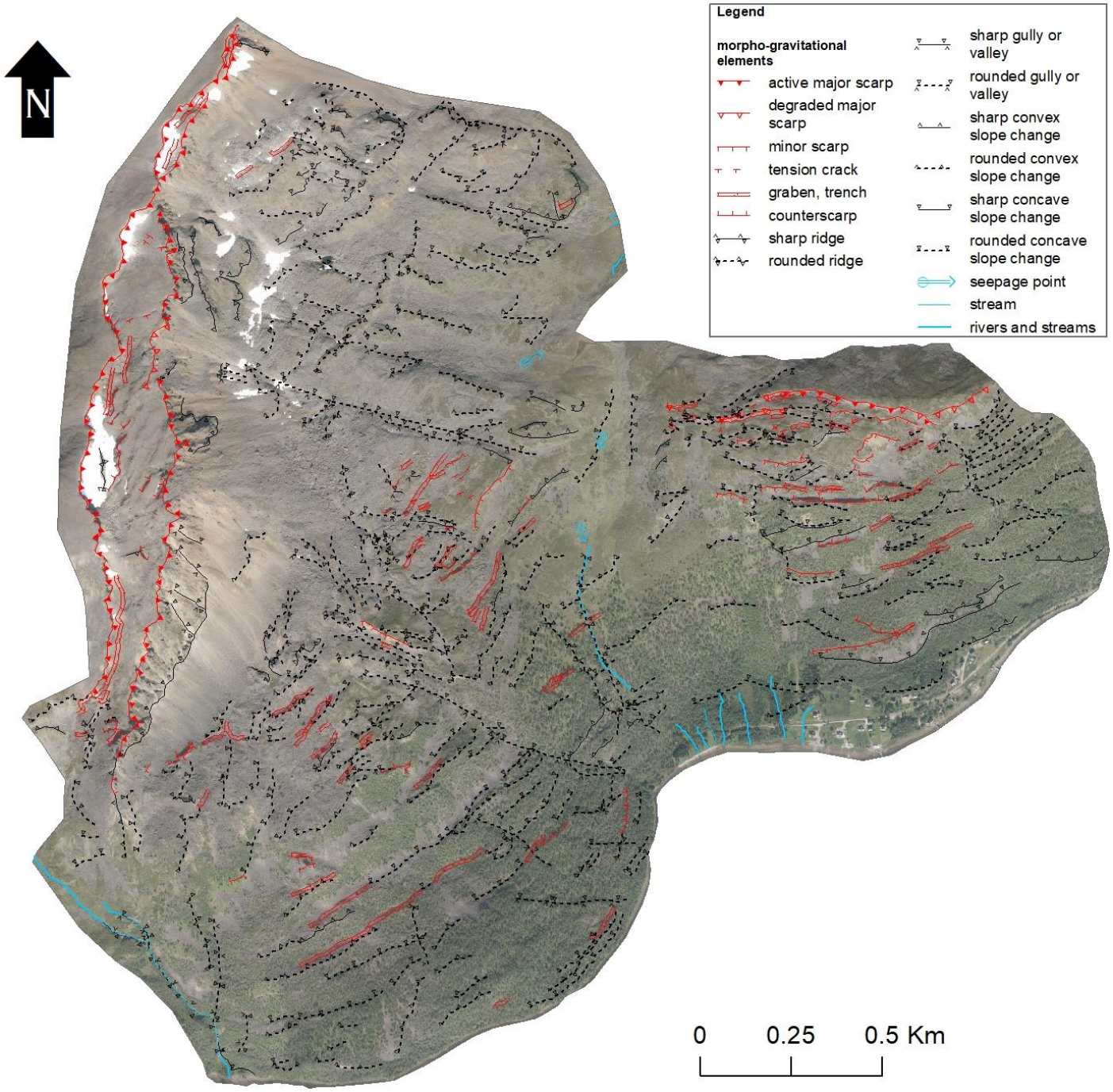

Figure 22: Morpho-gravitational map of the central study area (enlarged version in the appendix): the chosen extent covers the gravitationally deformed slopes; red symbols = morphological features clearly indicating gravitational deformation, black symbols = changes in slope morphology and possible signs for gravitational deformation. The base map is the high-resolution orthophoto overlain by the semi-transparent DEM.

7.1.3 Slope morphology of Dusnjarga

- ***Head scarps and the head domain***

The head domain marks the top of the deformation area and is characterized by a large unstable block delimited by two long, subparallel head scarps. The 1.5 km long major head

scarp forms the upper limit of the deformation areas separating it from the top ridge of Koppartinden (at around 800 m a.s.l.). This major head scarp is depicted in Figure 23 and has a morphological fresh appearance with a height of usually 20 to 30 m. It has a clear trench in front and is partly opposed by counterscarps. On most of its length, this head scarp separates a large N-S-stretching, displaced block from the mountain. At its front towards the central deformation area, this block is delimited again by an even higher back scarp (total height over 100 m) with massive talus fans. Both, upper and lower, head scarps are sub-parallel to each other, running N-S whereby at both the orientation and steepness shows a significant degree of variation. In most cases, dip orientations of 135 – 145° and dip angles of 70 – 85° were measured for the scarp faces.

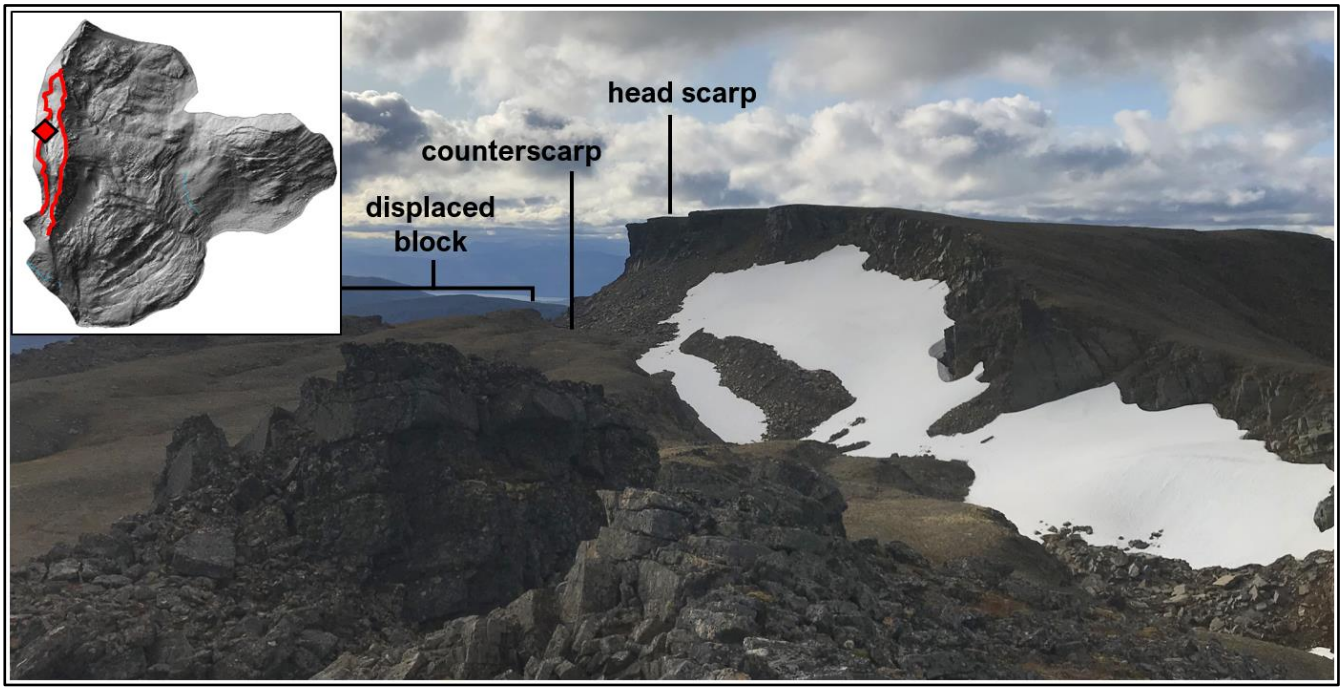

Figure 23: Dusnjarga's major head scarp at the top of Koppartinden: The view direction is towards S. It separates a major displaced block from the stable area (to the right). The rock face of the scarp has a height of 20 to 30m and the opposing counterscarp and trench are also recognizable. The position of the photo (diamond) and the locations of the two sets of head scarps (red lines) are indicated in the small overview map.

- ***The central domain and lateral flanks***

Below the talus fans of the described back scarps starts the central deformation area of Dusnjarga (Figure 24). This area consists mainly of disaggregated rock mass, is basically unvegetated and shows a chaotic pattern of trenches, ridges, isolated blocks, and few counterscarps (Figure 24, 31). This chaotic, heavily deformed morphology is especially strong in its center and decreases laterally. The slope inclination in the central domain is relatively

low compared to steep back scarps above (Figure 24A) or the steep steps in the morphology below (Figure 24D).

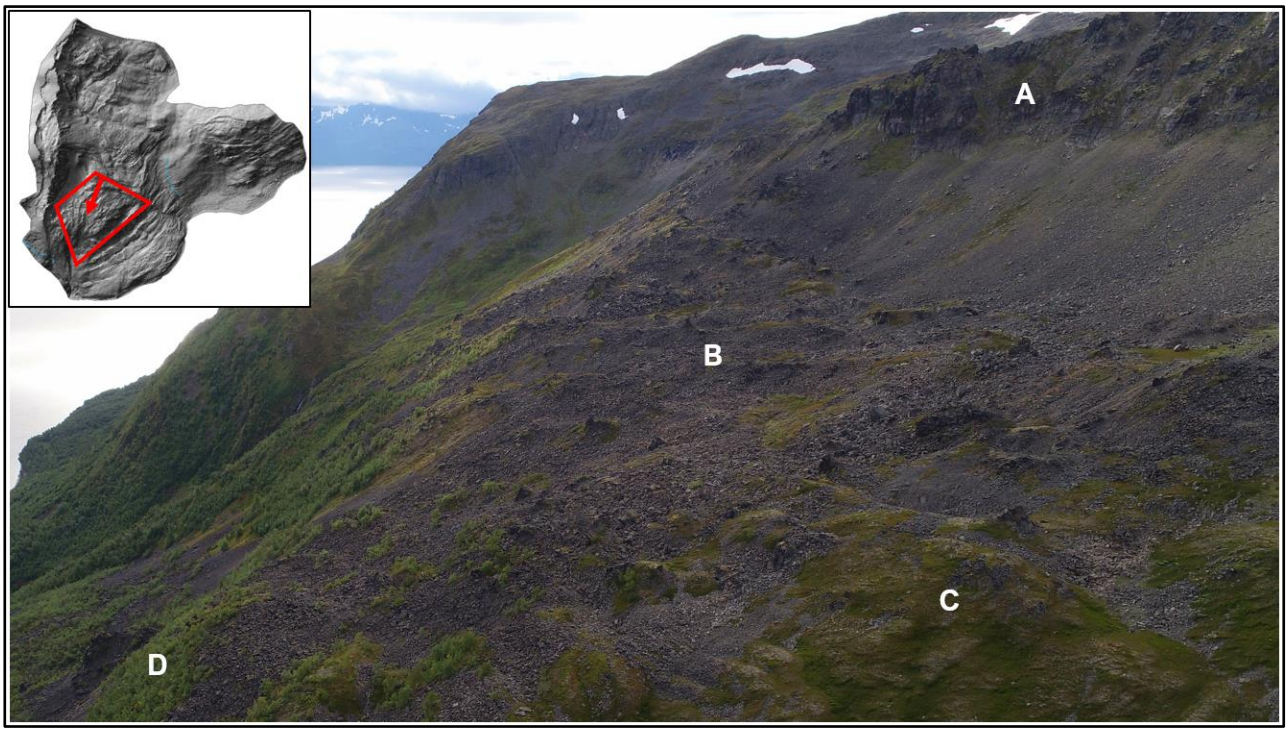

Figure 24: UAV-imagery depicting the central domain of Dusnjarga: The overview map indicates the approximate extent of the central domain (trapezoid) as well as the direction of view in the photo (arrow). A: The lower head scarp and its large talus fan delimit the central domain to the top. B: In the middle of the central domain dominate chaotic masses of disaggregated bedrock forming a system of convex ridges and trenches. C: Farther laterally, the grade of deformation seems lower indicated by vegetation cover and obviously less disaggregation. D: Steep steps transition to the frontal lobe where the morphology forms a more regular pattern.

Laterally, the central domain is on both sides delimited by a system of rounded trenches or small valleys that run slightly diagonal compared to the slope orientation (Figure 25). The NE lateral limit is morphologically stronger expressed than the SW limit. Towards the frontal domain, these complex systems of lateral trenches merge on each side to form one distinct.

Figure 25: One of several lateral trenches delimiting the central deformation area to the NE. The trench runs towards SE. Further downslope the trench unites with others and becomes deeper and wider. The position of the photo (diamond) and the loations of all lateral limits (red lines) are indicated in the small overview map.

- ***The frontal lobe: transverse ridges and grabens***

The lowest domain, the frontal lobe, has a quite regular morphology characterized by regularly alternating convex and concave coast-parallel features. These transversal features consist usually of gently rounded ridges with adjacent rounded trenches (Figure 26). They show consistently a strike around 140°.

Most parts of the frontal lobe are vegetated. The upslope transition towards the central domain is formed by two large and steep steps (Figure 21) with inclinations ranging around 40°, whereas most parts of the frontal lobe have slope inclinations of below 15°. At the toe, the frontal lobe forms a characteristic arched protrusion reaching for about 250 m out into the fjord compared to the neighboring coast. The frontal slope of this protrusion drops steeply down to the fjord (mostly ~40°).

Figure 26: A transverse ridge directly followed by a trench which is a good example for the typical pairs of convex and concave features found all over Dusnjarga's frontal lobe. The direction of view is SW. The photo's location (diamond) as well as the extent of the frontal lobe domain (red polygon) are indicated in the overview map.

7.1.4 Slope morphology of Låvan

This chapter dedicates to the description of Låvan's morphology and morpho-gravitational features which are a central part for the investigation of the slope deformation and for the final hazard analysis. Detailed observations of rock mass and structures are however not included in this chapter, but these results are presented with reference to the morpho-gravitational features in section 7.5.

The unstable slope of Låvan is shorter (about 850 m) but in average also considerably steeper (25°) than Dusnjarga's slope as indicated in the slope inclination map (Figure 21). The average slope inclination for the deformed area was calculated at 31° ±12°.

- ***Head domain: head scarp, tension cracks and minor scarps***

Låvan's top is situated at the edge of a high plateau with an overall relatively low slope inclination (< 10° in average). A 400m-long, prominent head scarp runs from W to E (overall strike ~0°) in a weekly curved shape (Figure 27A). The height of the head scarp face increases towards E from around 5 to more than 10 m. The head domain of Låvan is further characterized by a system of minor scarps, measuring usually 1 – 4 m in height, accompanied by distinct, narrow trenches that often transition into to tension cracks (Figure 27C).

These features mostly have a "fresh" and basically unweathered appearance and follow usually a distinct zigzag pattern. This zigzag pattern is formed by two directions: most

dominantly features strike WNW-ESE (105 - 110°) and secondly NE-SW (55 – 60°). The individual rock faces of the head and minor scarps follow also these directions.

Furthermore, gently rounded convex ridges appear in this top section running parallel to the main scarp direction.

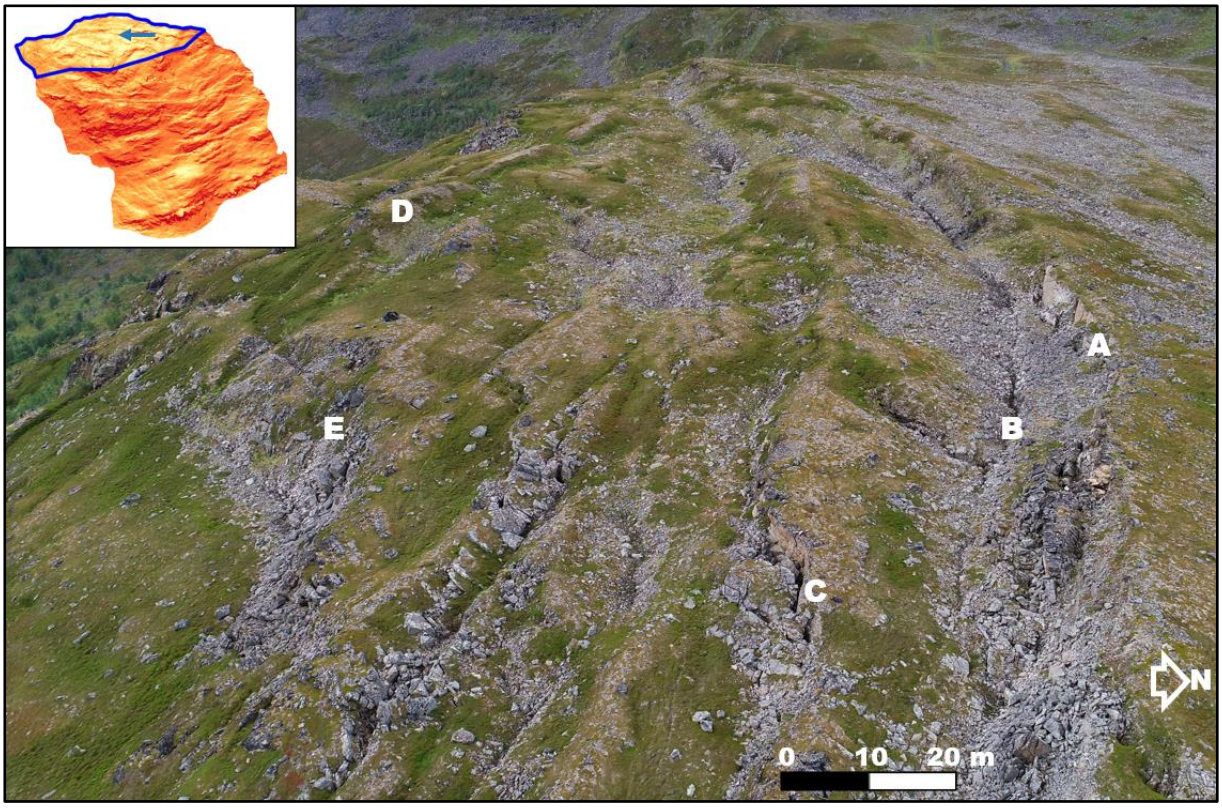

Figure 27: UAV-image overlooking the head domain of the deformation area Låvan: The limits of the head domain (blue line) and the location/direction of view (arrow) are indicated in the small overview map. The weekly curved head scarp (A) is followed by a narrow trench (B) and is progressively more weathered and obscured to the E. Minor scarps and tension cracks run approximately parallel to the head scarp and form usually a distinct zigzag pattern (e.g. C). Additionally, E-W-trending, rounded convex features are characteristic for this upper slope section (e.g. D). Several distinct cliffs/scarps form the transition to the steeper central slope section (E).

- ***Central domain: counterscarps and grabens***

The central domain starts at the border of the top plateau where the slope is suddenly getting steeper which transition is characterized by several minor scarps. The whole central slope domain remains consistently steep and has an average slope inclination of 35° ±11°. The minor scarps are followed below by various trenches and counterscarps forming a so-called 'saw-tooth morphology'. Typically, these features form angular shapes following the two orientations (here: strikes of ~115° and ~55°) which were observed at the features in the head domain. These gravitational features vary strongly in their grade of conservation ranging from very fresh scarps to very degraded appearance. Particularly outstanding is one very large counterscarp

running E-W (strike ~90°) across the whole deformation area on a length of about 200 m (Figure 28).

Below this counterscarp the rugged saw-tooth morphology gradually transitions into a more rounded stair-like morphology of alternating concave and convex morphologies (Figure 29 B/C). These transverse-running convex and concave features gradually loose the angular shape and strike at 60 to 75°.

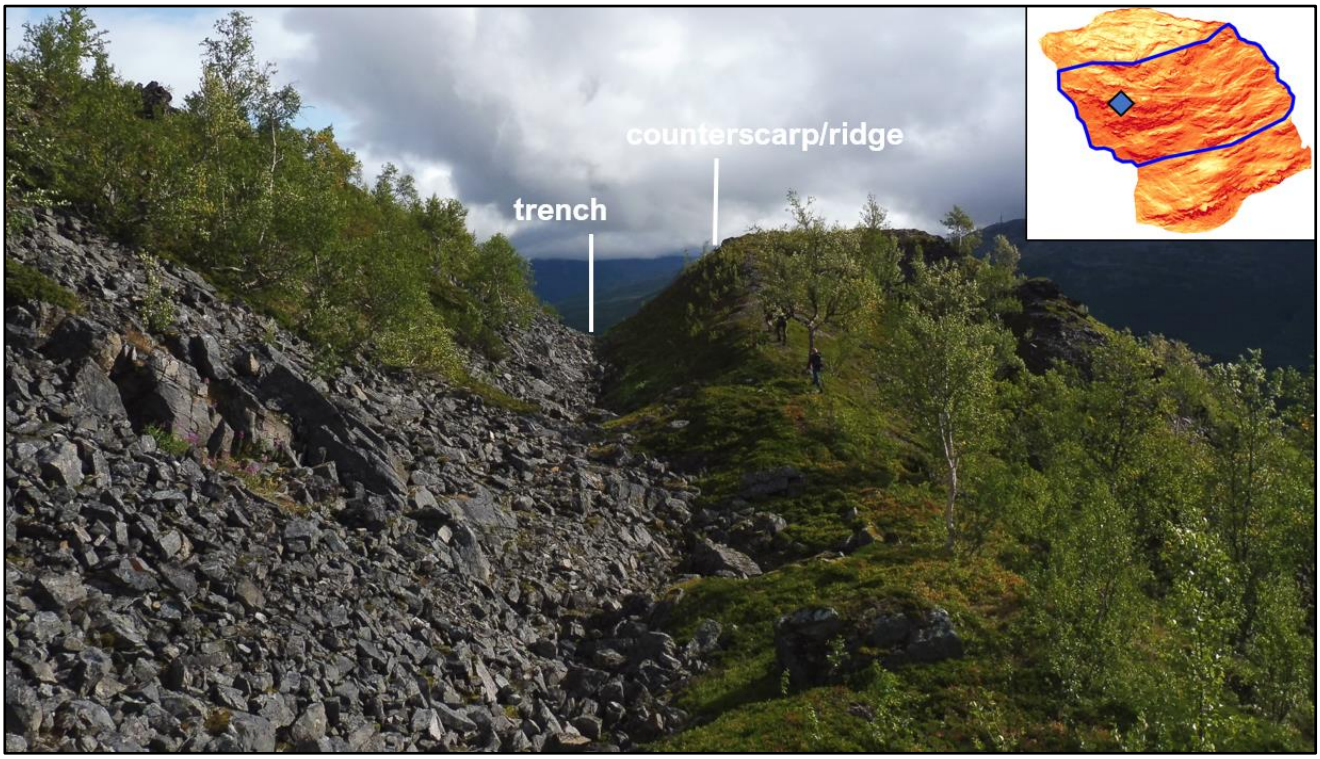

Figure 28: The picture shows the most prominent of counterscarp of Låvan spanning across the entire width of the deformation area (length of around 200m). It is situated in the zone of transition from the head to the central domain characterized by an abrupt steepening of the slope and accompanied by a variety of minor scarps and counterscarps (see also Figure 29A/B). Direction of view is towards E. As a scale, note the people walking on the ridge. The image location (diamond) and the extent of the central domain (blue line) are indicated in the small overview map.

- ***Lateral flanks***

The lateral flanks are not as clearly delimited as for Dusnjarga. To the W and to the E, the unstable slope can be delimited by the gradual disappearance of gravitational features, e.g. the limits of the head scarp or of the large counterscarp (e.g. Figure 21). The lateral limits delineated according to this criterion form quite irregular shapes and are oriented towards SE (azimuth of around 140 – 150°).

- ***Frontal lobe***

At the lowest slope section, the stair-like morphology becomes gradually less pronounced and the slope inclination decreases slightly (average: 31° ±11°). Further below, the deformed slope ends suddenly forming a toe cliff or scarp (~40 m in height) with a pronounced talus fan directly above the settlement Låvan (Figure 29D). A frontal lobe and accumulation zone are thus not well developed at Låvan compared to Dusnjarga. The flat coastal area in front of the deformation area forms a distinctly curved protrusion reaching out into the fjord (Figure 29E).

Figure 29: 3D-view of the deformation area Låvan (dashed line = limits of slope deformation): The small overview map depicts the direction of view (arrow) as well as the extents of the central (dashed, blue line) and frontal domain (full, blue line). A) The transition from the head domain to the steeper central domain is characterized by a system of minor scarps and counterscarps. B) Ridge belonging to the most prominent counterscarp (Figure 28). C) The rugged saw-tooth morphology of the upper central domain transitions into a more rounded stair-like morphology. D) A frontal lobe is only formed to a minor degree and ends abruptly at a cliff/scarp above the settlement Låvan (E) located on a flat coastal protrusion. The figure was created using *ArcGIS Pro*.

7.2 Quaternary geology

7.2.1 Quaternary geological map

A detailed Quaternary geological map for an area of 10.4 km² was compiled including Dusnjarga, Låvan and neighboring areas. The print version of the map is presented in Figure 30 in a resolution of 1:20,000. The Quaternary map serves as an important cornerstone to reconstruct landscape development in the area.

In the Quaternary map, polygon features represent the dominant type of surface cover, especially sedimentary cover, and point and line symbols represent Quaternary geomorphological, linear landforms, erosional features and streams. The symbology and feature classes are based on NGU's standard for Quaternary geological mapping (e.g. Bergstrøm 2001; Fredin et al. 2013; Hilger et al. 2019), but adapted for products of slow rock slope deformation. Specifically, this meant the introduction of two classes 'disintegrated bedrock' (= gravitationally deformed bedrock, still with rock bridges in-contact) and 'disaggregated bedrock' (= gravitationally deformed bedrock, disrupted blocks and out-of-contact).

The Quaternary map (Figure 30) shows that large parts of the study area are dominated by bedrock in different variations (pinkish colors). Consequently, only a minor proportion of the study area is covered by loose Quaternary deposits as glacial as periglacial sediments. Outstanding are the steep rock slopes and debris fans in the high mountain zone which are usually dominated by fast-moving landslide processes (reddish colors). Other exceptions represent the coastal areas at Låvan and Laslett which stand out by various and often thick Quaternary deposits, like glaciomarine (blue) and glaciofluvial products (orange). The Quaternary deposits and landforms are described in more detail in the following two sections.

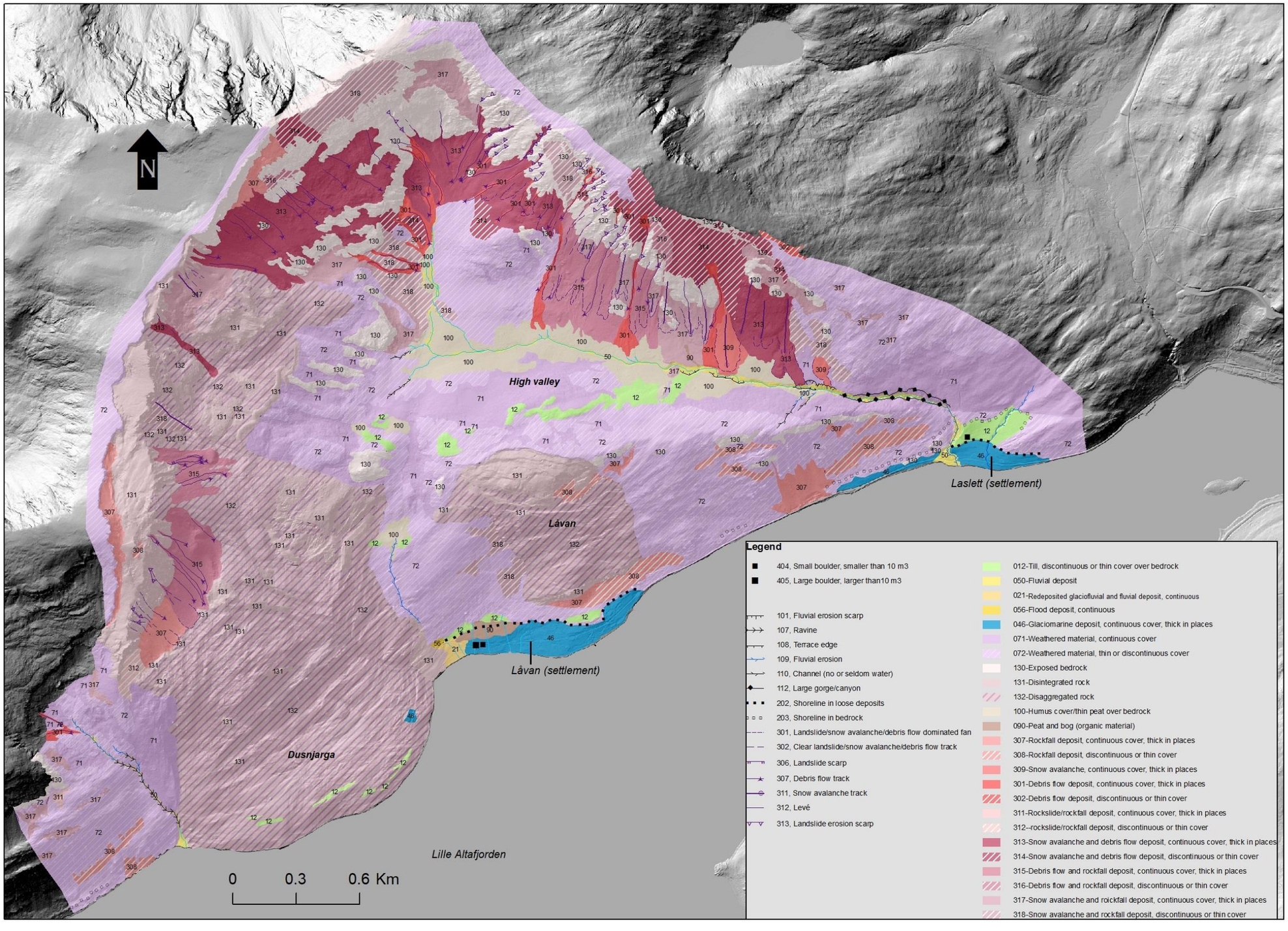

Figure 30: The created Quaternary geological map of the study area comprising the slope deformations Dusnjarga and Låvan.

7.2.2 Non-glacial Quaternary deposits and landforms

We divided the deposits and landforms presented in the Quaternary map (Figure 30) according to their origin into non-glacial and glacial/periglacial. The analyzes and descriptions for the latter category are much more detailed since these particularly allow to draw conclusions about the development during and after the last glaciation.

A. Exposed, disintegrated and disaggregated bedrock

In the Quaternary map (Figure 30), an area is classified as bedrock (pinkish colors) if Quaternary deposits are basically missing and bedrock covers more than 50 % of the area. In this case and if no significant slope deformation is noticed, it is classified as 'exposed bedrock'. Exposed bedrock is therefore only present at few patches outside the areas showing deep-seated deformation.

The deformation areas of Låvan and Dusnjarga are almost entirely covered by disintegrated and disaggregated bedrock. Especially at the head of both deep-seated deformations, the bedrock is still in-contact (disintegrated) whereas the central and foot zones of the deformation are usually covered by loose disrupted rock mass (disaggregated) occasionally interrupted by single outcrops of disintegrated rock (Figure 31). The proportion of rock mass disaggregation is generally higher at Dusnjarga than at Låvan.

Figure 31: The field picture from the central deformed area of Dusnjarga (view towards east) : centrally, one large block of intact bedrock (about 20 m in height) stands out, an example for disintegrated bedrock since it is located inside the DSGSD body. The disrupted rock fragments all around represent disaggregated bedrock which is characteristic for most parts of Dusnjarga below the head scarps.

B. Weathered rock material

In the Quaternary map (Figure 30), the class 'weathered material' (purple color) describes areas covered by loose bedrock material that was disaggregated through physical or chemical processes, but not through processes of deep-seated slope deformation. It is further separated between continuous and discontinuous cover depending on thickness (limit at 0.5 m) and covered proportion (50 %) of the area. Weathered material is the predominant type of surface cover of the non-deformed slopes and of the central high plateau/valley, typically consisting of weathered bedrock with a thin cover or vegetation and humus material. A good example for this is the south side of the central high valley above Låvan (Figure 32) which shows a gently undulating landscape of weathered rock material partially overlain by humus material and/or a thin cover of till.

Interpretation

The gabbroic rocks of the study area weather relatively fast. Therefore, flatter areas and slopes not steep enough for landslide processes are predominantly covered by weathered rock material.

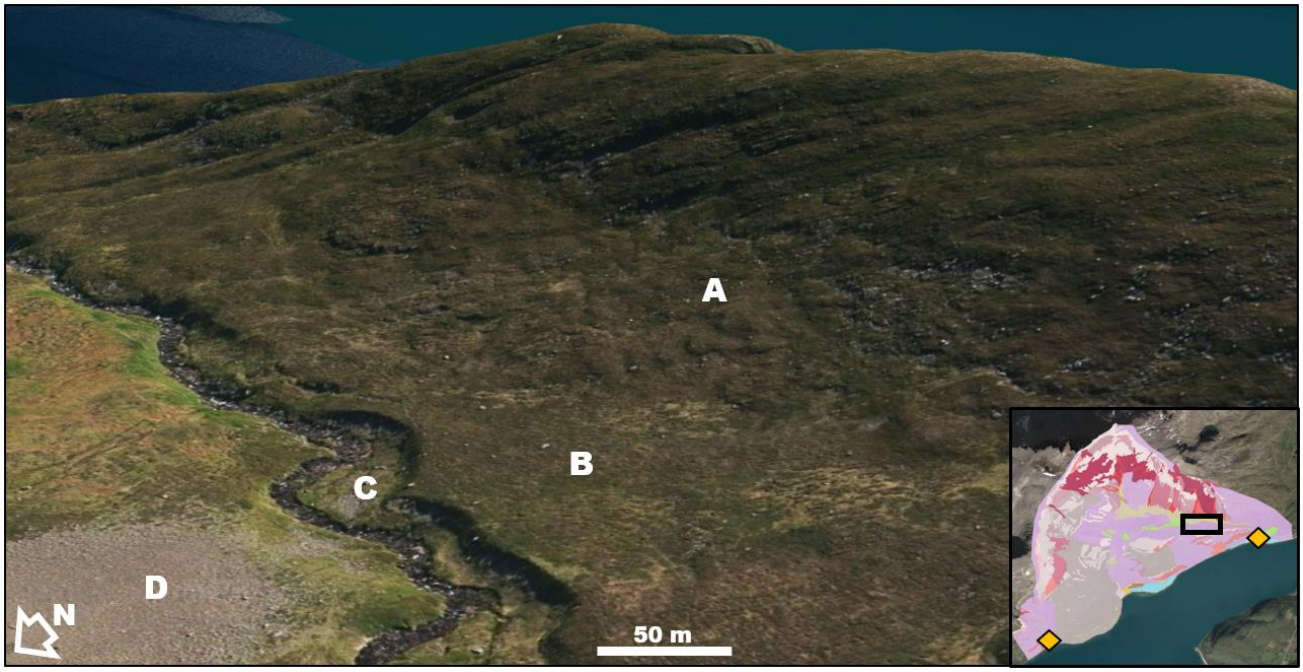

Figure 32: Aerial view (*ArcGIS Pro* model) depicting the typical landforms in the high valley (location = black rectangle): A – The southern side of the valley is characterized by a gentle undulating relief covered mainly by weathered bedrock material partly overlain by humus and/or thin till deposits. B – Especially closer to the river, the weathered rock material is covered by humus and peaty material. C – The river channel, flood plain and fluvial terraces are marked by fluvial deposits, mostly subrounded, gabbroic gravel and cobbles. Further locations with significant fluvial deposits are marked in the overview map (yellow diamonds). D – Debris fan of snow avalanche deposits, an example of landslide debris typical for north side of the valley (compare Fig. …).

C. Rockfall, debris flows and snow avalanches

Material from small- to medium-scale, fast-moving landslide processes (reddish colors) is classified in the Quaternary map (Figure 30) according to the dominating processes into snow avalanche, rockfall or debris flow deposits and according to continuity and thickness (see …). These deposits consist of loose debris and are deposited on steep slopes or as talus fans in front of these. Such debris occurs for example below the head scarps of Dusnjarga where debris flow tracks are well recognizable and along the steep, high mountainous slopes north of the central valley depicted in Figure 33.

Interpretation

At steep, rocky slopes, that are not subject to deep-seated slope deformation, the bedrock's high weatherability and high grade of dissection condition the formation of landslide deposits. Most likely their formation has been continuously going on since the last deglaciation.

Figure 33: Aerial view (*ArcGIS Pro* model) of the steep slopes at the northern side of the central high valley: These slopes and the north side of the river almost entirely overlain by debris from mass movements. A – Fan dominated by snow avalanche deposits, B – Fan dominated by snow avalanche and rock fall deposits from the cliff above. C – Debris flow track leading to tongue-shaped deposits from various debris flow events.

D. Peat, bog and humus cover

The category 'peat and bog' (brown color) classifies thick soils (thickness >0.5 m) formed by organic plant material. Peat is only found at one area close to the fjord overlying fine-grained glaciomarine deposits. Peat and organic material of 0.2 to 0.5 m thickness is classified as 'humus cover' (beige color) which in many places covers the weathered rock material in the central high valley (Figure 30).

E. Fluvial deposits and landforms

The class ‘fluvial deposits’ (yellow color) is defined as material deposited by streams and rivers typically found as flood plains, fans or terraces and usually dominated by well-sorted and -rounded sand and gravel. Fluvial deposits occur along the river in the central high valley and at its outlet at the settlement Laslett as well as at the outlet of the stream at the W-flank of Dusnjarga (Figure 30). Generally, streams, ravines and channels of fluvial erosion are mainly found outside the gravitationally deformed areas, e.g. in the inactive area between Låvan and Dusnjarga (Figure 30).

We investigated the fluvial deposits at the river outlet at Laslett which consist predominantly of gabbroic gravel and cobble (from angular to well-rounded) but contained as well some exotic lithologies (e.g. sandstone and gneiss).

Interpretation

The absence of surface run-off in the deformation areas is a recognized indicator for the disintegration of rock mass characterizing a DSGSD (e.g. Reitner and Linner 2009).

The characteristics of clasts and the absence of fine material indicates that the deposits at Laslett are of fluvial and not of glaciofluvial origin. The found sandstone and gneissic components must be however of glacial origin and were later incorporated in the fluvial deposits.

7.2.3 Glacial deposits and landforms

In order to analyze a most likely relative timeline of glacial, marine and rock slope deformation processes, it is important to focus particularly on Quaternary deposits with a glacial origin. The distribution of these units is highlighted in the map in Figure 34. During field work, we recorded eleven sediment profiles in these deposits and sampled each type of deposit. In this study, we present stratigraphic and sedimentological data charts as well as particle size distributions for selected profiles and samples from the most relevant deposits (locations in Figure 34).

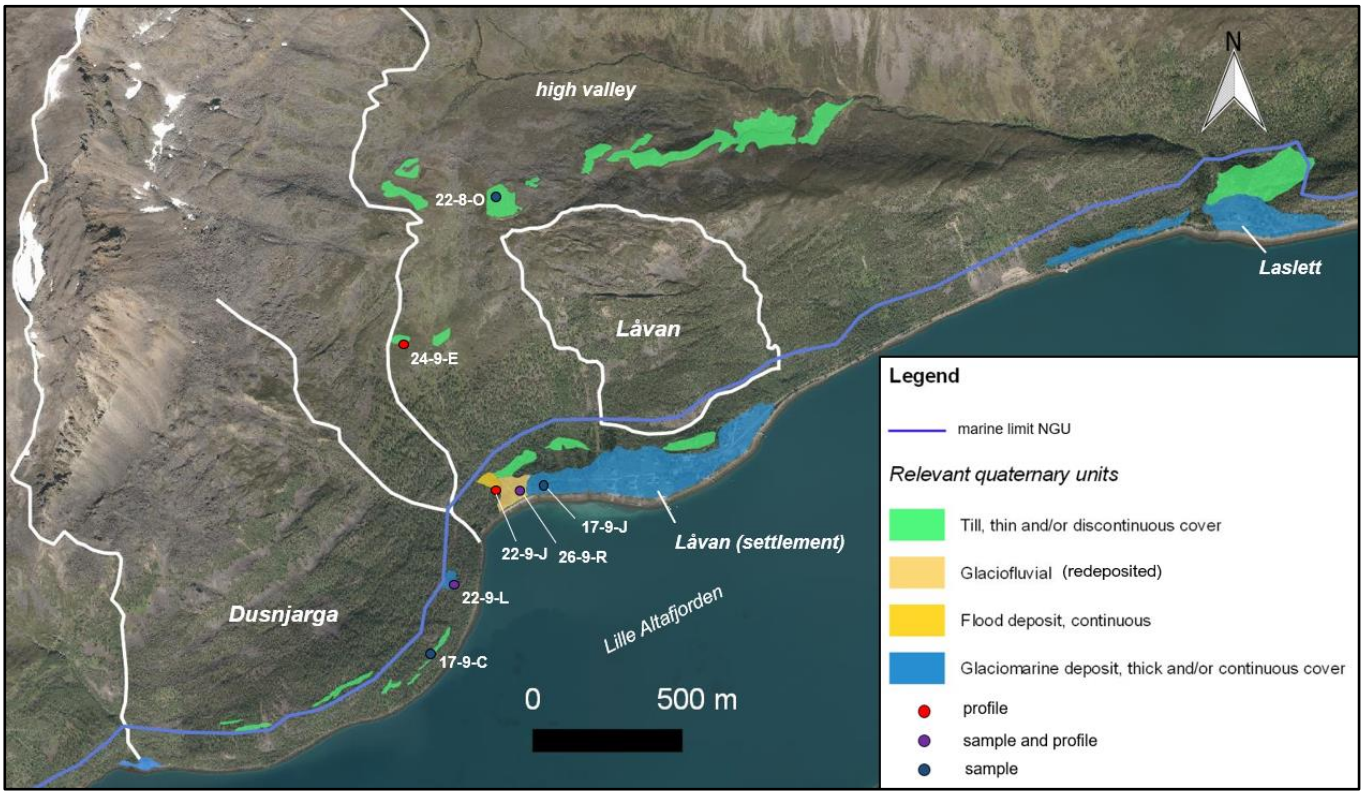

Figure 34: Map of the central study area depicting the marine locations of presented Quaternary profiles and analyzed sediment samples as well as distributions of the most relevant Quaternary deposits. The base map is the high resolution orthophoto overlain by the semi-transparent DEM.

The identification of non-local lithologies, that must be transported to the site of deposition by means of glacial processes, is an important indicator for inferring a glacial origin. Figure 35 presents handpieces of such identified non-local or ‘exotic’ lithologies that were found the most commonly in glacial deposits of the study area. According to the local geological maps (Roberts 1974; Roberts and Elvevold 2018), these litholgies (mostly variations of gneisses and metasandstone) dominate in the areas (orange) south of the Langfjord fault.

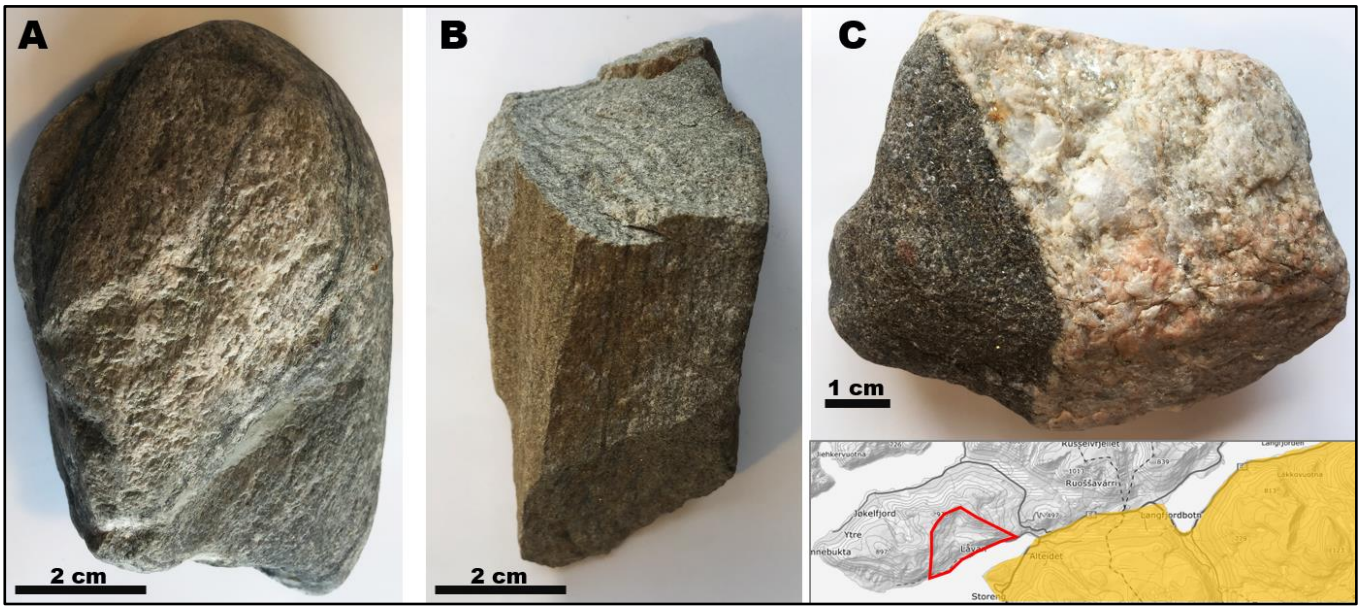

Figure 35: Examples of non-local/exotic clasts found in glacial deposits in the study area: A) Mylonitic quartz-feldspar gneiss: bullet-shaped clast found in glaciomarine deposits. B) Arkosic mica-rich metasandstone: clast found in glaciofluvial deposits. C) Granodioritic gneiss with pegmatitic dyke: clast found in glaciofluvial deposits. Overview map: red polygon = the study area, orange zone = area of provenance of the identified exotic lithologies.

A. Glacial till

As depicted on the maps in Figure 30 and 34, thin and/or discontinuous till (green color) is mapped in the southern part of the high valley and at several locations close to the fjord. In contrast to the original Quaternary map by NGU (Figure 7), thick or continuous deposits of glacial till do not occur in the study area.

- *Occurrence*

The southern part of the high valley has a rather flat, smoothly undulating landscape covered in the main part by weathered rock material (Figure 32). On protected, slightly elevated patches, protected from erosion, thin layers of till (thickness of 1-6 cm) can be found overlying the weathered bedrock and underlying the organic topsoil. Till was also identified at profile 24-9-E (Figure 39) which has a special location between high plateau and coast (270 m a.s.l.) on a shallow elevation forming the margin of a bowl-like depression (Figure 36).

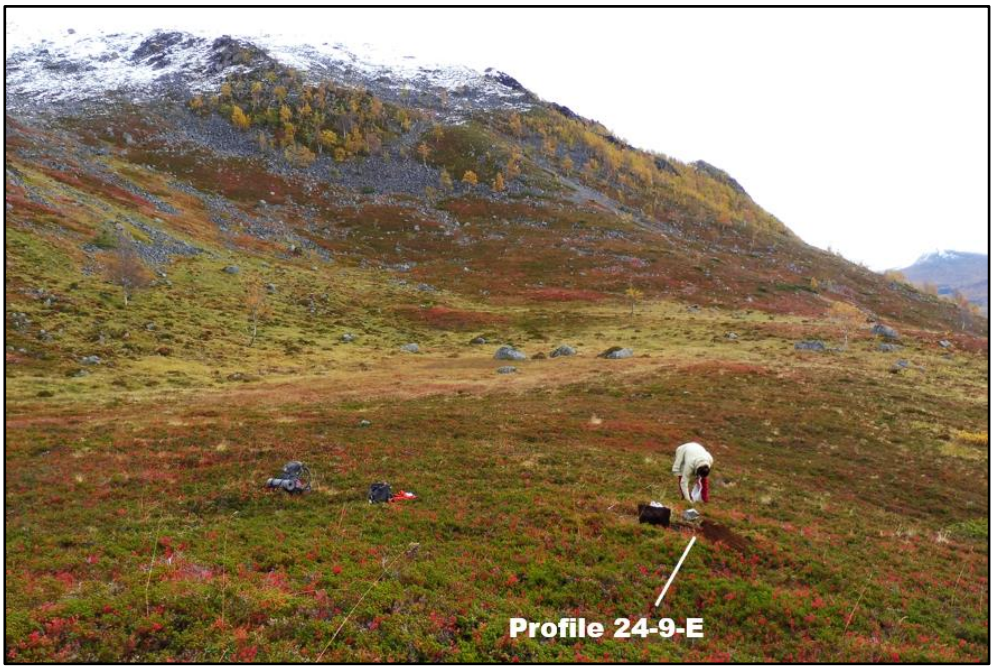

Figure 36: Morphology of the surrounding of profile 24-9-E situated in the gravitationally inactive area between Dusnjarga and Låvan. Till is found on the shallow, convex elevation in front of a peaty depression (center).

Furthermore, thin layers of till (1-10 cm thickness) are found at several locations closer to the fjord (Figure 34). They occur very irregularly on the frontal lobe of Dusnjarga limited to the flat, protected tops of terraces where the till overlies weathered and disaggregated rock (Figure 37A). The till layers are also found closer to the settlements Låvan and Laslett restricted to areas above a distinctive, gentle terrace at around 23 m a.s.l. (Figure 46) where the till also overlies weathered bedrock (Figure 37B).

Figure 37: A – Small profile on a terrace in the western frontal lobe of Dusnjarga. A grey layer (10 cm) of glacial till overlies reddish slope deformation products consisting of weathered gabbroic rock. B – A subrounded quartzitic-gneissic boulder found on a terrace where a thin till cover overlies weathered bedrock.

- *Characteristics and composition*

The till layers close to the fjord showed an obvious similarity to the high plateau tills. In all identified locations, the till was identified as thin layers of maximum 10 cm thickness showing a distinctive grey color, a considerable proportion of fines and/or fine sand, as well as clasts of different lithologies and grades of roundness. We identified several exotic lithologies (not from the study area) in these deposits, most prominently clasts of silvery, low-metamorphic sandstone as well as light-colored Gneiss which were typically subrounded to subangular and partly bullet-shaped.

Grain size distributions for selected samples of different Quaternary deposits are presented in Figure 38. This analysis includes a till sample from the high plateau (22-8-O) and a till sample from Dusnjarga's frontal lobe (17-9-C) (locations in Figure 34). The distributions for both types are relatively similar revealing relatively low, but significant shares of small grain sizes. The high share of clasts is partly due to subrounded, exotic lithologies, but mostly to gabbroic slope deformation products either mixed into the till layer or from the neighboring strata. The glacial till layers from the frontal lobe (e.g. Figure 37A) have a slightly higher share of gabbroic clasts and lower share of fines than the tills from the high valley as perceived in the field but also in the grain size analysis.

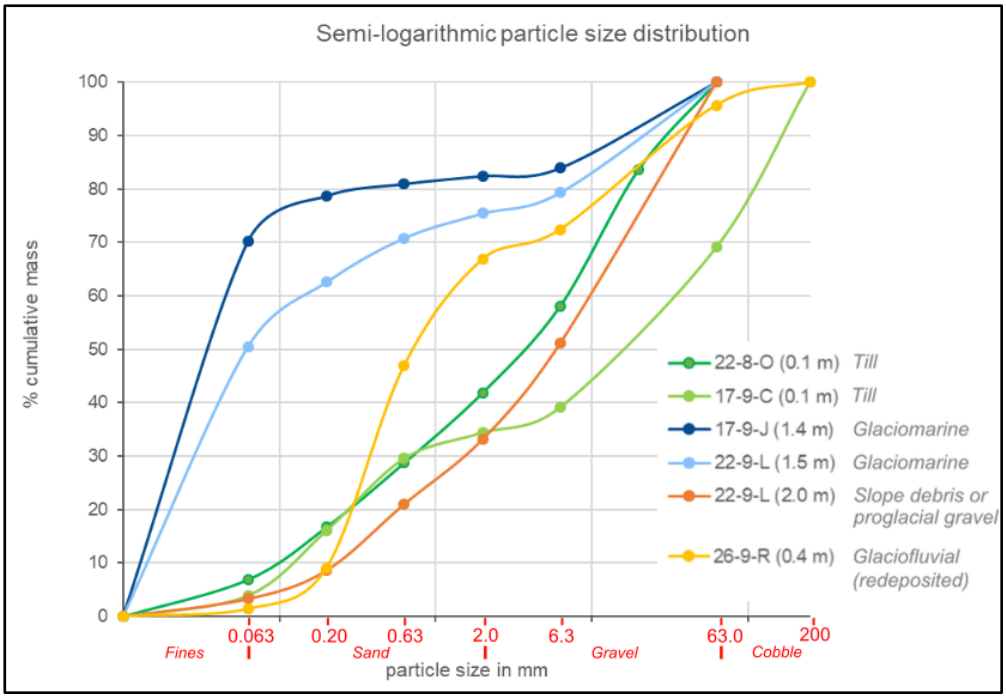

Figure 38: Results of the particle size analysis for six different Quaternary deposits obtained from wet-sieving: the results are presented as cumulative masses (of all finer fractions) and as semi-logarithmic distributions. The sample locations are displayed in Figure 34 and three of the analyzed samples were recovered from sediment profiles presented in this chapter. The fraction "fines" includes the clay and silt fraction which is not separable through sieving. The occasional occurrence of cobble could not be quantified for 22-9-L (1.5 m) and for 17-9-J (1.4 m), for this larger sample sizes would have been needed.

In Figure 39, a sedimentological data chart for profile 24-9-E (Figure 34) is presented. It includes a distinct grey till layer (unit III) which has very similar characteristics as the grey till layers found in other locations. As depicted in Figure 39, the till layer contains clasts of varying lithology and roundness including a high proportion of gneissic, subrounded clasts. The till layer overlies a diamicton (unit II) with a deep brown color in its upper part and with clasts dominated by subrounded gabbroic gravel.

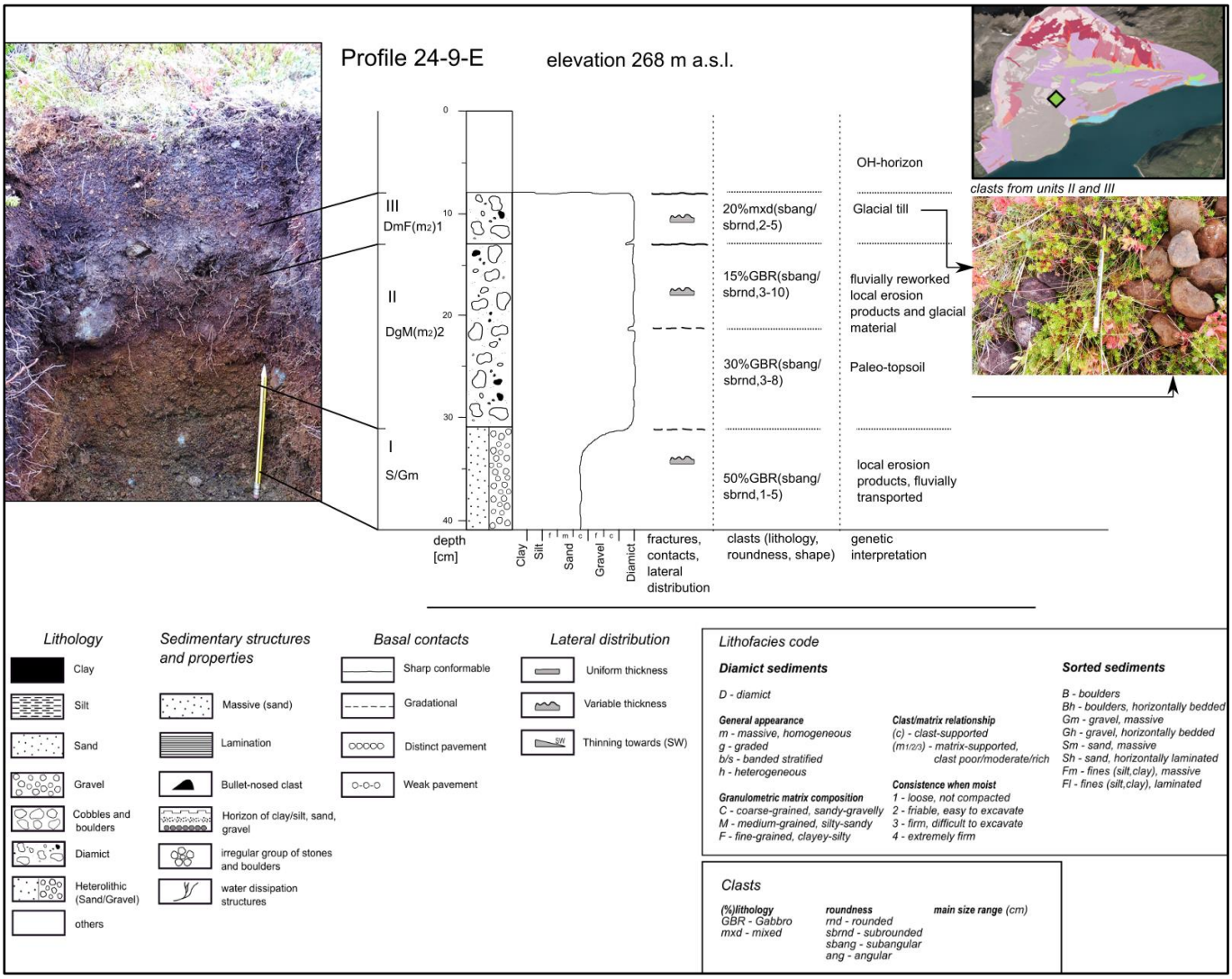

Figure 39: Stratigraphic and sedimentological data chart for profile 24-9-E situated between Låvan and Dusnjarga close to the high plain (location in Figure 34). The distinct grey layer (unit II) with a high share of fines is interpreted as glacial till, found in similar expositions at other locations in the study area. Below: the legend for all the presented profiles.

- *Interpretation*

The afore-described deposits are generally classified as glacial till due to their diamictic composition characterized by significant shares of fines and fine sand as well as by clasts of both local and exotic lithologies. The latter lithologies (mainly gneiss and sandstone) must have

been transported by glaciers since they do not exist in the local bedrock, but at locations further S and E (S of Lille Altafjorden and Langfjorden) (Roberts 1974). Their often subrounded and bullet-like shapes support their glacial provenance. We also observed that the weathering of the mentioned, mica-rich metasandstone is mainly responsible for the grey color and high sand content of the till. A more detailed classification of the till is complicated by the absence of structures, but the properties as the low grade of compaction and homogenous distribution as thin layers suggest a classification as a subglacial meltout till (e.g. Dreimanis 1989; Lukas and Rother 2016).

However, the sandy matrix with a relatively low share of fines, the low grade of compaction and the relatively high content in locally derived clasts might also indicate a possible reworking of primary deposits through e.g. melting processes. Thus, the definition as 'till' might be critical and a classification as secondary ablation diamicton could be more appropriate (Lukas and Rother 2016). This counts especially for the deposits on the terraces close to the fjord, e.g. on Dusnjarga's the frontal lobe, since these locations are situated below the pre-Holocene shoreline elevation. Nonetheless, on the Quaternary map the classification as glacial till is kept since these deposits are certainly primarily or secondarily formed by glaciers, thereby referring to a broader definition of the term till, e.g. by Dreimanis (1989).
Since all the identified glacial till deposits were found directly below the topsoil, they were most likely created during the last phase of glaciation which ended locally between 15 and 13 ka (section 4.3).

In the central high valley, the described morphology (Figure 32) and island-like distribution of glacial till was most likely created through a braided river system that dominated the valley during the glacial retreat and shortly after. Braided river systems are typical for proglacial settings and are important morphologic agents by exerting strong deposition and erosion through the frequent shift of channels and erosion of river banks (e.g. Bristow and Best 1993). To the north of the river, potential glacial tills were not identified due to burying under the more recent landslide debris (Figure 33).

The deep brown diamicton underlying the grey tills in profile 24-9-E (Figure 39) is interpreted as a paleo-topsoil preserved from an interstadial before the last glacial maximum.

We did not find till or glacial products in the high elevation zones (above 500 m a.s.l.) and around the mountain tops. This and the vast existence of block fields indicate that during the last glaciations, these zones were probably covered by cold-based ice leading to very little erosion rates (e.g. Linge et al. 2006; 2007; Fjellanger et al. 2006). Its existence as a nunatak is less likely because of the relatively low elevations (maximum below 1000 m a.s.l.) (e.g. Olsen et al. 2013; Sveian 2004).

B. Glaciomarine deposits

- *Occurrence*

As visible on the Quaternary map (Figure 30,34), continuous glaciomarine deposits (blue color) are generally found proximal to the fjord at two locations around the settlements Låvan and Laslett. These coastal locations are relatively flat and outside of the gravitationally deformed slopes. Strikingly at these locations, the deposits stop accurately at an elevation of about 27 m a.s.l. where a morphologically distinct terrace starts. To the west of Låvan, the glaciomarine deposits are overlain by (redeposited) glaciofluvial and flood deposits (e.g. Figure 42).

The glaciomarine deposits identified at profile 22-9-L (Figure 41, location in Figure 34) represent a great exception from this general distribution because this is the only location where we identified the glaciomarine deposits inside the active deformation area and also at a higher elevation (53 m a.s.l.).

- *Characteristics and composition*

The glaciomarine deposits found at the lower locations close to the settlements have typically a thick cover of at least 1 to 2 m and maybe significantly (observed e.g. at profile 17-9-J). At these locations, deposits are found as massive silty clays with a quite consistent composition.

Profile 17-9-J (Figure 40) is a representative example for which the grain size distribution was analyzed (Figure 38): the grey glaciomarine deposits are characterized by a high content of fines (around 70 %) and a considerable share of clasts. Cobble- and boulder-sized clasts of non-local, often gneissic, lithologies occur frequently (not included in grain size analysis), are often bullet-shaped (e.g. Figure 35A) and usually show striations. Outstanding are two large boulders (Figure 40B) found among these deposits that consist of garnet-bearing Gneiss and quartzitic Metasandstone (non-local) and are heavily striated. However, the gravel-sized clasts in the glaciomarine mud consist exclusive of angular to subangular gabbro clasts.

The silty clays have an abrupt upper contact either to the organic layer (Figure 40) or to the (redeposited) glaciofluvial products (Figure 42). As observed in profile 17-9-J, the silt and fine sand contents increase towards the top of the deposit whereas the clast content decreases. The silty clays have a massive appearance showing water dissipation structures but no other recognizable sedimentation structures.

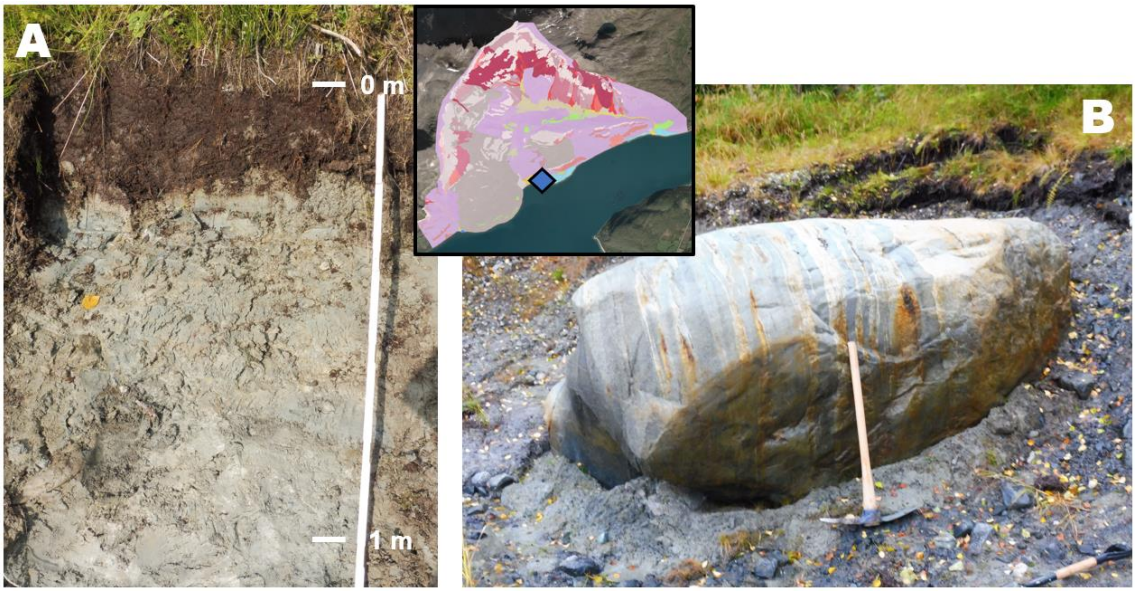

Figure 40: Glaciomarine deposits. A – Upper section of profile 17-9-J: a typical example for the glaciomarine deposits in the study area. Massive grey clay directly under the topsoil. This profile was sampled for grain size analyses. B – A large glacial boulder amidst the glaciomarine deposit (directly next to 17-9-J): The lithology is garnet-bearing gneiss and the boulder shows clear signs of glacial transport, such as numerous striations.

The glaciomarine deposits are also found at the outstanding location at profile 22-9-L and are presented in the sedimentological data chart in Figure 41. The glaciomarine deposits (unit II) are less thick in this location and dip towards SW (as do all units in this profile). The deposits' composition (22-9-L 1.5 m; Figure 38) is generally very similar to the glaciomarine deposits identified at lower elevations (e.g. profile 17-9-J), but the content in silt, sand and gabbroic gravel is higher. They have similar clast properties and show also dissipation structures. The deposits show a lower abrupt contact to a massive, strongly compacted deposit of coarse gabbroic gravel (unit I; Figure 41) for which the grain size distribution is also presented (22-9-L 2.0 m; Figure 38). The upper contact of the glaciomarine deposits in profile 22-9-L (Figure 41) is very gradual marked by decreasing compaction and an increase in silt, sand and gabbroic components. In the top of the profile, the deposits are gradually overlain by a clast-supported diamicton dominated by angular gabbroic components.

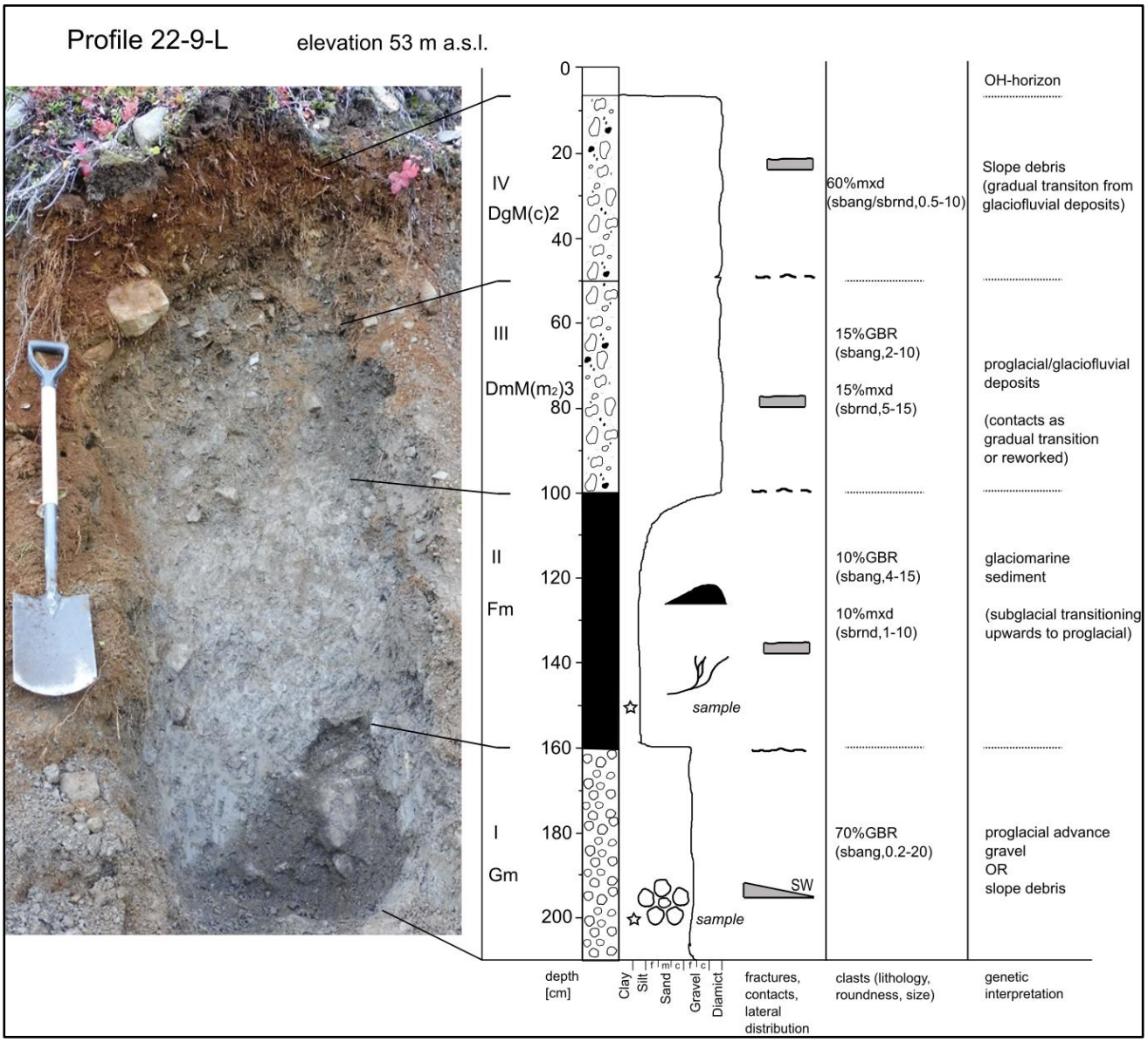

Figure 41: Stratigraphic and sedimentological data chart for profile 22-9-L situated at the eastern frontal lobe of the actively deforming area of Dusnjarga (location in Figure 34). It was the only location where glaciomarine together with glaciofluvial products could be identified inside the deformation area. Two samples were taken and analyzed for grain size (Figure 38). Legend presented in Figure 39.

- *Interpretation*

Clear indicators for the glacial origin of the described massive silty clays are the clast characteristics (the variety of lithologies, subrounded and bullet-like shapes, striations), the two large, striated boulders and the water dissipation structures. The domination of clayey and silty material indicates a marine, and thus glaciomarine, origin. Structures such as lamination could be expectable in such deposits but are often destroyed by bioturbation (Benn and Evans 2014).

The sediment must have been deposited in the last phase of glaciation when temperate glaciers filled the inner fjord systems, and which ended around 15 – 13 ka (Figure 8). Such glaciomarine sediments have usually different sources: subglacial meltwater streams flushing out basal sediments into the fjord tend to be the most important sediment source at temperate glacier margins (Powell and Domack 1995). The contribution of buoyant fresh water plumes of suspended sediment load is also very common in deglaciated fjord settings (Benn and Evans 2014; Nemec et al. 1995). The frequent occurrence of glacial cobbles and the two boulders speaks (at least partly) for an origin through ice-rafting and/or subglacial melting processes which provenance would classify the deposit as a dropstone mud or undermelt diamicton (Benn and Evans 2014; Powell and Domack 1995).

Coarsening upward as well as decreasing compaction was identified in the glaciomarine deposits at both lower (profile 17-9-J, Figure 40) and higher elevation (profile 22-9-L, Figure 41). A suggested reason for this observed increase in the silt and sand fraction is the progressing retreat and stronger melt processes of the fjord glacier leading to a gradually higher contribution of subglacial melt processes, ice-rafting and glaciofluvial input from the slopes. This later phase of formation of the glaciomarine sediments might correspond to Younger Dryas phase when the fjord glacier was based further back in the fjord. The relative fall in sea level should have led, additionally to the glacier retreat, to a gradually increasing sediment contribution from land. This transition becomes especially clear at profile 22-9-L (Figure 41) which is located just below (53 m a.s.l.) the expected Younger Dryas sea level and where the glaciomarine clay transitions upwards into a glaciofluvial diamicton. This diamicton is on the other hand more and more dominated by gabbroic, angular debris from the slope deformation which might further indicate an increasing slope deformation at Dusnjarga following the glacial retreat.

In profile in 22-9-L (Figure 41), a further important detail concerning the relation of slope deformation to the last glaciation is the abrupt basal transition of glaciomarine deposits to coarse, massive gravel (1.6 m depth). On one hand, this gravel may be interpreted as connected to glacial advance, accordingly as proglacial advance gravel. The gravel might however also represent older, local slope debris that was preserved under little erosive ice. Hence, further investigations of this basal contact and the according deposits would be of great importance due to their potential role in explaining the temporal activation of Dusnjarga's slope deformation in relation to the last glaciation.

C. Redeposited glaciofluvial and fluvial deposits

- *Occurrence*

As depicted in Figure 34, redeposited glaciofluvial occur together with fluvial deposits (beige polygon) in a zone close to the coast below the central, inactive slope between both deformation areas. To the north, these deposits start at an elevation of about 24 m a.s.l. and stretch down to the current shoreline. To the west, the deposits are limited by the slope deformation of Dusnjarga. The deposits overly the glaciomarine muds in most locations (e.g. Figure 42) and gradually thin out towards E.

- *Characteristics and composition*

The redeposited glaciofluvial and fluvial deposits are principally dominated by massive gravel and sand and show a high spatial variability in thickness and composition. Profile 26-9-R (Figure 42), situated close to the shore (Figure 34), is a representative example for the deposits. The (glacio-)fluvial deposits (unit II) consist here of massive, homogeneous, grey to brown sands that have a sharp lower contact to the glaciomarine mud (unit I) as well as a sharp upper contact to unconsolidated, massive gravel deposits dominated by angular gabbroic clasts. No sedimentation structures were recognizable in the profile. Inside the glaciofluvial sequence (unit II) occur two gravel-bearing layers: one between 0.57 and 0.60 m containing fine to medium, angular gabbroic gravel, and another layer between 0.25 and 0.4 m. For this second layer, a grain size distribution was analyzed (Figure 38) resulting in a gravelly sand. The clasts in this layer are typically subrounded and show a high lithological variation including gabbro, quartzite, gneiss and sandstone clasts (Figure 42).

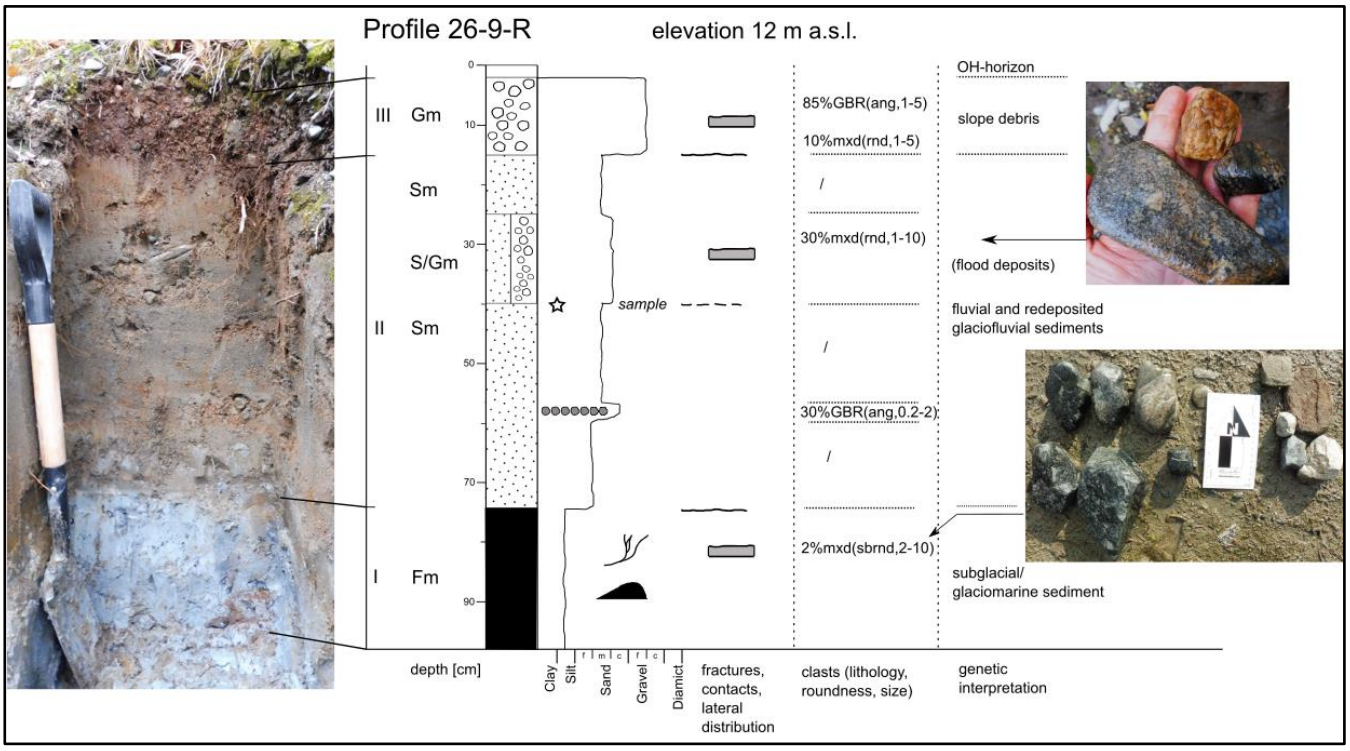

Figure 42: Stratigraphic and sedimentological data chart of profile 26-9-R located close to the present shore and in the inactive zone between the deformation areas (location in Figure 34). Massive sandy deposits (sample in Figure 38) overly firm grey clays, whereby both deposits include clasts of clear glacial origin. Legend presented in Figure 39.

Apart from the latter profile, we investigated several other profiles in these deposits and particularly four further profiles along a NW-trending transect line in order to characterize the spatial variations of the deposits. These results are summarized using a schematized profile line (Figure 43A) that runs from profile 26-9-R up to an elevation of 24 m a.s.l., the locally highest elevation where these massive sands and gravels as well as the underlying glaciomarine muds were recorded. Figure 43A shows that from SE to NW the massive sands become more and more enriched in gravel clasts of increasing size and various lithologies. Moreover, the proportion of gabbroic coarse sand and gravel grows with increasing elevation and is mainly concentrated on a central horizon which can be seen as a reddish layer in profile 26-9-R (0.57 – 0.6 m) and in profile 26-9-O (Figure 43B). Compared to profile 26-9-R, profile 26-9-O demonstrates the significantly coarser character of the deposits (sandy gravel) at this elevation (19 m a.s.l.). Along the whole profile line, the described sand and gravel deposits are underlain by glaciomarine mud (thickness not determined).

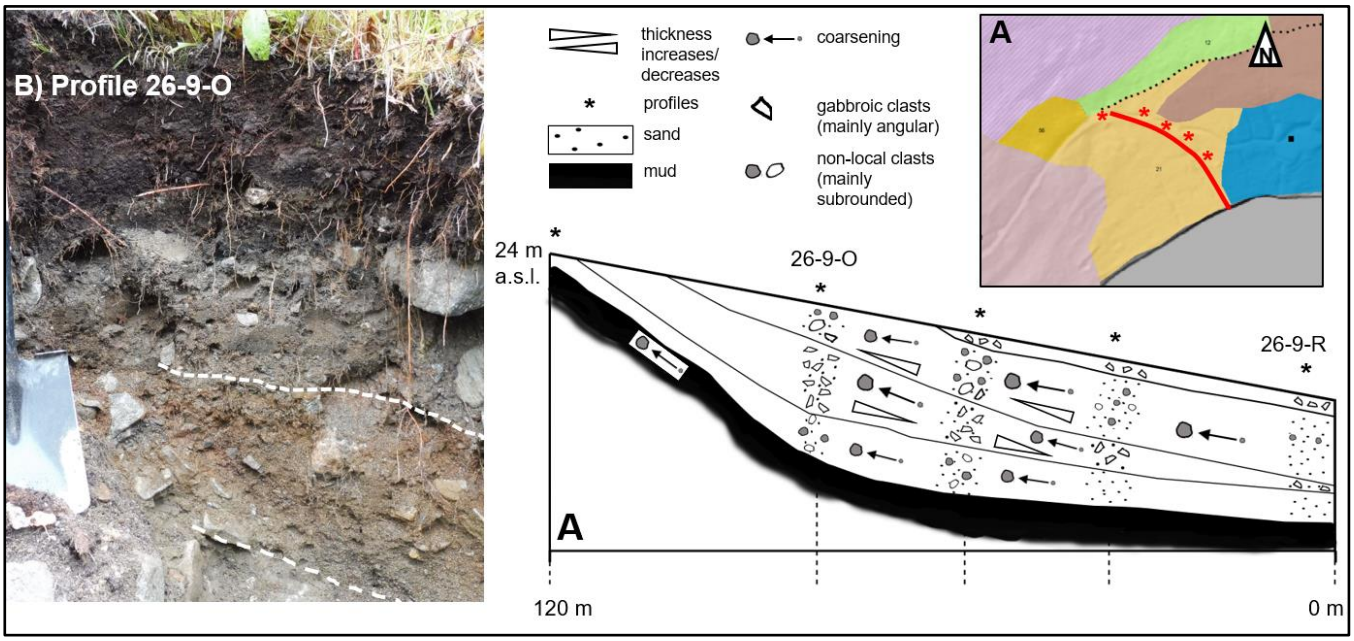

Figure 43: A) Schematized profile view of the sediment sequences in the central study area (location in right upper corner): The profile focusses on the glaciofluvial deposits which were logged at several positions (*; compare Figure 34) and for which the sedimentological variations are displayed along the profile. The profile is not true to scale. B) Profile 26-9-O which includes variating contents of glaciofluvial products and slope debris. The delimited sequences correspond to the schematized sequences in (A). The thickness of the glaciomarine mud is not known.

Interpretation

The described sediments have a fluvial origin which is expressed in the recorded stratification, the rounding of clasts, the grain size distribution (dominantly sand and gravel) and its variations along the analyzed profile (Figure 43A). The high proportion of typically subrounded clasts of exotic lithologies, which are found in all profiles of these deposits (e.g. Figure 42), indicates the incorporation of glacial material and therefore are these deposits interpreted as a combination of redeposited glaciofluvial and fluvial deposits.

The deposits are interpreted to have been deposited at a river outlet or small delta when the sediment-loaded flood met the waterfront at the former shoreline. This explains abrupt stop of these deposits at 24 m a.s.l., the presumed paleo-shoreline, and the fining of grain sizes with increasing shore distance. The sedimentation limit at 24 m a.s.l. fits to the elevation of the prominent paleo-shoreline identified at several locations in the study area (e.g. Figure 45). As described in detail in subsection E, this shoreline must have been created during the Early to Mid-Holocene and corresponds most likely to the Tapes transgression.

D. Flood deposits

- *Occurrence*

The afore-described (glacio-)fluvial deposits stop at an elevation of 24 m a.s.l. above which elevation the slope abruptly steepens. As indicated in the map in Figure 34, laminated or sheeted strata of flood deposits (yellow polygon) are found in a small area above this elevation (profile 22-9-J).

- *Characteristics and composition*

Figure 44 presents the analysis of profile 22-9-J which includes the mentioned sequence of sheeted flood deposits (unit II). The sheet flood deposits have a thickness of 15 to 20 cm, are well-sorted and show upward-fining. The lowest layer consists of fine-medium gravel which is overlain by a medium layer of sandy gravel with an upward-increasing sand content. The uppermost layer is formed by greyish colored silty sand, generally fine sand with an upward-increasing content of silt and a small share of fine to medium gravel. The clasts in the laminated flood deposits show a great variation from round to angular clasts, mostly from gabbroic lithologies but also from non-local (e.g. gneissic). The laminated strata have an average dip direction of 107° (dip angle of 29°).

The upper and the lower contact of these sheeted deposits is very abrupt. They are topped by reddish, unsolidified sandy gravel (unit III) with a chaotic structure and mostly coarse gravelly, angular components of gabbroic lithology. The deposits below the flood deposits are formed by subrounded gabbroic cobble (unit I) which is stacked in a very solid way.

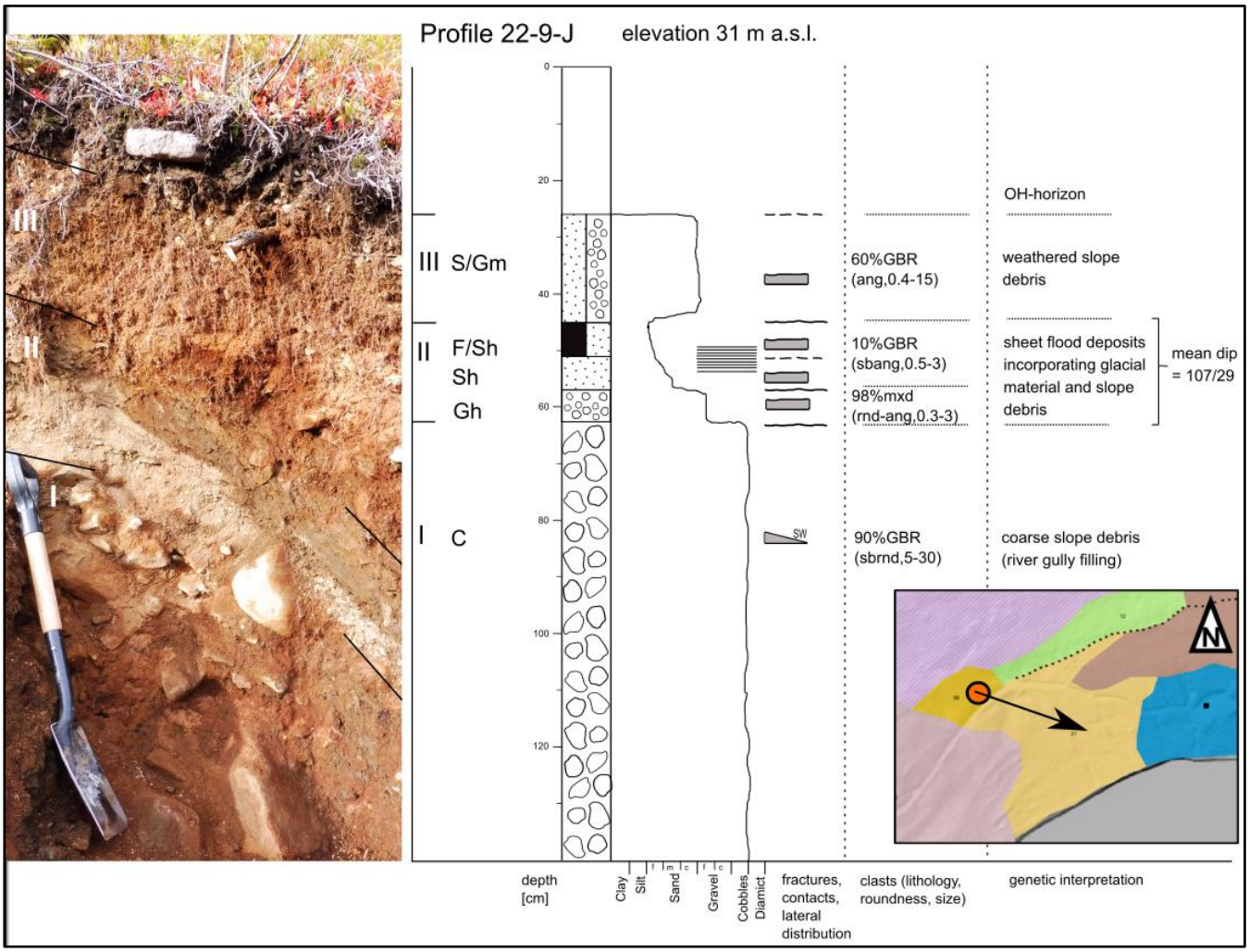

Figure 44: Stratigraphic and sedimentological data chart of profile 22-9-J situated directly east of Dusnjarga's eastern lateral limit (location in small map). A sequence of laminated deposits (unit II) is interpreted as sheet flood deposits, dipping towards ESE (arrow in map) and fining upwards from gravel to fines. Legend presented in Figure 39.

- *Interpretation*

The described sediment structures of unit II in profile 22-9-J (Figure 44), especially the lamination or sheeting and the grain size distribution, lead to the classification as a flood (or sheet flood) deposit. Unit II represents one complete fining upward sequence that probably goes back to one large flood event. Using the classification by Hungr et al. (2014), the deposit's genesis can be described by the term 'debris flood', a water flow in a steep channel that is very rapid and heavily charged with debris. As indicated in Figure 44, the recorded ESE-orientation of these sheeted deposits points directly towards the fluvial and redeposited glaciofluvial deposits found below 24 m a.s.l. (subsection C). Therefore, both deposits should be linked in their origin and whereby the deposits below 24 m a.sl. probably reflect a longer time range of sedimentation which is not only limited to one flood event. Correspondingly must the sheeted flood deposits (Figure 44) have been deposited just above the former (Tapes) shoreline.

Additionally, the greyish fine sandy and silty material forming the top of the sheeted flood deposits (Figure 44; unit II) resembles strongly the fine glacial deposits found on the high plain (subsection A) which further induces a relocation of glacial material. The thin greyish fine material found on terraces at lower elevation (Figure 37) might be also linked to the responsible flood event.

The underlying compacted cobble (unit I) can probably be interpreted as coarse slope debris due to the local lithology. The rounding and almost absence of matrix might indicate a gully filling of unknown age. The unsolidified gabbroic gravel (unit III) which overlies the flood deposits represents weathered slope debris, probably considerably younger than the flood deposits due to its loose character.

E. Raised shorelines

- *Occurrence*

Two distinct sets of raised shorelines were identified at several locations which are termed in the following 'Shoreline 1' (23 – 25 m a.s.l.) and 'Shoreline 2' (60 – 62 m a.s.l.). Both shorelines stood out by very consistent elevations and are indicated in Figure 45 as well as in the created Quaternary geological map (Figure 30).

Shoreline 1 is well expressed along the entire coast of the study area with exception to the gravitationally deformed slopes (e.g. the frontal lobe of Dusnjarga). Shoreline 1 is especially well recognizable at the loose deposits at Låvan and Laslett (e.g. Figure 46).

Laslett is the only location where Shoreline 2 is clearly expressed above Shoreline 1, but it is also indicated at the steep slopes between Låvan and Laslett.

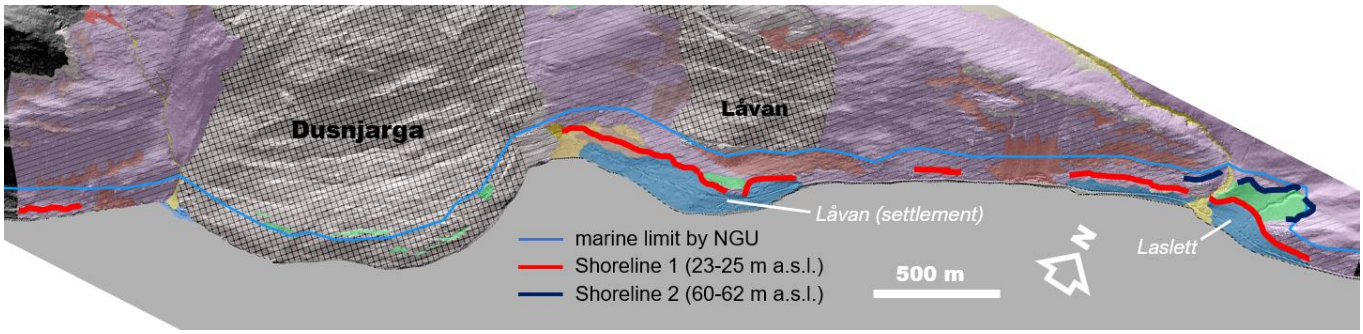

Figure 45: Distribution of the identified raised shorelines (Shoreline 1 and Shoreline 2). Base map is the compiled Quaternary map (Figure 30). The marine limit that was interpolated by NGU matches well Shoreline 2.

- *Characteristics and morphology*

Around the settlements of Låvan and Laslett, Shoreline 1 forms morphologically distinct convex terraces between 23 and 25 m a.s.l. (Figure 46). These terraces are formed by highly weathered rock material and are mostly draped by a thin layer of till. Apart from the sheet flood deposits (Figure 44) which occur just above this terrace, the distribution of all thicker glacial deposits (glaciomarine and glaciofluvial) is delimited by these terraces (Figure 45). But Shoreline 1 is also expressed as a shore-parallel, erosional notch in bedrock on the steep rocky slopes W of Dusnjarga and E of Låvan.

At Laslett, Shoreline 2 forms between 60 and 62 m a.s.l. the upper limit of the morphologically smooth slope (highly weathered bedrock covered by thin till) towards steeper slopes of more intact rock (Figure 46). At this elevation, shore-parallel erosional notches can be further observed at the steep rock slope between Låvan and Laslett, however less clearly expressed as Shoreline 1.

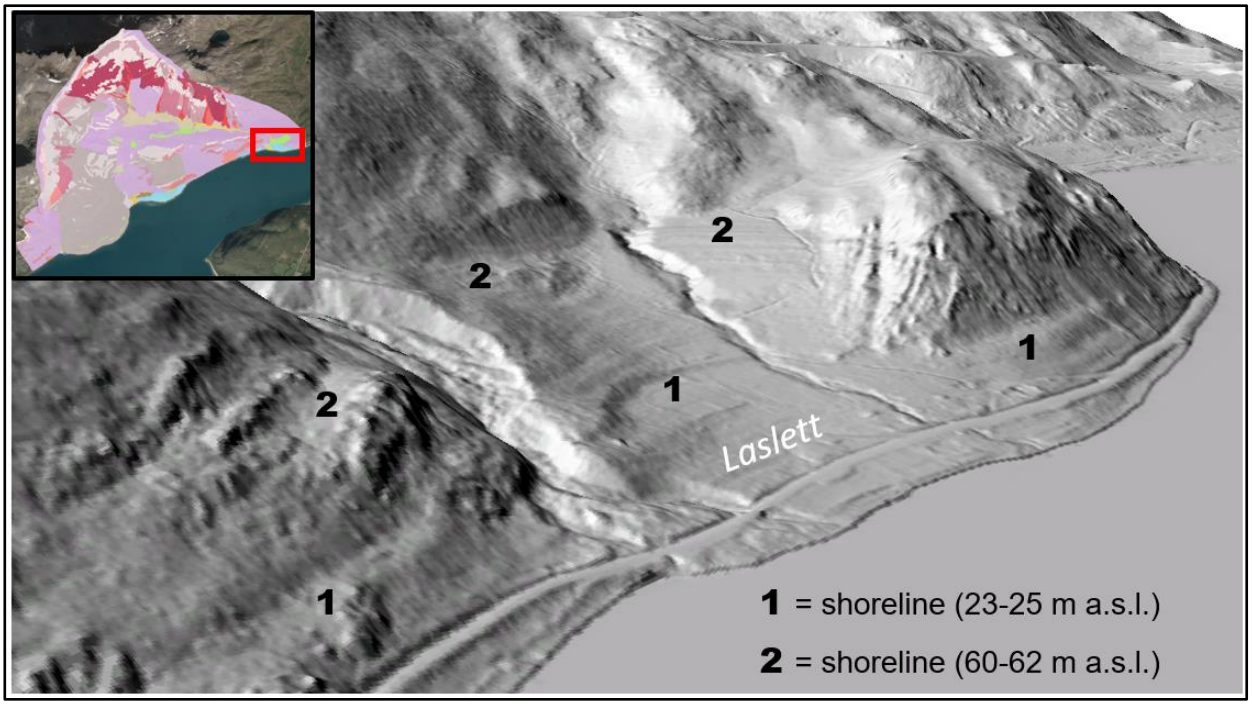

Figure 46: Geomorphological expression of paleo-shorelines at Laslett (eastern study area): a lower (1) and a higher (2) shoreline are morphologically well expressed in the digital elevation model, especially in the presented 3D-view.

- *Interpretation*

The elevation (23 – 25 m a.s.l.) and character of Shoreline 1 indicate that it is likely to correspond to the Tapes shoreline (section 4.3.3), a post-glacial shoreline going back to the Tapes transgression (Vorren et al. 2008). For instance, Corner and Haugane (1993) identified the Tapes shoreline as terraces or notches at 21 – 22 m a.s.l. in central Lyngen (Troms), an

area with a comparable isostatic uplift. Bondevik et al. (2019) dated the Tapes transgression maximum between 7600 and 5600 cal yr BP.

The elevation of Shoreline 2 between 60 and 62 m a.s.l corresponds well to the marine limit interpolated by NGU (Figure 45). Additionally, ice contact sediments recorded in the neighboring fjords at similar elevations (64 – 72 m a.s.l.) were interpreted by Evans et al. (2002) to represent the Main shoreline. Thus, Shoreline 2 should be interpreted as the Main shoreline. The Main shoreline was created during the Younger Dryas period and is mostly expressed as erosional notches (as here) in bedrock (Vorren et al. 2008). At many Norwegian coastal locations both Tapes and Main shoreline can be found (Vorren et al. 2008).

No raised shorelines were recognizable on the frontal lobe of Dusnjarga where compressional deformation features dominate. Most likely, the formerly expressed shoreline was overprinted and overrun by the slope deformation which is a further indicator for the slope deformation at Dusnjarga after the formation of these shorelines (after 7 ka).

7.3 Structural analysis of the deformation area Låvan

The analysis of structural data is a fundamental part in order to understand the nature of the gravitational deformation at Låvan. For the performed analysis, structural data is used from outcrops in the deformation area as well as in the stable area surrounding Låvan. In this work, the orientation data is always presented as dip angle and dip direction in degrees.

Figure 47 presents the location of the outcrops where the implemented structural data was collected. The data comprises 846 discontinuity plane measurements: 483 recordings for joint and 363 for foliation planes. The outcrops can be divided into two groups for which the structural data is presented separately. The first group is represented by five outcrops in the deformation area (highlighted zone) including two in-situ outcrops at the head scarp (22-8-L, 24-9-U) and three outcrops in disintegrated (displaced) bedrock. Secondly, data is presented for seven in-situ outcrops in the stable eastern part of the study area (including the stable head scarp). The result presentation for these in-situ outcrops differentiates between outcrops at low and at higher elevation (</> 200 m a.s.l.) since a high control of elevation on the pattern of structural data was observed.

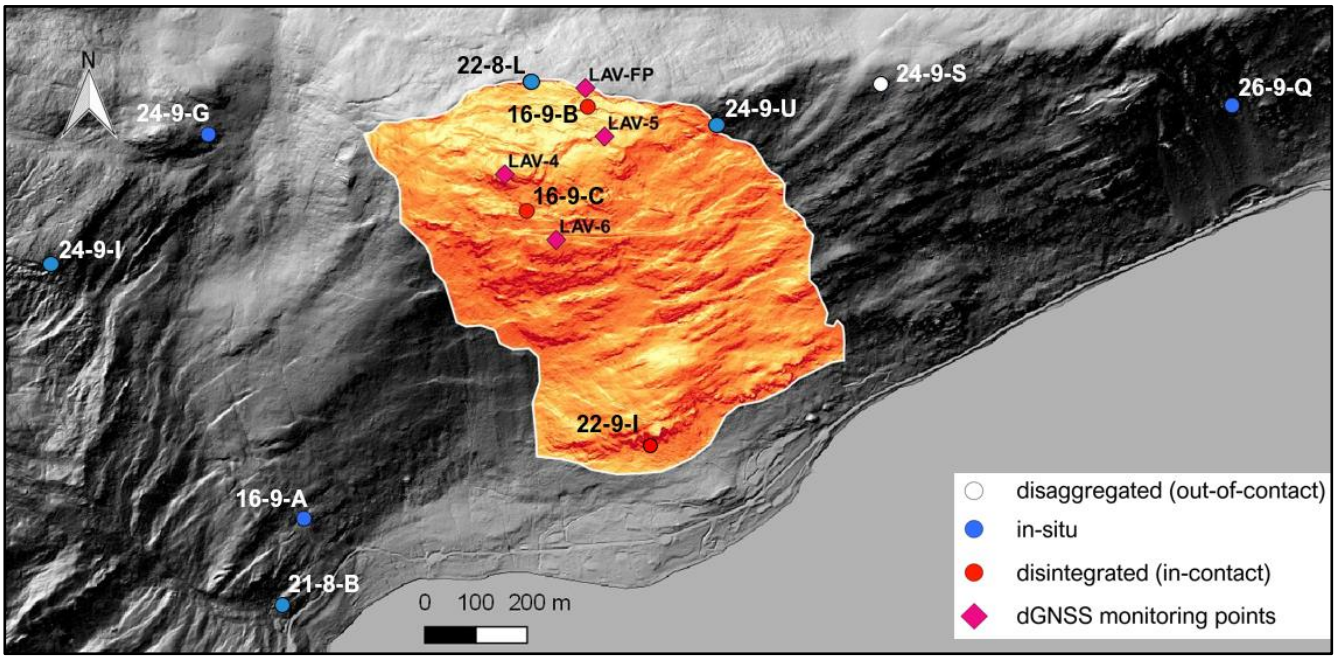

Figure 47: DEM of Låvan and its surrounding depicting the locations of dGNSS monitoring points (diamonds) and the outcrop locations (points) for which structural data is analyzed in this chapter. These outcrops are classified into disaggregated, disintegrated and in-situ bedrock (see section 7.2.2). Most important are measurements inside the deformation area of Låvan (typically disintegrated bedrock) and in-situ outcrops from the inactive surrounding and head scarp (blue dots) serving as a direct comparison to the displaced outcrops.

- ***Foliation planes***

Figure 48 presents the data of foliation planes for gravitationally inactive outcrops in the surrounding of Låvan (A) and for outcrops in the deformation area of Låvan (B).

For the inactive area (A), the foliation planes show a significantly different pattern depending on the elevation. Foliation planes at elevations above 200 m a.s.l. (SC1) are very consistent in their orientation and show a low variability. In general, they show a gentle, subhorizontal dip towards SE (mean orientation = 138/23 ±13°). Foliation planes recorded closer to the fjord (SC2) show a considerably different behavior compared to SC1. Their variability is significantly higher. They show usually also a low dip angle, but their dip orientation reaches from NE to NW (mean orientation = 007/21 ±23°).

The described pattern for the inactive area is also expressed in the data from the deformation area Låvan (B). Outcrops located at higher elevations (head and central domain) show usually a shallow dip towards SE whereas foliation planes at Låvan's front (22-9-I) dip towards NW.

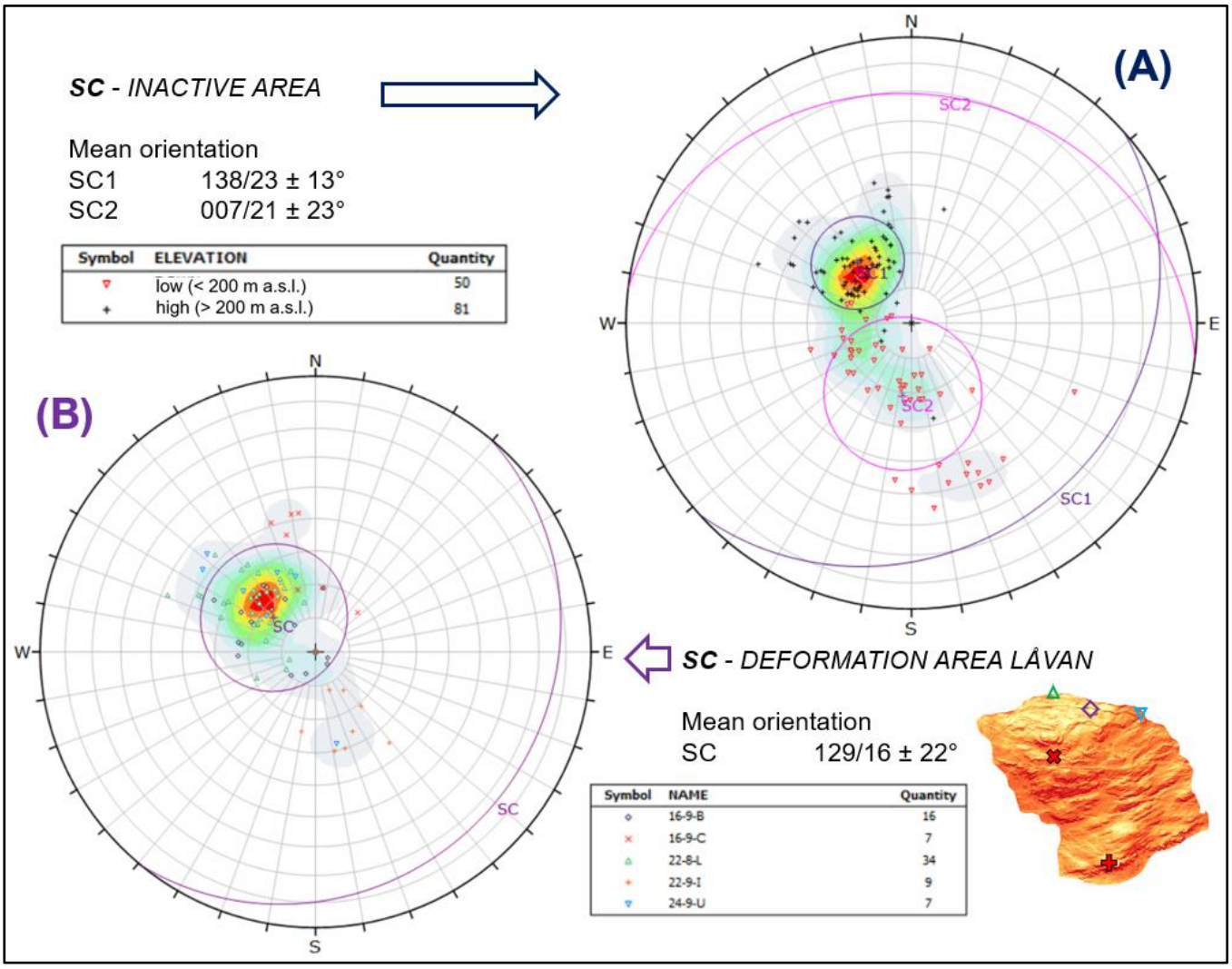

Figure 48: Stereonet plots of foliation (SC) planes (pole plot) in the inactive area surrounding Låvan (A) and inside the deformation area of Låvan (B): Colored 1σ variability cones and mean surfaces are presented for all defined discontinuity sets. (A) Inactive area: includes 131 SC planes recorded at 7 outcrops with in-situ bedrock (locations in Figure 47). The data is divided into outcrops at low elevation (below 200 m a.s.l.) and at higher elevation (above 200 m a.s.l.) and discontinuity sets (SC1 and SC2) are determined for each group. (B) Deformation area Låvan: includes 73 SC planes recorded at 5 outcrops which are presented as different symbols (locations in small map). Measurements were recorded at disintegrated bedrock (displaced and in-contact) and at in-situ bedrock (outcrops at the head scarp: 22-8-L, 24-9-U). The discontinuity set SC is calculated for all presented planes.

- ***Joint planes***

Figure 49 presents the data of joint planes for outcrops in the gravitationally inactive surrounding of Låvan (A) and for outcrops in the deformation area of Låvan (B).

In general, the joint plane data for the in-situ outcrops (A) show a very similar distribution as the JN data from the deformation area (B). Three main joint sets (JN1/2/3) were recognized that differ only marginally between the inactive surrounding and the deformation area.

JN1 is the most prominent set in the data. JN1 has a vertical to subvertical dip while striking NW-SE. At higher elevation (A) and at Låvan's head domain (B), JN1 shows a very small variability and strikes dominantly WNW-ESE. Contrastingly at lower elevations, JN1 has a much higher variability and is oriented differently compared to the higher areas (strikes in average NW-SE).

JN2 and JN3 are two further main discontinuity sets that are similarly represented in both data sets (A and B). JN2 dips moderately steep (~60°) towards SE and JN3 dips moderately steep (~50 - 55°) towards NW. Both sets are very similar in their variability which does not defer significantly depending on the elevation. It must be noted that the foliation at lower elevations (e.g. outcrop 22-9-I) has a similar orientation as JN3. The attribution to either discontinuity set will be further discussed.

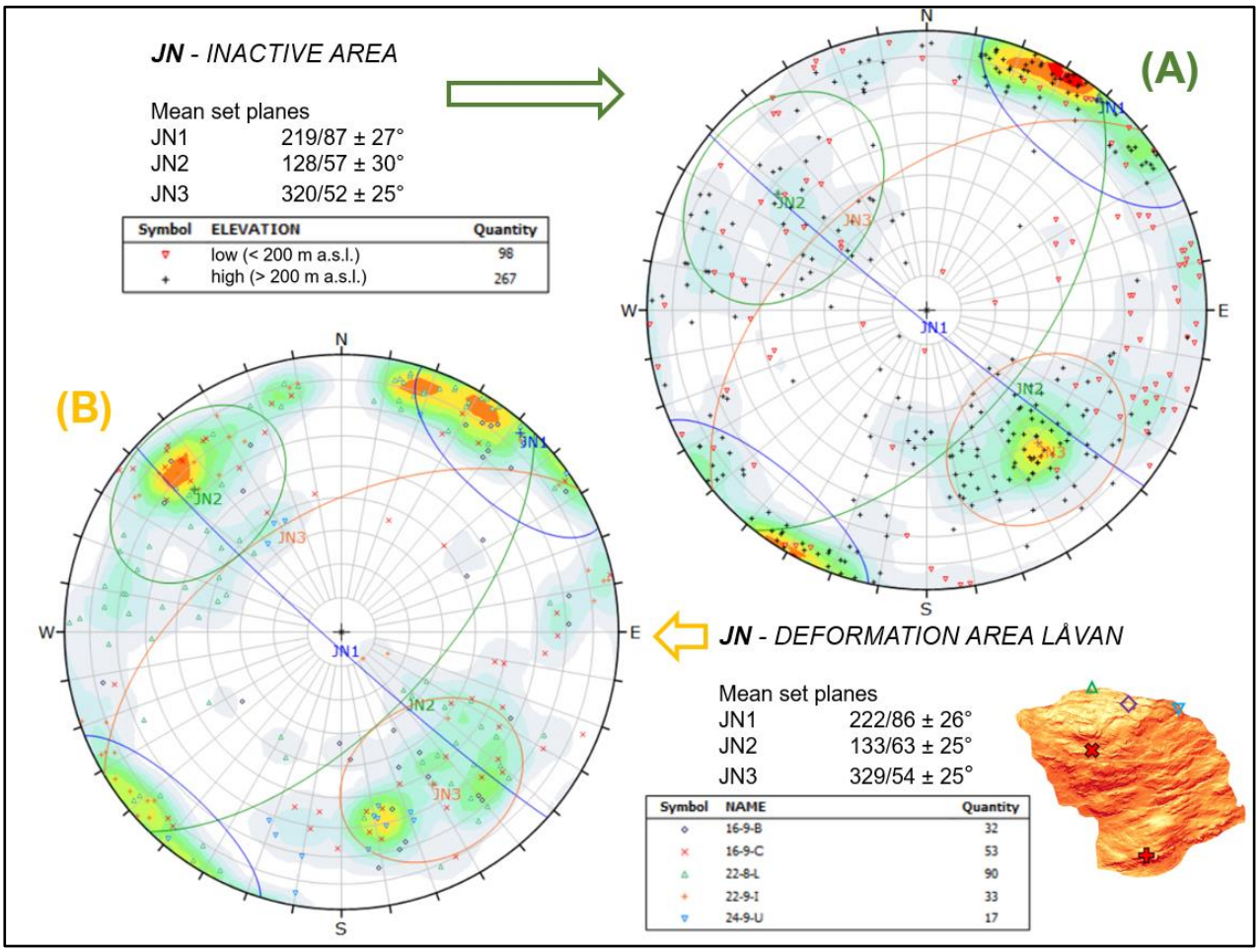

Figure 49: Stereonet plots of joint (JN) planes (pole plot)) in the inactive area surrounding Låvan (A) and inside the deformation area of Låvan (B): In each data set three discontinuity sets were defined (JN1, JN2, JN3) for which colored 1σ variability cones and mean surfaces are presented. (A) Inactive area: includes 365 JN planes recorded at 7 outcrops with in-situ bedrock (locations in Figure 47). The data is divided into outcrops at low elevation (below 200 m a.s.l.) and at higher elevation (above 200 m a.s.l.). (B) Deformation area Låvan: includes 225 JN planes recorded at 5 outcrops which are presented as different symbols (locations in small map). Measurements were recorded at disintegrated bedrock (displaced and in-contact) and at in-situ bedrock (outcrops at the head scarp: 22-8-L, 24-9-U).

- ***Structures in the morphological domains of Låvan***

In order to interpret on the deformation mechanism at Låvan, it is important to compare the structural results between the three different morphological domains that were defined in section 7.1.4. Figure 50 presents the specific discontinuity sets of foliation and joints as expressed at Låvan's head, central and frontal domain.

The head domain is represented by data from the main head scarp (22-8-L), a second, subordinate head scarp (16-9-B) and the transitioning section from head to lateral scarp (24-9-U), all with very intact rock mass. The data is quite consistent for the head scarp domain, especially for SC which dips gently towards SW. JN1 stands clearly out as the dominant joint set.

The central domain is defined by data from a minor scarp opposing a counterscarp in the top slope section (16-9-C), a feature typical for the saw-tooth morphology in this section. All the defined JN sets are expressed in the data. The rock mass was clearly more disintegrated than at the head scarp domain, and SC is dipping slightly steeper and more to the S.

The frontal domain is represented by data from the morphologically dominant frontal scarp (22-9-I) underlain by a large talus fan. Discontinuity sets SC, JN1 and JN2 are clearly given and very persistent. SC dips moderately into the slope (towards NW) which orientation corresponds also to JN3. The orientation of JN1 (SSE-NNW-striking) is clearly different here compared to the upslope domains (ESE-WNW-striking) which relation is also observed for instance at Dusnjarga.

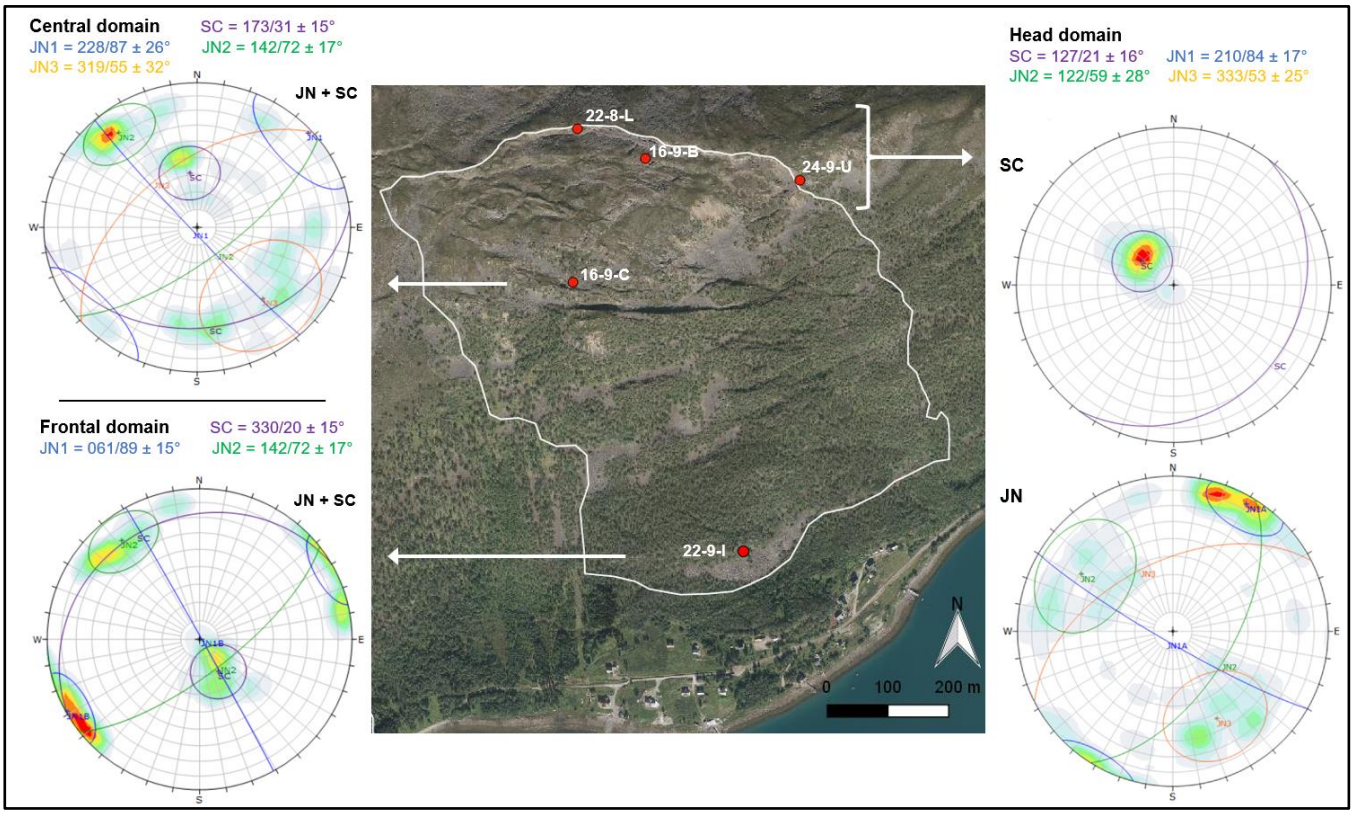

Figure 50: Structural subdomains at Låvan: contour plots of the foliation (SC) and joint (JN) surface poles are presented for the three outcrops of Låvan's head scarp domain as well as for the central and frontal domain (only one outcrop each). For each domain, the discontinuity sets' 1σ variability cones and mean surfaces (and their orientations) are displayed. The white line delimits the presumed actively deforming area and the base map is the high-resolution orthophoto.

7.4 Scanline data analysis

Apart from structural measurements and general observations during field work, we carried out line scans for rock mass characterization at 20 outcrops spread across the study area (Figure 51). Line scans were performed at eight undeformed (in-situ) outcrops, at seven deformed in-contact outcrops (disintegrated) and at five strongly displaced out-of-contact outcrops (disaggregated). Except for data from two disaggregated blocks (20-9-Q, 23-9-C), all the mapped discontinuities could be assigned to the previously defined discontinuity sets.

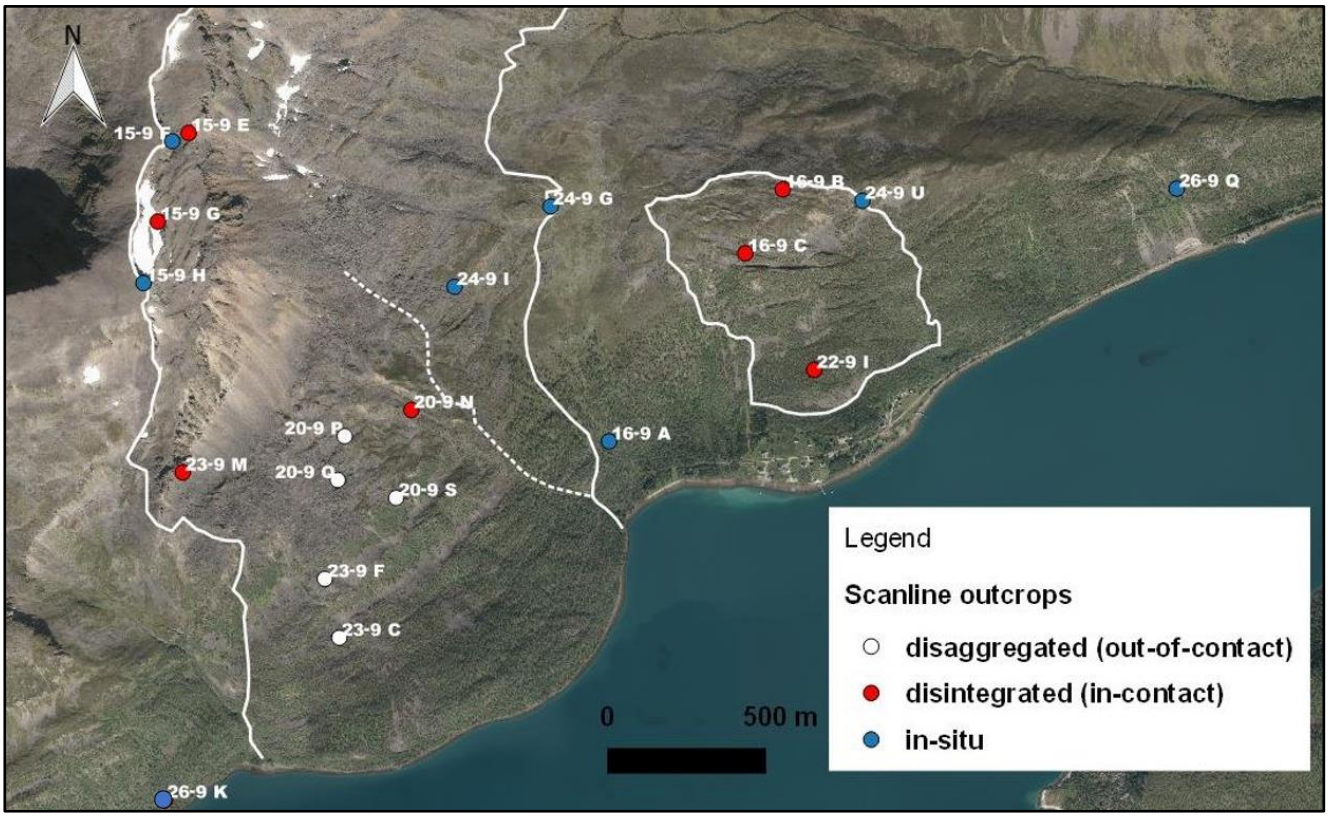

Figure 51: Overview map depicting the location of outcrops (n = 20) where line scans were performed. The limits (white lines) of the deformation areas of Låvan and Dusnjarga are indicated (whereby the dashed line delimits the central active part of Dusnjarga). Line scan locations are classified according to the bedrock character (legend).

We recorded the discontinuity characteristics (joints and foliation) comprising the following categories: defect type, orientation, spacing, length, type of termination, roughness, width, water condition, lithology and strength. For each discontinuity set, the detailed results are presented as histogram plots in Figure 52.

Figure 52: Data histograms displaying characteristics of the four main discontinuity sets based on the line scan data collected at 22 different localities in the field. The histograms present the recorded frequency (vertical axis) of the characteristics.

Figure 53 displays the orientations (strike directions) of the outcrops where line scans were performed which is relevant regarding the possible disproportionate representation of certain discontinuity orientation. The dominance of NE-SW-striking outcrops is logical due to the topography with typically SE-dipping slopes. It should be noted that all N-S-striking scanline outcrops were located at Dusnjarga's head scarp whereas the other orientations were relatively well distributed across the study area.

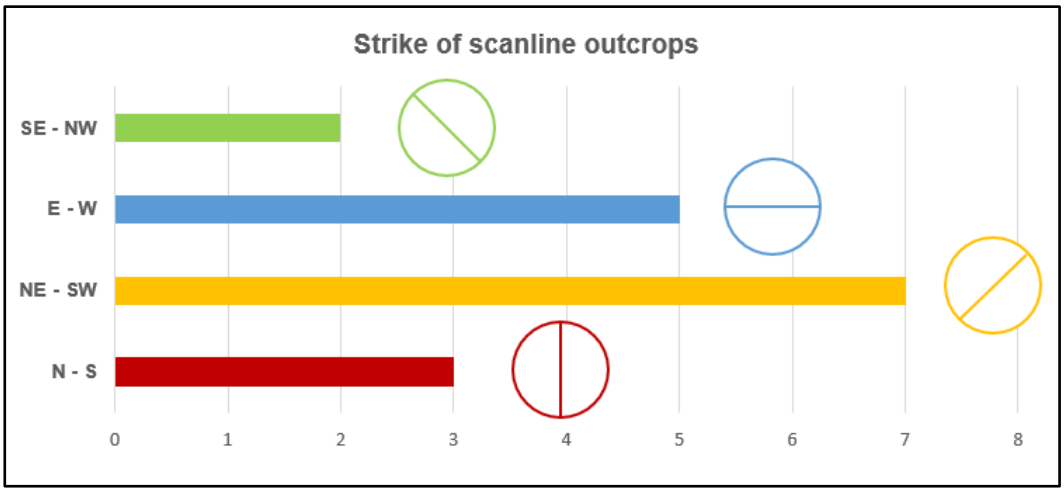

Figure 53: Chart displaying the frequency count of orientations (strike) of the outcrops where line scans were performed. It is displayed for 17 outcrop locations for which scanline data was analyzed

Table 4 summarizes the most relevant discontinuity set characteristics as mean values in addition to the more detailed data histograms (Figure 52).

JN1 was usually the most dominant joint set observed in the field. This is supported by the scanline data in which the set stands out by the highest persistence (length), a high joint width and frequent seepage.

JN2 shows a high similarity to JN3 in many aspects but it defers from JN3 through a greater width, less roughness, more seepage and more continuous fractures. This indicates a higher dominance for JN2 compared to JN3. This difference could be also a result of slope deformation. However, a comparison of the results from disaggregated with in-contact bedrock does not reveal any significant differences for JN2 or JN3.

In most cases the foliation (SC) fractures have a low persistence, were dry and form seldomly continuous fractures. The foliation is usually present but does not form the dominant discontinuities. On the other side, we witnessed that the foliation discontinuities can vary strongly in their characteristics depending on the lithology and stratigraphic location discussed in the following chapter.

Table 4: Summary of characteristics of the defined discontinuity sets: Orientation values are calculated based on the data from in-situ in the eastern part of the study area. Values are given as dip direction/dip angle in degrees. The categories (discontinuity) spacing, length (= persistence) and width (= thickness) are based on the collected scanline data (collected at 22 outcrops). Note the difference in the chosen units between width (mm) and length/spacing (m). All variabilities are given as ± *1σ*.

Summary of main discontinuity sets

Discontinuity set	mean orientation	mean spacing [m]	mean length [m]	mean width [mm]
JN1	219/87 ± 27°	0.5 ± 0.3	4.5 ± 2.8	54 ± 74
JN2	128/57 ± 30°	0.4 ± 0.2	2.4 ± 1.4	24 ± 39
JN3	320/52 ± 25°	0.3 ± 0.3	2.2 ± 3.0	2 ± 2
SC	129/16 ± 22°	0.5 ± 0.5	1.4 ± 1.2	11 ± 27

7.5 Rock mass observations

The dominant bedrock types observed in the study area were layered gabbro and gabbro gneiss, thus metamorphosed plutonic rocks. All the recorded rock types match the lithologies identified by Roberts and Elvevold (2018) in the neighboring Øksfjord area. Field estimations of uniaxial compressive strength according to the criteria by Hoek and Brown (1997) resulted in a rock strength ranging between strong (R4) and very strong (R5) for the observed bedrock types.

Generally, two different principal rock types dominate in the deformation area of Låvan: fine-grained, layered gabbro (herein termed ‘dark gabbro’) and coarse-grained anorthositic gabbro (herein termed ‘anorthositic gabbro’).

The dark gabbro is mainly distinguishable from the latter rock type through the darker color and small grain size (Figure 54). The dark color is most likely due to a high share in clinopyroxene which also forms its foliation and layering that is mostly but not always recognizable. The dark gabbro shows often strong surficial weathering and oxidation.

The anorthositic gabbro stood out by a lighter color due to a high share in coarse plagioclase crystals. It occurs often as layers of 5 - 50 cm surrounded by darker gabbro and shows often a clear foliation mainly formed by lengthy plagioclase crystals (Figure 54C). At Låvan, the frontal and central domains are dominated by the dark gabbro interspersed by layers of anorthositic gabbro that increase in number and size with higher elevation. Låvan’s head domain is finally dominated by anorthositic gabbro (e.g. Figure 54B).

Different rock types were observed at higher elevations at Dusnjarga where the head scarps are dominated by massive rock types as syenite and gabbro gneiss. The massive syenite shows rarely any layering or foliation. It has typically a porphyritic texture of large-grained

idiomorphic potash feldspar crystals dispersed in finer matrix of nepheline (Figure 54A). Massive garnet-bearing gabbro gneiss occurs predominantly at the uppermost head scarp section of Dusnjarga.

Apart from this, quartzitic veins (Figure 54D) were observed e.g. at the central domain of Dusnjarga but also close to the head domain of Låvan. These veins penetrating the gabbroic bedrock enclose sometimes brecciated rock material and form irregular shapes, not following any obvious discontinuities.

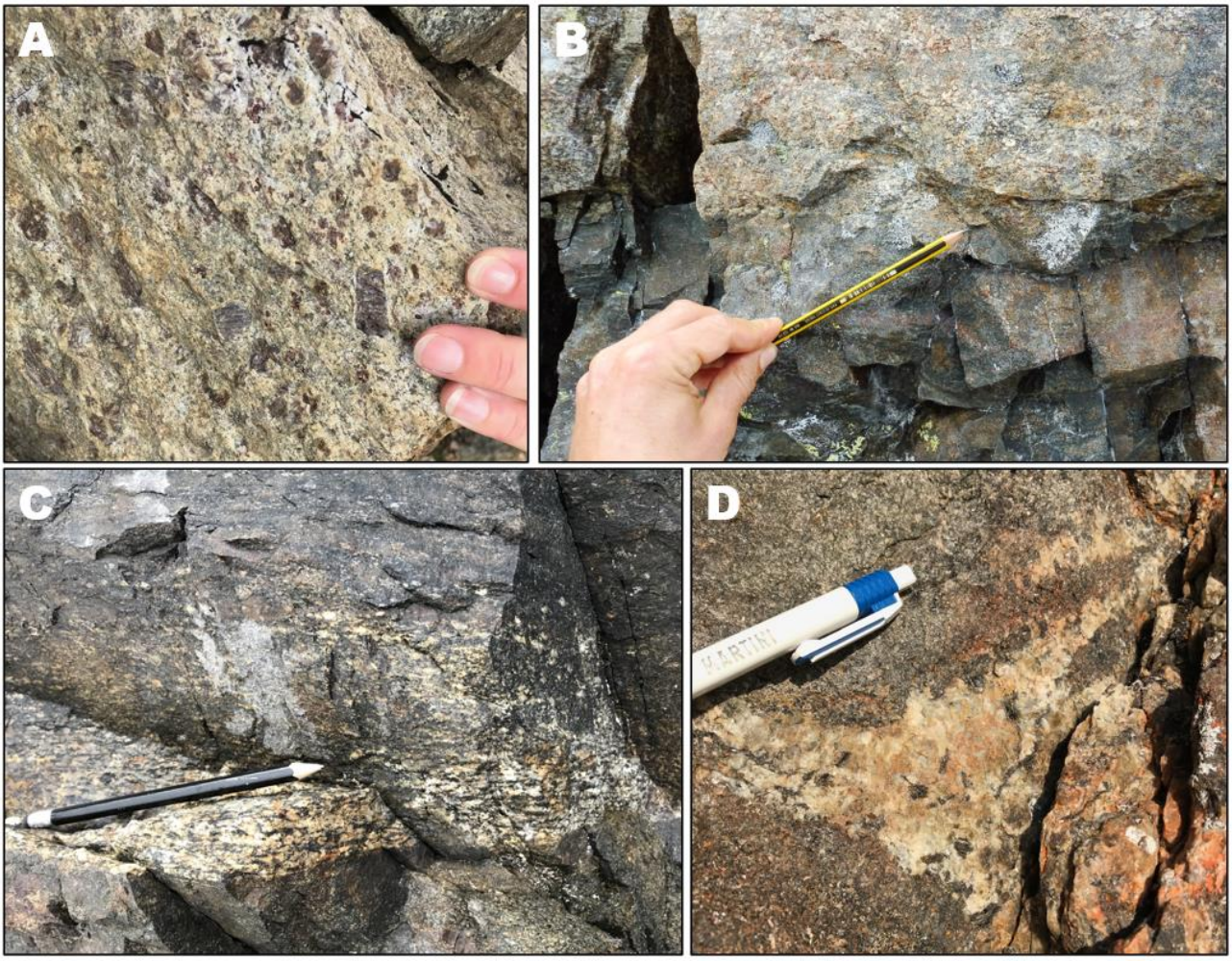

Figure 54: Characteristic rock mass in the study area: A) Syenitic rock close to Dusnjarga's head scarp. Idiomorphic potash feldspar crystals enveloped by a light matrix probably dominated by nepheline. B) Lithological change from dark gabbro to lighter rock (either anorthosite or syenite) at the head domain of Låvan: the different fracture behaviour of both lithologies is well recognizable. C) Foliation and layering in gabbro at Låvan's central domain. The foliation is better recognizable in the light layer rich in coarse plagioclase compared to the surrounding gabbro. D) Quartzitic vein inside fine-grained gabbro at Dusnjarga's central domain.

The described rock types differ also in their fracture behavior from each other. For instance, the darker gabbro at Låvan has usually a higher density of fractures than the anorthositic gabbro (Figure 54B). Observed fractures in the dark gabbro are usually shorter and less rough

than in the anorthositic gabbro. The observed downslope disintegration of rock mass at Låvan is not as strong as at Dusnjarga (where the central and frontal lobe consist predominantly of disaggregated rock mass). Nonetheless, the rock mass at Låvan's central and frontal domain is significantly more fractured than at the head (which observation might also be linked to the downslope increase in dark gabbro).

The expression and characteristics (e.g. spacing, roughness, width, persistence) of the foliation vary also significantly between the different lithologies. For instance, the foliation is comparably rough and not very persistent in the coarse-grained, anorthositic gabbro dominating the head domain (e.g. Figure 56) whereas foliation fractures are typically smoother in the fine-grained lithologies. Furthermore, persistent foliation fractures form typically at the locations of lithological transitions (e.g. from coarse- to fine-grained as in Figure 54B). Since the foliation has usually a subhorizontal orientation (section 7.3), it is morphologically expressed by forming the flat top surfaces of outcrops (Figure 56).

Most of the morphological features expressing the gravitational deformation at Låvan are developed along the three defined JN sets, such as back scarps, counterscarps, tension cracks or trenches. Particularly Låvan's top area just above the start of the steeper slope is characterized by very well developed morpho-gravitational features which usually can be attributed to the identified discontinuity sets. This morpho-structural relation becomes very clear in an aerial view of the head domain as displayed in Figure 27 and Figure 55. It is visible that many of the afore-mentioned morphological features follow the strike directions of JN1 (blue lines) and of JN2 and JN3 (same strike; yellow lines). The flatter part of the head domain is thus characterized by a zig-zag pattern of trenches, ridges, minor scarps and tension cracks following these discontinuity sets (Figure 55B). At the transition to the steeper, central slope domain (Figure 55C), several minor scarps and counterscarps show a distinct wedge-shape following also JN1 and JN2/3. The large counterscarp marking the boundary to Låvan's central is not following the structural trends as at the head domain and strikes rather transversal to the slope and the coastline (e.g. Figure 55D).

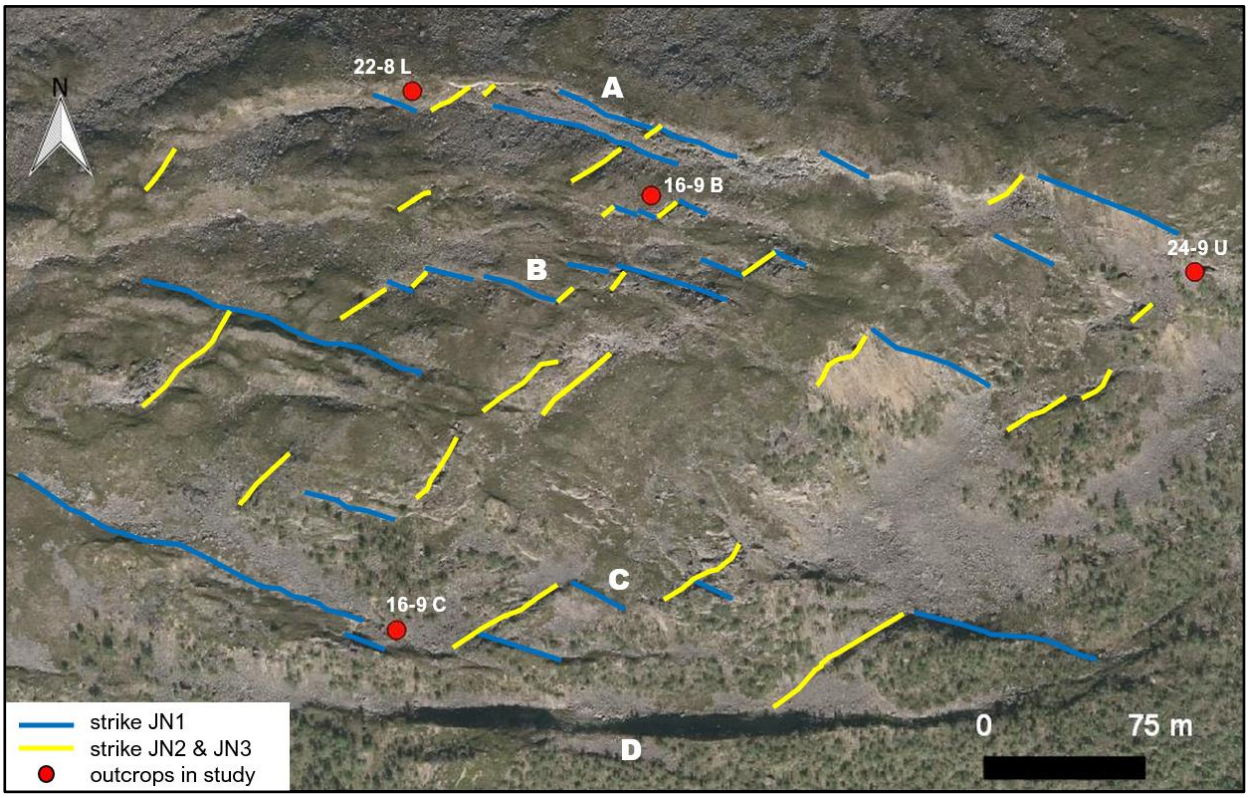

Figure 55: Orthophoto of the head domain of Låvan: as indicated by the lines, most of the morphological surface features (such as trenches, scarps, ridges or counterscarps) can be attributed to the local strike direction of the main JN sets: either JN1 striking ESE-WNW or JN2/JN3 striking SW-NE. A) Head scarp: large faces follow JN1 connected by small sections following JN2/3. B) Zigzag pattern of minor scarps, ridges, trenches and tension cracks dominating most parts of the head domain. C) Transition to the steeper slope: the wedge-shape of scarps and counterscarps follows JN1 and JN2/JN3. D) Large counterscarp marks the start of the central: the morpho-structural relation is not that clearly expressed in the central and frontal domain.

Morphological features following JN1 are typically more persistent and dominant compared to those following JN2/3. This is for instance expressed well at the head scarp (Figure 55,56A) or at the secondary scarp just S of it (Figure 56B). In its W-part shows the head scarp a curvy shape that seems to rather follow JN2/3, however in most parts the smooth faces of the major and subordinate head scarp follow principally JN1 whereby these dominant scarp faces are interrupted and connected by short sections following JN2/3 (Figure 56A). It is well visible that these short scarp sections are very rough which is reasoned by diamond-shaped rock pieces breaking out of the face along discontinuities JN2 and JN3 (Figure 56A).

The lateral limits of the deformation at Låvan have irregular shapes: the exact course of the eastern limit is hard to define due to disaggregated rock mass cover and the western limit has a very jagged shape. Their general SSE-NNW-striking orientation does not match any of the defined discontinuity sets. The head scarp however transitions gradually into the eastern lateral flank (26-9-U, e.g. Figure 55) and the flank's jagged course might be controlled partly by JN1.

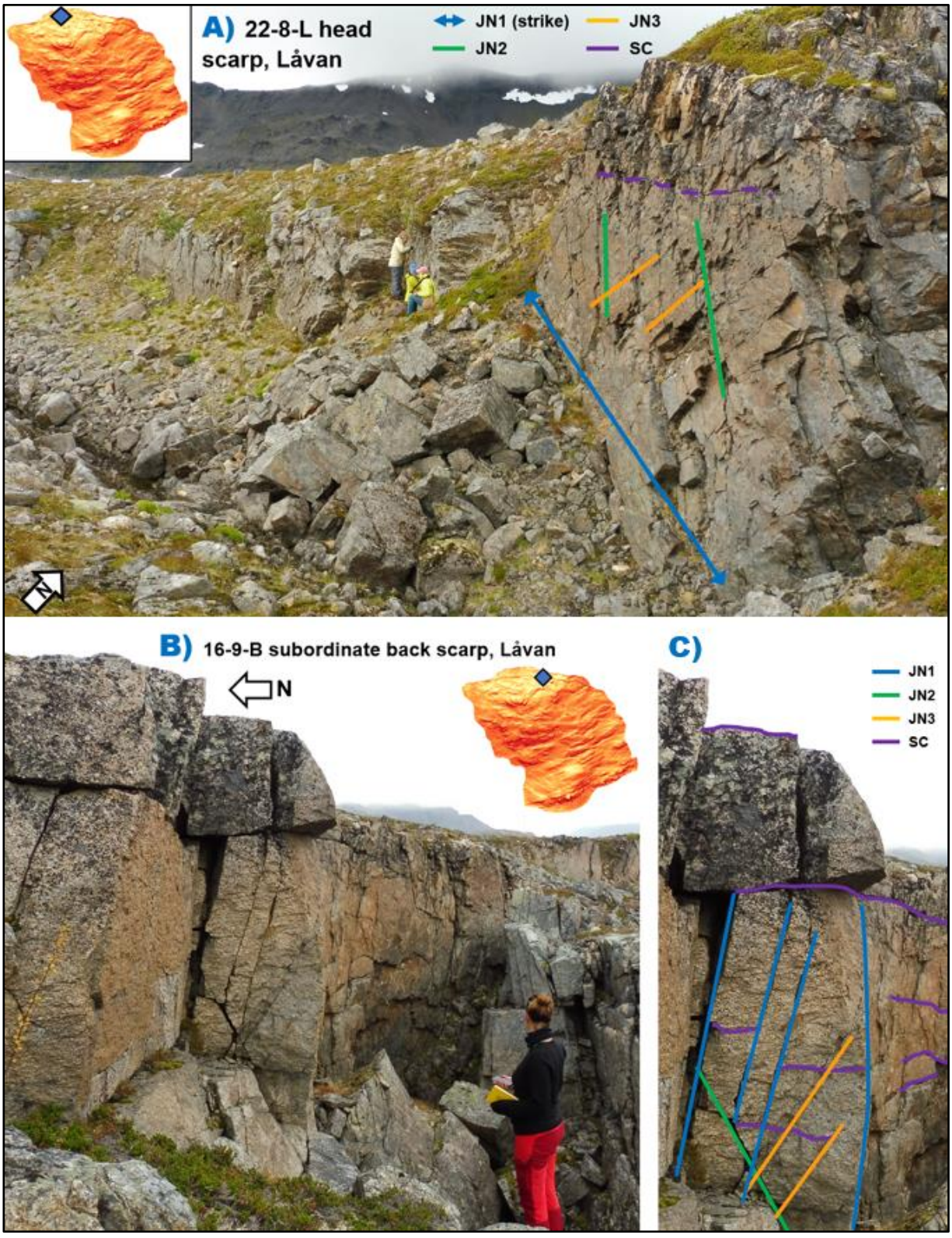

Figure 56: A) Låvan's head scarp (22-8-L) and associated trench: the scarp follows a zigzag pattern ruled by the strike of the dominant JN1 set and the strike of JN2 and JN3. The intersections of JN2 and JN3 form diamond-shaped blocks breaking out of the rock wall, while JN1 forms scarp sections with a smooth face. B) Subordinate head scarp and trench (16-9-B): it can be also interpreted as a large tension crack. The rock type at the head domain is coarse-grained anorthosite generally with a weekly developed foliation (SC). C) The visible fractures can all be assigned to the defined discontinuity sets. The scarp is mainly developed along the dominant, almost vertical oriented discontinuity set JN1. JN2 and JN3 have a moderate persistence and form perfectly symmetric wedges.

Rock mass and morphological expression of structures at the frontal domain defer to some degree the characteristics observable at the head domain. Fewer outcrops with intact rock mass can be found with exception for the prominent frontal scarp depicted in Figure 57. The rock is not very disintegrated at the frontal scarp and all discontinuity sets are very well developed and quite persistent, particularly JN1. JN3 follows the foliation surfaces that dip at a moderate angle into the slope in this lower elevated domain (compare to Figure 50). The large talus fan in front of the scarp exemplify dominant rock fall activity controlled by all four discontinuity sets (JN1, JN2, JN3/SC) leading to a rectangular fracture pattern. Additionally, some degree of toppling behaviour of some large frontal scarp blocks could be witnessed.

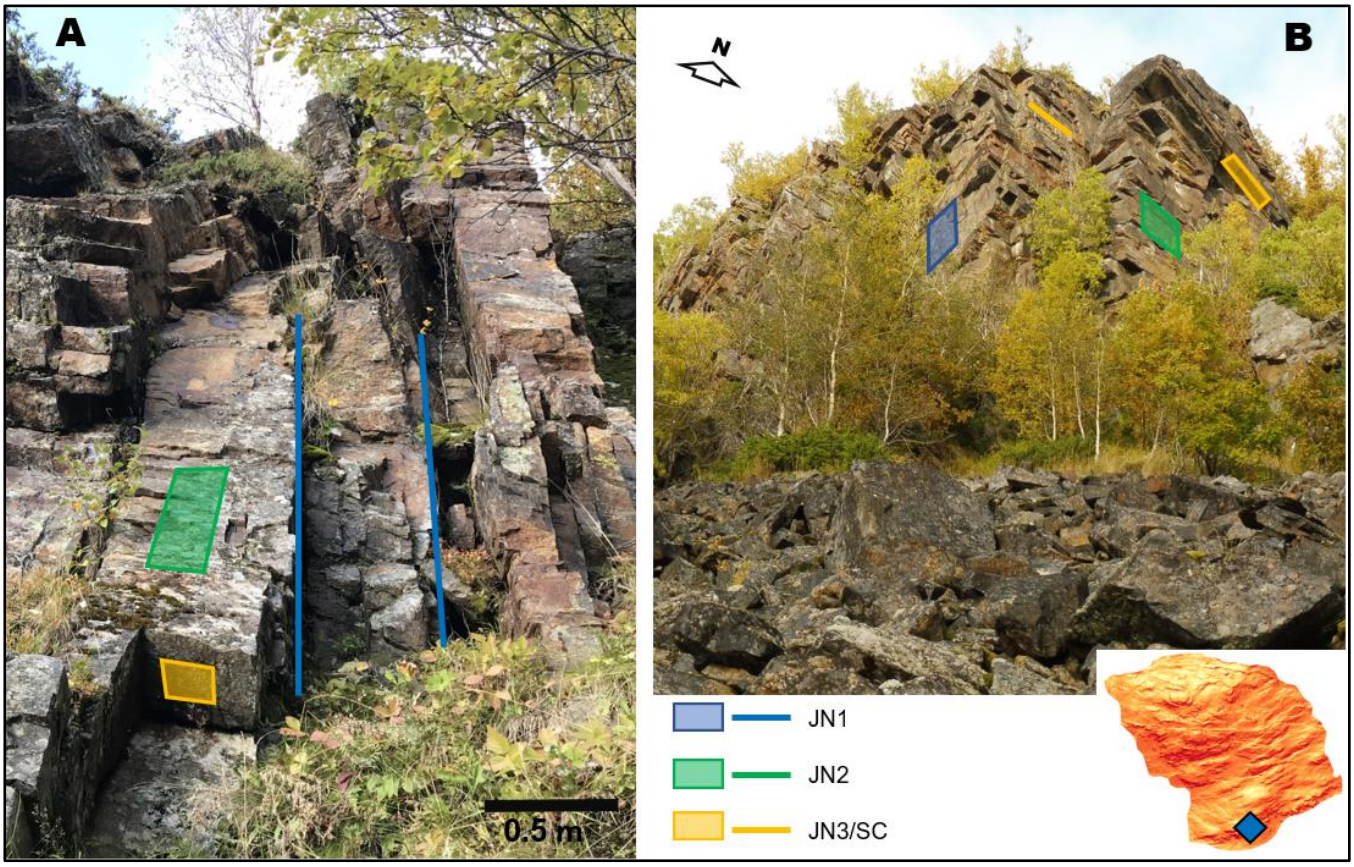

Figure 57: Låvan's frontal scarp (outcrop 22-8-I): A) All discontinuity sets are very persistent and well expressed but the bedrock is not extraordinarily dissected at the frontal scarp. JN3 follows the foliation (SC) dipping northwards into the slope. B) The scarp face follows JN1 and JN2. JN1 widens towards the front of the scarp and indicates some degree toppling of frontal scarp blocks. The talus fan in the foreground indicates extensive rockfall activity.

7.6 InSAR data analysis

The available InSAR data recorded from 2015 to 2019 (Figure 58) reveals for the ascending pathway a clearly delimited active deformation zone at Dusnjarga with an indicated down-and-eastward directed displacement. The highest indicated displacement rates in the top part

amount up to 16 mm yr^{-1}. This active displacement at Dusnjarga stands in contrast to Låvan for which the InSAR data does not reveal any significant displacement over the past five years, neither for the ascending nor the descending pathway.

- *Interpretation*

InSAR has problems with detecting directly north- or southwards directed displacement which cannot be excluded for Låvan, but an active displacement at Låvan seems unlikely since the displacement is very clearly expressed at Dusnjarga (Eriksen et al. 2017). The low density of data points at Låvan's lower slopes is due to the steepness and forest cover. This is another reason justifying the use of further methods to identify displacement (e.g. dGNSS monitoring points).

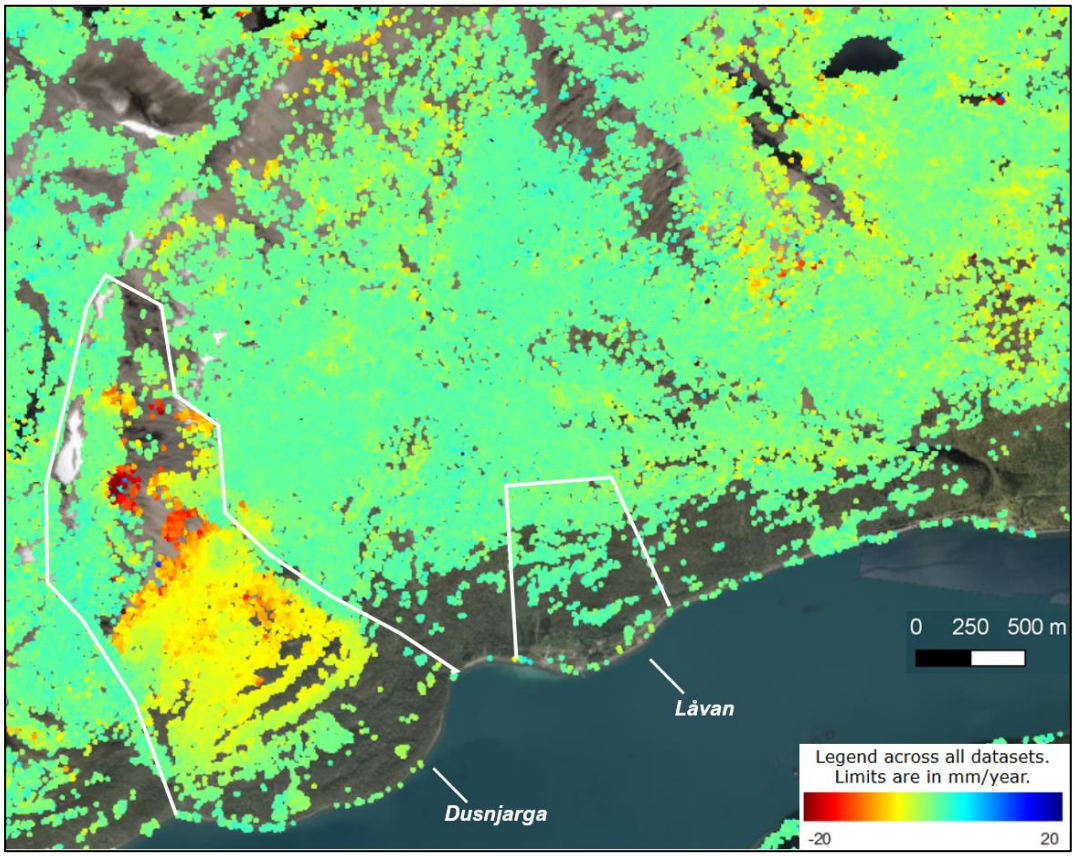

Figure 58: Overview map of the study area depicting the InSAR data for the ascending pathway (satellite moves northwards) collected for six consecutive years (2014 – 2019). Negative values indicate a relative movement away from the satellites line of sight, thus down and to the east. The unstable slope of Dusnjarga is quite clear delimited in this data through active displacement whereas for the deformed slope of Låvan no active displacement is indicated. *Data source: InSAR Norway (https://insar.ngu.no/).*

7.7 dGNSS monitoring point data analysis

At Låvan, three dGNSS monitoring points were installed in presumably unstable locations in 2010 (Figure 47). Points LAV-4 and LAV-5 are both situated in the top part of the deformation

area: LAV-4 is located on a large block right at the edge to the steeper slope and delimited by several trenches, and LAV-5 is located closer to the main scarp on a convex feature just behind a distinct, deep trench. LAV-6 is situated on top of the major counter scarp in the central slope of Låvan (Figure 28).

We had access to the results measured in 2010, 2012 and 2014 (Figure 59). It is clearly visible that the uncertainties (3σ variabilities) for all the recorded measurements surpass the amount of displacement. Accordingly, the displacement has to be regarded as insignificant or uncertain for all three monitoring points. Especially at LAV-6, the indicated displacements are highly insignificant since they followed opposing trends.

- *Interpretation*

The insignificant displacement of all three monitoring points at Låvan fits to the InSAR data and both data sets indicate that despite its morphologically active appearance the mountain slope Låvan is not actively deforming at present. This contrasts the data for Dusnjarga where both InSAR and dGNSS data indicate active deformation (e.g. vertical movements of more than 4 mm a^{-1}). However, the availability of only three monitoring points and three measurement periods is very little and longer time series available in the future should allow more valid interpretations.

After all, neglecting the high uncertainties for LAV-4 and LAV-5, trends of a vertical downward movement (~1 mm a^{-1}) could be suggested which would be expectable for this top part of the slope.

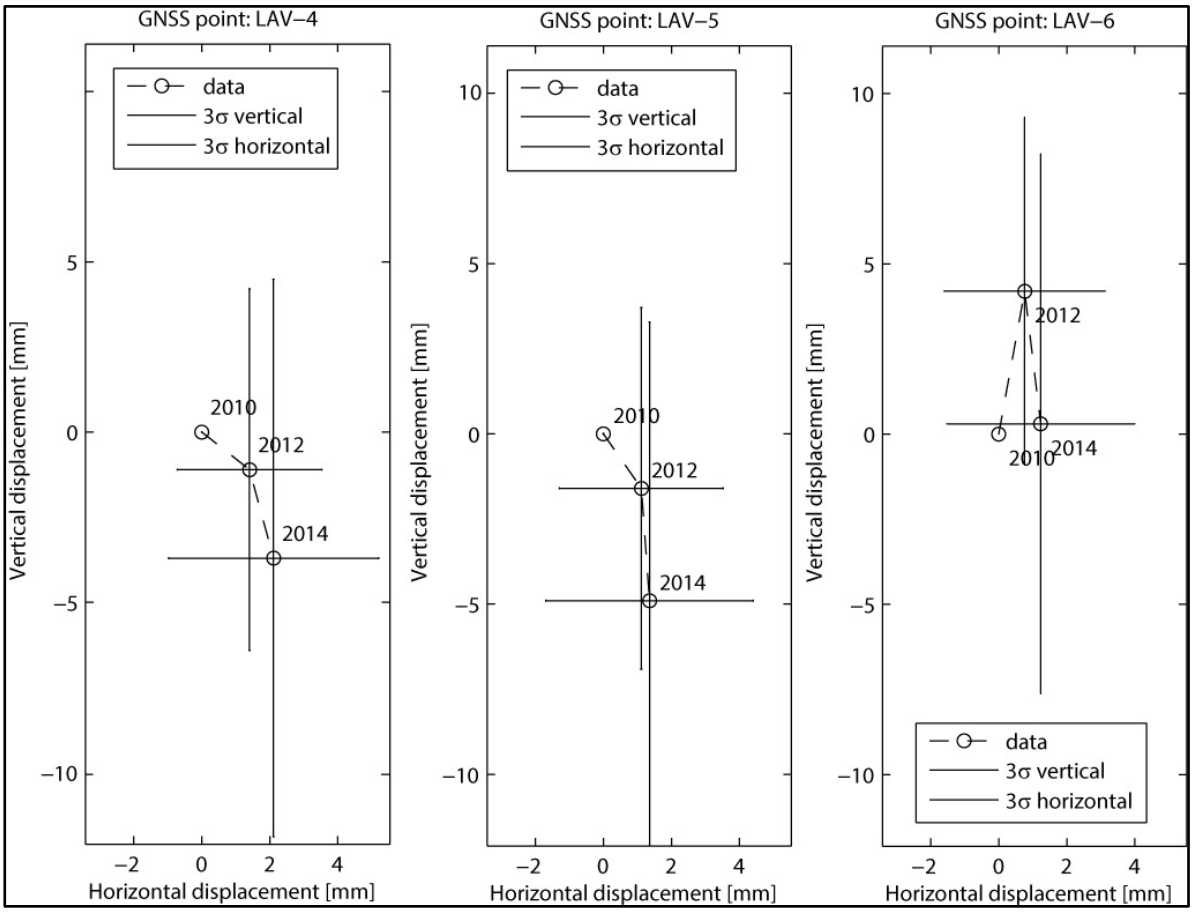

Figure 59: Horizontal and vertical displacements of the three dGNSS monitoring points placed in the deformation area of Låvan recorded between 2010 and 2014. Uncertainties of the measurements are indicated as 3σ variabilities.

7.8 Kinematic failure analysis for Låvan

With the help of the software *Dips 7.0*, a kinematic analysis was performed based on the structural data from in-situ outcrops in the eastern study area close to Låvan (Figure 47).

In order to test for the different failure modes, certain kinematic parameters need to be defined. We calculated the mean slope orientation at 165° ±49° and the mean slope inclination at 31° ±12° for the whole deformation area of Låvan. The central and frontal domain are however considerably steeper (33° ±11°) than the head domain (19° ±10°). Consequently, in the kinematic analyses a slope inclination of 33° is applied, however with special consideration to potential steeper slope section due to the variance of 11°.

The unstable slope covers a relatively large area (about 900 x 550 m). A larger size of a slope deformation justifies the selection of a high lateral limit (chosen here at 30°) since a higher variation of the slope face and an involvement of more complex structures is more likely (Hermanns et al. 2012a).

The friction angle is probably the most critical parameter for the results of the analyzes and it is unfortunately also most difficult to choose. Bieniawski (1988) generally attributed friction angles of 35 to 45° to 'good' rock and 15 to 25° to 'poor' rock. For instance, analyzes by Wines and Lilly (2003) gave basic friction angles around 30° for comparable rock types which were 3-4° lower in case of wetness. In a failure analysis, one should assume the worst scenario, therefore Hermanns et al. (2012a) recommended using a friction angle of 20° as a conservative value for large unstable rock slopes in Norway which is also the friction angle we used for the presented models. For a more site-specific approach, it would be necessary to perform mechanical analyzes of the local samples or to drill for a basal detachment which was not possible in the context of this work.

- *Planar sliding*

Planar sliding is only possible if a gliding surface exists that dips roughly parallel to the slope face, but it must also daylight in the slope face. For a kinematic feasibility, the gliding plane must dip steeper than the angle of friction and release surfaces must exist laterally and at the upper end (Hencher 2013).

Regarding the obtained structural data, these conditions are best given for the joint set JN2 and the foliation (SC) since both are oriented SSW, thus similar to the slope face. The relevant tests for planar failure are presented in Figure 60.

For the chosen parameters, only a minor proportion (2.5%) of JN2 planes plots in the critical pole vector zone under the assumed conditions. JN2 is usually dipping steeper (mean dip of 57°) and more towards east (128°) than Låvan's SSE-facing slope.

Contrastingly, a significantly high proportion (25.7%) of foliation planes from above 200 m a.s.l. (SC1) plots in the critical zone and a big part of the remaining poles plots in the direct vicinity. These results are most sensitive to parameter changes of the friction angle and the slope orientation. For instance, a lower friction angle of 16-18° combined with a more SE oriented slope (140°) would yield more than 50 % critical foliation planes.

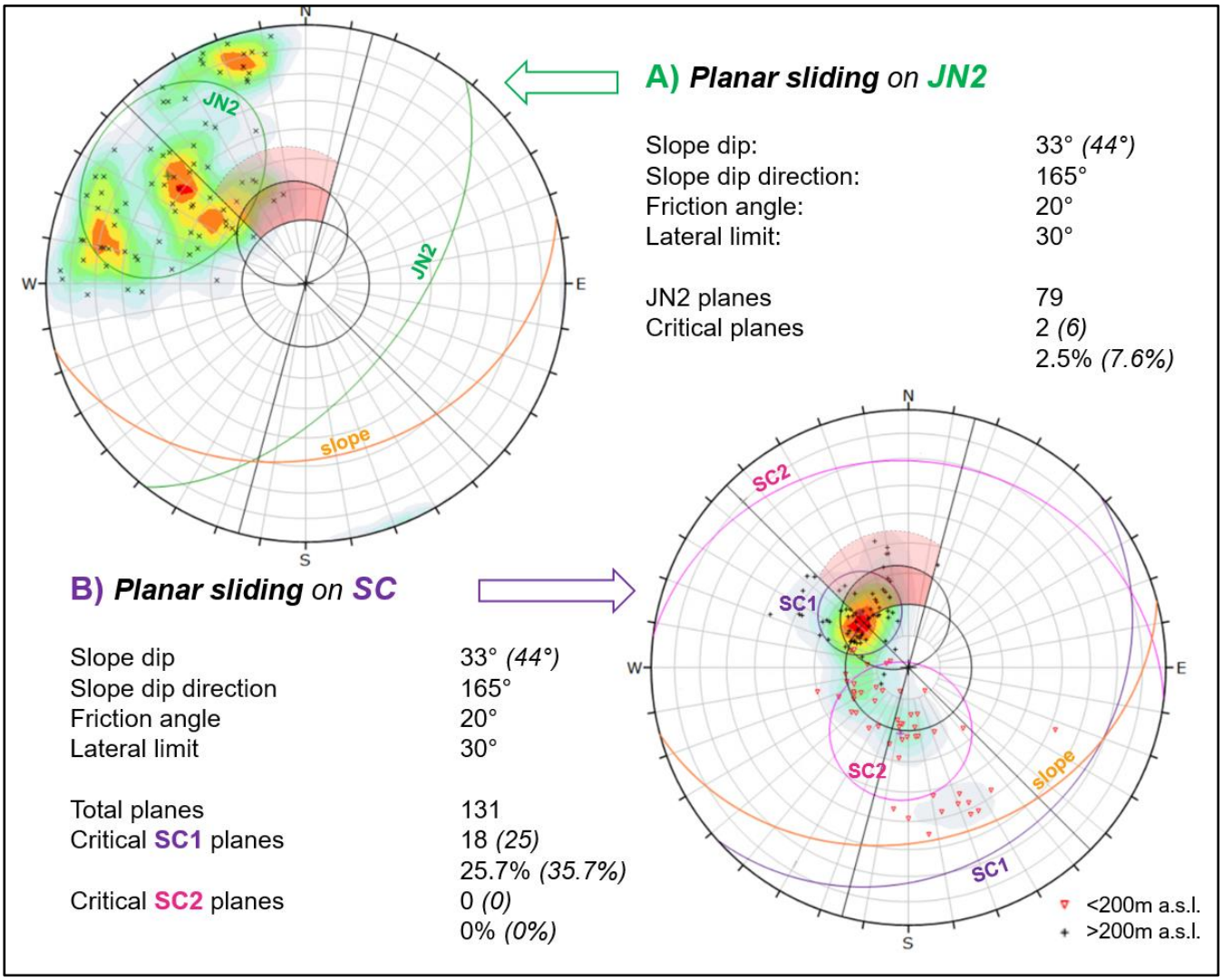

Figure 60: Kinematic analyses for planar sliding: A) Planar sliding along joint set JN2. B) Planar sliding along the foliation SC which is divided into data from above (SC1) and below (SC2) 200m of elevation. The discontinuity sets are indicated by 1σ variability cones and mean surfaces. The critical pole vector zone (red area) is delimited by the pole friction cone (inner black circle), the lateral limits (black straight lines) and the daylight envelope (outer black circle). A potential higher slope inclination (1σ variability) is included by the extension of the critical zone (pale red area) and by the values shown in italics. The displayed structural data was recorded at 7 in-situ outcrops in the eastern study area (Figure 47).

- *Wedge failure*

Wedge failure can occur on two gliding surfaces along their line of intersection or on one of two planes if its orientation is more favorable than the line of intersection. The lines of intersections are the central elements of the analysis. In order to enable a wedge failure, the lines of intersection must daylight and be oriented similar as the slope (Hencher 2013).

These conditions are matched best by two pairs of discontinuities: JN1-JN2 (mean intersection line = 130/16) and JN1-SC (mean intersection line = 133/57). The kinematic analyses for both combinations are presented in Figure 61.

The presented results support that wedge failure is kinematically possible along both pairs of discontinuity sets. However, failure along JN1-SC-wedges stands out by a much higher proportion of critical intersection lines (13.0 %) than for JN1-JN2 (6.5 %). The analysis for JN1-SC (Figure 61) reveals that the main cluster of intersection lines (blue points) plots partly in the critical zone (red zone) whereas for JN1-JN2 most intersection lines cluster outside of the critical zone. Slope dip and friction angle are sensitive parameters for both pairs, but the JN1-SC-wedges stand out by an increasing likelihood of failure for a more SE-oriented slope.

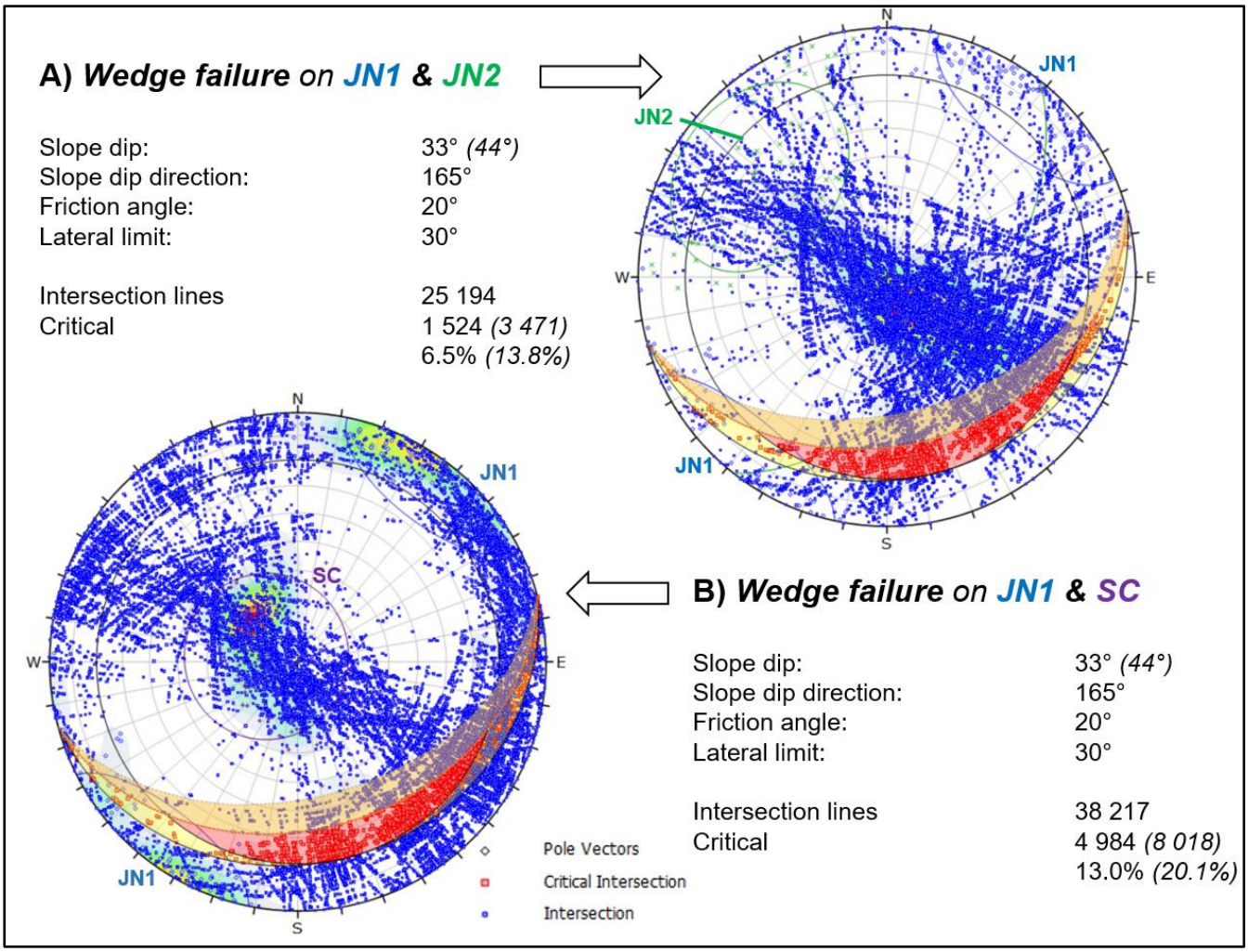

Figure 61: Kinematic analysis for wedge failure: A) Wedge failure along the joint sets JN1 and JN2. B) Wedge failure along joint set JN1 and the foliation SC. The critical intersections are highlighted in the critical zone (red points/zone) which is delimited by the plane friction cone (black circle) and the slope plane (orange surface). A potential higher slope inclination (1σ variability) is included by the extension of the critical zone (pale orange area) and by the result values shown in italics. The vectors of all intersections are displayed by the blue points. The displayed structural data was recorded at 7 in-situ outcrops in the eastern study area (Figure 47).

- *Toppling*

For a large-scale toppling failure, it is necessary to identify continuous and closely spaced discontinuity planes that dip steeply into the slope (Hencher 2013). *Dips 7.0* allows kinematic analyses for direct toppling and flexural toppling.

Direct toppling depends on a pair of two intersecting discontinuity sets whose lines of intersection dip steeply into the slope and which can form discrete toppling blocks. These discrete blocks would usually form minor rock volumes breaking out of steep cliffs or scarps which is why this mechanism is of minor relevance for the large-scale rock slope deformation. However other modes of toppling and particularly flexural toppling have been identified as the responsible mechanisms for a significant number of large-scale rock slope deformations (e.g. De Freitas and Watters 1973; Nichol et al. 2002; Reitner and Linner 2009).

Figure 62 presents the results of the kinematic analysis for flexural toppling as defined in Goodman (1980). JN1 and JN3 are the two potentially critical discontinuity sets but only minor proportions of planes (2.8% and 1.5%) plot in the critical zone for flexural toppling. A higher slope inclination has little effect on these results.

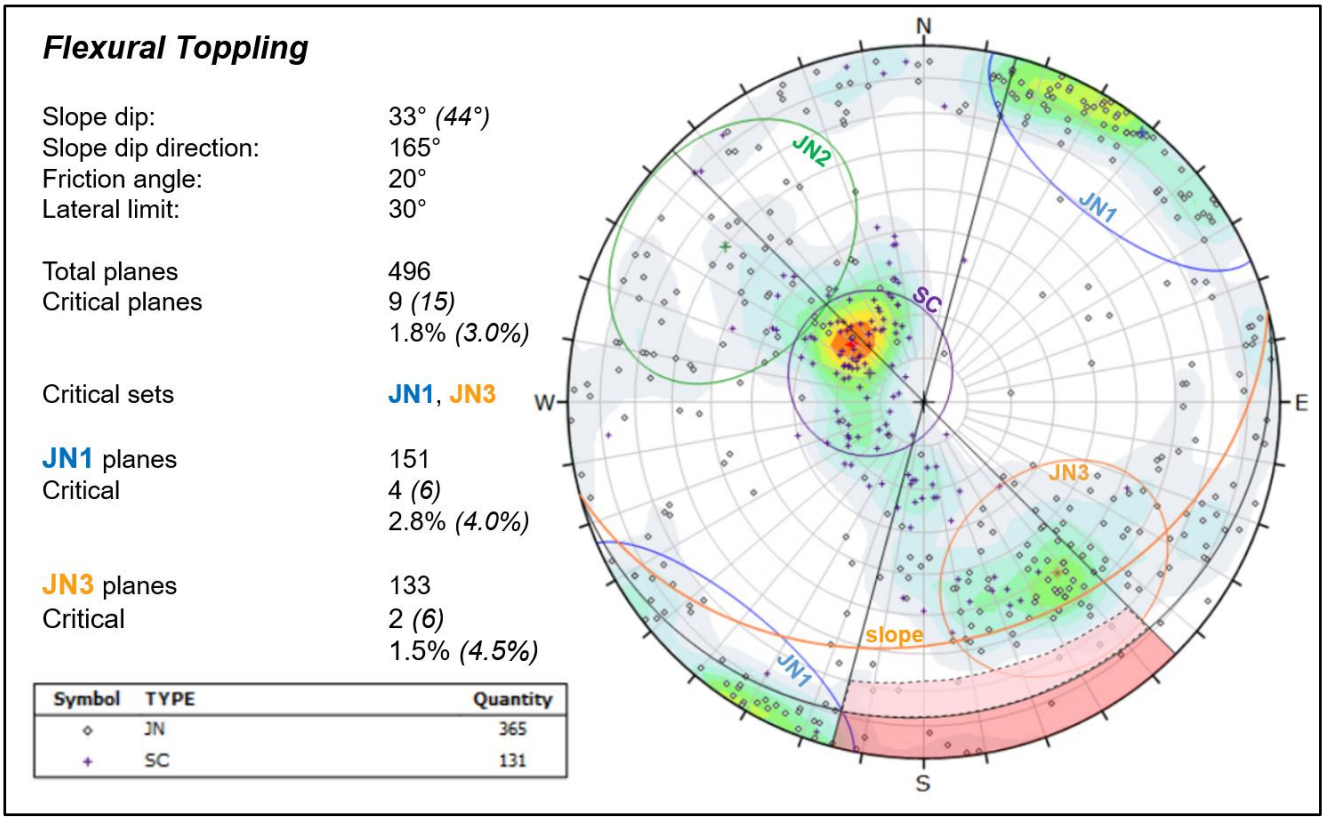

Figure 62: Kinematic analysis for flexural toppling based on the total structural data recorded at in-situ outcrops (n=7) in the eastern study area (Figure 47): Discontinuity surfaces are displayed as pole and contour plots. Discontinuity sets are indicated by 1σ variability cones. The red area highlights the critical zone of kinematic feasibility which is delimited by the lateral limits (black straight lines) and by the slip limit (black semicircle) calculated from the slope dip and friction angle. A potential higher slope inclination (1σ variability) is included by the extension of the critical zone (pale red area) and by the result values shown in italics.

- *Interpretation*

According to the performed analyses are planar sliding along the foliation (Figure 60) and wedge sliding along the foliation and joint set JN1 (Figure 61) the most likely kinematic failure mechanisms. This counts however only for higher elevated areas (above 200 m a.s.l.) since at lower elevations the foliation changes its orientation towards dipping into the slope. Wedge failure along joint sets JN1 and JN2 (Figure 61) should also not be excluded according to these results. All these feasible options are very sensitive to variations in the slope inclination and in the slope orientation. Both parameters are possible to show locally significant variations as indicated by their high variabilities.

The missing of appropriate discontinuity set orientations excludes toppling and in particular flexural toppling from playing a major role for the large-scale slope deformation.

It is essential to compare the results of this analysis with the other available resources (e.g. field observations, scanline data) in order to conclude on the eventual failure mechanism and deformation at Låvan (section 8.2).

8 Discussion

In general, the discussion of results in this study can be divided into two major parts. The first part (8.1) comprises the findings on the Quaternary landscape development and the long-term slope deformation at Dusnjarga and Låvan which findings are largely based on the detailed analysis and mapping of Quaternary deposits in the study area. The second major part (8.2) dedicates exclusively to Låvan thereby discussing in detail the present rock slope deformation. This includes further a final hazard analysis (8.3) for Låvan.

8.1 Quaternary landscape development and long-term slope deformation

The detailed analysis of the local Quaternary geology helps to reconstruct the development of the study area from the last glacial maximum until today. Especially important in this approach is the interaction of Quaternary deposits either with the morphologic elements of the slope deformation (such as grabens or counterscarps) or with deposits caused by the slope deformation (such as slope debris or disaggregated bedrock). The study of these interactions allows to infer on the relative chronological development of the slope deformations and is a traditional approach as implemented in studies like Agliardi et al. (2009a) or Hilger et al. (2018).

The Quaternary geological analysis and presented interpretations are based on the detailed Quaternary mapping, field observations, sedimentological profiles and samples as well as the digital map resources and imagery (e.g. orthophotos, DEM).

All in all, the largest part of the study area is covered by weathered bedrock and the products of slope deformation. Contrastingly, a minor part of the study area is covered by glacial sediments or redeposited glacial material with the only thick successions mapped close to the present shore, at Låvan and Laslett (Figure 30). For one part, this is due to the dominance of steep slopes with sparse vegetation characterizing the study area leading to the study area being largely dominated by strong erosion. Especially the large unstable slopes are basically free of Quaternary deposits. In particular at Dusnjarga, the strong deformation and bedrock disaggregation are supposed to have destroyed and incorporated the formerly existent sediment successions. Låvan shows no Quaternary deposits at all which should be largely due to its very steep character, but it can also hint the higher activity status of a slope.

Among the Quaternary deposits and landforms, those of a direct or indirect glacial origin (Figure 34) were of particular interest and comprised:

- *Thin glacial till deposits*, mainly small patches of secondary till deposits, found mainly as small patches in the high valley and on low-elevated terraces (between 23 and 60 m a.s.l.)

- *Glaciomarine deposits* found as thick sequences of glaciomarine mud with dropstones and dissipation structures that indicate the glacial origin
- *Sheeted flood deposits* and *redeposited glaciofluvial material* found as fan-like deposits directly above the present shore that include a significant share of glacial material
- *Shoreline sets* identified in the coastal morphology and correlated to the Tapes shoreline (Early/Mid-Holocene) and the Main shoreline (Younger Dryas)

8.1.1 Model of development of Quaternary morphology and deposits

The scheme in Figure 63 illustrates the creation of the present geomorphology and Quaternary deposits in the study area as interpreted from the results obtained in this thesis. The scheme focusses on five periods between the last glacial maximum (LGM) and today that were central for the local landscape development and which interpretations are described subsequently.

A. LGM (*23 – 21 ka)*

The large ice masses of the Scandinavian ice-sheet covered Lille Altafjorden and the whole study area during the LGM. During deglaciation, the ice margin did not reach the outer coast before 17 ka (Hughes et al. 2015; Patton et al. 2017). Cold-based ice prevailed at higher elevations where little erosion occurred and therefore also little deposition of glacial products (e.g. Linge et al. 2006; 2007; Fjellanger et al. 2006). However, first subglacial products might have already been deposited and probably increased towards the end of the LGM through the increase in melt-out processes. The ice masses stabilized the slope which is why no deformation is supposed during the glaciation.

B. Lateglacial interstadial (15 – 13 ka)

This period is generally characterized by ice streams filling the fjords of western Scandinavia and this phase comprises the Bølling interstadial (15.3 – 14.1 ka), the Older Dryas stadial (14.1 – 13.8 ka) and the Allerød interstadial (13.8 – 12.9 ka) (Hughes et al. 2016; Patton et al. 2017). According to data presented by Evans et al. (2002) and Hughes et al. (2015), the study area was deglaciated either during the Bølling or the Alllerød interstadial (or during both). The deglaciation occurred probably quite rapidly in the study area and in the local main fjord, the Kvænangen fjord, similarly to other wide and basal over-deepened fjords that showed typically rapid retreat rates up to more than 100m per year (Stokes et al. 2014). Supposedly during this period, most of the till in the high valley was deposited as subglacial melt-out till at the receding glacier(s). The glacial retreat in the high valley was probably accompanied by a braided river system that already eroded and deposited some of the till and shaped the valley's morphology preserved as elevated, lengthy patches (Figure 32). In the fjord, strong deposition of

glaciomarine mud should have occurred in the fjord, for instance through subglacial meltwater streams (e.g. Powell and Domack 1995). This is supported by the dissipation structures (e.g. Figure 42) identified in the lower sequences of the glaciomarine muds which testify local compression through glacial load, thus before. The glaciomarine muds should have been deposited up to the lateglacial shoreline which means higher than 60 m a.s.l. even though the highest identified glaciomarine deposits were at 53 m a.s.l.. The upward-coarsening in the glaciomarine muds and the increasing content of dropstones in these deposits (e.g. Figure 41) are interpreted to mark the recede of the fjord glacier this phase which also led to increasing material input from land, e.g. from the meltwater streams and the braided river system.

C. Younger Dryas (around 12 ka)

Overall, Norwegian glaciers readvanced significantly during the stadial of the Younger Dryas lasting from 12.9 –to 11.7 ka (Hughes et al. 2016; Patton et al. 2017). The study area was apparently not glaciated again following the results from Evans et al. (2002) and Hughes et al. (2015), but the local glaciers should have terminated further within the fjord. The locally preserved Main shoreline is locally preserved as an erosional notch, most likely due to frost - weathering (Vorren et al. 2008), and its existence further supports the absence of fjord glaciers at this time.

It is difficult to certainly assign any Quaternary units in the study area to the Younger Dryas phase. On land, no distinct glacial landforms or indications for an ongoing or renewed glaciation at the higher elevations could be identified. But probably some erosion and redeposition of glacial material (tills) occurred on land. Glaciomarine sedimentation is supposed to have continued especially through ice-rafting which is supported by a growing proportion of glacial clasts in the deposit's upper sequences as well as by the absence of dissipation structures (Figure 41). Profile 22-9-L (Figure 41) is important in this respect: compact glaciomarine deposits are gradually overlain by a undermelt diamicton that involves a significantly growing share of slope deformation products. This is a possible indicator for slope deformation (at Dusnjarga) starting after the Younger Dryas since this profile is situated just below the Main shoreline (53 m a.s.l.). But otherwise, there is no indication in the sedimentological record for increasing slope deformation during this period.

D. Early to Mid-Holocene (8 – 5 ka)

The Early to Mid-Holocene coincides with the phase of the Tapes transgression with its maximum probably between 7600 and 5600 cal a BP (Bondevik et al. 2019). The transgression is interpreted to be well expressed in the study area through the distinct shoreline that is present along large parts of the study area's coast and forms the lower terraces between 23 and 25 m a.s.l.. These lower terraces form typically the upper limit of the glaciomarine muds

(section 7.2.3), and as the terraces partly consist of glaciomarine muds (e.g. profile 22-9-L), these have been probably eroded above the Tapes shoreline. This paleo-shoreline forms also the upper limit of the sequence of fluvial and redeposited glaciofluvial products. It is likely that the material was deposited fluvially and/or by floods just below the former sea level during this period (compare section 7.2.3). This sand and gravel fan below the shoreline was partially supplied by a debris flood event creating the sheet flood deposits (Figure 43) appearing in its vicinity just above the paleo-shoreline. The flood and fluvial processes creating the afore-mentioned deposits as well as probably eroding of the glaciomarine deposits above the Tapes shoreline indicate extensive surface water runoff during this period. The blanketing of the terraces above the Tapes shoreline with a thin redeposited till layer is most likely also connected to these events that involved strong erosion and redeposition of glacial material.

Holocene climate optimum which lasted in Norway approximately from 8 to 5 ka coincides with this period (Lilleøren et al. 2012). It was especially characterized by warmer winters and towards its end by a greater seasonality, likely involving strong annual snow melt events that might be related to the described deposits (e.g. Hilger et al. 2019). A small outburst flood from a lake at the depression bowl next to profile 24-9-E (Figure 36) might be another hypothesis for the creation of the flood deposits (profile 24-9-E; e.g. Figure 39).

The flood and redeposited (glacio)fluvial sequences were deposited in the stable area just in between the lateral flanks of Dusnjarga and Låvan. The sequences indicate substantial redeposition of glacial material, but they also include a high share of local slope debris (angular gabbroic components) possibly indicating an activation of the lateral limit of Dusnjarga that contributed to the slope debris deposits. The slope deformation in the formerly mentioned upper sequence of profile 22-9-L (Figure 44) could also well be redeposited from this period.

E. Late Holocene (after 4 ka)

This phase is supposed to represent the whole second half of the Holocene during which phase the sea level continued to sink relatively. The thin till patches found on the frontal lobe of Dusnjarga (7.2.3 A)lie below Younger Dryas sea level which implies that they constitute the remnants of mostly eroded glaciomarine deposits, or they redeposited from upslope area. It is here suggested that these till patches were redeposited through flood events in the Early to Mid-Holocene, similarly to the other till deposits found on the terraces above the Tapes shoreline. The necessity of surface water runoff on Dusnjarga's frontal lobe at this time would indicate that the bedrock was not very disaggregated. Today the strong disaggregation of the frontal lobe obstructs all surface runoff. This is a hint that deformation processes of the frontal part of Dunsjarga continued in the Late Holocene.

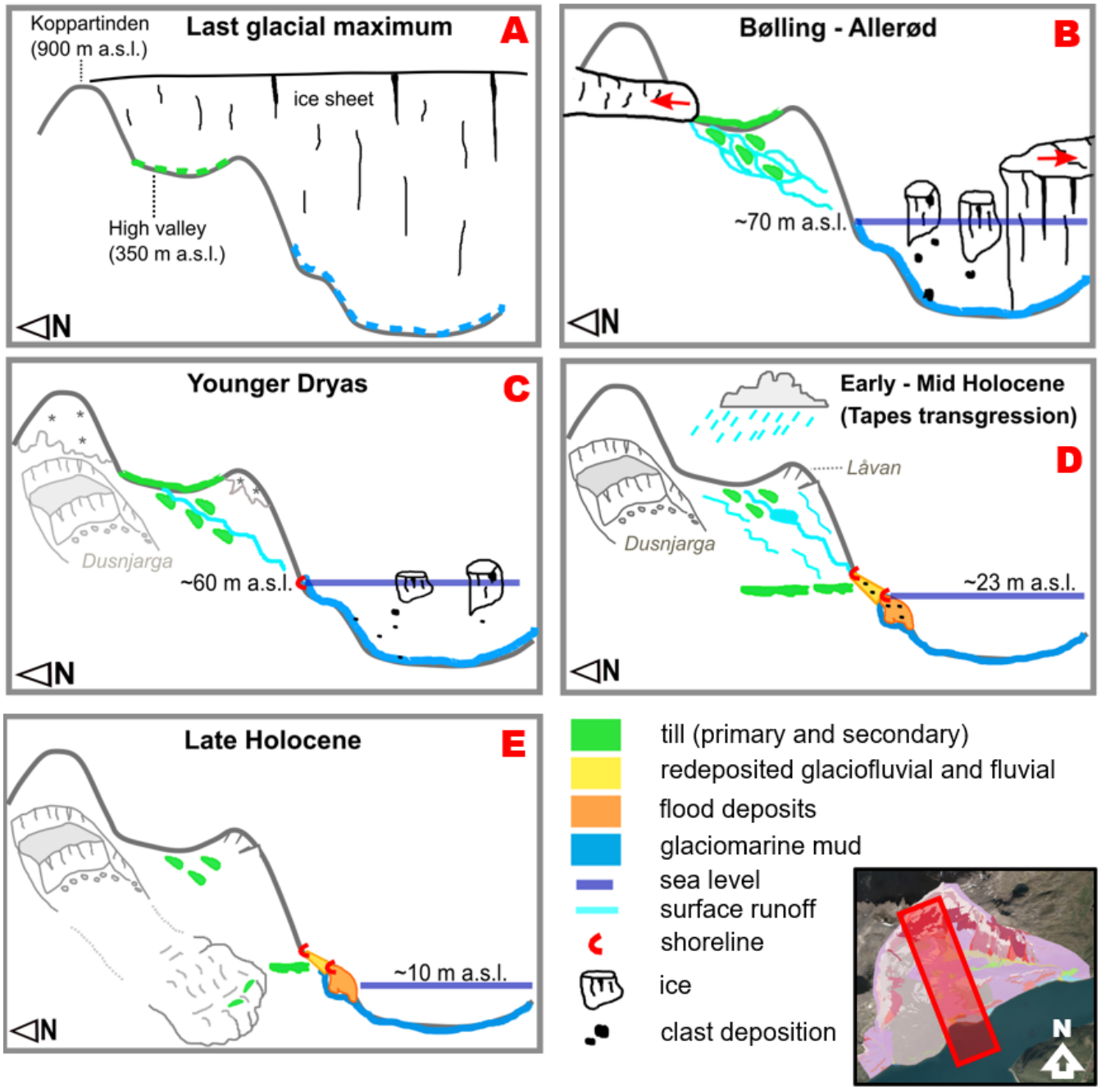

Figure 63: Schematized development of Quaternary morphology and deposits in the study area: The scheme serves only as a visual interpretation of processes described in text, but as a precise representation in terms of time and space. The section roughly covers the area indicated in the small map. A) LGM (~23 – 21 ka): fjord and high valley are covered by glaciers; maybe already some deposition of subglacial material. B) Bølling and Allerød interstadials (~15 – 13 ka): deglaciation in the study area; deposition of till and glaciomarine mud and dropstones; braided river system in the high valley. C) Younger Dryas (~12 ka): erosion creates the main shoreline; glaciers are further within fjord and deposition of glaciomarine mud continues; first activity of Dusnjarga after this phase. D) Early to Mid-Holocene involving the Tapes transgression (~8 – 5 ka): debris flood (re)deposits of glaciofluvial material below and sheet flood products above the shoreline, likely caused by extensive precipitation events and/or a lake outburst; tills redeposited on Younger Dryas terraces; presumed increase of slope deformation. E) Late Holocene (<4 ka): ongoing slope deformation; frontal protrusion of Dusnjarga disrupts shorelines and sediment sequences; further decreasing sea level.

8.1.2 Indications for the chronological development of the rock slope deformations

- *Dusnjarga*

The coarse deposits (unit I) underlying glaciomarine mud at profile 22-9-L (Figure 41) are an important chronological indicator for the deformation at Dusnjarga. Unfortunately, it could not be determined if they represent slope debris or proglacial advance gravel. In case of slope debris, this would indicate gravitational activity of Dusnjarga's frontal domain before the deposition of glaciomarine deposits, at least before Younger Dryas. In case of proglacial advance gravel, slope deformation would most likely have started after the Younger Dryas as indicated by the increasing content of slope debris in the profile's upper sequences.

The identified flood deposits (Figure 44) and the (glacio-)fluvial fan deposits (Figure 43) below contain in certain sequences a high amount of local slope debris. This might indicate increasing slope deformation around the time of the Tapes transgression which is the most likely time of deposition. Likely these deformation products descended from Dusnjarga's eastern lateral flank leading to the hypothesis of increasing deformation of Dusnjarga's central domain and the development of its flanks around the Tapes transgression. The suspected climatic events causing floods in this time (e.g. strong precipitation or snow melt events) might also hypothetically be connected to this local deformation.

It is likely that strong deformation occurred during the Early to Mid-Holocene since probably redeposited glacial till is found in the sheet flood deposits (Figure 44) and on the terraces just above the Tapes shoreline (section 7.2.3 E). This fluvial deposition depends on surface water runoff. The thin till patches on Dusnjarga's frontal lobe should either have the aforementioned origin or be remnants of eroded glaciomarine deposits. Assuming the former, this would indicate that the principal deformation of Dusnjarga's frontal lobe and the connected extensive rock mass disaggregation occurred after the till redeposition, thus after the Tapes transgression, maybe only in the Late Holocene and continuing up to the present-day.

- *Låvan*

At Låvan, no Quaternary sediment sequences were found in the deformation area which hampers the interpretations on its relative timing. At least for the head domain, the generally 'fresh' appearance (typically little surface weathering and little lychen or moss cover) of the morpho-gravitational surface features (e.g. head and subordinary scarps) must be interpreted with caution, but could possibly limit the deformation at the head domain to comparably young ages.

The distinct coastal bulge at Låvan's front is conformably overlain by glaciomarine mud which deposits stop at the well-expressed Tapes shoreline. Especially, the local existence and constant elevation of the Tapes shoreline along this frontal protrusion indicate that the main (compressional) deformation at creating the protrusion occurred before the Tapes transgression and likely after the Younger Dryas.

- *Failure chronology with respect to Norwegian rock slope failures*

As was described in section 5.6, studies by Böhme et al. (2015), Longva et al. (2009) and Hermanns et al. (2017) identified clusters of rock slope failures in the Early to Mid-Holocene between 8 and 5 ka in S- and W-Norway. In studies by Böhme et al. (2019) and Hilger et al. (2018) increased rock slope failure activity was indicated for the Mid-Holocene, roughly between 6 and 4 ka. Interestingly, these periods include the presumed period of the Tapes transgression maximum between 7600 and 5600 cal yr BP (Bondevik et al. 2019). This would for instance match the timing of the afore-suggested increase in activity at Dusnjarga's central domain and eastern lateral flank. Reasons remain speculative but the period coincides with the Holocene climate optimum in Norway during which stronger precipitation, increasing snow melt or thawing permafrost might have been possible factors (Lilleøren et al. 2012).

However, the real start of the slope activity might have also occurred well before. At least most rock slope failures and rock avalanches in S- and W-Norway were activated shortly after the deglaciation (Böhme et al. 2015; Hermanns et al. 2017). The early deformation might just not appear in the scarce sedimentological record and for instance at Dusnjarga might have been limited to the head domain and head scarp. The described findings at profile 22-9-L (section 7.2.3) might also indicate a start of deformation directly following the deposition of the glaciomarine mud (thus likely after the Lateglacial interstadial or the Younger Dryas)

- *Future potential and requirement*

A potential, more detailed investigation of the Quaternary deposits is expected to lead to very limited improvement of the presented relative chronology, mainly because of the scarcity of Quaternary sediments at Dusnjarga and Låvan that can be analyzed. Trenching of the sediment filling in deformation features e.g. at the trench of a head scarp (as in McCalpin and Hart 2003) has not much potential either since none of the observed trenches or deformation features shows a considerable sediment infill.

Nonetheless, specific recommendations on how to improve the relative chronology of slope deformation would be the following: This would be firstly a further investigation of the sediment sequence including glaciomarine deposits at profile 22-9-L where a thorough analysis of both the upper coarsening contact of the glaciomarine deposits as well as their lower contact to potential proglacial gravel (or slope debris?) would be especially important. But the lower

contact of the glaciomarine deposits should be also determined and investigated at other locations with the aim of characterizing the likely glacial products below.

The highest potential however to improve the chronology at Dusnjarga and Låvan could be reached through absolute dating methods. Particularly TCN dating (e.g. as in Böhme et al. 2019; Hippolyte et al. 2006; 2012; Hormes et al. 2008) would have the greatest potential and could be performed on the head scarps and other scarps in the head domains of Dusnjarga and Låvan. Apart from the head scarps, TCN dating of the large boulders in Dusnjarga's central domain would be of interest. At Låvan, it would be additionally important to date the frontal scarp limiting the frontal domain (Figure 57) that could theoretically collapse, or to date the smaller rockslide at the eastern head domain (Figure 64). Furthermore, radiocarbon dating (e.g. as in Agliardi et al. 2009; McCalpin and Irvine 1995) could be also performed in order to improve the deformation chronology in the study area. This would however depend on dateable organic material which is probably not easy to find in the deformation area since no lakes or swamps exist and surface features as trenches do not seem to contain much sediment material. Therefore, another strategy would be to use optical stimulated luminescence dating on the sheet flood deposits (e.g. as in Alexanderson and Murray 2012).

8.2 Låvan: characterization of rock mass and failure mechanisms

8.2.1 Rock mass characterization and interpretation

The local discontinuities form the weaknesses within the rock at Låvan and are most relevant for the slope instabilities due to the generally high strength of the intact rock that was recorded (Stead and Wolter 2015). Both the foliation and the three defined joint sets control the slope stability.

The foliation is generally weakly expressed which is also reflected in the analyzed scanline data (Figure 52), e.g. by its relatively low persistence. At no location formed the foliation the dominant discontinuity, but spatial and lithological variations of the expression of the foliation were recorded (section 7.5). For instance, at the head domain it seems that the bedrock is stronger foliated in the lower slope sections due to lithological changes. Very relevant for the slope's failure mechanism is the foliation's change of orientation and dip depending on the elevation (e.g. Figure 50): in the deformed slope as well as in the stable surrounding, it changes from a gentle SE-dip (mean orientation = 138/23 ±13°) in the upslope areas (>200 m a.s.l.) to moderately NW- or NE-dipping (mean orientation = 007/21 ±23°) in the lower areas (<200 m a.s.l.). This behavior was observed similarly in deformed and undeformed slopes which contradicts a hypothesis of strong downslope rotation. The foliation in the lower slopes is

similar oriented as a N-dipping, Caledonian thrust-fault of the Seiland Igneous Province that, as suggested by Roberts and Elvevold (2018), underlies the local rock unit (Figure 6B; section 4.2), and as a theory the foliation might align to this thrust contact. Krauskopf (1954) suggested a basin structure for the Seiland Igneous Province whereby overall a complex pattern recorded for the foliation complicate this interpretation.

Joints are commonly created by tectonic stresses, but frequently non-tectonic joints, e.g. exfoliation joints or sheeting joints, are also found (McColl 2012). Especially, sheeting joints created as an effect of debuttressing (e.g. Figure 13B) are typical for deglaciated areas and show characteristics such as a very local extent and oriented sub-parallel to the surface (Nichols 1980). At Låvan however, typical sheeting joints were not identified, and the defined joint sets are generally interpreted as post-Caledonian brittle structures created by tectonic stresses.

JN1 (mean orientation = 119/87 ± 27°) is the dominant JN set as expressed in the structural data and field observations at basically all investigated outcrops. In the scanline data (Figure 52), JN1 shows for instance by far the highest persistence and highest width which supports the dominance of the set. Furthermore, JN1 shows its dominance also in the deformation area's morphology where many features (e.g. counterscarps, trenches, head scarp) follow its orientation (section 7.5). JN1 seems to follow the orientation (SE-NW) of several faults recorded in the nearby Øksfjord area (Krauskopf 1954; Roberts and Elvevold 2018). Generally, most joints develop as extensional fractures (Hencher 2013). The vertical orientation of JN1 fits to an extensional genesis and its orientation is normal to the direction of Mesozoic rifting indicating its possible provenance (e.g. Nøttvedt and Johannessen 2008).

JN2 and JN3 showed generally very similar characteristics as expressed in the scanline data (Figure 52). A clear dominance relation between JN3 and JN2 was not indicated but differed between different outcrop locations. It is also important to notice that the scanline data is based on a variety of outcrop orientations (Figure 53) among which NE-SW-striking outcrops were most frequent. This might lead for instance to an underrepresentation (or a higher resulting spacing) of JN2 and JN3 in the data from those outcrops. Many surface features in the deformation area follow the NE-SW-strike which is similar for JN2 and JN3 (Figure 49). It is usually difficult to say if the features follow the orientation of one specific discontinuity set specific or both, and it could be observed that scarp faces often follow a pattern of small surfaces composed by both sets (Figure 56A). Typically, JN2 and JN3 form an X-pattern with an angle of around 60° between both sets (Figure 56B). This fact, the same strike direction and the similar joint characteristics might possibly mark JN2 and JN3 as a pair of conjugate shear fractures, for example created through stress release during exhumation (e.g. Hancock 1985).

In the field no specific faults were identified at Låvan, but as indicated in section 8.2.4 (Figure 66) a larger fault might follow the major counterscarp in the central slope.

At Låvan, the rock mass disintegration increased relatively little from the head towards the frontal domain standing in strong contrast to Dusnjarga dominated in most parts by strong rock mass disaggregation. Reasons for this aspect at Låvan are further discussed in the following sections.

8.2.2 Assessment of the failure mechanism

The performed failure analysis (section 7.8) shows that planar failure on the foliation (SC) is kinematically the most likely failure mechanism (Figure 60). Wedge failure on SC and JN1 has also a high potential (Figure 61) and likely the ruling failure mechanism is a combination of planar and wedge sliding on SC and JN1 whereby the main part of sliding will always happen on SC with JN1 acting rather as either as a very steep, lateral wedge sliding surface or a lateral release surface.

JN1 forms principally both good lateral and good back release surface as e.g. indicated by the orientation of scarp faces and the back scarps gradual transition to the eastern lateral flank (e.g. Figure 55,56). The scarps and other surface features show that JN2 and JN3 together combined form also good back release surfaces (e.g. Figure 55). In general, back release surfaces are much better given than lateral release surfaces which is also visible in the hardly traceable lateral limits.

Large unstable rock slopes show generally much more complex structures and interactions of multiple failure mechanisms than smaller instabilities show (Stead et al. 2006). Låvan's basal sliding surface should be mainly defined by the foliation but is most likely a more complex surface constituted by multiple connected and stepped basal surfaces as it is often the case at deep-seated rockslides in crystalline rock (e.g. Bonzanigo et al. 2000; Ganerød et al. 2008) or as exemplified for the Norwegian Åknes rock slide (Blikra 2012). Persistence has a strong influence on the magnitude of rock slope instabilities (Molina 2010), and the principally low persistence and small width of SC (Table 4) support the theory of multiple connected sliding surfaces. JN2 that dips also in downslope direction but steeper than the slope is likely to connect the interrupted sliding surfaces. These characteristics are visualized in the interpreted geological cross section (Figure 66) in section 8.2.4. The sliding will be focused on zones were the foliation is particularly well expressed and continuous. The foliation showed strong spatial variations (mostly depending on the stratigraphy) in its expression and characteristics (e.g. persistence, width). The foliation was particularly well expressed in the dark gabbro and at the lithological transitions between the coarse-grained, anorthositic and the finer, dark gabbro

(section 7.5) which is why sliding is supposed to follow preferably these observed weaknesses. Particularly strongly weathered, sheared or brecciated layers were however not recorded which also speaks against a very low shear friction angle (e.g. lower than 20°). But further geological investigation as core drilling or more extensive mapping would be needed to support this suggestion.

The observed change of the foliation's orientation at lower slope elevation from SE- to roughly N-dipping (Figure 50) is highly relevant for failure interpretation of the instable slope since the foliation is supposed to control the failure. On the N-dipping foliation, planar and/or wedge sliding is however kinematically impossible resulting in a complication of the failure behavior in the frontal domain. The elevation of 200 m a.s.l. for the change of the foliation is a rough estimation since no outcrops could be recorded in the central slope section and it is questionable if the foliation changes very gradually or rather abrupt (e.g. at a fault). None of the discontinuity sets recorded for the frontal block and its scarp (22-9-I; Figure 57) allow kinematically for sliding, however strong compression should take place and resulted probably in the pushing out of this frontal block along the relatively persistent discontinuities formed by the foliation and JN3. This is illustrated and is shown in further detail in section 8.2.4.

At the frontal scarp, small-scale toppling (controlled by JN1, JN2, JN3/SC) was also witnessed leading to large talus fan (Figure 57). Toppling can however be excluded from being relevant for the large-scale failure behavior due to the results from the failure analysis (section 7.8).

A slope orientation more towards SE (approximating 140°) would yield significantly more critical discontinuity orientations in all tests for planar (Figure 60) and wedge sliding (Figure 61) and would thus favor these failure mechanisms. This is expressed in the morphology of the deformation area and demonstrated in Figure 64. It depicts a minor, relatively fresh rock slope failure (A) and a neighboring, instable block (B) in the eastern head domain which both indicate displacement towards SE. The eastern part of the central domain (C-D) is less topographically confined in SE-direction and shows a higher density of gravitational deformation features, such as counterscarp-like, uphill-facing "wedges". This implies the development of a smaller subarea deforming independently from the large unstable rock slope and with different and probably on a shallower sliding plane.

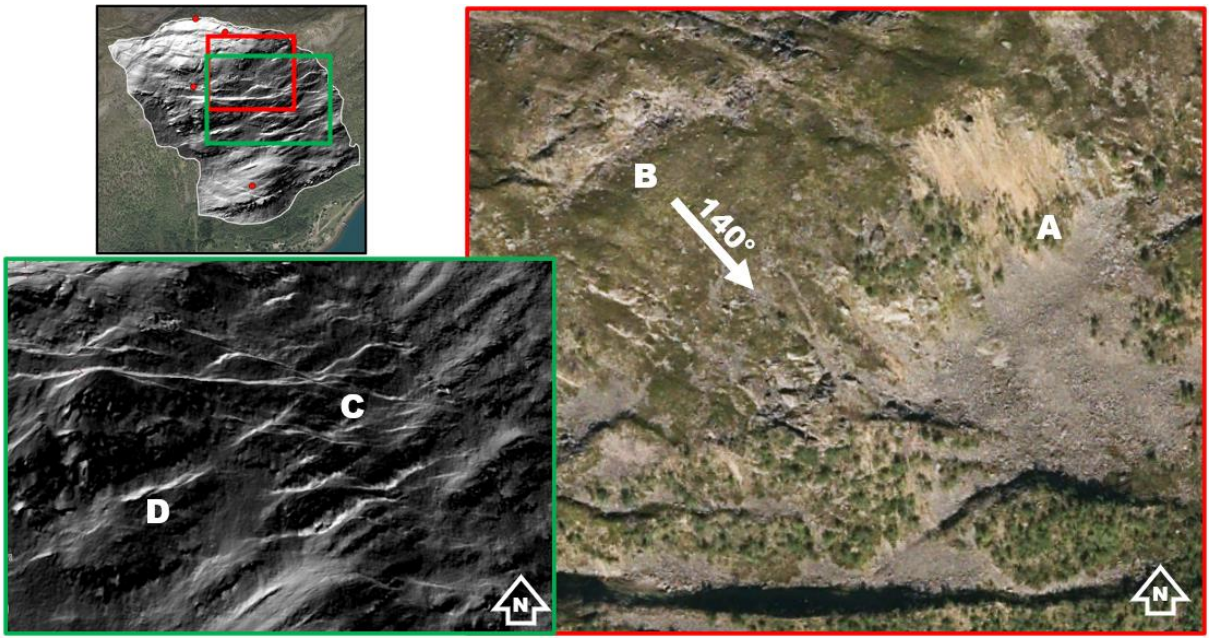

Figure 64: A) Scarp and talus fan of relatively recent, smaller rockslides and rock fall. Slide direction was obviously towards SE and the scarp shows the typical orientations matching the strike of JN1 and JN2-JN3. B) Unstable block that shows displacement towards SE. This is indicated by the opening of the trench to the NW (along JN2-JN3) whereas no trench opens at its NE-side, but it is also indicated by the increasing rock fall at the SE-side of the block. The arrow indicates the kinematically optimal orientation for sliding. C) Eastern part of the deformed slope (central domain): the high density of small counterscarps implies many wedge-shaped sliding blocks that could develop in this part due to less confinement in SE-direction. D) Vice versa, the area west of it shows less morpho-gravitational features and hints the existence of a more integrated central sliding block.

8.2.3 Classification of the rock slope failure

Most of the characteristic criteria for a deep-seated gravitational slope deformation (DSGSD) that were defined by Agliardi et al. (2001; 2012) apply for the slope deformation at Låvan, such as:

- great thickness and large volume (>0.5 km³)
- The deformation stretches across the whole length of the slope.
- The boundaries are not clearly defined.
- typical morpho-gravitational features (mainly extensional) in the head and upper central domain (e.g. trenches, scarps, counterscarps)
- absence of surface water run-off

The central, steep slope of Låvan shows a dense pattern of counterscarps and graben structures that form a ‘saw-tooth surface’ (e.g. Figure 29) which is also characteristic for deep-seated deformations (Reitner and Linner 2009). Creep movement (even though not quantified for the present-day) can be inferred to be responsible for the observable deformation. The zone of accumulation is for instance much better developed at Dusnjarga (toe bulge and

buckling), nonetheless Låvan can be classified as DSGSD or as sackung (sagging slope), a synonym referring to the complex, deep-seated deformation style (Hutchinson 1988).

Characteristic for a sackung is that the majority of deformation and displacement occurs at the upper part (head domain) whereas being less clearly expressed at the frontal domain which applies also to Låvan (Zischinsky 1966). The typical sackung shows a downslope increase of rock mass disintegration through stress at the toe which is very prominent at Dusnjarga where the rock mass collapses into joint-controlled particles (Zischinsky 1966; 1969). This downslope rock mass disintegration is not very pronounced at Låvan which can be thus interpreted as an intermediate state of sackung showing graben structures, counter scarps and bulging toe at the coast (Poisel 1998).

Regarding the commonly used landslide classification by Varnes (1978) and Hungr et al. (2014) (Table 2), the class 'mountain slope deformation' describes phenomena as DSGSDs and sackung features. Nevertheless, it is important to determine the dominant type of sliding at Låvan (section 5.3).

Rotational slides are quite rare in Norway since it is not expected to occur in strong rock which in fact speaks against this failure type for Låvan. Låvan's head scarp is low in height and rather indicates a combination of horizontal and vertical displacement. In case of rotation, it should be also measurable in form of a significant back tilt of marker beds (Cruden and Varnes 1996). As displayed in Figure 67, rotation is not indicated at the head and the discontinuities at the front are relatively similarly oriented as outcrops in stable locations at the same elevations (section 7.3). Thus, rotational sliding is not expected to be the dominant failure style at Låvan.

Translational sliding is kinematically possible as planar failure on the foliation as presented in the failure analysis and translational slides are very common to occur in Norway (e.g. Bunkholt et al. 2012). However, the characteristics of the foliation at Låvan (e.g. the low persistence and the change of dip at lower elevations) as well as the missing of sheared and weathered bands within it indicate that classical translational sliding on one or several basal planes is unlikely to define the overall deformation style.

Låvan has probably a complex rupture surfaces consisting of several planes maybe with an uneven curvature which would apply to a compound slide as schematically illustrated in Figure 65 (Hungr et al. 2014). It is common for compound slides to have an active proximal block with horst and graben structures that drives a relatively stable passive block (Hungr et al. 2014). At Låvan, these two blocks might be separated from each other by the large counterscarp. According to Hutchinson (2006), internal shear to the rear of the slide as well as internal distortion is particularly important to enable failure and usually results in the formation of a graben delimiting the top from the lower sliding block which fits again to the large graben or

counterscarp at Låvan (e.g. Figure 29). Sliding surfaces in compound slides can be classified either as unevenly curved (listric) or bilinear on two or more sliding planes which latter case is likely for Låvan due to the high rock strength and the exemplified characteristics of the foliation (Hutchinson 1988).

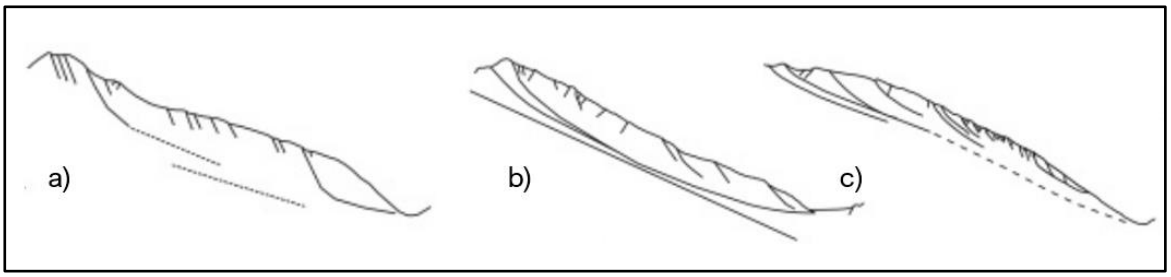

Figure 65: Exemplary mechanisms and failure surfaces of three theoretical examples of large compound slides as presented in the literature. *Source: a-b) Ambrosi and Crosta (2006), c) Agliardi et al. (2001).*

8.2.4 Interpretation of slope deformation

An interpreted cross section for Låvan is presented in Figure 66. It crosses the slope deformation from NNW to SSE (azimuth 155°) which is the interpreted direction of displacement. It should be noted that JN1 which forms dominant discontinuities in all domains of Låvan, is underrepresented in this profile direction (due to its similar strike direction).The interpreted deformation is based on the presented results and becomes increasingly interpretative with depth. In particular, the depth and exact trace of the basal sliding plane is speculative, and its surface is expected to be more complex (e.g. stepped or uneven). It does not daylight visibly on the slope and the lower end might daylight below the coastal bulge in the fjord. A detailed discussion treating the slope deformation as presented in the cross section follows in the subsequent paragraphs.

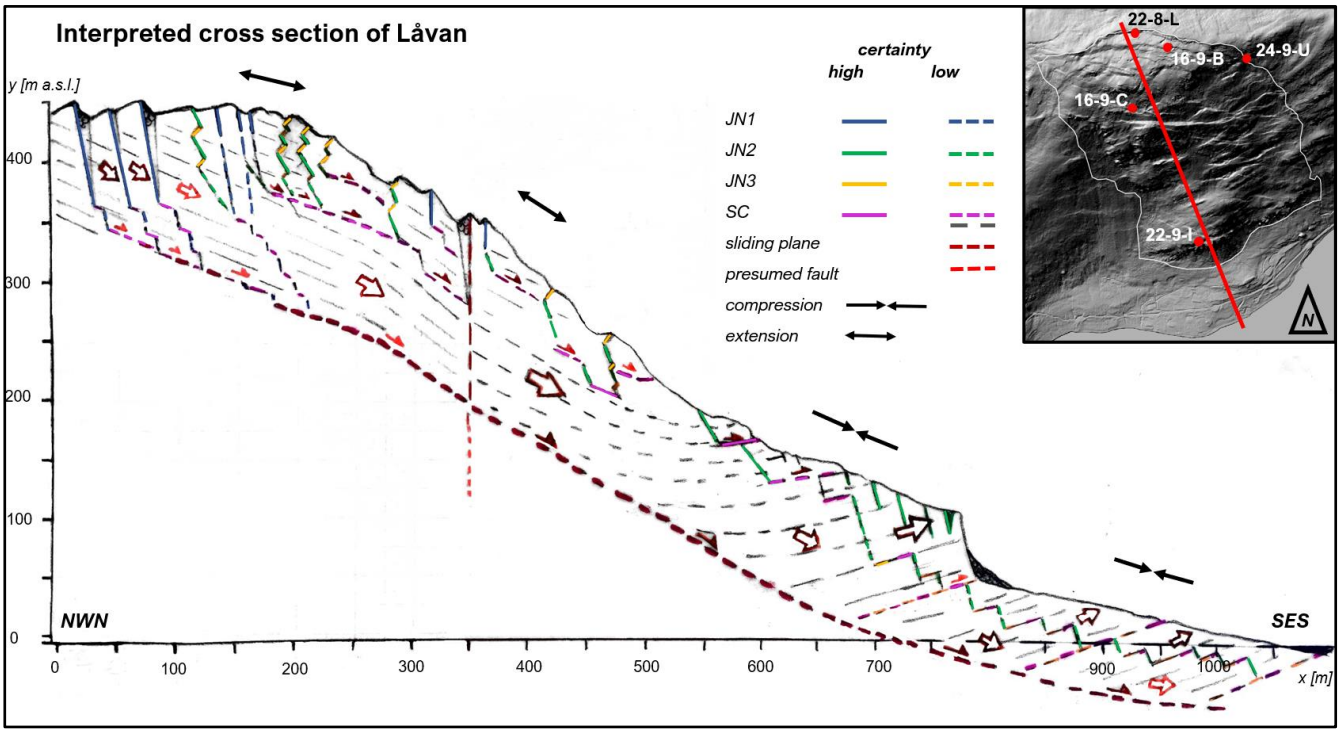

Figure 66: Interpreted cross section across the rock slope deformation Låvan (bearing 155°).

Låvan's head scarp is accompanied by a distinct trench and tension cracks (e.g. Figure 27) that indicate not only vertical but also horizontal displacement and thus extension. An uppermost sliding block is displaced along the head scarp as visible in Figure (67A). The block's surface has approximately the same inclination as the stable surface behind the head scarp which is why back tilt of the block (connected to rotation) cannot be justified. However, characteristics as the scarp's curved shape at its western side and the scarp's decrease in height towards the sides would speak for a listric character (e.g. Hungr et al. 2014). Hence, the actual sliding surface might be a hybrid between a listric and a bilinear character, but it is illustrated as bilinear in the cross section (Figure 66) due to the strong afore-mentioned arguments. The upper sliding block is followed by a second, weathered back scarp that forms transitions to a trench and tension cracks which delimit a second sliding block (Figure 67B). The area in front of these upper sliding blocks (Figure 67C) shows a dense pattern of tension cracks, trenches and horst and graben structures that indicates complex deformation of multiple, separated sliding blocks dominating the head domain. As indicated also in Figure 66, the separated blocks are controlled by the defined JN sets and can differ in their sliding behavior, comparable to observations made at the rockslides at Åknes (Ganerød et al. 2008) or Jettan (Blikra et al. 2015)

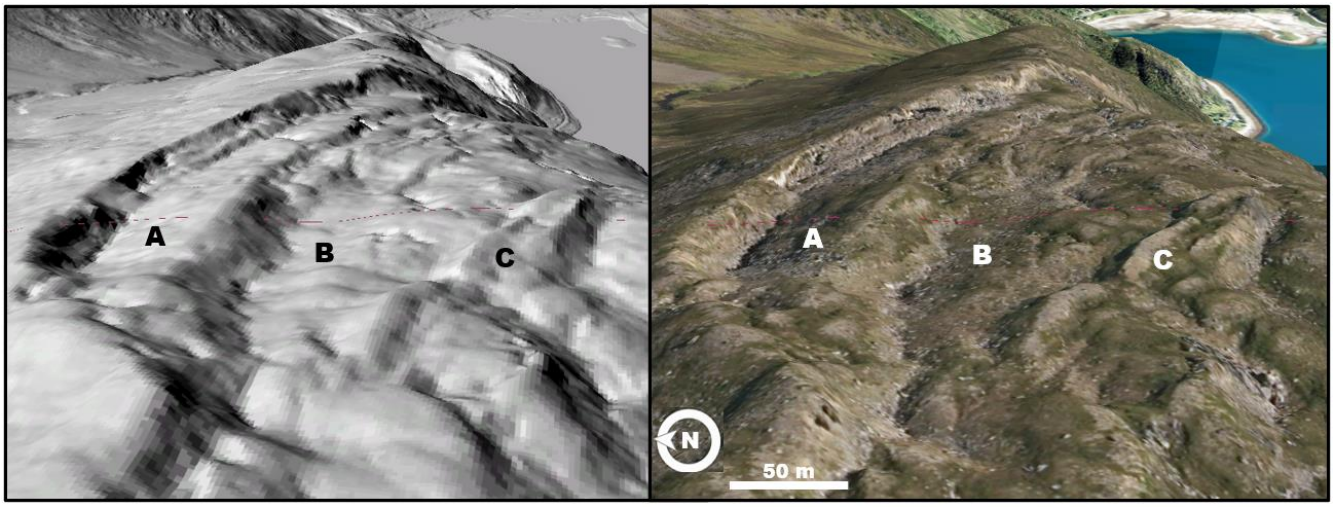

Figure 67: 3D-view *(ArcGIS Pro)* of Låvan's head domain: Left: DEM; right: orthophoto. A: Uppermost sliding block is displaced along the head scarp and tension cracks. The block's inclined surface matches the inclination in the stable area next to it. B: The second sliding block's surface is separated from the upper block by trenches, tension cracks or a subordinary back scarp which indicates horizontal and vertical displacement. C: A system of trenches, tension cracks and horst and graben structures indicates the existence of multiple sliding blocks showing complex displacement patterns dominated by extension.

The large counterscarp in the central slope (e.g. Figure 28) represents a crucial element for the slope deformation and is interpreted to separate the strongly dissected block of the head domain from a large, more intact sliding block forming the central domain as displayed in the cross section (Figure 66). It is the most dominant morphologic element at Låvan apart from the head scarp and stands out by its persistence running transverse to the slope and thereby, unlike most other features, not following the discontinuity sets. In the geomorphology, the trace of the counterscarp can be even followed outside the deformed slope. As highlighted in the DEM in Figure 68, the trace follows a line of increased surface erosion that can be followed from the fjord up to Dusnjarga's head scarp. The large counterscarp is thus interpreted to be developed along a fault. Future field investigation of this fault would be necessary in the future. It might be related to JN1 justifying its nearly vertical orientation in the cross section.

The large counterscarp forms a predominantly extensional feature created by the downslope sliding of the central block which is also driven by the push from the head domain block. Morpho-gravitational features are not well expressed in the central block which seems to be a quite coherent block in contrast to the heavily dissected head domain. One reason for this is the change of the foliation's orientation that should occur somewhere below the counterscarp and hampers planar sliding. The change in the foliation's orientation is displayed as gradual in Figure 66 but might also occur abruptly at a not-recorded fault. The basal rupture surface is however interpreted to roughly follow its trend from above due to increasing rock mass disintegration in depth. Another reason for the lesser degree of dissection and gravitational

morphology in the central block is probably the topographical confinement of the block in SE-direction as explained in section 8.2.2 (Figure 64).

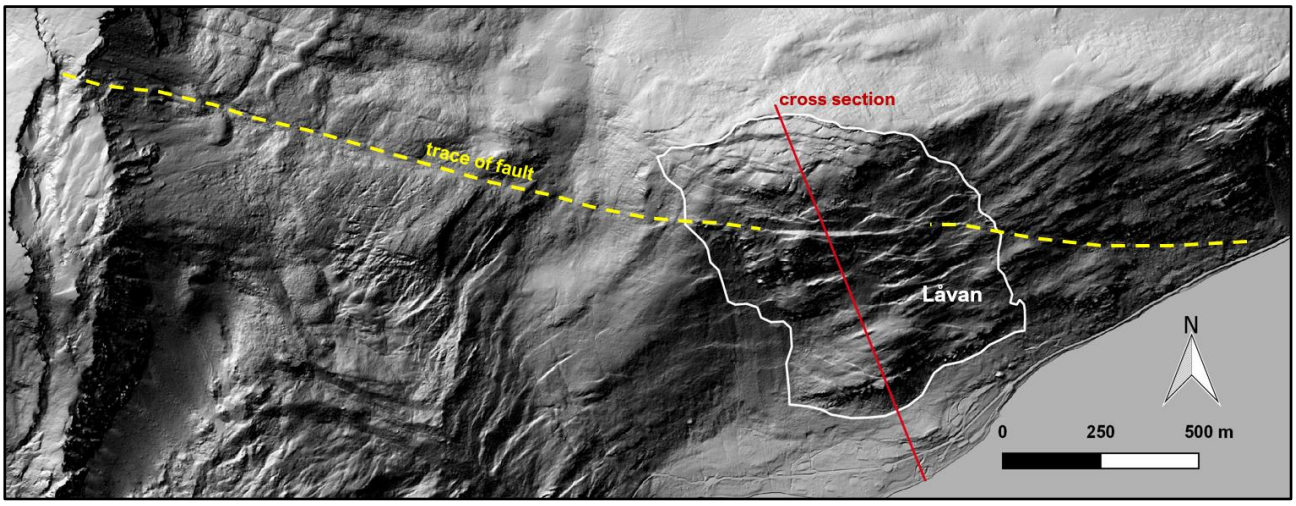

Figure 68: The DEM hints that the large counterscarp in the center of Låvan follows a fault that is traceable from the fjord up to Dusnjarga's head scarp. This explains why the large counterscarp does not follow the trends of discontinuity sets.

The transition from the steep slope of the central domain to the protruding frontal block is morphologically quite abrupt (Figure 69A). The frontal block is dominated by convex shapes and appears as a relatively coherent block with few signs of internal dissection. Solely some small trenches following JN1 indicate some degree of internal extension and dissection (Figure 69B), but the frontal block is clearly characterized by a compressional regime. Its size and integrity in depth is unsure but the block was obviously pushed outward along a rupture surface that must be situated below the frontal scarp, likely hidden under the talus fan (Figure 69C). Rock segments prone to collapse and rock fall occur at the frontal scarp (Figure 57) even though discontinuity sets at the frontal domain (Figure 50) themselves do kinematically not suggest failure. This indicates that this block has been pushed out by forces from the upper slope and is principally forming an outward-pushed buttress to the rest of the slope. It might be consequently a critical part for sudden failure and a further investigation of other outcrops in this domain is recommended, particularly regarding the settlement's situation below.

The settlement itself is situated on a coastal protrusion (Figure 69D) as well created by compressional deformation. No outcrops for structural data were available in this part which is why it is structurally and genetically interpreted similarly to the frontal block with sliding surfaces cropping out above and/or below the present coastline. Supposedly however, the creation of the coastal protrusion is considerably older and longer inactive than the frontal block and the frontal scarp. This is indicated by the smooth, flat morphology but also by the well-preserved Tapes shoreline as discussed in section 8.1.2

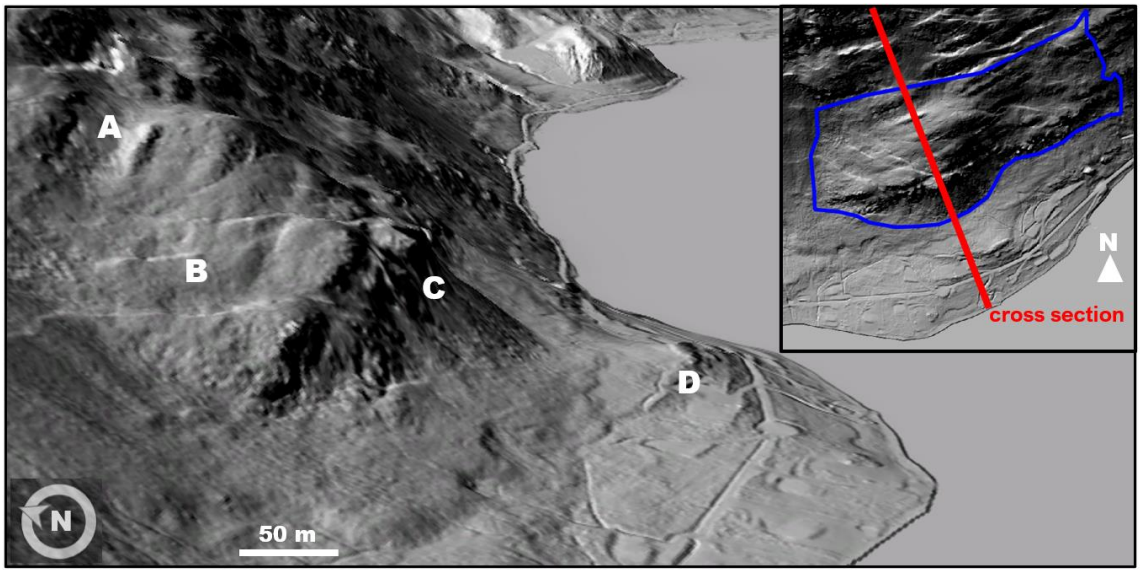

Figure 69: DEM 3D-view of the frontal block (domain) and coastal protrusion of Låvan: The small map depicts the morphological limits of the frontal domain (blue line). Transition from the extensional regime of the central domain to the compressional regime of the frontal block. B) The frontal block shows some signs of internal collapse/extension as here visible by small trenches following JN1. C) The basal sliding plane of the frontal block (probably following JN3 and SC) should be hidden somewhere under the frontal talus fan. D) The whole coastal protrusion is interpreted as an own displaced block pushed out into the fjord.

8.2.5 Controlling factors

As always with unstable rock slopes, geology and topography together have preconditioned the development of the rock slope instability at Låvan (McColl 2012). The weak link, regarding the local geology, is formed by the afore-described structures in the local rock allowing and controlling the rock slope failure.

The Quaternary glaciations surely had a strong impact on the slope instability being responsible for several preparatory factors. Låvan's topography is characterized by a steep walled fjord setting that was shaped during the former glaciations. Thus glacial erosion and wall steepening prepared this slope instability by increasing the self-weight shear stress leading to failure if rock mass strength is exceeded (e.g. Caine 1982). Additionally, the vertical isostatic uplift following the deglaciation amounts around 50 height meters and thereby contributed to the present-day elevation of the slope (Vorren et al. 2008). Isostatic uplift conditions also seismic activity but the effect of seismic weakening on this slope deformation is hard to assess. Debuttressing through stress release in the course of deglaciation is often identified as one of the main preparatory or triggering factors identified for slope failures, e.g. (Agliardi, et al. 2001). The absence of typical debuttressing or sheeting does not exclude a major effect of debuttressing for Låvan since stress release can also follow existing discontinuities in an already dissected rock mass as at Låvan (e.g. Wyrwoll 1977).

Climatic factors and future climatic changes are especially important as triggering factors that could cause a future reactivation of the rock slope failure. Water flow occurs exclusively as groundwater flow inside the deformed slope and is likely to occur preferentially at the basal sliding surface. Deep-seated slope deformations as Låvan deep-seated landslides are usually less sensitive to short maximum precipitations but need prolonged periods of heavy rainfall to be triggered (van Asch et al. 2009). Moreover, the impact of snow melt events on groundwater flow can be substantial and, especially relevant for northern Norway, has to be considered in terms of the future slope stability together with the expected increase in average precipitation (Figure 2).

The role of permafrost as a trigger in the foreseeable future should be marginal for Låvan due to its relatively low elevation. The limit of discontinuous permafrost is at around 1000 m a.s.l. but sporadic permafrost is theoretically possible down to sea level (Magnin et al. 2019). Ice wedging that was e.g. quantified in its destabilizing effect by Blikra et al. (2015) should be also rather relevant for higher elevated areas as the head domain of Dusnjarga.

Seismicity is commonly seen as one of the main triggers for rock slope failures (e.g. Henderson and Saintot 2011). It cannot be excluded as a future trigger but Låvan is located in one of the least seismically active regions in Norway (Fjeldskaar et al. 2000).

8.3 Hazard analysis of Låvan

The results and interpretations presented in this study enable a hazard analysis for the unstable rock slope Låvan according to the hazard classification system by Hermanns et al. (2012a; 2013a). Thereby, nine criteria are evaluated for Låvan and each is assigned a specific score from 0 to 1 (Table 5). The sum of these nine values gives a specific hazard score (ranging from 0 to 12) which is intended to correspond to the rock slope's likelihood of failure (Hermanns et al. 2013a).

The existence of differently behaving sliding blocks at Låvan is likely as indicated by minor scarps, tension cracks and depressions, but neither the displacement data nor the geological structures show clear spatial variations. Therefore, this hazard analysis is performed for one major failure scenario involving the whole deformation area as delimited by the morpho-gravitational features (e.g. section 7.1).

In the following, each hazard class and its attributed score are discussed. Table 5 summarizes the main results for each hazard class which results exclude uncertainties.

Table 5: Results of the hazard classification for Låvan based on the classification system by Hermanns et al. (2012a). The table presents the main results for each hazard class whereby the respective uncertainties are not displayed.

Hazard class		Result	Score
1	Head scarp	Open over the full width of the slide body	1
2	Potential sliding structures	No penetrative structures dip out on the slope	0
3	Lateral release surfaces	Partially developed on 2 sides	0.5
4	Kinematic feasibility test	Failure is kinematically possible and the movement is less than ±30° to the slope orientation	0.75
5	Morphologic expression of rupture surface	No clear indication for a rupture surface in the morphology	0
6	Displacement rates	No significant movement indicated	0
7	Acceleration	No acceleration or change in displacement rates	0
8	Increase of rock fall activity	Local increase in rock fall activity	1
9	Past events	No post-glacial event of similar size	0

1. ***Back-scarp*** *- Is it developed and open?*

The back- or main scarp is well recognizable and runs over the full width of the unstable rock slope (e.g. Figure 55). Its degree of development is very heterogeneous: it often forms an only slightly weathered scarp face of several meters in height whereas e.g. towards its eastern side, the scarp becomes increasingly weathered and less distinct. Nonetheless, it is classified as a fully open back scarp with the assigned score of 1.

2. ***Potential sliding structures*** *- Do penetrative structures daylight on the slope face and do they dip with more than 20° towards the slope?*

The most likely sliding structure is represented by the foliation (138/23 ± 13°). It dips in slope direction, daylights in the slope and has an average dip angle of slightly more than 20° (Figure 48). However, reasoned by the low persistence of the foliation (1.4 ± 1.2 m) and by the change of its orientation in the lower slope sections, the sliding structures are generally regarded as favorable for stability and a general score of 0 is attributed. On the other hand, it cannot be excluded that the foliation forms very locally persistent discontinuities that could not be mapped leading to some uncertainty for this score.

3. ***Lateral release surfaces*** *- Are they developed or are the sides free?*

None of the lateral boundaries is fully developed as a lateral release surface. But the lateral limits of deformation are recognizable in the terrain and both boundaries are traceable in the DEM (e.g. Figure 19). At the central domain, the eastern flank bordering the central domain could even be interpreted as a free slope section. Based on this reasoning, the lateral release surfaces are generally regarded as partially developed on two sides (score of 0.5) with some uncertainty to a higher score.

4. ***Kinematic feasibility test*** *- Are toppling, planar or wedge sliding possible? Are persistent discontinuities oriented similar as the slope?*

The kinematic analysis using *Dips 7.0* (section 7.8) shows that both planar sliding on the foliation (Figure 60) as well as wedge failure on the foliation and JN1 (Figure 61) are likely failure mechanisms with a significant proportion of critical orientations. Wedge failure on JN1 and JN2 might also be possible. All these failure mechanisms indicate a movement direction of less than 30° compared to the slope orientation. The mechanisms relying on the foliation are however only feasible above an elevation of 200 m due to the recorded change in the foliation's orientation.

Furthermore, persistence has a strong influence on the possible size of the rock slope failures and can influence the score (Hermanns et al. 2012a; Molina 2010). JN1 is the most persistent discontinuity set in the study area whereas the foliation (compare hazard class 2) and JN2 (2.4 ± 1.4) are low persistent.

In conclusion, failure is kinematically possible by means of three different kinematic failure modes and the movement is less than ±30° to the slope orientation. The persistence characteristics and spatial changes in foliation however act stabilizing which is why a score of 0.75 is applied.

5. ***Morphologic expression of the rupture surface*** *- Do clear morphologic signs exist and can the rupture surface be delimited?*

The rupture surface should be expected to crop out below the frontal buttress maybe hidden below the large talus fan (Figure 69C). The rupture surface does however not visibly crop out on the slope, and characteristic signs as a distinct frontal bulge, a series of springs, fault breccia or fault gouge could also not be determined. This leads to a general score of 0 with some uncertainty to a higher score.

6. ***Displacement rates*** *- Quantify the movement*

Available displacement data from InSAR (2015 – 2019) and dGNSS monitoring points (2010 – 2014) was analyzed. Both data sets resulted in insignificant displacement values that do not indicate any present deformation at Låvan. This corresponds to a score of 0.

The short periods of measurement should however be considered, and a future reevaluation of displacement data will be necessary justifying some uncertainty for this score.

7. ***Acceleration*** *– Has there been a clear acceleration in recent time?*

No acceleration of displacement is indicated since no present displacement is recorded.

8. ***Increase of rockfall activity*** spatial increase compared to others

Overall, rockfall activity appears to be significantly higher at Låvan than on adjacent slopes. Especially, the talus fan in front of the frontal scarp (Figure 57) and a talus fan below a subordinary failure scarp in the eastern head domain (Figure 64) show abundant also relatively fresh rockfall. This results in a general score of 1.0 for this class.

9. ***Past events*** *- Can further evidences for post-glacial slope deformations be found?*

Dusnjarga and Vassnestind are actively deforming areas that are larger than Låvan, but as indicated none of both has led to a large catastrophic failure. There is no indication (e.g. morphological) for a catastrophic rock slope avalanches event of a comparable dimension that occurred in the vicinity since the last deglaciation leading to a score of 0 for this class.

Figure 70 displays the final score of the hazard analysis including uncertainties for each hazard class.

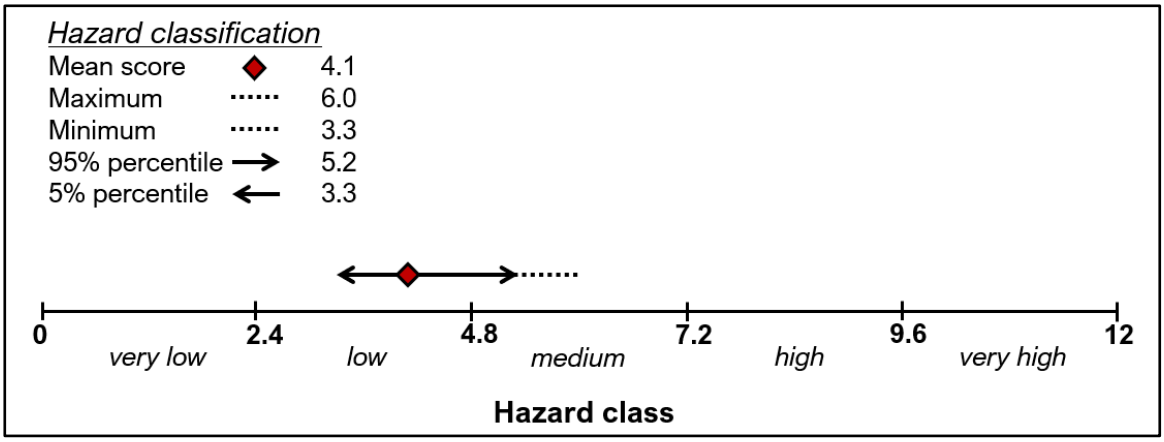

Figure 70: Final results of the hazard analysis for Låvan: hazard score and uncertainties.

- ***Implications for the future displacement and hazard of Låvan***

According to the results of the hazard analysis (Figure 70) and the average hazard score of 4.1, Låvan can be classified as a low hazard object. However, Låvan could also potentially be a medium hazard object due to the high uncertainties that exist for several hazard classes. This is expressed by the significant deviation of the maximum hazard score (6.0) from the mean score (4.1).

The estimated low hazard at Låvan is heavily based on the assessment of its displacement rates (and acceleration) for which the lowest (0) rating was given. As presented in section 7.6 and 7.7, the available dGNSS and InSAR displacement data did not indicate any significant displacement. Both methods have however potential incapacities and especially the time series of the dGNSS data was very limited (only three measurement periods). Therefore, a special focus in the future should be set on the collection and analysis of more displacement data for Låvan. The gravitational features especially at Låvan's head domain show little surface weathering and little moss and lychen cover compared to stable locations which can be a hint for a relatively recent deformation. The installation of a new dGNSS point on the frontal block (Figure 69) is recommended since data is entirely missing for the lower domains (tree cover impedes InSAR) and especially due to its critical vicinity to the settlement.

Rockslides in Troms county that show a similar deformation style as Låvan (compound slide-type sagging slopes) were interpreted by Bunkholt et al. (2012) as slides that do probably not move as a coherent mass and that do not show any signs for catastrophic collapses. The low displacement rates that are commonly observed in compound slides are supposed to go back to kinematic locking of the upper sliding block in these typically brittle slides (Hutchinson 2006). But in case of failure, sudden and strong acceleration of the slide can be possible since the failure occurs as a brittle, first-time internal shear (Hutchinson 2006). The Vaiont slide is the most dramatic example of a catastrophic failure for such an originally locked compound slide (Hendron and Patton 1985). Even though the condtions for this latter event differed strongly from Låvan, it can be a reminder that initially low displacement rates should not be overvalued in case of such complex deformation mechanisms.

9 Conclusion

Dusnjarga and Låvan are two large unstable rock slopes located on the Dusnjarga peninsula in Troms. It is the county with the most recorded unstable rock slopes in Norway whereby former studies largely focused on the slopes in the central but not the northeastern part of the county (e.g. Bunkholt et al. 2012; Oppikofer et al. 2015). Dusnjarga and Låvan stand clearly out as slope deformations by their characteristic surface morphology but had preliminarily only been roughly investigated by NGU (Bunkholt et al. 2011). The need for a thorough investigation of both objects was further reasoned by the potential danger emanating from the unstable rock slopes for people living along Lille Altafjorden, and particularly in the settlement Låvan, and thereby to contribute to NGU's effort to systematically map Norway's unstable rock slopes. On the other hand, such studies are important in their contribution to scientific knowledge about rock slope deformations on a Norwegian and international scale.

Essentially, the work presented in this study can be divided in two central parts for which central results and interpretations are presented in the following:

(i) Analysis of the Quaternary geology and landscape evolution

- A high-detail Quaternary geological map (10.4 km²) was produced which shows that Quaternary deposits cover only a minor part of the study area. Deposits with a glacial origin comprised glaciomarine, thin till and redeposited glaciofluvial material whereby thick or continuous successions are limited to locations at the shore.
- This map in combination with the detailed analyses of glacial deposits (profile logging and grain size analyzes) and the study of the morphology allowed a reconstruction of landscape evolution since the last glacial maximum.
- Several chronological interpretations on the development of the deep-seated rock slope deformations could be made based on the Quaternary geological analysis and especially on the identified paleo-shorelines, even though overall the reconstructions were heavily complicated by the scarcity of Quaternary deposits at the unstable slopes.
- For Dusnjarga, strong slope deformation is suggested for the period around the Tapes transgression, especially for its central domain and eastern flank as indicated by the partially high content of slope debris in flood and redeposited glaciofluvial deposits. The main deformation for Dusnjarga's frontal bulge is however suggested for the second half of the Holocene.
- A minimum age for the deformation at Låvan is set by the well-preserved Tapes shoreline on its frontal protrusion whereas further chronological interpretations are hampered by the absence of Quaternary sediments which also counts for the upper areas of Dusnjarga.

(ii) Detailed analysis of the deep-seated slope deformation Låvan:

- The analysis of structural data, focusing on outcrops inside the active deformation area and in its inactive surrounding, resulted in the definition of four discontinuity sets (JN1, JN2, JN3, SC). The sets' characteristics were investigated by the implementation of scanline data.
- In the kinematic failure analysis, planar failure on the foliation SC as well as wedge failure on SC and JN1 stood out as the most likely failure mechanisms and probably a combination of both active mechanisms seems logical whereby JN1 forms mainly back and lateral release surfaces.
- Additional investigation of rock mass characteristics and mapping of the slope morphology allowed a detailed interpretation of the slope deformation at Låvan.
- The application of various criteria characterizes Låvan as DSGSD and sackung (sagging slope).
- Bilinear compound sliding is suggested as the dominating deformation style since sliding movement on a stepped or multiple sliding surfaces is supposed. This is reasoned by the complex surface morphology and the low persistence of the foliation fractures which might be linked by the steeply dipping set JN2.
- Låvan's head domain is characterized by complex extensional deformation on multiple sliding blocks that are developed along all four defined discontinuity sets. A fault along which a large counterscarp is expressed separates this domain from a central more compact block. The foliation's orientation changes at lower elevations towards dipping into the slope. This complicates the sliding movement at the frontal domain where several frontal blocks are pressed outward along the foliation, e.g. visible at the frontal scarp belonging to a block that might pose the greatest hazard for the settlement situated below.
- A hazard analysis was performed according to Hermanns et al. (2012a) and classified Låvan as a low-hazard object whereby considerable uncertainties existed for several hazard classes. These were mainly connected to the displacement data (InSAR and dGNSS) which did not indicate significant displacement but was only available for very limited time series.

Further conclusions and recommendations for future work consequently result from the presented findings.

To significantly improve the established chronology of deformation for Dunsjarga and Låvan, it would be most sensible to use absolute dating methods, especially TCN and/or optically stimulated luminescence dating.

Låvan's classification as a low-hazard object does not justify extensive further monitoring measures (Hermanns et al. 2012a). Nonetheless, its hazardous location above the settlement and the high uncertainties attributed to the displacement data imply to follow up the displacement measurements and amplify them through for instance new dGNSS monitoring points (e.g. above the frontal scarp). From a scientific point of view, the slope deformation and its mechanisms could be further investigated by several measures: e.g. further structural measurements and rock mass observations, or borehole logging which could finally allow for detailed 3D-modelling of its failure surfaces and kinematics.

Bibliography

Agliardi, F., G. B. Crosta, and P. Frattini. 2012. 'Slow Rock-Slope Deformation'. *Landslides: Types, Mechanisms and Modeling*, 207.

Agliardi, F., G. B. Crosta, P. Frattini, and M. G. Malusà. 2013. 'Giant Non-Catastrophic Landslides and the Long-Term Exhumation of the European Alps'. *Earth and Planetary Science Letters* 365: 263–74.

Agliardi, F., G. B. Crosta, A. Zanchi, and C. Ravazzi. 2009. 'Onset and Timing of Deep-Seated Gravitational Slope Deformations in the Eastern Alps, Italy'. *Geomorphology*, Dating, triggering, modelling, and hazard assessment of large landslides, 103 (1): 113–29. https://doi.org/10.1016/j.geomorph.2007.09.015.

Agliardi, Federico, Giovanni Crosta, and Andrea Zanchi. 2001. 'Structural Constraints on Deep-Seated Slope Deformation Kinematics'. *Engineering Geology* 59 (1–2): 83–102.

Agliardi, Federico, Andrea Zanchi, and Giovanni B Crosta. 2009a. 'Tectonic vs. Gravitational Morphostructures in the Central Eastern Alps (Italy): Constraints on the Recent Evolution of the Mountain Range'. *Tectonophysics* 474 (1–2): 250–70.

Alexanderson, Helena, and Andrew Murray. 2012. 'Problems and Potential of OSL Dating Weichselian and Holocene Sediments in Sweden'. *Quaternary Science Reviews* 44: 37–50.

Ambrosi, Christian, and Giovanni B Crosta. 2006. 'Large Sackung along Major Tectonic Features in the Central Italian Alps'. *Engineering Geology* 83 (1–3): 183–200.

———. 2011. 'Valley Shape Influence on Deformation Mechanisms of Rock Slopes'. *Geological Society, London, Special Publications* 351 (1): 215–33.

Andersen, Bjørn Grothaug. 1968. *Glacial Geology of Western Troms, North Norway*. Universitetsforlaget.

Asch, Th WJ van, L. P. H. Van Beek, and T. A. Bogaard. 2009. 'The Diversity in Hydrological Triggering Systems of Landslides'. In *Proceedings of The First Italian Workshop on Landslides*, 8–10.

Augustinus, Paul C. 1995. 'Glacial Valley Cross-Profile Development: The Influence of in Situ Rock Stress and Rock Mass Strength, with Examples from the Southern Alps, New Zealand'. *Geomorphology* 14 (2): 87–97.

Ballantyne, Colin K. 2002. 'Paraglacial Geomorphology'. *Quaternary Science Reviews* 21 (18–19): 1935–2017.

Ballantyne, Colin K., John O. Stone, and L. Keith Fifield. 1998. 'Cosmogenic Cl-36 Dating of Postglacial Landsliding at the Storr, Isle of Skye, Scotland'. *The Holocene* 8 (3): 347–51.

Benn, Douglas, and David JA Evans. 2014. *Glaciers and Glaciation*. Routledge.

Bergstrøm, Bjørn. 2001. 'NGU-Rapport 2001-018'. www.ngu.no.

Bieniawski, Z. 1988. 'The Rock Mass Rating (RMR) System (Geomechanics Classification) in Engineering Practice'. In *Rock Classification Systems for Engineering Purposes*. ASTM International.

Bigot-Cormier, F., Regis Braucher, D. Bourlès, Y. Guglielmi, M. Dubar, and J.-F. Stéphan. 2005. 'Chronological Constraints on Processes Leading to Large Active Landslides'. *Earth and Planetary Science Letters* 235 (1–2): 141–50.

Blikra, Lars H, and Hanne H Christiansen. 2013. 'A Field-Based Model of Permafrost-Controlled Rockslide Deformation in Northern Norway'. *Geomorphology* 208: 34–49.

Blikra, Lars Harald, Hanne H Christiansen, Lene Kristensen, and Mario Lovisolo. 2015. 'Characterization, Geometry, Temporal Evolution and Controlling Mechanisms of the Jettan Rock-Slide, Northern Norway'. In *Engineering Geology for Society and Territory-Volume 2*, 273–78. Springer.

Blikra, LH, O Longva, A Braathen, E Anda, JF Dehls, and K Stalsberg. 2006. 'Rock Slope Failures in Norwegian Fjord Areas: Examples, Spatial Distribution and Temporal Pattern'. In *Landslides from Massive Rock Slope Failure*, 475–96. Springer.

Böhme, M., R. L. Hermanns, J. Gosse, P. Hilger, T. Eiken, T. R. Lauknes, and J. F. Dehls. 2019. 'Comparison of Monitoring Data with Paleo–Slip Rates: Cosmogenic Nuclide Dating Detects Acceleration of a Rockslide'. *Geology* 47 (4): 339–42.

Böhme, M, T Oppikofer, O Longva, M Jaboyedoff, RL Hermanns, and M-H Derron. 2015. 'Analyses of Past and Present Rock Slope Instabilities in a Fjord Valley: Implications for Hazard Estimations'. *Geomorphology* 248: 464–74.

Böhme, Martina. 2014. *Spatial and Temporal Variability of Rock Slope Instability in Western Norway:: Implications for Susceptibility and Hazard Assessment*. Norges teknisk-naturvitenskapelige universitet, Fakultet for ingeniørvitenskap og teknologi, Institutt for geologi og bergteknikk. https://brage.bibsys.no/xmlui/handle/11250/236254.

Böhme, Martina, R. L. Hermanns, L. Fischer, T. Oppikofer, H. Bunkholt, M. H. Derron, D. Carrea, M. Jaboyedoff, and T. Eiken. 2012. 'Detailed Assessment of the Deep-Seated Gravitational Deformation at Stampa above Flåm, Norway'. *Landslides and Engineered Slopes: Protecting Society through Improved Understanding, Taylor & Francis Group, London*, 647–52.

Böhme, Martina, Reginald L Hermanns, Thierry Oppikofer, Luzia Fischer, Halvor SS Bunkholt, Trond Eiken, Andrea Pedrazzini, Marc-Henri Derron, Michel Jaboyedoff, and Lars H Blikra. 2013. 'Analyzing Complex Rock Slope Deformation at Stampa, Western Norway, by Integrating Geomorphology, Kinematics and Numerical Modeling'. *Engineering Geology* 154: 116–30.

Böhme, Martina, Aline Saintot, Iain HC Henderson, Helge Henriksen, and Reginald L. Hermanns. 2011. 'Rock Slope Instabilities in Sogn and Fjordane County, Norway: A Detailed Structural and Geomorphological Analysis'. *Geological Society, London, Special Publications* 351 (1): 97–111.

Bondevik, Stein, Trond Klungseth Lødøen, Christine Tøssebro, Hanne Årskog, Kari Loe Hjelle, and Ingvild K. Mehl. 2019. 'Between Winter Storm Surges – Human Occupation on a Growing Mid-Holocene Transgression Maximum (Tapes) Beach Ridge at Longva, Western Norway'. *Quaternary Science Reviews* 215 (July): 116–31. https://doi.org/10.1016/j.quascirev.2019.05.006.

Bonzanigo, L., E. Eberhardt, and S. Loew. 2000. 'Measured Response to a Drainage Adit in a Deep Creeping Slide Mass'. In *Landslides in Research, Theory and Practice: Proceedings of the 8th International Symposium on Landslides Held in Cardiff on 26–30 June 2000*, 1: 151-156. Thomas Telford Publishing.

Böse, Margot, Christopher Lüthgens, Jonathan R Lee, and James Rose. 2012. 'Quaternary Glaciations of Northern Europe'. *Quaternary Science Reviews* 44: 1–25.

Brain, Matthew J., Nicholas J. Rosser, Emma C. Norman, and David N. Petley. 2014. 'Are Microseismic Ground Displacements a Significant Geomorphic Agent?' *Geomorphology* 207: 161–73.

Bristow, C. S., and J. L. Best. 1993. 'Braided Rivers: Perspectives and Problems'. *Geological Society, London, Special Publications* 75 (1): 1–11. https://doi.org/10.1144/GSL.SP.1993.075.01.01.

Brückl, Ewald, and Miltiades Parotidis. 2005. 'Prediction of Slope Instabilities Due to Deep-Seated Gravitational Creep'. *Natural Hazards and Earth System Science* 5 (2): 155–72.

Bunkholt, H., S. Otterå, F.X. Yugsi Molina, R.L. Hermans, J. Dehls, P.T. Osmundsen, T.F. Redfield, T. Eiken, and M. Böhme. 2013. 'Undersøkelser av ustabile fjellpartier i Troms - status og planer etter feltarbeid 2011 og 2012'. *Norges Geologiske Undersøkelse*.

Bunkholt, H., T.F. Redfield, P.T. Osmundsen, T. Oppikofer, R.L. Hermans, T.R. Lauknes, T. Eiken, and J-S. L'Heureux. 2011. 'ROS Fjellskred i Troms: Status Og Analyzer Etter Feltarbeid i 2010. NGU Rapport 2011.031'. *Norges Geologiske Undersøkelse*.

Bunkholt, H. S. S., T. F. Redfield, P. T. Osmundsen, T. Oppikofer, R. L. Hermanns, and J. Dehls. 2012. 'Landslide Processes in Hard Rock in Troms, Norway'. *Landslides and Engineered Slopes: Protecting Society through Improved Understanding. Taylor & Francis Group, London*, 855–61.

Caine, Nel. 1982. 'Toppling Failures from Alpine Cliffs on Ben Lomond, Tasmania'. *Earth Surface Processes and Landforms* 7 (2): 133–52.

Chemenda, A. I., T. Bois, S. Bouissou, and E. Tric. 2009. 'Numerical Modelling of the Gravity-Induced Destabilization of a Slope: The Example of the La Clapière Landslide, Southern France'. *Geomorphology* 109 (3–4): 86–93.

Clark, Peter U, Arthur S Dyke, Jeremy D Shakun, Anders E Carlson, Jorie Clark, Barbara Wohlfarth, Jerry X Mitrovica, Steven W Hostetler, and A Marshall McCabe. 2009. 'The Last Glacial Maximum'. *Science* 325 (5941): 710–14.

Cossart, Etienne, Regis Braucher, Monique Fort, DL Bourlès, and Julien Carcaillet. 2008. 'Slope Instability in Relation to Glacial Debuttressing in Alpine Areas (Upper Durance Catchment, Southeastern France): Evidence from Field Data and 10Be Cosmic Ray Exposure Ages'. *Geomorphology* 95 (1–2): 3–26.

Crosta, G., and A. Zanchi. 2000. 'Deep Seated Slope Deformations: Huge, Extraordinary, Enigmatic Phenomena'. In *Landslides in Research, Theory and Practice: Proceedings of the 8th International Symposium on Landslides Held in Cardiff on 26–30 June 2000*, 1: 351-358. Thomas Telford publishing.

Crosta, GB, C Di Prisco, P Frattini, Gabriele Frigerio, Riccardo Castellanza, and F Agliardi. 2014. 'Chasing a Complete Understanding of the Triggering Mechanisms of a Large Rapidly Evolving Rockslide'. *Landslides* 11 (5): 747–64.

Crosta, GB, P Frattini, and F Agliardi. 2013. 'Deep Seated Gravitational Slope Deformations in the European Alps'. *Tectonophysics* 605: 13–33.

Cruden, David M. 1991. 'A Simple Definition of a Landslide'. *Bulletin of the International Association of Engineering Geology-Bulletin de l'Association Internationale de Géologie de l'Ingénieur* 43 (1): 27–29.

Cruden, David M, and David J Varnes. 1996. 'Landslides: Investigation and Mitigation. Chapter 3-Landslide Types and Processes'. *Transportation Research Board Special Report*, no. 247.

D'Alessandro, G. R., M. Berti, A. Urbani, and P. R. Tecca. 2002. 'Geomorphology, Stability Analyses and the Stabilization Works on the Montepiano Travertinous Cliff (Central Italy)'. *Applied Geomorphology—Theory and Practice. Wiley, New York*, 21–38.

Davies, Michael CR, Omar Hamza, and Charles Harris. 2001. 'The Effect of Rise in Mean Annual Temperature on the Stability of Rock Slopes Containing Ice-filled Discontinuities'. *Permafrost and Periglacial Processes* 12 (1): 137–44.

De Freitas, M. H., and R. J. Watters. 1973. 'Some Field Examples of Toppling Failure'. *Geotechnique* 23 (4): 495–513.

Díez, Alberto González, Luis Salas, José Ramon Díaz de Terán, and Antonio Cendrero. 1996. 'Late Quaternary Climate Changes and Mass Movement Frequency and Magnitude in the Cantabrian Region, Spain'. *Geomorphology* 15 (3–4): 291–309.

Dortch, Jason M., Lewis A. Owen, William C. Haneberg, Marc W. Caffee, Craig Dietsch, and Ulrich Kamp. 2009. 'Nature and Timing of Large Landslides in the Himalaya and Transhimalaya of Northern India'. *Quaternary Science Reviews* 28 (11–12): 1037–54.

Dreimanis, Aleksis. 1989. 'Tills: Their Genetic Terminology and Classification'. In , 17–83.

Dyrrdal, Anita Verpe, Alex Lenkoski, Thordis L. Thorarinsdottir, and Frode Stordal. 2015. 'Bayesian Hierarchical Modeling of Extreme Hourly Precipitation in Norway'. *Environmetrics* 26 (2): 89–106. https://doi.org/10.1002/env.2301.

Eberhardt, E., H. Willenberg, S. Loew, and H. Maurer. 2001. 'Active Rockslides in Switzerland-Understanding Mechanisms and Processes'. In *International Conference on Landslides-Causes, Impacts and Countermeasures*, 25–34.

Eriksen, Harald Øverli, Tom Rune Lauknes, Yngvar Larsen, Geoffrey D Corner, Steffen G Bergh, John Dehls, and Halfdan Pascal Kierulf. 2017. 'Visualizing and Interpreting Surface Displacement Patterns on Unstable Slopes Using Multi-Geometry Satellite SAR Interferometry (2D InSAR)'. *Remote Sensing of Environment* 191: 297–312.

Evans, David JA, Brice R Rea, James D Hansom, and W Brian Whalley. 2002. 'Geomorphology and Style of Plateau Icefield Deglaciation in Fjord Terrains: The Example of Troms-Finnmark, North Norway'. *Journal of Quaternary Science: Published for the Quaternary Research Association* 17 (3): 221–39.

Evans, Stephen G, and John J Clague. 1994. 'Recent Climatic Change and Catastrophic Geomorphic Processes in Mountain Environments'. In *Geomorphology and Natural Hazards*, 107–28. Elsevier.

Fenton, Cassandra R., Reginald L. Hermanns, Lars H. Blikra, Peter W. Kubik, Charlotte Bryant, Samuel Niedermann, Anette Meixner, and Mirjam M. Goethals. 2011. 'Regional 10Be Production Rate Calibration for the Past 12 Ka Deduced from the Radiocarbon-Dated Grøtlandsura and Russenes Rock Avalanches at 69 N, Norway'. *Quaternary Geochronology* 6 (5): 437–52.

Fischer, L, Ross S Purves, Christian Huggel, Jeannette Noetzli, and Wilfried Haeberli. 2012. 'On the Influence of Topographic, Geological and Cryospheric Factors on Rock Avalanches and Rockfalls in High-Mountain Areas'. *Natural Hazards and Earth System Science* 12 (1): 241–54.

Fjeldskaar, Willy, Conrad Lindholm, John F. Dehls, and Ingrid Fjeldskaar. 2000. 'Postglacial Uplift, Neotectonics and Seismicity in Fennoscandia'. *Quaternary Science Reviews* 19 (14–15): 1413–22.

Fjellanger, Jakob, Leif Sørbel, Henriette Linge, Edward J Brook, Grant M Raisbeck, and Françoise Yiou. 2006. 'Glacial Survival of Blockfields on the Varanger Peninsula, Northern Norway'. *Geomorphology* 82 (3–4): 255–72.

Fredin, Ola, Bjørn Bergstrøm, Raymond Eilertsen, Louise Hansen, Oddvar Longva, Atle Nesje, and Harald Sveian. 2013. 'Glacial Landforms and Quaternary Landscape Development in Norway'. *Quaternary Geology of Norway. Geological Survey of Norway, Special Publication* 13: 5–25.

Furseth, Astor. 1985. *Dommedagsfjellet: Tafjord 1934*. Gyldendal Norsk Forlag.

Ganerød, Guri Venvik, Guro Grøneng, Jan Steinar Rønning, Einar Dalsegg, Harald Elvebakk, Jan Fredrik Tønnesen, Vidar Kveldsvik, Trond Eiken, Lars Harald Blikra, and Alvar Braathen. 2008. 'Geological Model of the Åknes Rockslide, Western Norway'. *Engineering Geology* 102 (1–2): 1–18.

Gisnås, Kjersti, Bernd Etzelmüller, Cristian Lussana, Jan Hjort, A. Britta K. Sannel, Ketil Isaksen, Sebastian Westermann, Peter Kuhry, Hanne H. Christiansen, and Andrew Frampton. 2017. 'Permafrost Map for Norway, Sweden and Finland'. *Permafrost and Periglacial Processes* 28 (2): 359–78.

Glade, Thomas, and Michael J. Crozier. 2005. 'The Nature of Landslide Hazard Impact'. *Landslide Hazard and Risk. Wiley, Chichester*, 43–74.

Goodman, RE. 1980. 'Introduction to Rock Mechanics, Edited John Wiley and Sons'. *New York*.

Gutiérrez-Santolalla, F., Enrique Acosta, Santiago Ríos, Jesús Guerrero, and Pedro Lucha. 2005. 'Geomorphology and Geochronology of Sackung Features (Uphill-Facing Scarps) in the Central Spanish Pyrenees'. *Geomorphology* 69 (1): 298–314. https://doi.org/10.1016/j.geomorph.2005.01.012.

Hancock, PL. 1985. 'Brittle Microtectonics: Principles and Practice'. *Journal of Structural Geology* 7 (3–4): 437–57.

Hanssen-Bauer, I, H Drange, EJ Førland, LA Roald, KY Børsheim, H Hisdal, D Lawrence, A Nesje, S Sandven, and A Sorteberg. 2009. 'Climate in Norway 2100'. *Background Information to NOU Climate Adaptation (In Norwegian: Klima i Norge 2100. Bakgrunnsmateriale Til NOU Klimatilplassing), Oslo: Norsk Klimasenter*.

Harbitz, C. B., G. Pedersen, and B. Gjevik. 1993. 'Numerical Simulations of Large Water Waves Due to Landslides'. *Journal of Hydraulic Engineering* 119 (12): 1325–42.

Harbor, Jonathan M, Bernard Hallet, and Charles F Raymond. 1988. 'A Numerical Model of Landform Development by Glacial Erosion'. *Nature* 333 (6171): 347–49.

Hencher, S. R., S. G. Lee, T. G. Carter, and L. R. Richards. 2011. 'Sheeting Joints: Characterisation, Shear Strength and Engineering'. *Rock Mechanics and Rock Engineering* 44 (1): 1–22.

Hencher, Steve. 2013. 'Practical Engineering Geology'.

Henderson, Iain HC, and Aline Saintot. 2011. 'Regional Spatial Variations in Rockslide Distribution from Structural Geology Ranking: An Example from Storfjorden, Western Norway'. *Geological Society, London, Special Publications* 351 (1): 79–95.

Hendron Jr, A. J., and Franklin D. Patton. 1985. 'The Vaiont Slide. A Geotechnical Analysis Based on New Geologic Observations of the Failure Surface. Volume 1. Main Text'. ARMY ENGINEER WATERWAYS EXPERIMENT STATION VICKSBURG MS GEOTECHNICAL LAB.

Hermanns, Reginald L, Lars H Blikra, Einar Anda, Aline Saintot, Halgeir Dahle, Thierry Oppikofer, Luzia Fischer, Halvor Bunkholt, Martina Böhme, and John F Dehls. 2013. 'Systematic Mapping of Large Unstable Rock Slopes in Norway'. *Landslide Science and Practice*, 29–34.

Hermanns, Reginald L, and Oddvar Longva. 2012. 'Rapid Rock-Slope Failures'. *Landslides: Types, Mechanisms and Modeling*, 59–70.

Hermanns, Reginald L, T Oppikofer, E Anda, LH Blikra, M Böhme, H Bunkholt, GB Crosta, H Dahle, G Devoli, and L Fischer. 2012a. 'Recommended Hazard and Risk Classification System for Large Unstable Rock Slopes in Norway'. *NGU Rapport*.

Hermanns, Reginald L, THIERRY Oppikofer, EINAR Anda, L. Blikra, Martina Böhme, Halvor Bunkholt, G. Crosta, Halgeir Dahle, GRAZIELLA Devoli, and Luzia Fischer. 2013a. 'Hazard and Risk Classification for Large Unstable Rock Slopes in Norway'.

Hermanns, Reginald L., Thierry Oppikofer, Freddy X. Yugsi Molina, John F. Dehls, and Martina Böhme. 2014. 'Approach for Systematic Rockslide Mapping of Unstable Rock Slopes in Norway'. In *Landslide Science for a Safer Geoenvironment*, edited by Kyoji Sassa, Paolo Canuti, and Yueping Yin, 129–34. Cham: Springer International Publishing. https://doi.org/10.1007/978-3-319-04996-0_21.

Hermanns, Reginald L, Markus Schleier, Martina Böhme, Lars Harald Blikra, John Gosse, Susan Ivy-Ochs, and Paula Hilger. 2017. 'Rock-Avalanche Activity in W and S Norway Peaks after the Retreat of the Scandinavian Ice Sheet'. In , 331–38. Springer.

Hermanns, RL, T Oppikofer, M Böhme, JF Dehls, FX Yugsi Molina, and IM Penna. 2016. 'Rock Slope Instabilities in Norway: First Systematic Hazard and Risk Classification of 22 Unstable Rock Slopes from Northern, Western and Southern Norway'. In , 12:19.

Highland, Lynn, and Peter T Bobrowsky. 2008. *The Landslide Handbook: A Guide to Understanding Landslides*. US Geological Survey Reston.

Hilger, Paula, Reginald L Hermanns, John C Gosse, Benjamin Jacobs, Bernd Etzelmüller, and Michael Krautblatter. 2018. 'Multiple Rock-Slope Failures from Mannen in Romsdal Valley, Western Norway, Revealed from Quaternary Geological Mapping and 10Be Exposure Dating'. *The Holocene* 28 (12): 1841–54.

Hilger, Paula, G. Sandøy, Lena Rubensdotter, Kari Sletten, Knut Stalsberg, Raymond Eilertsen, and Line Nygård. 2019. 'Detailed Quaternary Geological Maps in Steep Terrain as Basis for Landslide-Hazard Evaluation'. In .

Hippolyte, Jean-Claude, Didier Bourlès, Laëtitia Léanni, Régis Braucher, Frédéric Chauvet, and Anne Elisabeth Lebatard. 2012. '10Be Ages Reveal> 12 Ka of Gravitational Movement in a Major Sackung of the Western Alps (France)'. *Geomorphology* 171: 139–53.

Hippolyte, Jean-Claude, Gilles Brocard, Marc Tardy, Gérard Nicoud, Didier Bourles, Regis Braucher, Gilles Ménard, and Blaise Souffaché. 2006. 'The Recent Fault Scarps of the Western Alps (France): Tectonic Surface Ruptures or Gravitational Sackung Scarps? A Combined Mapping, Geomorphic, Levelling, and 10Be Dating Approach'. *Tectonophysics* 418 (3–4): 255–76.

Hoek, Evert, and Edwin T. Brown. 1997. 'Practical Estimates of Rock Mass Strength'. *International Journal of Rock Mechanics and Mining Sciences* 34 (8): 1165–86.

Høgaas, F, L Hansen, BI Rindstad, H Sveian, and L Olsen. 2012. 'Database for Registrering Av Marine Grense (MG) i Norge'. *NGU Rapport*.

Hormes, Anne, Susan Ivy-Ochs, Peter W. Kubik, Luca Ferreli, and Alessandro Maria Michetti. 2008. '10Be Exposure Ages of a Rock Avalanche and a Late Glacial Moraine in Alta Valtellina, Italian Alps'. *Quaternary International* 190 (1): 136–45.

Hughes, Anna, Richard Gyllencreutz, Øystein S Lohne, Jan Mangerud, and John Inge Svendsen. 2015. 'DATED-1: Compilation of Dates and Time-Slice Reconstruction of the Build-up and Retreat of the Last Eurasian (British-Irish, Scandinavian, Svalbard-Barents-Kara Seas) Ice Sheets 40-10 Ka'. PANGAEA. https://doi.org/10.1594/PANGAEA.848117.

———. 2016. 'The Last Eurasian Ice Sheets–a Chronological Database and Time-slice Reconstruction, DATED-1'. *Boreas* 45 (1): 1–45.

Hungr, Oldrich, Serge Leroueil, and Luciano Picarelli. 2014. 'The Varnes Classification of Landslide Types, an Update'. *Landslides* 11 (2): 167–94.

Hutchinson, J. N. 1988. 'Morphological and Geotechnical Parameters of Landslides in Relation to Geology and Hydrogeology'. In *Proc., Fifth International Symposium on Landslides, 1988*. Lausanne, AA.

———. 2006. 'Massive Rock Slope Failure : Perspectives and Retrospectives on State-of-the-Art'. In *Landslides from Massive Rock Slope Failure*, edited by Stephen G. Evans, Gabriele Scarascia Mugnozza, Alexander Strom, and Reginald L. Hermanns, 619–62. NATO Science Series. Dordrecht: Springer Netherlands. https://doi.org/10.1007/978-1-4020-4037-5_32.

Hutchinson, J. N., E. N. Bromhead, and J. F. Lupini. 1980. 'Additional Observations on the Folkestone Warren Landslides'. *Quarterly Journal of Engineering Geology and Hydrogeology* 13 (1): 1–31.

Ivy-Ochs, Susan, A. V. Poschinger, H.-A. Synal, and M. Maisch. 2009. 'Surface Exposure Dating of the Flims Landslide, Graubünden, Switzerland'. *Geomorphology* 103 (1): 104–12.

Jia, Hailiang, Wei Xiang, and Michael Krautblatter. 2015. 'Quantifying Rock Fatigue and Decreasing Compressive and Tensile Strength after Repeated Freeze-thaw Cycles'. *Permafrost and Periglacial Processes* 26 (4): 368–77.

Keefer, David K. 1984. 'Landslides Caused by Earthquakes'. *Geological Society of America Bulletin* 95 (4): 406–21.

Kinakin, D., and D. Stead. 2005. 'Analysis of the Distributions of Stress in Natural Ridge Forms: Implications for the Deformation Mechanisms of Rock Slopes and the Formation of Sackung'. *Geomorphology* 65 (1–2): 85–100.

Kirkland, Christopher L, J Stephen Daly, and Martin J Whitehouse. 2007. 'Provenance and Terrane Evolution of the Kalak Nappe Complex, Norwegian Caledonides: Implications for Neoproterozoic Paleogeography and Tectonics'. *The Journal of Geology* 115 (1): 21–41.

Krauskopf, Konrad B. 1954. 'Igneous and Metamorphic Rocks of the Øksfjord Area, West Finnmark'. *Norges Geol Unders* 188: 29–50.

Krautblatter, M, and K Leith. 2015. 'Glacier-and Permafrost-Related Slope Instabilities'. *The High-Mountain Cryosphere; Huggel, C., Carey, M., Clague, JJ, Kaab, A., Eds*, 147–65.

Krautblatter, Michael, Daniel Funk, and Friederike K Günzel. 2013. 'Why Permafrost Rocks Become Unstable: A Rock–Ice-mechanical Model in Time and Space'. *Earth Surface Processes and Landforms* 38 (8): 876–87.

Krogh, Erling J, and Synnøve Elvevold. 1990. 'A Precambrian Age for an Early Gabbro–Monzonitic Intrusive on the Øksfjord Peninsula, Seiland Igneous Province, Northern Norway'. *Norsk Geologisk Tidsskrift* 70 (4): 267–73.

Krüger, Johannes, and Kurt Henrik Kjær. 1999. 'A Data Chart for Field Description and Genetic Interpretation of Glacial Diamicts and Associated Sediments…with Examples from Greenland, Iceland, and Denmark'. *Boreas* 28 (3): 386–402. https://doi.org/10.1111/j.1502-3885.1999.tb00228.x.

Le Roux, Olivier, Stéphane Schwartz, Jean François Gamond, Denis Jongmans, Didier Bourles, Regis Braucher, William Mahaney, Julien Carcaillet, and Laetitia Leanni. 2009. 'CRE Dating on the Head Scarp of a Major Landslide (Séchilienne, French Alps), Age Constraints on Holocene Kinematics'. *Earth and Planetary Science Letters* 280 (1–4): 236–45.

Leroueil, S., J. Locat, J. Vaunat, L. Picarelli, and H. Lee. 1996. 'Geotechnical Characterization of Slope Movements'. In *Landslides*, 53–74.

Lilleøren, Karianne S., Bernd Etzelmüller, Thomas V. Schuler, Kjersti Gisnås, and Ole Humlum. 2012. 'The Relative Age of Mountain Permafrost—Estimation of Holocene Permafrost Limits in Norway'. *Global and Planetary Change* 92: 209–23.

Linge, Henriette, Edward J Brook, Atle Nesje, Grant M Raisbeck, Françoise Yiou, and Heather Clark. 2006. 'In Situ 10Be Exposure Ages from Southeastern Norway: Implications for the Geometry of the Weichselian Scandinavian Ice Sheet'. *Quaternary Science Reviews* 25 (9–10): 1097–1109.

Linge, Henriette, Lars Olsen, Edward J Brook, Jessica R Darter, David M Mickelson, GM Roisbeck, and Françoise Yiou. 2007. 'Cosmogenic Nuclide Surface Exposure Ages from Nordland, Northern Norway: Implications for Deglaciation in a Coast to Inland Transect'. *Norsk Geologisk Tidsskrift* 87 (1/2): 269.

Longva, Oddvar, Lars Harald Blikra, and JF Dehls. 2009. 'Rock Avalanches: Distribution and Frequencies in the Inner Part of Storfjorden, Møre Og Romsdal County, Norway'. *Geological Survey of Norway* 32.

Lukas, Sven, and Henrik Rother. 2016. 'Moränen versus Till: Empfehlungen Für Die Beschreibung, Interpretation Und Klassifikation Glazialer Landformen Und Sedimente'. *E & G Quaternary Science Journal* 65 (2): 95–112.

MacGregor, KR, RS Anderson, SP Anderson, and ED Waddington. 2000. 'Numerical Simulations of Glacial-Valley Longitudinal Profile Evolution'. *Geology* 28 (11): 1031–34.

Magnin, Florence, Bernd Etzelmüller, Sebastian Westermann, Ketil Isaksen, Paula Hilger, and Reginald Hermanns. 2019. 'Permafrost Distribution in Steep Rock Slopes in Norway: Measurements, Statistical Modelling and Implications for Geomorphological Processes'.

Mangerud, Jan. 2004. 'Ice Sheet Limits on Norway and the Norwegian Continental Shelf'. *Quaternary Glaciations—Extent and Chronology* 1: 271–94.

McCalpin, James P, and Earl W Hart. 2003. 'Ridge-Top Spreading Features and Relationship to Earthquakes, San Gabriel Mountains Region, Southern California: Part A. Distribution and Description of Ridge-Top Depressions (Sackungen): Part B. Paleoseismic Investigations of Ridge-Top Depressions'. *Ridge-Top Spreading in California. California Geological Survey, Open-File Report* 1.

McCalpin, JAMES P, and James R Irvine. 1995. 'Sackungen at the Aspen Highlands Ski Area, Pitkin County, Colorado'. *Environmental & Engineering Geoscience* 1 (3): 277–90.

McColl, Samuel T. 2012. 'Paraglacial Rock-Slope Stability'. *Geomorphology* 153: 1–16.

McColl, Samuel T, and Timothy RH Davies. 2013. 'Large Ice-contact Slope Movements: Glacial Buttressing, Deformation and Erosion'. *Earth Surface Processes and Landforms* 38 (10): 1102–15.

Meteorologisk Institutt, Norges vassdrags- og energidirektorat NVE, Norwegian Research Center AS NORCE, and Bjerknes Center for Climate Research. 2020. 'Norsk Klimaservicesenter'. Norwegian Climate Service Center. 2020. https://klimaservicesenter.no/observations/.

Miller, Daniel J., and Thomas Dunne. 1996. 'Topographic Perturbations of Regional Stresses and Consequent Bedrock Fracturing'. *Journal of Geophysical Research: Solid Earth* 101 (B11): 25523–36.

Molina, Freddy XY. 2010. 'Structural Control of Multi-Scale Discontinuities on Slope Instabilities in Crystalline Rock'. ETH Zurich.

Moore, Jeffrey R., Valentin Gischig, Jan Burjanek, Simon Loew, and Donat Fäh. 2011. 'Site Effects in Unstable Rock Slopes: Dynamic Behavior of the Randa Instability (Switzerland)'. *Bulletin of the Seismological Society of America* 101 (6): 3110–16.

Moro, Marco, Michele Saroli, Stefano Salvi, Salvatore Stramondo, and Fawzi Doumaz. 2007. 'The Relationship between Seismic Deformation and Deep-Seated Gravitational Movements during the 1997 Umbria–Marche (Central Italy) Earthquakes'. *Geomorphology* 89 (3–4): 297–307.

Nemec, W, MN Oti, and G Postma. 1995. 'The Dynamics of Deltaic Suspension Plumes'. *Geology of Deltas*, 31–93.

Nesje, Atle, and Ian M. Whillans. 1994. 'Erosion of Sognefjord, Norway'. *Geomorphology* 9 (1): 33–45.

NGU, Norges Geologiske Undersøkelse. 2015. 'Maps and Data - NGU'. 29 January 2015. https://www.ngu.no/en/topic/maps-and-data.

———. 2020a. 'Unstable Rock Slope Inventory Map'. Online map. 2020. https://geo.ngu.no/kart/ustabilefjellparti_mobil/.

———. 2020b. 'About the Mapping Service - NGU'. 29 January 2020. https://www.ngu.no/en/topic/about-mapping-service.

Nichol, Susan L., Oldrich Hungr, and S. G. Evans. 2002. 'Large-Scale Brittle and Ductile Toppling of Rock Slopes'. *Canadian Geotechnical Journal* 39 (4): 773–88.

Nichols, T. C. 1980. 'Rebound, Its Nature and Effect on Engineering Works'. *Quarterly Journal of Engineering Geology and Hydrogeology* 13 (3): 133–52.

Nøttvedt, A., and E. P. Johannessen. 2008. 'The Source of Norway's Oil Wealth'. *The Making of a Land–Geology of Norway. Norsk Geologisk Forening, Trondheim, Norway* 384: 417.

Olsen, Lars, Harald Sveian, Bjørn Bergstrøm, Dag Ottesen, and Leif Rise. 2013. 'Quaternary Glaciations and Their Variations in Norway and on the Norwegian Continental Shelf'. *Quaternary Geology of Norway* 13: 27–78.

Oppikofer, Thierry, Reginald L Hermanns, Martina Böhme, and Aline Saintot. 2017. 'Different Stages of Progressive Failure in Unstable Rock Slopes in Møre & Romsdal County, Western Norway'. In . International Society for Rock Mechanics and Rock Engineering.

Oppikofer, Thierry, Bobo Nordahl, Halvor Bunkholt, Magnus Nicolaisen, Alexandra Jarna, Sverre Iversen, Reginald L. Hermanns, Martina Böhme, and Freddy X. Yugsi Molina. 2015. 'Database and Online Map Service on Unstable Rock Slopes in Norway—From Data Perpetuation to Public Information'. *Geomorphology* 249: 69–81.

Pánek, Tomáš, Jan Hradecký, Jozef Minár, Oldrich Hungr, and Radek Dušek. 2009. 'Late Holocene Catastrophic Slope Collapse Affected by Deep-Seated Gravitational Deformation in Flysch: Ropice Mountain, Czech Republic'. *Geomorphology* 103 (3): 414–29.

Pánek, Tomáš, and Jan Klimeš. 2016. 'Temporal Behavior of Deep-Seated Gravitational Slope Deformations: A Review'. *Earth-Science Reviews* 156: 14–38.

Patton, Henry, Alun Hubbard, Karin Andreassen, Amandine Auriac, Pippa L. Whitehouse, Arjen P. Stroeven, Calvin Shackleton, Monica Winsborrow, Jakob Heyman, and Adrian M. Hall. 2017. 'Deglaciation of the Eurasian Ice Sheet Complex'. *Quaternary Science Reviews* 169 (August): 148–72. https://doi.org/10.1016/j.quascirev.2017.05.019.

Patton, Henry, Alun Hubbard, Karin Andreassen, Monica Winsborrow, and Arjen P Stroeven. 2016. 'The Build-up, Configuration, and Dynamical Sensitivity of the Eurasian Ice-Sheet Complex to Late Weichselian Climatic and Oceanic Forcing'. *Quaternary Science Reviews* 153: 97–121.

Pedrazzini, Andrea. 2012. 'Characterization of Gravitational Rock Slope Deformations at Different Spatial Scales Based on Field, Remote Sensing and Numerical Approaches'.

Penna, Ivanna M, Reginald L Hermanns, Samuel Niedermann, and Andrés Folguera. 2011. 'Multiple Slope Failures Associated with Neotectonic Activity in the Southern Central Andes (37–37 30′ S), Patagonia, Argentina'. *Bulletin* 123 (9–10): 1880–95.

Poisel, R. 1998. 'Kippen, Sacken, Gleiten'. *Felsbau* 16 (3): 135–40.

Porter, Stephen C., and Giuseppe Orombelli. 1981. 'Alpine Rockfall Hazards: Recognition and Dating of Rockfall Deposits in the Western Italian Alps Lead to an Understanding of the Potential Hazards of Giant Rockfalls in Mountainous Regions'. *American Scientist* 69 (1): 67–75.

Powell, RD, and E Domack. 1995. 'Glacial Environments, Vol. 1. Modern Glacial Environments: Processes, Dynamics and Sediments'.

Reitner, Jürgen M., and Manfred Linner. 2009. 'Formation and Preservation of Large Scale Toppling Related to Alpine Tctonic Structures - Eastern Alps.' *Austrian Journal of Earth Sciences* 102 (2).

Riiber, K. 2000. 'Løsmasse Kart. Manuskart 1:250 000'. http://geo.ngu.no/kart/losmasse/.

Roberts, D. 1974. 'Hammerfest: Description to the 1: 250.000 Bedrockgeological Map'. *Norges Geologiske Undersøkelse* 301: 1–66.

Roberts, D, and S Elvevold. 2018. 'Berggrunnskart Øksfjord 1835-3, M 1:50 000. Norges Geologiske Undersøkelse'.

Roberts, David, and Stephen J Lippard. 2005. 'Inferred Mesozoic Faulting in Finnmark: Current Status and Offshore Links'. *Norges Geologiske Undersøkelse Bulletin* 443 (55–60).

Roberts, R. J., F. Corfu, T. H. Torsvik, L. D. Ashwal, and D. M. Ramsay. 2006. 'Short-Lived Mafic Magmatism at 560–570 Ma in the Northern Norwegian Caledonides: U–Pb Zircon Ages from the Seiland Igneous Province'. *Geological Magazine* 143 (6): 887–903. https://doi.org/10.1017/S0016756806002512.

Robins, B., and P. M. Gardner. 1975. 'The Magmatic Evolution of the Seiland Province, and Caledonian Plate Boundaries in Northern Norway'. *Earth and Planetary Science Letters* 26 (2): 167–78.

Romundset, Anders, Naki Akçar, Ola Fredin, Dmitry Tikhomirov, Regina Reber, Christof Vockenhuber, Marcus Christl, and Christian Schlüchter. 2017. 'Lateglacial Retreat Chronology of the Scandinavian Ice Sheet in Finnmark, Northern Norway, Reconstructed from Surface Exposure Dating of Major End Moraines'. *Quaternary Science Reviews* 177: 130–44.

Romundset, Anders, Stein Bondevik, and Ole Bennike. 2011. 'Postglacial Uplift and Relative Sea Level Changes in Finnmark, Northern Norway'. *Quaternary Science Reviews* 30 (19–20): 2398–2421.

Sanchez, G., Yan Rolland, M. Corsini, Regis Braucher, D. Bourlès, M. Arnold, and G. Aumaître. 2010. 'Relationships between Tectonics, Slope Instability and Climate Change: Cosmic Ray Exposure Dating of Active Faults, Landslides and Glacial Surfaces in the SW Alps'. *Geomorphology* 117 (1–2): 1–13.

Scheidegger, Adrian E. 1973. 'On the Prediction of the Reach and Velocity of Catastrophic Landslides'. *Rock Mechanics* 5 (4): 231–36.

Sollid, J. L., S. Andersen, N. Hamre, O. Kjeldsen, O. Salvigsen, S. Sturød, T. Tveitå, and A. Wilhelmsen. 1973. 'Deglaciation of Finnmark, North Norway'. *Norsk Geografisk Tidsskrift - Norwegian Journal of Geography* 27 (4): 233–325. https://doi.org/10.1080/00291951.1973.9728306.

Stead, Doug, and Andrea Wolter. 2015. 'A Critical Review of Rock Slope Failure Mechanisms: The Importance of Structural Geology'. *Journal of Structural Geology* 74: 1–23.

Stephens, MB, H Furnes, B Robins, and BA Sturt. 1985. 'Igneous Activity within the Scandinavian Caledonides'. *The Caledonide Orogen—Scandinavia and Related Areas* 2: 623–57.

Stokes, Chris R, Geoffrey D Corner, Monica CM Winsborrow, Katrine Husum, and Karin Andreassen. 2014. 'Asynchronous Response of Marine-Terminating Outlet Glaciers during Deglaciation of the Fennoscandian Ice Sheet'. *Geology* 42 (5): 455–58.

Sveian, H. 2004. 'Isen Kom–Og Forsvant'. *Ka Dokker Mein Førr Stein*.

———. 2005. *Troms Fylke: Løsmassekart*. Norges Geologiske Undersøkelse.

Trauth, Martin H, Ricardo A Alonso, Kirk R Haselton, Reginald L Hermanns, and Manfred R Strecker. 2000. 'Climate Change and Mass Movements in the NW Argentine Andes'. *Earth and Planetary Science Letters* 179 (2): 243–56.

Tyldum Skogen, Ellen. in prep. 'Structural assessment and controlling factors of the unstable rock slope Dusnjarga in Kvænangen'. Master thesis, Tromsø: University of Tromsø.

Varnes, David J. 1978. 'Slope Movement Types and Processes'. *Special Report* 176: 11–33.

Vorren, TO, J Mangerud, LH Blikra, A Nesje, and H Sveian. 2008. 'The Emergence of Modern Norway'. *The Making of Land: Geology of Norway. Geological Society of Norway, Trondheim*, 534–59.

Willenberg, Heike, Keith F. Evans, Erik Eberhardt, Thomas Spillmann, and Simon Loew. 2008. 'Internal Structure and Deformation of an Unstable Crystalline Rock Mass above Randa (Switzerland): Part II—Three-Dimensional Deformation Patterns'. *Engineering Geology* 101 (1–2): 15–32.

Wines, David, and P. Lilly. 2003. 'Estimates of Rock Joint Shear Strength in Part of the Fimiston Open Pit Operation in Western Australia'. *International Journal of Rock Mechanics and Mining Sciences - INT J ROCK MECH MINING SCI* 40 (September): 929–37. https://doi.org/10.1016/S1365-1609(03)00020-0.

Wyllie, Duncan C., and Chris Mah. 2004. *Rock Slope Engineering*. CRC Press.

Wyrwoll, Karl-Heinz. 1977. 'Causes of Rock-Slope Failure in a Cold Area: Labrador-Ungava'. *Geological Society of America Reviews in Engineering Geology* 3: 59–67.

Zangerl, Christian, Christoph Prager, Rainer Brandner, Ewald Brückl, Stefan Eder, Wolfgang Fellin, Ewald Tentschert, Gerhard Poscher, and Helmut Schönlaub. 2008. 'Methodischer Leitfaden Zur Prozessorientierten Bearbeitung von Massenbewegungen'. *Geo. Alp* 5: 1–51.

Zischinsky, Ulf. 1966. 'On the Deformation of High Slopes'. In . International Society for Rock Mechanics and Rock Engineering.

———. 1969. 'Über Sackungen'. *Rock Mechanics* 1 (1): 30–52.

Appendix

Supplements Quaternary geology

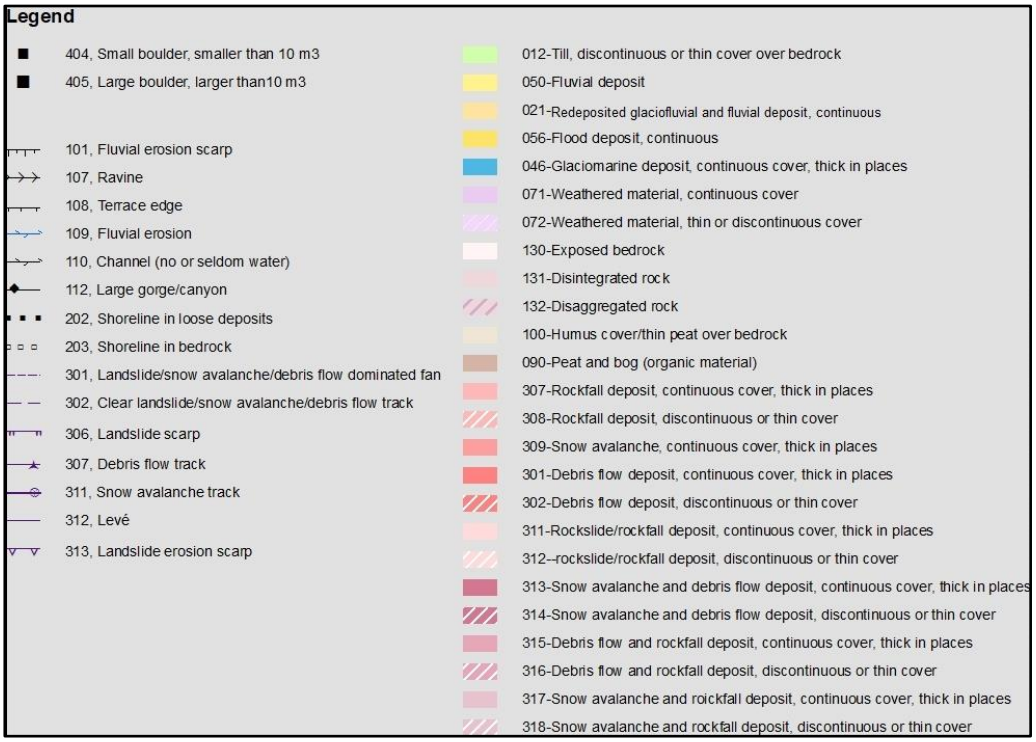

Appendix 1: Legend Quaternary geological map.

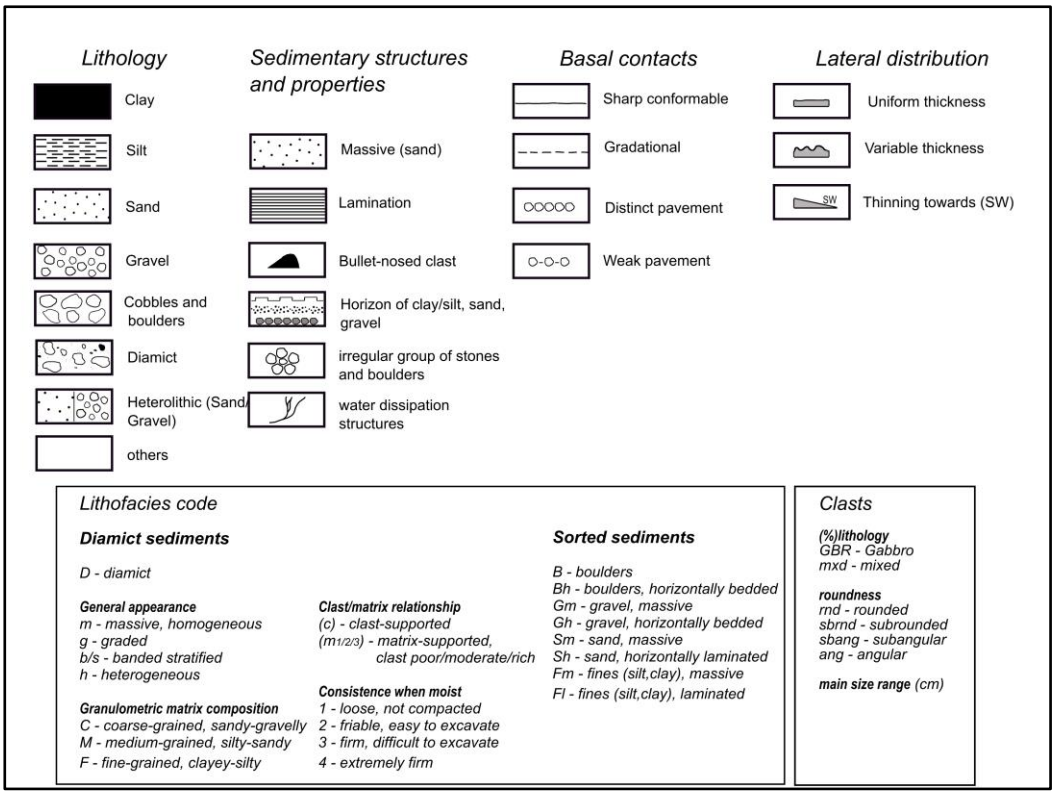

Appendix 2: Legend sedimentary logs of Quaternary deposits.

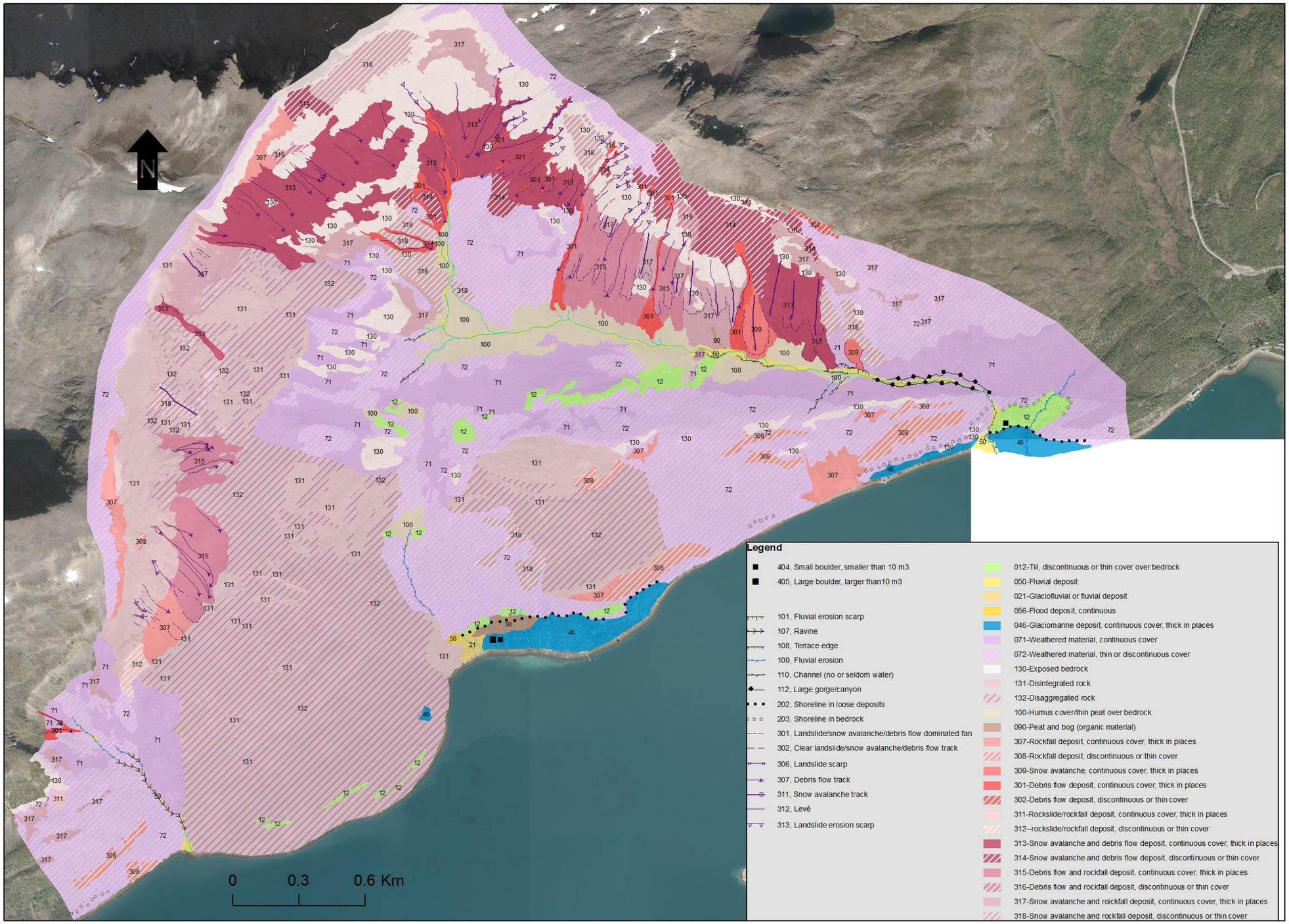

Appendix 3: Quaternary geological map: no transparency and orthophoto base map.

Supplements morphological analysis

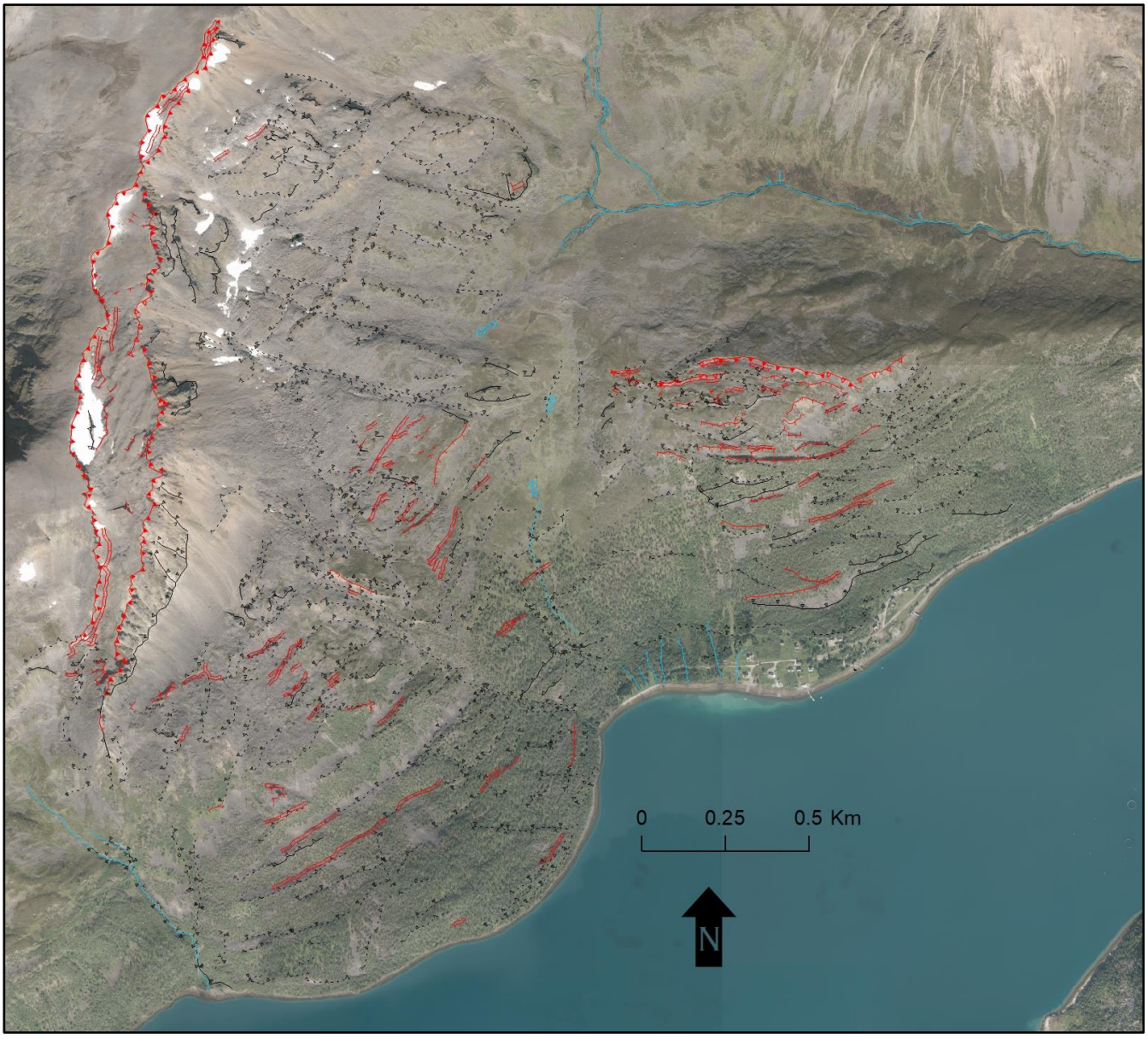

Appendix 4: Morpho-gravitational map with orthophoto base map.

Supplementary displacement data

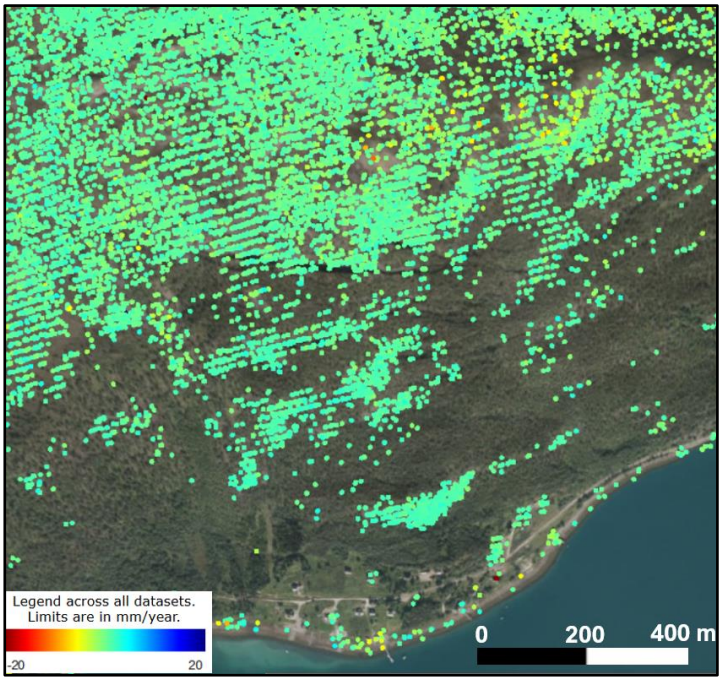

Appendix 5: InSAR data for Låvan. Ascending pathway.

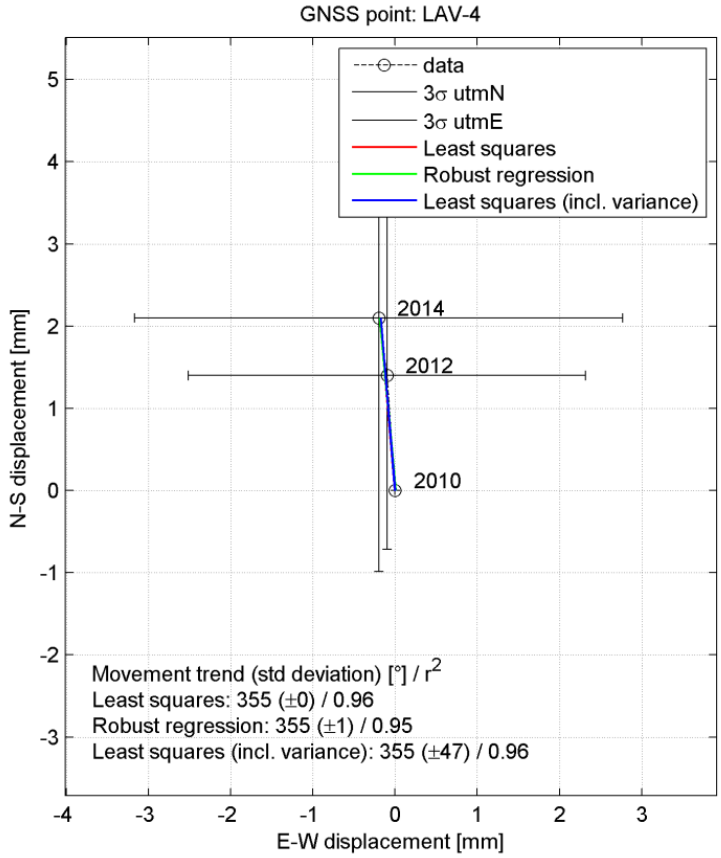

Appendix 6: dGNSS Låvan for point LAV-4. Horizontal displacement.

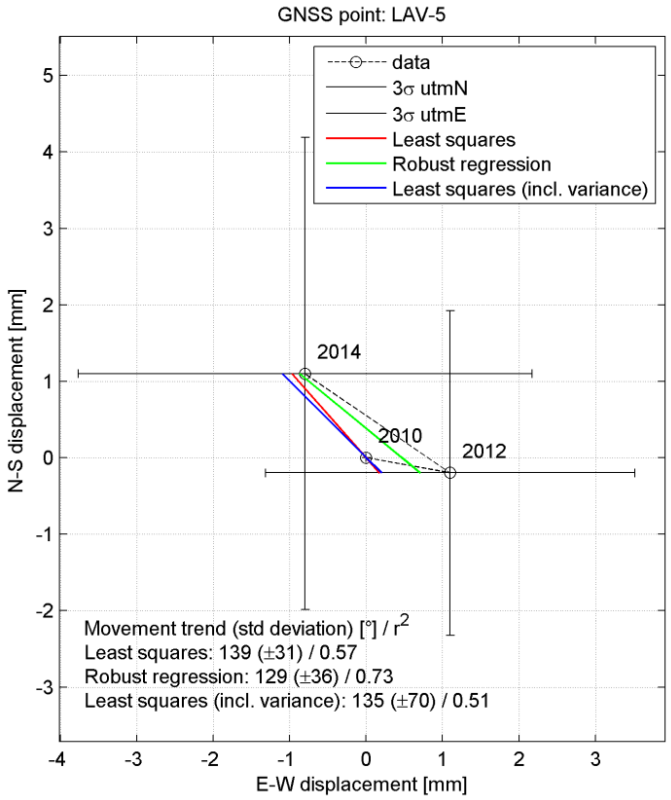

Appendix 7: dGNSS Låvan for point LAV-5. Horizontal displacement.

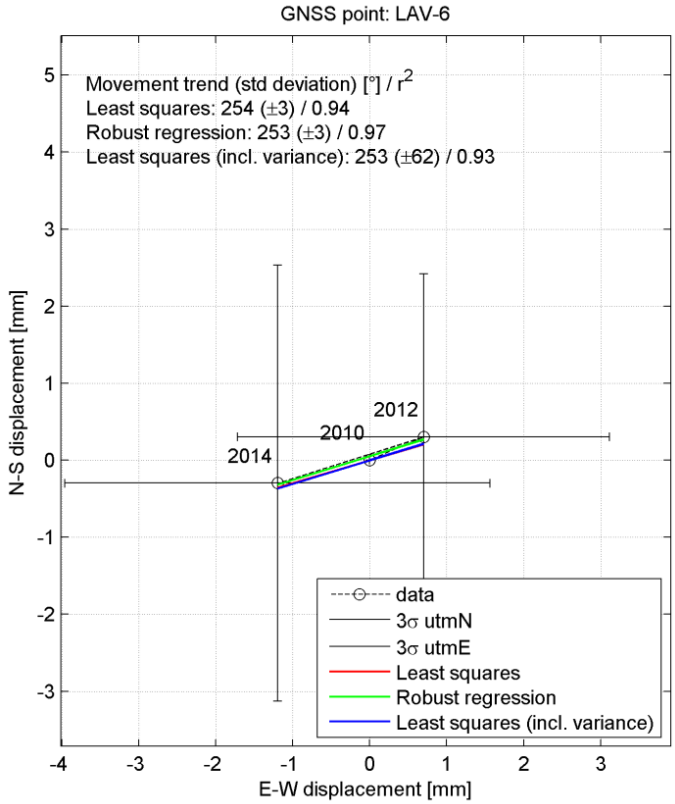

Appendix 8: dGNSS Låvan for point LAV-6. Horizontal displacement.

Supplementary structural data

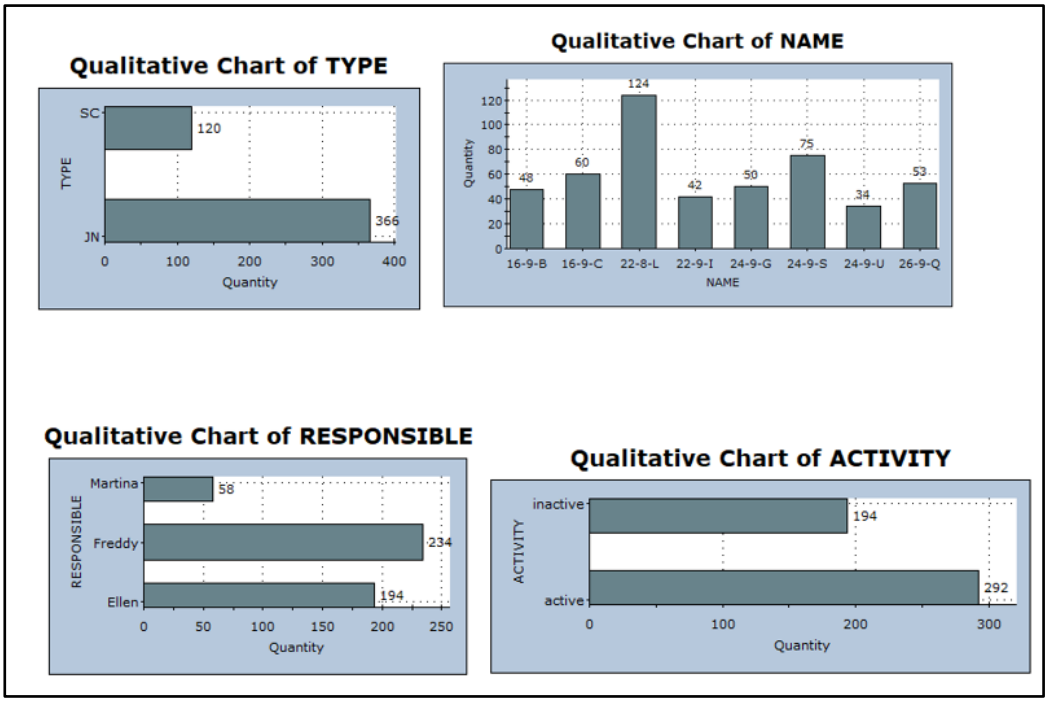

Appendix 9: Statistics of structural data for Låvan and surrounding stable locations that were implemented in the result chapter.

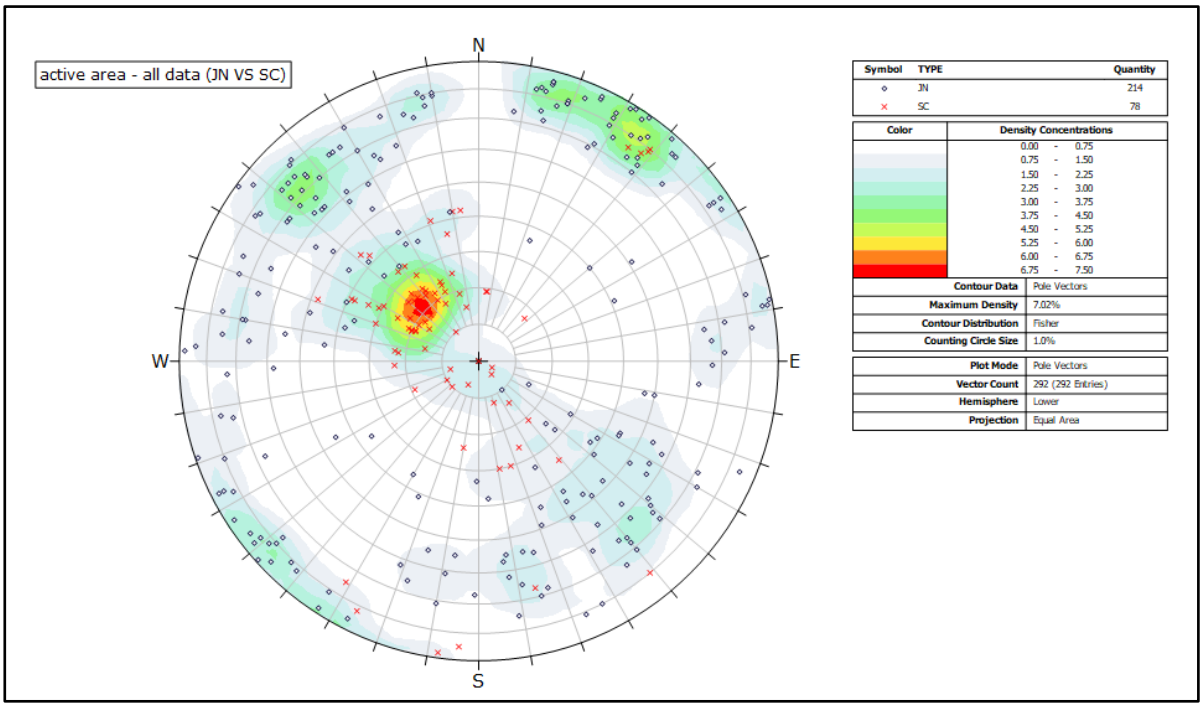

Appendix 10: All structural data from the deformation area Låvan.

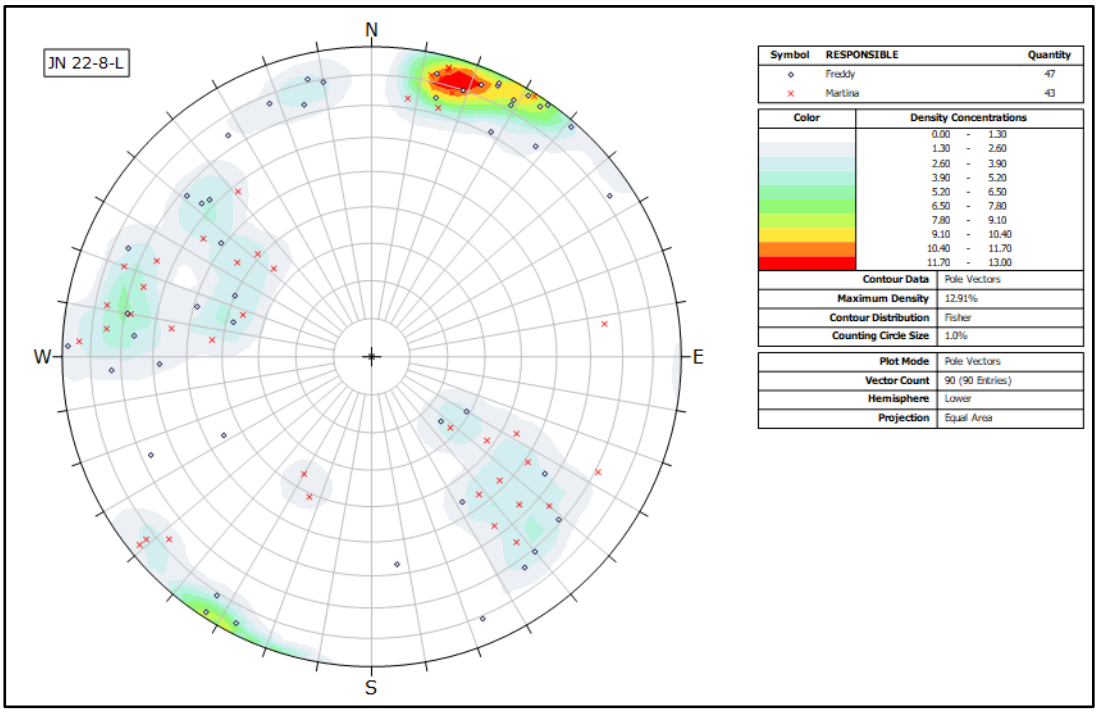

Appendix 11: Joint orientations for outcrop 22-8-L in the deformation area Låvan.

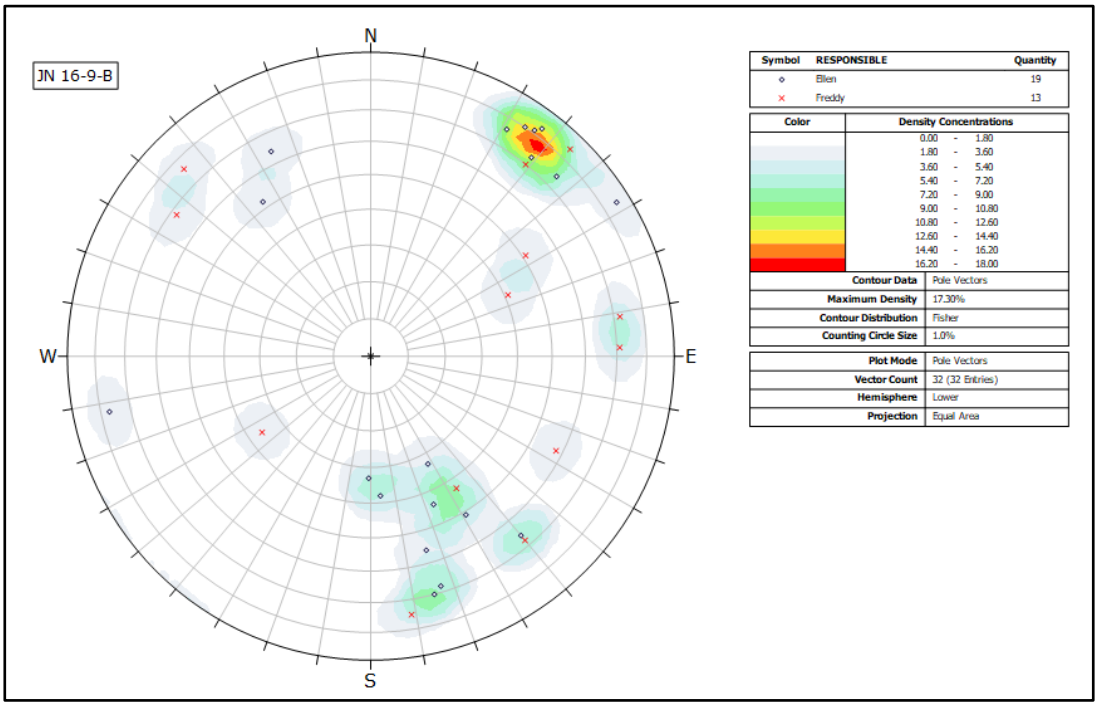

Appendix 12: Joint orientations for outcrop 16-9-B in the deformation area Låvan.

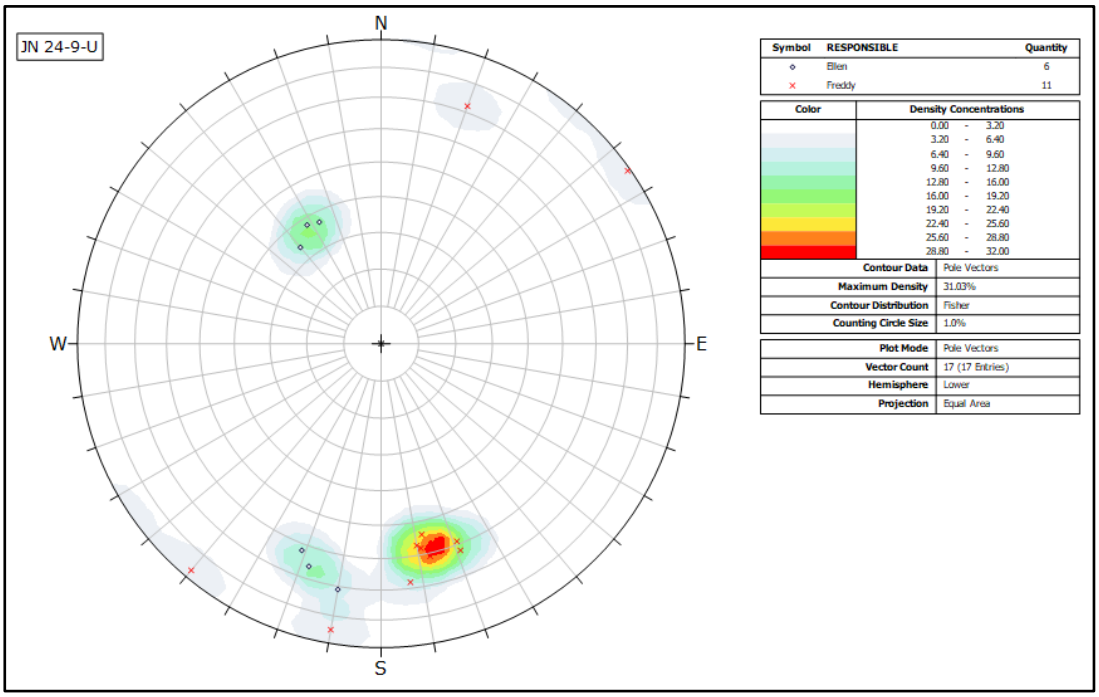

Appendix 13: Joint orientations for outcrop 24-9-U in the deformation area Låvan.

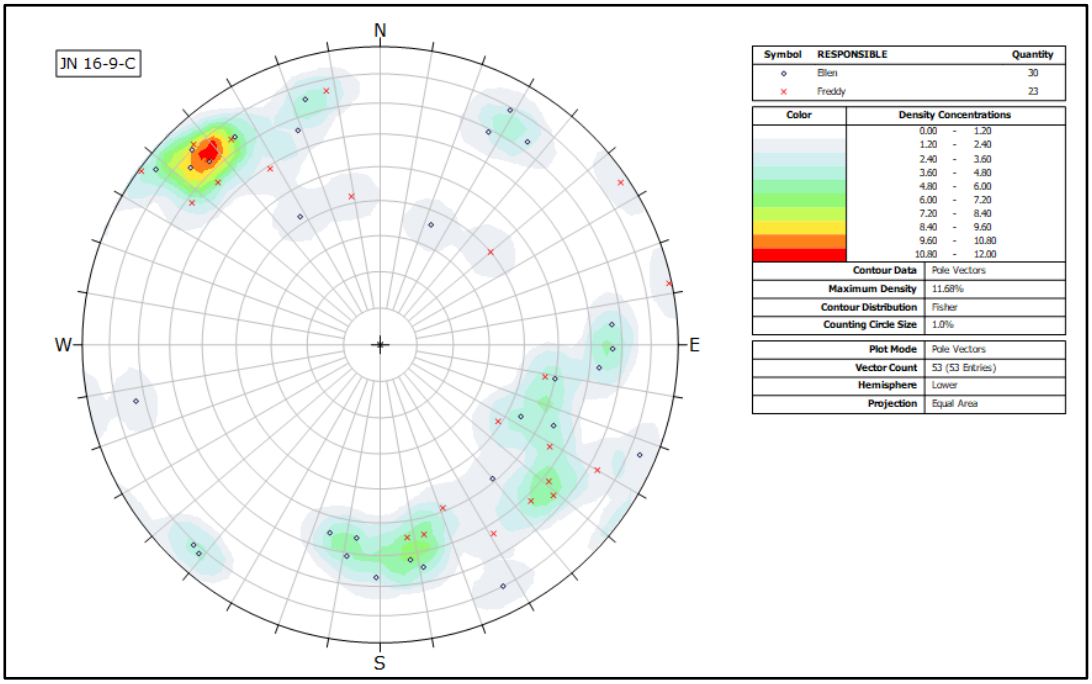

Appendix 14: Joint orientations for outcrop 16-9-C in the deformation area Låvan.

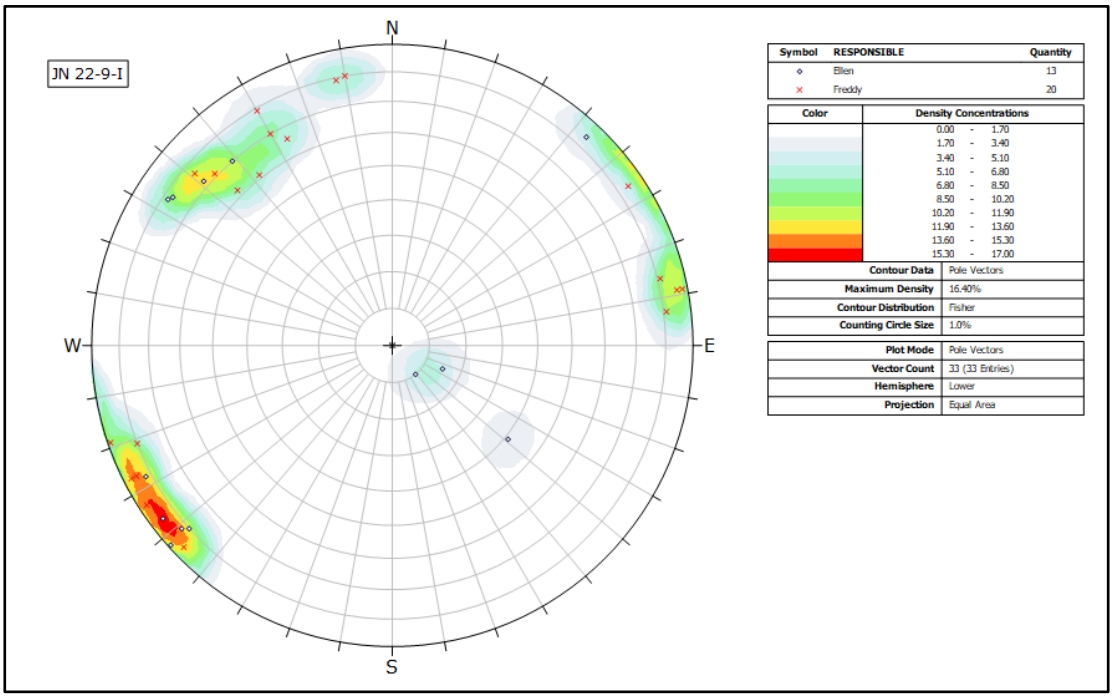

Appendix 15: Joint orientations for outcrop 22-9-I in the deformation area Låvan.

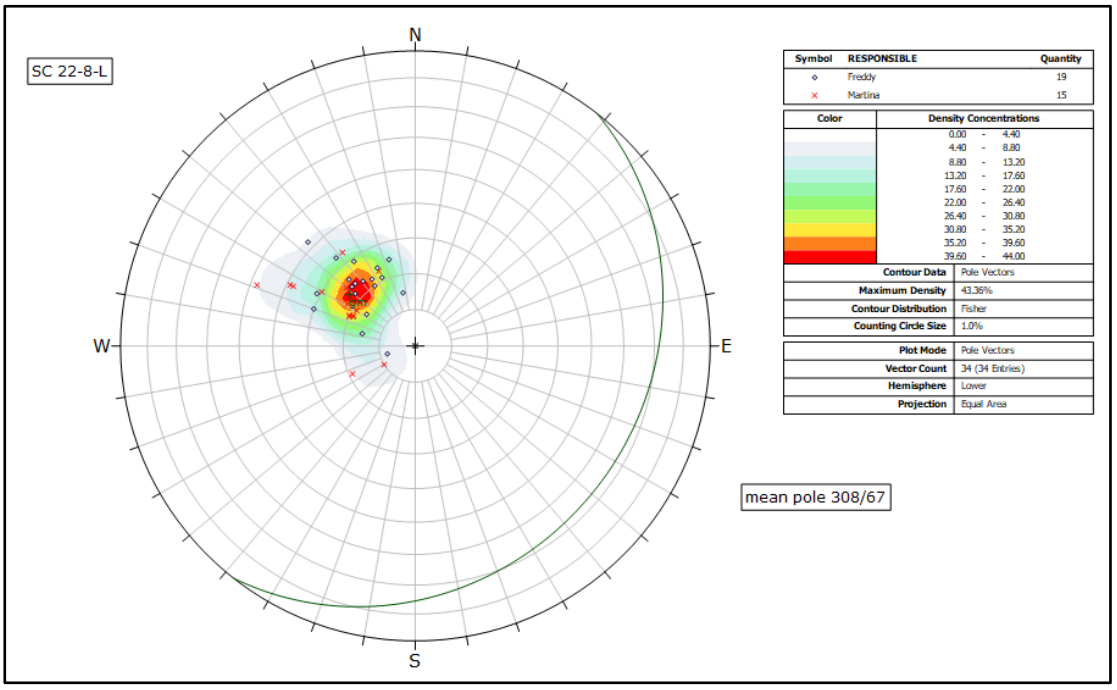

Appendix 16: Foliation (SC) data for outcrop 22-8-L in the deformation area Låvan.

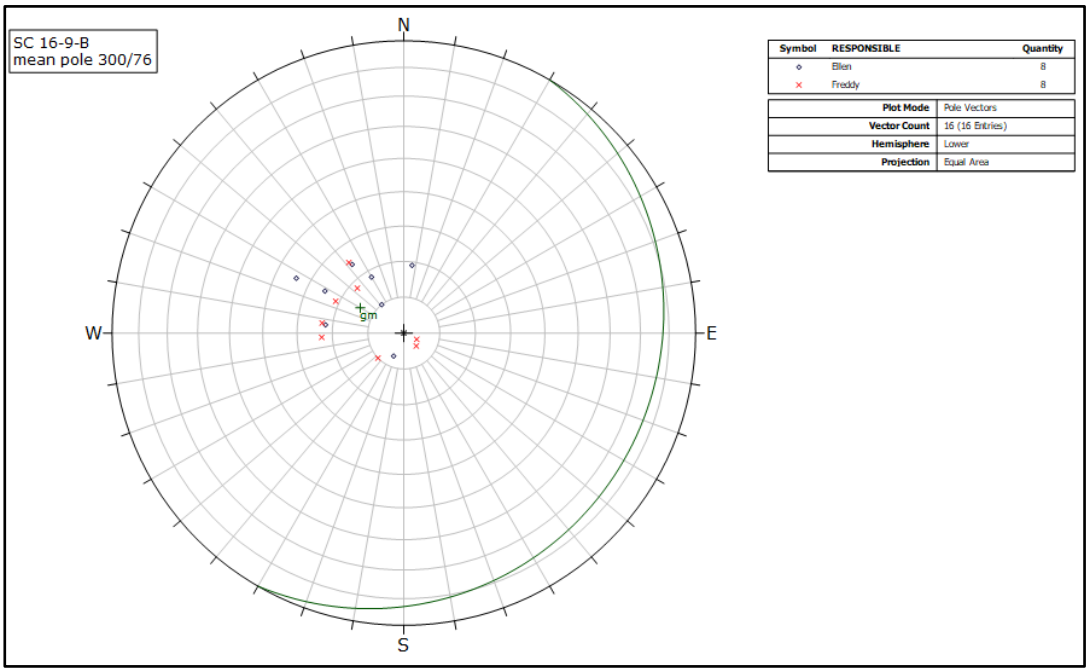

Appendix 17: Foliation (SC) data for outcrop 16-9-B in the deformation area Låvan.

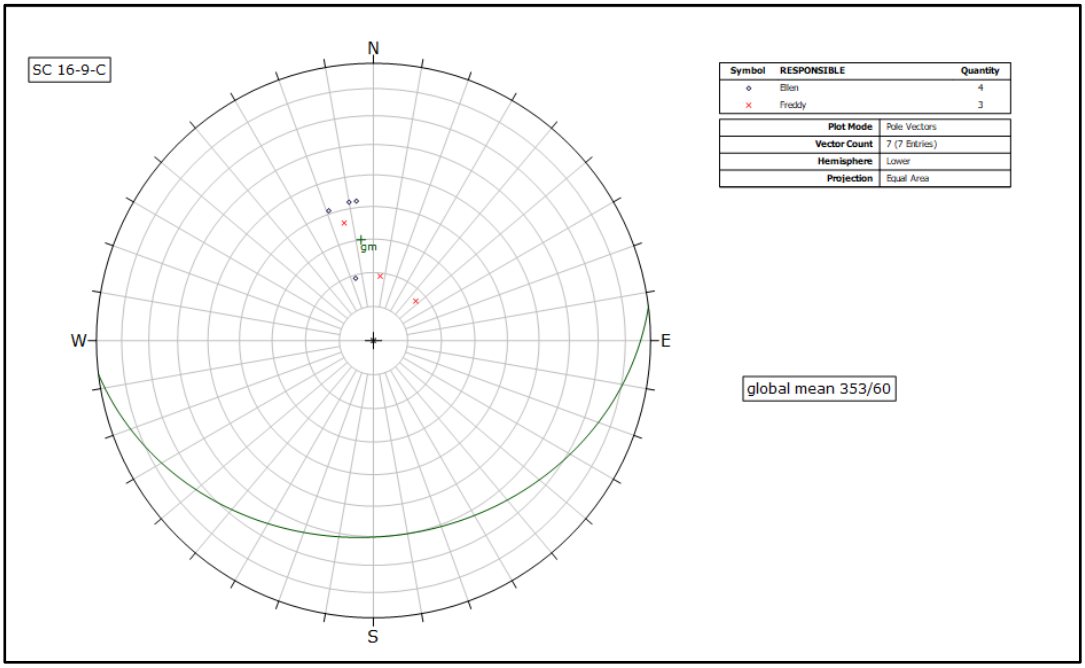

Appendix 18: Foliation (SC) data for outcrop 16-9-C in the deformation area Låvan.

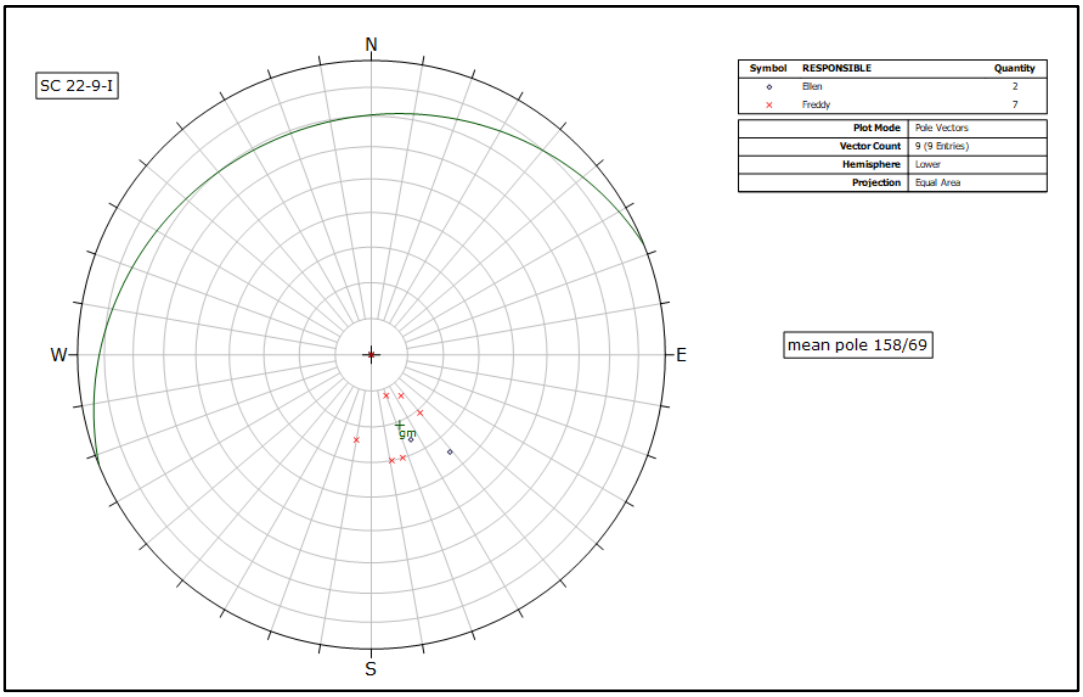

Appendix 19: Foliation (SC) data for outcrop 22-9-I in the deformation area Låvan.

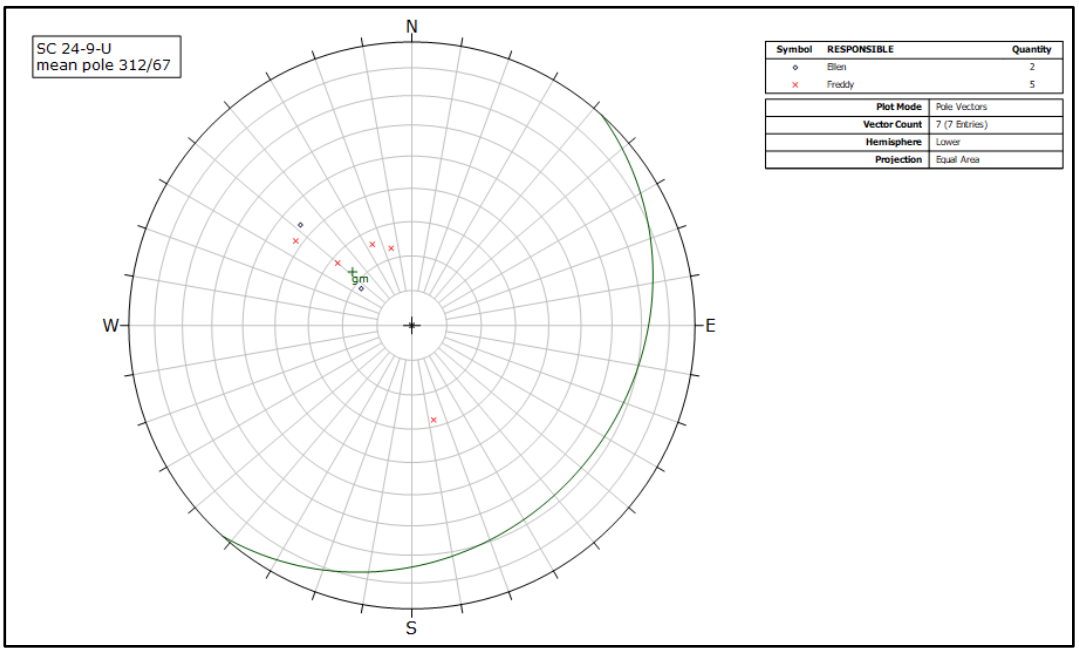

Appendix 20: Foliation (SC) data for outcrop 24-9-U in the deformation area Låvan.